SECTION 3

REACTOR

TABLE OF CONTENTS

TABLE OF CONTENTS (CONT'D)

TABLE OF CONTENTS (CONT'D)

TABLE OF CONTENTS (CONT'D)

TABLE OF CONTENTS (CONT'D)

LIST OF TABLES

LIST OF TABLES (CONT'D)

LIST OF FIGURES

LIST OF FIGURES (CONT'D)

LIST OF FIGURES (CONT'D)

LIST OF FIGURES (CONT'D)

LIST OF FIGURES (CONT'D)

LIST OF FIGURES (CONT'D)

SECTION 3 REACTOR

3.1 SUMMARY DESCRIPTION

This chapter describes:

1. the mechanical components of the reactor and reactor core including the fuel rods and fuel assemblies, reactor internals, and the control rod drive mechanisms

2. the nuclear design

3. the thermal-hydraulic design

The reactor core is comprised of an array of one type or a combination of 17 x 17 Standard (STD), VANTAGE 5H (V5H), VANTAGE+, and/or Robust Fuel Assemblies (RFA/RFA-2).

The significant new mechanical design features of the VANTAGE 5H fuel assembly design are described in References 1 and 2. These features include the following:

- Integral Fuel Burnable Absorbers (IFBAs)

- Axial Blankets - The axial blanket region is the nominal 6 inches of fuel pellets located at each end of the fuel rod pellet stack. The fuel pellets in the axial blanket region may be natural, mid-enriched or fully enriched solid or annular pellets. The annular blanket pellets are used to increase the void volume for gas accommodation within the fuel rod.

- Replacement of six intermediate Inconel grids with Zircaloy grids

- Slightly longer fuel rods and thinner top and bottom nozzle and plates to accommodate extended burnup

- Reconstitutable Top Nozzles (RTNs)

- Redesigned fuel rod bottom end plug to facilitate reconstitution capability

- Reduction in guide thimble and instrumentation tube diameter

Beginning with Beaver Valley Unit 1 Cycle 13, features of the VANTAGE+ fuel assembly design were incorporated into the fresh fuel feed regions. The VANTAGE+ fuel assembly design (Reference 5) included the following features: ZIRLO™ clad fuel rods, thimble tubes, and instrumentation tubes. The intermediate grid strap material was also changed to ZIRLO™. As an added debris mitigation feature, a protective bottom grid was incorporated.

Beginning with Beaver Valley Unit 1 Cycle 15, the Robust Fuel Assembly (RFA/RFA-2) design was incorporated into the fresh fuel regions. The significant new mechanical design features relative to the V5H and VANTAGE+ designs are:

- Modified Low Pressure Drop (LPD) mid-grids. This will provide increased DNB margin and increased resistance to fuel rod wear.

- The addition of three Intermediate Flow Mixer (IFM) grids between the top three mid-grid spans (grids 4 through 7). This will provide increased DNB margin.

- Increased guide and instrument thimble wall thickness by approximately 25 percent with no change to the inside diameters. This improves the stiffness of the tubes and addresses incomplete rod insertion considerations.

Beginning in Cycle 17, the RFA-2 design was incorporated into the fresh fuel regions. The RFA-2 design is the same as the RFA with the exception that the mid-grids of the RFA-2 have increased contact area between the dimples/springs and the fuel rods.

In Cycle 22, the RFA-2 fuel assemblies integrated the following design features:

- Standardized Debris Filter Bottom Nozzle (SDFBN) to improve the debris mitigation performance of the bottom nozzle.

- Robust Protective Grid (RPG) to help address the issues of fatigue failures and failures due to stress corrosion cracking within the rod support dimples.

- Low Strain Radius Mid-Grids and IFM Grids to lower the strain imposed on the formed features and improve the manufacturability.

In Cycle 26, the RFA-2 fuel assemblies incorporated the Westinghouse Integral Nozzle (WIN) with the following design and manufacturing improvements.

- The spring pads are now integral to the top nozzle casting.

- The springs are assembled into the nozzle pad and pinned in place which provides a wedged rather than a clamped (bolted) joint to transfer the fuel assembly holddown forces into the top nozzle structure.

The core is cooled and moderated by light water at a pressure of 2250 psia in the Reactor Coolant System. The moderator coolant contains soluble boron as a neutron poison. The concentration of boron in the coolant is varied as required to control relatively slow reactivity changes including the effects of fuel burnup. Additional boron, in the form of Integral Fuel Burnable Absorbers (IFBAs) and/or discrete burnable absorber rods, may be used to limit the moderator temperature coefficient (MTC) and the total power peaking that can be achieved.

Two hundred and sixty-four fuel rods are mechanically joined in a square array to form a fuel assembly. The fuel rods are supported in intervals along their length by grid assemblies, and IFMs for the RFA/RFA-2, which maintain the lateral spacing between the rods throughout the design life of the assembly. The grid assembly consists of an "egg-crate" arrangement of interlocked straps. The straps contain spring fingers and dimples for fuel rod support as well as coolant mixing vanes. The fuel rods consist of slightly enriched uranium dioxide ceramic cylindrical pellets contained in slightly cold worked Zircaloy-4 or ZIRLO® tubing, or partially re-crystallized Optimized ZIRLO™ tubing which is plugged and seal welded at the ends to encapsulate the fuel.[1] All fuel rods are pressurized with helium during fabrication to reduce stresses and strains to increase fatigue life. A protective bottom grid has been added just

[1] Optimized ZIRLO and ZIRLO are trademarks or registered trademarks of Westinghouse Electric Company LLC, its affiliates and/or its subsidiaries in the United States of America and may be registered in other countries throughout the world. All rights reserved. Unauthorized use is strictly prohibited. Other names may be trademarks of their respective owners.

above the bottom nozzle. The grid straps intersect the nozzle flow holes, thus, further reducing the possibility of fuel rod damage due to debris induced fuel rod fretting. In addition, the ZIRLO® and Optimized ZIRLO™ fuel rods will be oxide coated at the lower end for additional protection against fretting.

Fuel assemblies may also contain non-fueled rods (stainless steel, Zircaloy-4 or ZIRLO™ filler rods). Non-fueled rods may be used in core locations where fuel damage has occurred or may occur. The use of non-fueled rods began when fuel inspections performed during the fifth refueling outage identified leaking fuel rods in a peripheral assembly. It was determined that the fuel rod leakage was attributable to baffle jetting.

The solution to this problem, recommended by Westinghouse and used by other utilities, involves fuel assembly reconstitution as a means to allow the insertion of non-fueled rods into a fuel assembly. In the reconstitution process, the fuel rods in positions subject to problem conditions would be removed and replaced with non-fueled rods. The reconstituted fuel assemblies meet essentially the same design requirement as the original fuel assembly, and the use of reconstituted assemblies will not result in a change to existing safety criteria and design limits. The effects of fuel assembly reconstitution are evaluated in accordance with the methods described in Reference 4.

The center position in the assembly is reserved for the in-core instrumentation, while the remaining 24 positions in the array are equipped with guide thimbles joined to the grids and the top and bottom nozzles. Depending upon the position of the assembly in the core, the guide thimbles are used as core locations for rod cluster control assemblies, neutron source assemblies, and burnable absorber rods.

The bottom nozzle is a box-like structure which serves as a bottom structural element of the fuel assembly and directs the coolant flow distribution to the assembly.

The top nozzle assembly functions as the upper structural support element of the fuel assembly in addition to providing a partial protective housing for the rod cluster control assembly or other components. The Reconstitutable Top Nozzle (RTN) may be removed between operating cycles to provide access for fuel rod examination or reconstitution of damaged fuel.

The rod cluster control assemblies consist of individual absorber rods fastened at the top end to a spider assembly. These assemblies contain full length absorber material to control the reactivity of the core under operating conditions. The full length control rod assemblies shall contain a nominal 142 inches of absorber material. The nominal values of absorber material shall be 80 percent silver, 15 percent indium and 5 percent cadmium. All control rods shall be clad with stainless steel tubing.

The control rod drive mechanisms for the full length rod cluster control assemblies are of the magnetic latch type. The latches are controlled by three magnetic coils. They are so designed that upon a loss of power to the coils, the rod cluster control assembly is released and falls by gravity to shutdown the reactor.

The components of the reactor internals are divided into three parts consisting of the lower core support structure (including the entire core barrel and neutron shield pad assembly), the upper core support structure and the in-core instrumentation support structure. The reactor internals support the core, maintain fuel alignment, limit fuel assembly movement, maintain alignment between fuel assemblies and control rod drive mechanisms, direct coolant flow past the fuel

elements and to the pressure vessel head, provide gamma and neutron shielding, and provide guides for the in-core instrumentation.

The nuclear design analyses and evaluation establish physical locations for control rods and burnable absorbers and physical parameters such as fuel enrichments and boron concentration in the coolant such that the reactor core has inherent characteristics which, together with corrective actions of the reactor control, protective and emergency cooling systems, provide adequate reactivity control even if the highest reactivity worth rod cluster control assembly is stuck in the fully withdrawn position.

The design also provides for inherent stability against diametral and azimuthal power oscillations.

The thermal-hydraulic design analyses and evaluation establish coolant flow parameters which assure that adequate heat transfer is assured between the fuel cladding and the reactor coolant. The thermal design takes into account local variations in dimensions, power generation, flow distribution and mixing. The mixing vanes incorporated in the fuel assembly spacer grid design induce additional flow mixing between the various flow channels within a fuel assembly as well as between adjacent assemblies.

Instrumentation is provided in and out of the core to monitor the nuclear, thermal-hydraulic, and mechanical performance of the reactor and to provide inputs to automatic control functions.

The reactor core design, together with corrective actions of the reactor control, protection and emergency cooling systems can meet the reactor performance and safety criteria specified in Section 3.2.

Table 3.1-1 presents the principal nuclear, thermal-hydraulic and mechanical design parameters for the Beaver Valley 17 x 17 STD, VANTAGE 5H, VANTAGE+ and Robust Fuel Assemblies, including the effects of fuel densification.

The effects of fuel densification were evaluated with the methods described in Reference 6.

The analysis techniques employed in the core design are tabulated in Table 3.1-2. The loading conditions considered in general for the core internals and components are tabulated in Table 3.1-3.

Specific or limiting loads considered for design purposes of the various components are listed as follows: fuel assemblies in Section 3.2.1.1.2; reactor internals in Section 3.2.2.3 and Table 4.1-10; neutron absorber rods, burnable absorber rods, neutron source rods and thimble plug assemblies in Section 3.2.3.1.3; full-length control rod drive mechanisms in Section 3.2.3.1.4. The dynamic analyses, input forcing functions, and response loadings are presented in Section B.3.

References for Section 3.1

1. S. L. Davidson (Ed.), et. al., "VANTAGE 5H Fuel Assembly," WCAP-10444-P-A, Addendum 2-A (February 1989).

2. S. L. Davidson (Ed.), et. al., "VANTAGE 5 Fuel Assembly Reference Core Report," WCAP-10444-P-A (September 1985).

3. Deleted by Revision 16.

4. W. H. Slagle (Ed.), "Westinghouse Fuel Assembly Reconstitution Evaluation Methodology," WCAP-13060-P-A (July 1993).

5. S. L. Davidson, D. L. Nufer (Ed.), "Vantage+ Fuel Assembly Reference Core Report," WCAP-12610-P-A and Appendices A through D (April 1995).

6. P. J. Kersting et. al., "Assessment of Clad Flattening and Densification Power Spike Elimination in Westinghouse Nuclear Fuel," WCAP-13589-A (March 1995).

3.2 MECHANICAL DESIGN

The plant conditions for design are divided into four categories in accordance with their anticipated frequency of occurrence and risk to the public: Condition I - Normal Operation; Condition II - Incidents of Moderate Frequency; Condition III - Infrequent Incidents; Condition IV - Limiting Faults.

The reactor is designed so that its components meet the following performance and safety criteria:

1. The mechanical design of the reactor core components and their physical arrangement, together with corrective actions of the reactor control, protection, and emergency cooling systems (when applicable) assure that:

   a. Fuel damage is not expected during Condition I and Condition II events. Fuel damage as used here is defined as penetration of the fission product barrier (that is, the fuel rod clad). It is not possible, however, to preclude a very small number of rod failures resulting in the release of fission products. The chemical and volume control system (CVCS) is designed to remove these fission products from the reactor coolant, keeping the reactor coolant activity within BVPS-1 design basis limits.

   b. The reactor can be brought to a safe state following a Condition III event with only a small fraction of fuel rods damaged, although sufficient fuel damage might occur to preclude resumption of operation without considerable outage time. The fraction of fuel rods damaged must be limited to meet regulatory dose guidelines.

   c. The reactor can be brought to a safe state and the core can be kept subcritical with acceptable heat transfer geometry following transients arising from Condition IV events.

2. The fuel assemblies are designed to accommodate expected conditions for design, handling during assembly, inspection, and refueling operations and shipping loads.

3. The fuel assemblies are designed to accept control rod insertions in order to provide the required reactivity control for power operations and reactivity shutdown conditions.

4. All fuel assemblies have provisions for the insertion of incore instrumentation necessary for plant operation.

5. The reactor internals, in conjunction with the fuel assemblies, direct reactor coolant through the core to achieve acceptable flow distribution and to restrict bypass flow so that the heat transfer performance requirements can be met for all modes of operation. In addition, the internals provide core support and distribute coolant flow to the pressure vessel head so that the temperature difference between the vessel flange and head do not result in leakage from the flange during the Condition I and II modes of operation. Required in-service inspection can be carried out as the internals are removable and provide access to the inside of the pressure vessel.

The following section provides the fuel system design bases and design limits. This information augmented by the clarifying information[32] submitted to the NRC during their review of Reference 21, provided information consistent with the acceptance criteria of the Standard Review Plan (SRP) 4.2.

3.2.1 Fuel

3.2.1.1 Design Bases

For the 17 x 17 STD, VANTAGE 5H, VANTAGE+, and RFA/RFA-2 fuel assemblies, the fuel rod and fuel assembly design bases are established to satisfy the general performance and safety criteria presented in Section 3.2 and specific criteria noted below. Fuel rods may be replaced by non-fueled rods during reconstitution. For a description of the use of non-fueled rods in the reconstitution process, see Section 3.1.

Design values in Section 3.2.1 for the properties of the materials which comprise the fuel rod, fuel assembly and the incore control components are given in References 24 and 25 for Zircaloy-4 Reference 26 for ZIRLO® and Reference 35 for Optimized ZIRLO™ clad fuel. Other supplementary fuel design criteria/acceptance limits are given in Reference 27.

3.2.1.1.1 Fuel Rods

The integrity of the fuel rods is ensured by designing to prevent excessive fuel temperatures, excessive internal rod gas pressures due to fission gas releases, and excessive cladding stresses and strains. This is achieved by designing the fuel rods so that the following conservative design bases are satisfied during Condition I and Condition II events over the fuel lifetime:

1. Fuel Pellet Temperatures - The center temperature of the hottest pellet is to be below the melting temperature of the UO_2 (melting point of 5,080°F[1] unirradiated and reducing by 58°F per 10,000 MWD/MTU). While a limited amount of center melting can be tolerated, the design conservatively precludes center melting. A calculated centerline fuel temperature of 4,700°F has been selected as an overpower limit to assure no fuel melting. This provides sufficient margin for uncertainties, as described in Sections 3.4.1.2 and 3.4.2.10.1. To preclude fuel melting, the peak local power experienced during Condition I and II events can be limited to a maximum value which is sufficient to ensure that the fuel centerline temperatures remain below the melting temperature at all burnups. Design evaluations for Condition I and II events have shown that fuel melting will not occur for achievable local power and burnups up to 75,000 MWD/MTU (Reference 26). Note: The US NRC approved design evaluations up to 60,000 MWD/MTU rod burnup in Reference 26 and up to 62,000 MWD/MTU in Reference 27.

2. Internal Gas Pressure - The internal pressure of the lead rod (maximum internal pressure) in the reactor will be limited to a value below that which could cause, 1) the diametral gap to increase due to outward cladding creep during the steady state operation and, 2) extensive DNB propagation to occur.

3. Clad Stress - The effective clad stresses are less than that which would cause general yield of the clad. While the clad has some capability for accommodating plastic strain, the yield stress has been accepted as a conservative design basis.

4. Clad Tensile Strain - The clad tangential strain range is less than one percent. The clad strain design basis addresses slow transient strain rate mechanisms where the clad effective stress never reaches the yield strength due to stress relaxation. The 1 percent strain limit has been established based upon tensile and burst test data from irradiated clad. Irradiated clad properties are appropriate due to irradiation effects on clad ductility occurring before strain-limiting fuel clad interaction during a transient event can occur.

5. Strain Fatigue - The cumulative strain fatigue cycles are less than the design strain fatigue life. This basis is consistent with proven practice.

The effective clad stress is less than that which would cause general yield of the clad. While the clad has some capability for accommodating plastic strain, the yield strength has been accepted as a conservative design basis limit. Radial, tangential, and axial stress components due to pressure differential and fuel clad contact pressure are combined into an effective stress using the maximum-distortion-energy theory. The von Mises criterion is used to evaluate if the yield strength has been exceeded. Von Mises' criterion states that an isotropic material under multiaxial stress will begin to yield plastically when the effective stress (i.e. combined stress using maximum-distortion-energy theory) becomes equal to the material yield stress in simple tension as determined by an uniaxial tensile test. Since general yielding is to be prohibited, the volume average effective stress determined by integrating across the clad thickness increased by an allowance for local non-uniformity effects before it is compared to the yield strength. The yield strength correlation is that appropriate for irradiated clad since the irradiated properties are attained at low exposure whereas the fuel/clad interaction conditions which can lead to minimum margin to the design basis limit always occurs at much higher exposure.

The detailed fuel rod design establishes such parameters as pellet size and density, clad-pellet diametral gap, gas plenum size, and helium pre-pressure. The design also considers effects such as fuel density changes, fission gas release, clad creep, and other physical properties which vary with burnup.

The fuel rods are designed for extended burnup operation using the NRC approved Westinghouse extended burnup design methods, models and criteria in References 26, 27, 28, 29, and 33.

An extensive irradiation testing and fuel surveillance operational experience program was being conducted to verify the adequacy of the fuel performance and design bases. This program is discussed in References 6, 24, 26, 29 and 30. Fuel surveillance and testing results, as they become available, are used to improve fuel rod design and manufacturing processes and assure that the design bases and safety criteria are satisfied.

3.2.1.1.2 Fuel Assembly Structure

Structural integrity of the fuel assemblies is assured by setting limits on stresses and deformations due to various loads and by determining that the assemblies do not interfere with the functioning of other components. Three types of loads are considered.

1. Non-operational loads such as those due to shipping and handling,

2. Normal and abnormal loads which are defined for Conditions I and II,

3. Abnormal loads which are defined for Conditions III and IV.

These criteria are applied to the design and evaluation of the top and bottom nozzles, the guide thimbles, the grids and the thimble joints.

The design bases for evaluating the structural integrity of the fuel assemblies are:

1. Non-Operational - 4g axial and 6g lateral loading with dimensional stability,

2. Normal Operation (Condition I) and Incidents of Moderate Frequency (Condition II),

   For the normal operating (Condition I) and upset conditions (Condition II), the fuel assembly component structural design criteria are classified into two material categories, namely, austenitic steels and Zirconium alloys. The stress categories and strength theory presented in the ASME Boiler and Pressure Vessel Code, Section III, are used as a general guide. The maximum shear-theory (Tresca criterion) for combined stresses is used to determine the stress intensities for the austenitic steel components. The stress intensity is defined as the numerically largest difference between the various principal stresses in a three dimensional field. The allowable stress intensity value for austenitic steels, such as nickel-chromium-iron alloys, is given by the lowest of the following:

   a. 1/3 of the specified minimum tensile strength or 2/3 of the specified minimum yield strength at room temperature;

   b. 1/3 of the tensile strength or 90 percent of the yield strength at temperature but not to exceed 2/3 of the specified minimum yield strength at room temperature.

      The stress limits for the austenitic steel components are given below:

      1) General Primary Membrane Stress Intensity limit is 9 S_m

      2) Local Primary Membrane Stress Intensity limit is 1.5 S_m

      3) Primary Membrane plus Bending Stress Intensity limit is 1.5 S_m

      4) Total Primary plus Secondary Stress Intensity limit is 3.0 S_m

   The zircaloy/ZIRLO^{TM} structural components which consist of guide thimble and fuel tubes are in turn subdivided into two categories because of material differences and functional requirements. The fuel tube design criteria is covered separately in Section 3.2.1.3.1. The maximum stress theory is used to evaluate the guide thimble design. The maximum stress theory assumes that yielding due to combined stresses occur where one of the principal stresses are equal to the simple tensive or compressive yield stress. The zircaloy and the ZIRLO^{TM} unirradiated properties are used to define the stress limits.

3. Abnormal loads during Conditions III or IV - worst cases represented by combined seismic and blowdown loads.

   a. Deflections of components cannot interfere with the reactor shutdown or emergency cooling of the fuel rods.

   b. The fuel assembly structural component stresses under faulted conditions are evaluated using primarily the methods outlined in Appendix F of the ASME Boiler and Pressure Vessel Code Section III. Since the current analytical methods utilize elastic analysis, the stress allowables are defined as the smaller value of 2.4 Sm or .70 Su (ultimate tensile strength) for primary membrane and 3.6 Sm or 1.05 Su for primary membrane plus primary bending. For the austenitic steel fuel assembly components, the stress intensity is defined in accordance with the rules described in the previous section for normal operating conditions. For the zircaloy/ZIRLO™ components the stress limits are set at two-thirds of the material yield strength, Su, at reactor operating temperature. This results in zircaloy/ZIRLO™ stress intensity limits being the smaller of 1.6 Sy (0.2% offset yield strength) or .70 Su for primary membrane and 2.4 Sy or 1.5 Su for primary membrane plus bending. For conservative purposes, the zircaloy and the ZIRLO™ unirradiated properties are used to define the stress limits. The grid component strength criteria are based on experimental tests. The grid component strength criterion is based on the lower 95 percent confidence level on the true mean from distribution of grid crush strength data at temperature.

The properties of the fuel assembly and core component materials are given in Reference 24 for Zircaloy-4 and in Reference 26 for ZIRLO™.

3.2.1.2 Design Description

The fuel assembly and fuel rod design data are given in Table 3.3-1.

Each 17 x 17 fuel assembly consists of two hundred and sixty-four fuel rods, twenty-four guide thimble tubes and one instrumentation thimble tube are arranged within a supporting structure. The instrumentation thimble is located in the center position and provides a channel for insertion of an incore neutron detector if the fuel assembly is located in an instrumented core position. The guide thimbles provide channels for insertion of either a rod cluster control assembly, a neutron source assembly, a burnable absorber assembly or a plugging device, depending on the position of the particular fuel assembly in the core. Figure 3.2-1 shows a cross-section of the fuel assembly array, and Figure 3.2-2 shows a fuel assembly full length view. The fuel rods are loaded into the fuel assembly structure so that there is clearance between the fuel rods ends and the top and bottom nozzles.

The VANTAGE 5H fuel assembly design is shown in Figure 3.2-2A. The design changes from the 17 x 17 STD to the VANTAGE 5H design include reduced guide thimble and instrumentation tube diameters and replacement of the six intermediate (mixing vane) Inconel grids with zircaloy grids. The debris filter bottom nozzle (DFBN) design has been incorporated into the VANTAGE 5H fuel assemblies. The DFBN design is similar to the standard bottom nozzle design except that it is thinner and has a new pattern of smaller flow holes. The DFBN helps to minimize passage of debris particles that could cause fretting damage to fuel rod cladding.

The VANTAGE 5H assembly has the same cross-sectional envelope as the 17 X 17 STD fuel assembly. However, the VANTAGE 5H assembly overall length has been increased to accommodate extended burnup.

The VANTAGE+ assembly skeleton is identical to the VANTAGE 5H assembly skeleton except for those modifications necessary to accommodate the intended fuel operation to higher burnups. The modifications consist of the use of ZIRLO® guide thimbles, instrumentation tubes, cladding, and small skeleton dimensional alterations to provide additional fuel assembly and rod growth space at the extended burnup levels. The VANTAGE+ fuel assembly is shorter than the VANTAGE 5H fuel assembly. The grid centerline elevations of the VANTAGE+ are identical to those of the VANTAGE 5H fuel assembly, except for the top, first and second grids. The VANTAGE+ top grid and second grid have been lowered slightly and the first grid has been raised slightly. The first and second grids have been adjusted to stiffen the lower span to reduce the likelihood of grid-to-rod fretting failures, in addition to allowing space for the Protective Bottom Grid. However, since the VANTAGE+ fuel is intended to replace the VANTAGE 5H fuel, the VANTAGE+ exterior assembly envelope is equivalent in design dimensions, and the functional interface with the reactor internals is also equivalent to those of previous Westinghouse fuel designs. Also the VANTAGE+ fuel assembly is designed to be mechanically and hydraulically compatible with the VANTAGE 5H fuel assembly. The same functional requirements and design criteria established for the Westinghouse VANTAGE 5H fuel assembly remains valid for the VANTAGE+ fuel assembly. The VANTAGE+ fuel assembly design is provided in Figure 3.2-2B.

The Robust Fuel Assembly (RFA/RFA-2) design is shown in Figure 3.2-2C. The design changes from the VANTAGE+ to the RFA/RFA-2 design include: modified Low Pressure Drop (LPD) mid-grids, the inclusion of three Intermediate Flow Mixer (IFM) grids, thicker guide thimbles and instrument tube, and Standardized Debris Filter Bottom Nozzle (SDFBN) shown in Figure 3.2-2D. Based on Post Irradiation Examinations (PIE) data on fuel assembly growth with ZIRLO® guide thimbles, the fuel assembly and fuel rod lengths were increased by 0.200 inch relative to the VANTAGE+ design. The mid-grid centerlines are identical to the VANTAGE+ design with the exception of the top grid, which was raised 0.200 inch along with the increase in fuel assembly length of the RFA/RFA-2 design. The RFA/RFA-2 design continues to utilize the protective bottom grid and ZIRLO® or Optimized ZIRLO™ fuel rods and skeleton. The VANTAGE+ and RFA/RFA-2 assembly exterior envelope is equivalent in design dimensions to the STD and VANTAGE 5H assembly. The functional interface with the reactor internals is also equivalent to those of the STD and VANTAGE 5H fuel assembly designs. The VANTAGE+ and RFA/RFA-2 are designed to be mechanically and hydraulically compatible with the STD and VANTAGE 5H, and the same functional requirements and design criteria as previously established for the Westinghouse VANTAGE 5H fuel assembly remain valid for the VANTAGE+ and RFA/RFA-2. The RFA-2 design has an increased contact area between the mid-grid dimples/springs and the fuel rods relative to the RFA design.

Each fuel assembly is installed vertically in the reactor vessel and stands upright on the lower core plate, which is fitted with alignment pins to locate and orient the assembly. After all fuel assemblies are set in place, the upper support structure is installed. Alignment pins, built into the upper core plate, engage and locate the upper ends of the fuel assemblies. The upper core plate then bears downward against the fuel assembly top nozzle via the holddown springs to hold the fuel assemblies in place.

3.2.1.2.1 Fuel Rods

The fuel rods consist of uranium dioxide ceramic pellets contained in slightly cold worked Zircaloy-4 or ZIRLO® tubing, or partially re-crystallized Optimized ZIRLO™ tubing which is plugged and seal welded at the ends to encapsulate the fuel. Schematics of the 17 x 17 STD, VANTAGE 5H, VANTAGE+, and RFA/RFA-2 fuel rods are shown in Figures 3.2-3, 3.2-3A, 3.2-3B, and 3.2-3C. The fuel pellets are right circular cylinders consisting of enriched uranium-dioxide powder which has been compacted by cold pressing and then sintered to the required density. The ends of each pellet are dished slightly to allow greater axial expansion at the center of the pellets. The fuel rods may also contain annular pellets in the upper and lower six inch axial blanket regions which have no dish on the pellet ends, but are hollow for additional gas volume.

The VANTAGE 5H fuel rod is of the same design as the 17 x 17 STD fuel rod except that the VANTAGE 5H fuel rod is longer to provide a longer plenum and bottom end plug. The bottom end plug has an internal grip feature to facilitate rod loading on both designs. The bottom end plug is also longer to provide an improved lead-in for the removable top nozzle reconstitution feature.

The VANTAGE+ fuel rod represents a modification to the VANTAGE 5H fuel rod intended to support operation for fuel clad in place of Zircaloy-4 clad. The ZIRLO® alloy is a zirconium alloy similar to Zircaloy-4 that has been specifically developed to enhance corrosion resistance. The Optimized ZIRLO™ alloy is similar to ZIRLO® with a reduced tin concentration to further enhance the corrosion resistance. The VANTAGE+ fuel rods will contain, as in VANTAGE 5H fuel rod, enriched uranium dioxide fuel pellets and an Integral Fuel Burnable Absorber (IFBA) coating on some of the enriched fuel pellets.

The VANTAGE+ fuel rod has the same clad wall thickness as the VANTAGE 5H design. The VANTAGE+ fuel tube is shorter to provide room for the required fuel rod growth. To offset the reduction in the plenum length, the VANTAGE+ fuel rod has a variable pitch plenum spring. This spring has smaller wire and coil diameters and a shorter free length. The variable pitch plenum spring provides the same support as the regular VANTAGE+ plenum spring but with fewer spring turns which translates to less spring volume. The top end plug on the VANTAGE+ fuel rod has an external grip feature to facilitate fuel rod loading. The VANTAGE+ fuel rod also has an oxide coating at the bottom end of the fuel rod. The extra layer of oxide coating provides additional debris induced rod fretting wear protection.

The RFA fuel rod utilizes the same ZIRLO® or Optimized ZIRLO™ cladding material and clad wall thickness as the VANTAGE+ design. The RFA/RFA-2 fuel rod is longer than the VANTAGE 5H and VANTAGE+ designs but maintains sufficient margin for fuel rod growth. This provides additional plenum length to accommodate fission gas release associated with high burnup. The remaining fuel rod features of the RFA fuel rod are the same as the VANTAGE+ design with the exception of the external gripper feature of the VANTAGE+ top end plug which has been eliminated for the RFA/RFA-2 design to also afford additional plenum volume. The RFA and RFA-2 fuel rod designs are identical. The Optimized ZIRLO™ alloy is similar to ZIRLO® with a reduced tin concentration to further enhance the corrosion resistance.

The Beaver Valley Unit 1 17 x 17 STD, VANTAGE 5H, VANTAGE+, and RFA/RFA-2 fuel may have axial blankets and will use a standardized fuel pellet design.

The standardized fuel pellet design is a refinement to the chamfered pellet design. The standard design helps to improve manufacturability while maintaining or improving performance (e.g., improved pellet chip resistance during manufacturing and handling).

The IFBA coated pellets are identical to the enriched uranium dioxide pellets except for the addition of a thin boron coating on the pellet cylindrical surface. Coated pellets occupy the central portion of the fuel column. The number and pattern of IFBA rods within an assembly may vary depending on specific application. The ends of the enriched coated pellets and enriched uncoated pellets are dished to allow for greater axial expansion at the pellet centerline and void volume for fission gas release. An evaluation and test program for the IFBA design features are given in Section 2.5 of Reference 20.

The axial blanket region is the nominal six inches of the fuel pellets at each end of the fuel rod pellet stack that may be natural, mid-enriched, or fully enriched uranium dioxide. Natural and mid-enriched axial blankets reduce neutron leakage and improve fuel utilization. The axial blanket pellets may be either solid or annular. The annular axial blanket pellets are used to increase the void volume for gas accommodation within the fuel rod. The axial blanket pellets are of the same design as the enriched and IFBA pellet designs except for an increase in length. The length difference in the axial blanket pellets will help prevent accidental mixing with the enriched and IFBA pellets.

To avoid overstressing of the cladding or seal welds, void volume and clearances are provided within the rods to accommodate fission gases released from the fuel, differential thermal expansion between the cladding and the fuel, and fuel density changes during burnup. Shifting of the fuel within the cladding during handling or shipping prior to core loading is prevented by a stainless steel helical spring which bears on top of the fuel. At assembly the pellets are stacked in the cladding to the required fuel height, the spring is then inserted into the top end of the fuel tube and the end plugs pressed into the ends of the tube and welded. All fuel rods are internally pressurized with helium during the welding process in order to minimize compressive clad stresses and creep due to coolant operating pressures. The helium pre-pressurization may be different for each fuel region. Fuel rod pressurization is dependent on the planned fuel burnup as well as other fuel design parameters and fuel characteristics (particularly densification potential).

The cold helium design pressure for current Westinghouse PWR fuel rods is several hundred psi. The precise design pressure values for BVPS-1 fuel regions depend on detailed performance evaluations. Such detailed design information is proprietary to Westinghouse and will not be included in the Updated Final Safety Analysis Report.
The fuel rods are designed such that 1) the internal gas pressure of the lead rod will not exceed the value which causes the fuel-clad diametral gap to increase due to outward cladding creep during steady-state operation, 2) extensive DNB propagation will not occur, 3) the cladding stress-strain limits (Section 3.2.1.1.1) are not exceeded for Condition I and II events, and 4) clad flattening will not occur during the fuel core life.

3.2.1.2.2 Fuel Assembly Structure

The fuel assembly structure consists of a bottom nozzle, top nozzle, guide thimbles and grids, as shown in Figure 3.2-2.

Bottom Nozzle

The bottom nozzle is a box-like structure which serves as a bottom structural element of the fuel assembly and directs the coolant flow distribution to the assembly. The square nozzle is fabricated from type 304 stainless steel and consists of a perforated plate and four angle legs with bearing plates as shown in Figures 3.2-2A and 3.2-2B. The legs form a plenum for the inlet coolant flow to the fuel assembly. The plate itself acts to prevent a downward ejection of the fuel rods from their fuel assembly. The bottom nozzle is fastened to the fuel assembly guide tubes by locking cup or weld-locked screws which penetrate through the nozzle and mate with an inside fitting in each guide tube.

The Debris Filter Bottom nozzle (DFBN) design has been introduced into the Beaver Valley Unit 1 Region 10 fuel assemblies to help reduce the possibility of fuel rod damage due to debris-induced fretting. The 304 stainless steel DFBN is similar to the conventional bottom nozzle design used previously for Beaver Valley. However, the DFBN design incorporates a modified flow hole size and pattern (described below) and a decreased nozzle height and thinner top plate to accommodate the high burnup fuel rods. The DFBN retains the design reconstitution feature that facilitates easy removal of the nozzle from the fuel assembly.

The relatively large flow holes in a conventional bottom nozzle are replaced with a new pattern of smaller flow holes in the DFBN. The holes are sized to minimize passage of debris particles large enough to cause damage. The hole sizing was also designed to provide sufficient flow area, comparable pressure drop, and continued structural integrity of the nozzle. Tests to measure pressure drop and demonstrate structural integrity have been performed to verify that the DFBN is totally compatible with the current design.

Coolant flow through the fuel assembly is directed from the plenum in the bottom nozzle upward through the penetrations in the plate to the channels between the fuel rods. The penetrations in the plate are positioned between the rows of the fuel rods.

Axial loads (holddown) imposed on the fuel assembly and the weight of the fuel assembly are transmitted through the bottom nozzle to the lower core plate. Indexing and positioning of the fuel assembly is controlled by alignment holes in two diagonally opposite bearing plates which mate with locating pins in the lower core plate. Any lateral loads on the fuel assembly are transmitted to the lower core plate through the locating pins.

Westinghouse has developed the Standardized Debris Filter Bottom Nozzle (SDFBN) for 17x17 fuel which is designed to have a loss coefficient that is independent of the nozzle sub-supplier and varies less from nozzle to nozzle within each sub-supplier. The SDFBN (as shown in Figure 3.2-2D) has the same nominal loss coefficient as the DFBN and has been introduced into the Beaver Valley Unit 1 Region 24 fuel assemblies. The SDFBN has eliminated the side skirt communication flow holes as a means of improving the debris mitigation performance of the bottom nozzle. This nozzle has been extensively evaluated and analyzed and it was demonstrated that it meets all of the applicable mechanical design criteria.

Top Nozzle

The top nozzle assembly functions as the upper structural element of the fuel assembly in addition to providing a partial protective housing for the rod cluster control assembly or other components. It consists of an adapter plate, enclosure, top plate, and pads. The integral welded assembly has holddown springs mounted on the assembly as shown in Figure 3.2-2.

The springs and bolts are made of Inconel 718 and Inconel 600 respectively, whereas other components are made of type 304 stainless steel.

Beginning with Beaver Valley Unit 1 Cycle 15, the top nozzle assembly utilizes a composite (cast) design. The top nozzle holddown spring screws are made of Inconel-718 and bead-blasted (shot peened) in the shank-to-thread area of the spring screw to inhibit initiation and propagation of Primary Water Stress Corrosion Cracking (PWSCC). The nozzle adapter plate, thimble holes and flow hole pattern remain unchanged, thus there is no impact on flow conditions.

The reconstitutable top nozzle for the VANTAGE 5H, VANTAGE+, and RFA/RFA-2 fuel assemblies differ from the conventional design in two ways: a groove is provided in each thimble through hole in the nozzle plate to facilitate attachment and removal, and the nozzle plated thickness is reduced to provide additional axial space for fuel rod growth.

In the VANTAGE 5H, VANTAGE+, and RFA/RFA-2 reconstitutable top nozzle design (including the WIN), a stainless steel nozzle insert is mechanically connected to the top nozzle adapter plate by means of a preformed circumferential bulge near the top of the insert. The insert engages a mating groove in the wall of the adapter plate thimble tube through hole. The insert has four equally spaced axial slots that allow the insert to deflect inwardly at the elevation of the bulge, thus permitting the installation or removal of the nozzle. The insert bulge is positively held in the adapter plate mating groove by placing a lock tube with a uniform ID identical to that of the thimble tube into the insert.

To remove the top nozzle, a tool is first inserted through the lock tube and expanded radially to engage the bottom edge of the tube. An axial force is then exerted on the tool that overrides the local lock tube deformations and withdraws the lock tube from the insert. After the lock tubes have been withdrawn, the nozzle is removed by raising it off the upper slotted ends of the nozzle inserts which deflect inwardly under the axial lift load. With the top nozzle removed, direct access is provided for fuel rod examination or replacement. Reconstitution is completed by the remounting of the nozzle and the insertion of new lock tubes. The design bases and evaluation of the reconstitutable top nozzle are given in Section 2.3.2 of Reference 20.

The adapter plate is provided with round penetrations and semicircular ended slots to permit the flow of coolant upward through the top nozzle. Other round holes are provided to accept sleeves which are welded to tubes. The ligaments in the plate cover the tops of the fuel rods and prevent their upward ejection from the fuel assembly. The enclosure is a sheet metal shroud which sets the distance between the adapter plate and the top plate. The top plate has a large square hole in the center to permit access for the control rods and the control rod spiders. Holddown springs are mounted on the top plate and are fastened in place by bolts and clamps located at two diagonally opposite corners. On the other two corners integral pads are positioned which contain alignment holes for locating the upper end of the fuel assembly.

The WIN design, while similar to the RTN, incorporates design and manufacturing improvements to eliminate the Alloy 718 spring screw for attachment of the holddown springs. In the WIN nozzle, the springs are assembled into the nozzle pad and pinned in place. The WIN design provides a wedged rather than a clamped (bolted) joint for transfer of the fuel assembly holddown forces into the top nozzle structure. Integral pads which contain alignment holes for locating the upper end of the fuel assembly are positioned on the other two corners for the WIN. The flow plate, thermal characteristics, method of attachment of the top nozzle, and handling of the fuel assembly are all unchanged from the RTN top nozzle design.

Guide and Instrument Thimbles

The guide thimbles are structural members which also provide channels for the neutron absorber rods, burnable absorber rods or neutron source assemblies. Each one is fabricated from Zircaloy-4 or ZIRLO™ tubing having two different diameters. The larger diameter at the top provides a relatively large annular area to permit rapid insertion of the control rods during a reactor trip as well as to accommodate the flow of coolant during normal operation. Four holes are provided on the thimble tube above the dashpot to reduce the rod drop time. The lower portion of the guide thimbles has a reduced diameter to produce a dashpot action and to accommodate the outflow of water from the dashpot during a reactor trip. The dashpot is closed

at the bottom by means of an end plug which is provided with a small flow port to avoid fluid stagnation in the dashpot volume during normal operation. The top end of the guide thimble is fastened to a tubular sleeve by three expansion swages. The sleeve fits into and is welded to the top nozzle adapter plate. The lower end of the guide thimble is fitted with an end plug which is then fastened into the bottom nozzle by a locking cup or weld-locked screw.

The central instrumentation thimble of each fuel assembly is not attached to either the top or bottom nozzles, but the thimble is constrained by its seating in counterbores of each nozzle. The thimbles internal diameter does not vary, and in-core neutron detectors pass through the bottom nozzle's large counterbore into the center thimble.

With the exception of a reduction in the guide thimble diameter and increased length above the dashpot, the VANTAGE 5H or VANTAGE+ guide thimbles are identical to those in the 17 x 17 STD design. A reduction in the guide thimble outside and inside diameters is required due to the thicker zircaloy or ZIRLO™ grid straps. The VANTAGE 5H or VANTAGE+ guide thimble tube ID provides adequate clearance for the control rods. The reduced VANTAGE 5H or VANTAGE+ thimble tube also provides sufficient diametral clearance for burnable absorber rods, source rods, and dually compatible thimble plugs. The thimble plugs used before Region 10 are not the dually compatible type and cannot be inserted into the VANTAGE 5H or VANTAGE+ guide thimbles.

The VANTAGE 5H or VANTAGE+ instrumentation tube diameter has also been decreased relative to the 17 x 17 STD assembly instrumentation tube. This decrease still allows sufficient diametral clearance for the flux thimble to traverse the tube without binding.

The RFA/RFA-2 design features include a thicker wall guide thimble tube and thicker wall instrumentation tube relative to the VANTAGE 5H and VANTAGE+ designs. The wall thickness increase was obtained by increasing the outside diameter while maintaining the same inside diameter for control rod insertions. The ZIRLO™ mid and IFM grids had the grid cells with the guide thimble or instrument tube locations embossed (radial) to accommodate the thicker guide thimble and instrument tube. The guide thimble and instrument tube wall thickness is increased by approximately 25% to improve stiffness and mitigate Incomplete Rod Insertion (IRI).

The top Inconel grid sleeve, insert, and thimble of the VANTAGE 5H, VANTAGE+, or RFA/RFA-2 design are joined together using three bulge joint mechanical attachments similar to that used in the 17 x 17 STD design. This bulge joint connection was mechanically tested and was found to meet all applicable design criteria.

The intermediate zircaloy/ZIRLO™ grids of the VANTAGE 5H, VANTAGE+, or RFA/RFA-2 design employ a single bulge connection to the sleeve and thimble as compared to a double bulge connection used in the Inconel grids. Mechanical testing of this bulge joint connection showed that it meets all applicable design criteria.

Grid Assemblies

The fuel rods, as shown in Figure 3.2-2, are supported laterally at intervals along their length by grid assemblies which maintain the lateral spacing between the rods throughout the design life of the assembly. Each fuel rod is afforded lateral support at six contact points within each grid by the combination of support dimples and springs. The grid assembly consists of individual slotted straps interlocked and brazed in an "egg-crate" arrangement to join the straps permanently at their points of intersection. The straps contain spring fingers, support dimples and mixing vanes.

The magnitude of the grid restraining force on the fuel rod is set high enough to minimize possible fretting, without overstressing the cladding at the points of contact between the grids and fuel rods. The grid assemblies also allow axial thermal expansion of the fuel rods without imposing restraint sufficient to develop buckling or distortion of the fuel rods.

Up to four types of grid types are used in each fuel assembly: mid-grids (structural grids with flow mixing vanes), Intermediate Flow Mixing (IFM) grids (non-structural with flow mixing vanes), top and bottom structural grids without mixing vanes, and the protective grid. The flow mixing vanes project from the edge of the inner grid strap into the coolant stream to promote mixing of the coolant in the high heat flux region of the fuel assembly. The top and bottom structural grids do not contain mixing vanes on the internal straps. The outside straps on all grids contain mixing vanes which, in addition to their mixing function, aid in guiding the grids and fuel assembly past projecting surfaces during fuel handling and loading/unloading the core.

The top and bottom Inconel (non-mixing vane) grids of the LOPAR, V5H, VANTAGE+, and RFA/RFA-2 assemblies are nearly identical in design. The only differences are: 1) V5H, VANTAGE+, and RFA/RFA-2 interactions during core loading/unloading, 2) V5H, VANTAGE+, and RFA/RFA-2 top and bottom grids have dimples which are rotated 90 degrees to minimize fuel rod fretting and dimple cocking, 3) V5H, VANTAGE+, and RFA/RFA-2 top and bottom grid heights have been increased to 1.522 inches, 4) the V5H, VANTAGE+, and RFA/RFA-2 top grid spring force has been reduced to minimize rod bow, and 5) the V5H, VANTAGE+, and RFA/RFA-2 top grid uses 304L stainless steel sleeves.

The six mid structural (mixing vane) grids are made of zircaloy or ZIRLO™ material rather than Inconel which was used in the LOPAR design. These V5H grids (known as the VANTAGE 5H zircaloy grid), and VANTAGE+ and RFA/RFA-2 grids (known as ZIRLO™ grids) are designed to give the same pressure drop as the Inconel grid. Relative to the Inconel grid, the V5H zircaloy, VANTAGE+ and RFA/RFA-2 ZIRLO™ grid strap thickness and strap height are increased for structural performance. In addition to the snag-resistant design noted above, the upstream strap edges of the V5H zircaloy, and VANTAGE+ and RFA/RFA-2 ZIRLO™ grids are chamfered and a diagonal grid spring is employed to reduce pressure drop. The V5H zircaloy grids, and VANTAGE+ and RFA/RFA-2 ZIRLO™ grids incorporate the same grid cell support configuration as the Inconel grids (six support locations per cell: four dimples and two springs). The zircaloy and ZIRLO™ grid interlocking strap joints and grid/sleeve joints are fabricated by laser welding, whereas the Inconel grid joints are brazed. The RFA-2 design has an increased contact area between the mid-grid dimples/springs and the fuel rods relative to the RFA design. The increased contact area is intended to further reduce fretting wear.

The V5H zircaloy, and VANTAGE+ and RFA/RFA-2 ZIRLO™ mid structural grid have superior dynamic structural performance relative to the inconel grid. Structural testing was performed and analyses have shown the V5H zircaloy grid and ZIRLO™ grid seismic/LOCA load margin is superior to that of the Inconel grid.

The RFA/RFA-2 fuel assembly design incorporates three ZIRLO™ Intermediate Flow Mixing (IFM) grids positioned at the mid-spans of the four uppermost mid-grids to further increase the flow turbulence in the axial zone where departure from nucleate boiling (DNB) is limiting. Each IFM grid cell contains four dimples, which are designed to prevent mid-span channel closure in the spans containing IFMs and fuel contact with the mixing vanes. For the RFA/RFA-2 design, the modified low pressure drop mid-grids and IFM grids are embossed to accept the larger diameter guide thimble tubes and instrument tube. An additional feature incorporated in the Mid-Grid and IFM Grid designs is the Low Strain Radius which is designed to lower the strain imposed on the formed features and improve manufacturability.

The RFA/RFA-2 fuel assembly design also incorporates an Inconel protective grid. The protective grid is a partial height grid similar in configuration to the IFM grid but without mixing vanes. It is located between the bottom Inconel grid and the bottom nozzle, nearly on the surface of the bottom nozzle. The intersections of the inner straps of the protective grid align with the flow holes of the Debris Filter Bottom Nozzle (DFBN), effectively bisecting the flow path through the flow hole into four quarters. This provides an effective barrier against small debris. To reduce fatigue failures and failures due to stress corrosion cracking within the rod support dimples of the protective grid, Westinghouse developed the Robust Protective Grid (RPG). The RPG implements design changes such as increasing the maximum nominal height of the grid, increasing the ligament length and the radii of the ligament cutouts, and the use of four additional spacers to help support the grid. The nominal height of the grid was increased to allow “V-notch” window cutouts to help minimize flow-induced vibration caused by vortex shedding at the trailing edge of the inner grid straps. In conjunction with the protective grid, the fuel rod bottom end plug is changed to a longer design such that the portion of the fuel rod engaged in the protective grid and extending up past the top of the protective grid is solid end plug material. This provides a protective zone where trapped debris cannot fret through the fuel rod and cause failure. The hydraulic effects of the protective grid are minimized by positioning the fuel rods 0.085 inches above the bottom nozzle. The combination of lowered fuel rod position and the longer fuel rod end plug results in no change to the axial fuel stack height from the previous VANTAGE+ design.

3.2.1.3 Design Evaluation

3.2.1.3.1 Fuel Rods

The fuel rods are designed to assure the design bases are satisfied for Condition I and II events. This assures that the fuel performance and safety criteria (Section 3.2) are satisfied.

Materials - Fuel Cladding

The desired fuel rod cladding is a material which has a superior combination of neutron economy (low absorption cross section), high strength (to resist deformation due to differential pressures and mechanical interaction between fuel and clad), high corrosion resistance (to coolant, fuel and fission products), and high reliability. Zircaloy-4, ZIRLO® and Optimized ZIRLO™ have this desired combination of cladding properties. As shown in Reference 8, there is considerable PWR operating experience on the capability of zircaloy and ZIRLO® as cladding material. Clad hydriding has not been a significant cause of clad perforation since current controls on fuel contained moisture levels were instituted.[8]

Metallographic examination of irradiated commercial fuel rods have shown occurrences of fuel/clad chemical interaction. Reaction layers of < 1 mil in thickness have been observed between fuel and clad at limited points around the circumference. Westinghouse metallographic data indicates that this interface layer remains very thin even at high burnup. Thus, there is no indication of propagation of the layer and eventual clad penetration.

Stress corrosion cracking is another phenomenon related to fuel/clad chemical interaction. Out-of-reactor tests as well as operational experience have shown that in the presence of high clad tensile stresses, large concentrations of iodine will chemically attack the zircaloy tubing and can lead to eventual clad cracking.

Materials - Fuel Pellets

Sintered, high density uranium dioxide fuel reacts only slightly with the cladding, at core operating temperatures and pressures. In the event of cladding defects, the high resistance of uranium dioxide to attack by water protects against fuel deterioration although limited fuel erosion can occur. As has been shown by operating experience and extensive experimental work, the thermal design parameters conservatively account for changes in the thermal performance of the fuel elements due to pellet fracture which may occur during power operation. The consequences of defects in the cladding are greatly reduced by the ability of uranium dioxide to retain fission products including those which are gaseous or highly volatile.

Observations from several operating Westinghouse PWR's has shown that fuel pellets can densify under irradiation to a density higher than the manufactured values.[6][8] Fuel densification and subsequent incomplete settling of the fuel pellets results in local and distributed gaps in the fuel rods.

An extensive analytical and experimental effort[9] was performed by Westinghouse in 1973 to characterize the fuel densification phenomenon and identify improvements in pellet manufacturing to eliminate or minimize this anomaly (see Section 1.5).

Fuel rod design methodology has been introduced that reduces the densification power spike factor to 1.0 and Reference 30 demonstrates that clad flattening will not occur in Westinghouse fuel designs.

Materials - Strength Considerations

One of the most important limiting factors in fuel element duty is the mechanical interaction of fuel and cladding. This fuel-cladding interaction produces cyclic stresses and strains in the cladding, and these in turn consume cladding fatigue life. The reduction of fuel-cladding interaction is therefore a principal goal of design. In order to achieve this goal and to enhance the cyclic operational capability of the fuel rod, the technology for using pre-pressurized fuel rods in Westinghouse PWR's has been developed.

Initially the gap between the fuel and cladding is sufficient to prevent hard contact between the two. However, during power operation a gradual compressive creep of the cladding onto the fuel pellet occurs due to the external pressure exerted on the rod by the coolant. Cladding compressive creep eventually results in hard fuel-cladding contact, changes in power level could result in significant changes in cladding stresses and strains. By using pre-pressurized fuel rods to partially offset the effect of the coolant external pressure, the rate of cladding-creep toward the surface of the fuel is reduced. Fuel rod pre-pressurization delays the time at which substantial fuel-cladding interaction and hard contact occur and hence significantly reduces the number and extent of cyclic stresses and strains experienced by the cladding both before and after fuel-cladding contact. These factors result in an increase in the fatigue life margin of the cladding and lead to greater cladding reliability. If gaps should form in the fuel stacks, clad flattening will be prevented by the rod pre-pressurization so that the flattening time will be greater than the fuel core life.

A two-dimensional (r,θ) finite element model has been developed to investigate the effects of radial pellet cracks on stress concentrations in the clad. Stress concentrations, herein, are defined as the difference between the maximum clad stress in the θ-direction and the mean clad stress. The first case has the fuel and clad in mechanical equilibrium, and, as a result, the stress in the clad is close to zero. In subsequent cases, the pellet power is increased in steps and the resultant fuel thermal expansion imposes tensile stress in the clad. In addition to uniform clad stresses, stress concentrations develop in the clad adjacent to radial cracks in the pellet. These radial cracks have a tendency to open during a power increase, but the frictional forces between fuel and clad oppose the opening of these cracks and result in localized increases in clad stress. As the power is further increased, large tensile stresses exceed the ultimate tensile strength of UO_2 and additional cracks in the fuel are created which limit the magnitude of the stress concentration in the clad. As part of the standard fuel rod design analysis, the maximum stress concentration evaluated from finite element calculations is added to the volume averaged effective stress in the clad as determined from one-dimensional stress/strain calculations. The resultant clad stress is then compared to the temperature dependent zircaloy / ZIRLO® / Optimized ZIRLO™ yield stress in order to assure that the stress/strain criteria are satisfied.

Steady State Performance Evaluation

In the calculation of the steady-state performance of a nuclear fuel rod, the following interacting factors must be considered:

1. Clad creep and elastic deflection

2. Pellet density changes, thermal expansion, gas release, and thermal properties as a function of temperature and fuel burnup

3. Internal pressure as a function of fission gas release, rod geometry, and temperature distribution.

These effects are evaluated using an overall fuel rod design model[28,26,33]. The model modifications for time dependent fuel densification are given in Reference 30. With these interacting factors considered, the model determines the fuel rod performance characteristics for a given rod geometry, power history, and axial power shape. In particular, internal gas pressure, fuel and cladding temperatures, and cladding deflections are calculated. The fuel rod is divided lengthwise into several sections and radially into a number of annular zones. Fuel density changes, cladding stresses, strains and deformations, and fission gas releases are calculated separately for each segment. The effects are integrated to obtain the internal rod pressure.

The initial rod internal pressure is selected to delay fuel/clad mechanical interaction and to avoid the potential for flattened rod formation. It is limited, however, by the rod internal pressure design basis given in Section 3.2.1.1.1. The plenum height of the fuel rod has been designed to ensure that the maximum internal pressure of the fuel rod will not exceed the value which would cause the fuel clad diametral gap to increase during steady-state operation.

The gap conductance between the pellet surface and the cladding inner diameter is calculated as a function of the composition, temperature, and pressure of the gas mixture, and the gap size or contact pressure between clad and pellet. After computing the fuel temperature for each pellet annular zone, the fractional fission gas release is calculated based on local temperature and burnup. The total amount of gas released is based on the average fractional release within each axial and radial zone and the gas generation rate which in turn is a function of burnup. Finally, the gas released is summed over all zones and the pressure is calculated.

The model shows good agreement in fit for a variety of published and proprietary data on fission gas release, fuel temperatures and clad deflection.[28,33] Included in this spectrum are variations in power, time, fuel density, and geometry. The in-pile fuel temperature measurement comparisons used are referenced in Section 3.4.2.2.

Initially, the gap between the fuel and clad is sufficient to prevent hard contact between the two. However, during power operation, a gradual compressive creep of the clad onto the fuel pellet occurs due to the external pressure exerted on the rod by the reactor coolant. Clad compressive creep eventually results in the fuel/clad contact. Once fuel/clad contact occurs, changes in power level result in changes in clad stresses and strains. By using prepressurized fuel rods to partially offset the effect of the reactor coolant external pressure, the rate of clad creep toward the surface of the fuel is reduced. Fuel rod prepressurization delays the time at which fuel/clad interaction and contact occurs, and significantly reduces the number and extent of cyclic stresses and strains experienced by the clad both before and after fuel/clad contact. These factors result in an increase in the fatigue life margin of the clad and lead to greater clad reliability. If gas should form in the fuel stacks, clad flattening will be prevented by the rod prepressurization so that the flattening time will be greater than the fuel core life.

Typical fuel clad inner diameter and the fuel pellet outer diameter as a function of exposure are presented in Figure 3.2-4.

The cycle-to-cycle changes in the pellet outer diameter represent the effects of power changes as the fuel is moved into different positions as a result of refueling. The gap size at any time is merely the difference between clad inner diameter and pellet outer diameter. The figure represents hot fuel dimensions for a fuel rod operating at the power level shown in Figure 3.2-5. Figure 3.2-5 illustrates representative fuel rod internal gas pressure and linear power for the lead burnup rod vs. irradiation time. The "best estimate" fission gas release model was used in determining the internal gas pressures as a function of irradiation time.

The clad stresses at a constant local fuel rod power are low. Compressive stresses are created by the pressure differential between the coolant pressure and the rod internal gas pressure.

Tensile stresses could be created once the clad has come in contact with the pellet. These stresses would be induced by the fuel pellet swelling during irradiation. As shown in Figure 3.2-4, there is very limited clad pushout after pellet-clad contact. Fuel swelling can result in small clad strains (<1 percent) for expected discharge burnups but the associated clad stresses are very low because of clad creep (thermal and irradiation-induced creep). Furthermore, the 1 percent strain criterion is extremely conservative for fuel-swelling driven clad strain because the strain rate associated with solid fission products swelling is very slow ($\sim 5 \times 10^{-7}$ hr^{-1}). In-pile experiments[10] have shown that zircaloy tubing exhibits "super-plasticity" at slow strain rates during neutron irradiation. Uniform clad strains of >10 percent have been achieved under these conditions with no sign of plastic instability.

Transient Evaluation Method

Pellet thermal expansion due to power increases is considered the only mechanism by which significant stresses and strains can be imposed on the clad. Power increases in commercial reactors can result from fuel shuffling, reactor power escalation following extended reduced power operation, and control rod movement. In the mechanical design model, lead rods are depleted using best estimate power histories as determined by core physics calculations. During the depletion, the amount of diametral gap closure is evaluated based upon the pellet expansion-cracking model, clad creep model, and fuel swelling model. At various times during the depletion the power is increased locally on the rod to the burnup dependent attainable power density as determined by core physics calculations. The radial, tangential, and axial clad stresses resulting from the power increases are combined into a volume average effective clad stress.

The von Mises criterion is used to evaluate if the clad yield stress has been exceeded. This criterion states that an isotropic material in multiaxial stress will begin to yield plastically when the effective stress exceeds the yield stress as determined by a uniaxial tensile test. The yield stress correlation is that for irradiated cladding since fuel/clad interaction occurs at high burnup. Furthermore, the effective stress is increased by an allowance, which accounts for stress concentrations in the clad adjacent to radial cracks in the pellet, prior to the comparison with the yield stress. This allowance was evaluated using a two-dimensional (r,θ) finite element model. Slow transient power increases can result in large clad strains without exceeding the clad yield stress because of clad creep and stress relaxation. Therefore, in addition to the yield stress criterion, a criterion on allowable clad positive strain is necessary. Based upon high strain rate burst and tensile test data on irradiated tubing, 1% strain was determined to be the lower limit on irradiated clad ductility and thus adopted as a design criterion.

In addition to the mechanical design models and design criteria, Westinghouse relies on performance data accumulated through transient power test programs in experimental and commercial reactors, and through normal operation in commercial reactors.

It is recognized that a possible limitation to the satisfactory behavior of the fuel rods in a reactor which is subjected to daily load follow is the failure of the cladding by low cycle strain fatigue. During their normal residence time in reactor, the fuel rods may be subjected to 1,000 cycles with typical changes in power level from 50 to 100% of their steady-state values.

The assessment of the fatigue life of the fuel rod cladding is subjected to a considerable uncertainty due to the difficulty of evaluating the strain range which results from the cyclic interaction of the fuel pellets and claddings. This difficulty arises, for example, from such highly unpredictable phenomena as pellet cracking, fragmentation, and relocation. Nevertheless, since early 1968, Westinghouse has been investigating this particular phenomenon both analytically and experimentally. Strain fatigue tests on irradiated and nonirradiated hydrided Zircaloy-4 claddings were performed which permitted a definition of a conservative fatigue life limit and recommendation of a methodology to treat the strain fatigue evaluation of the Westinghouse reference fuel rod designs.

However, Westinghouse is convinced that the final proof of the adequacy of a given fuel rod design to meet the load follow requirements can only come from in-pile experiments performed on actual reactors. The Westinghouse experience in load follow operation dates back to early 1970 with the load follow operation of the Saxton reactor. More recently, successful load follow operation has been performed on reactor A (300 load follow cycles) and reactor B (150 load follow cycles). In both cases, there was no significant coolant activity increase that could be associated with the load follow mode of operation. Reference 31 provides the most recent experience with Westinghouse fuel designs.

The following paragraphs present briefly the Westinghouse analytical approach to strain fatigue.

A comprehensive review of the available strain-fatigue models was conducted by Westinghouse as early as 1968. This included the Langer-O'Donnel model, the Yao-Munse model, and the Manson-Halford model. Upon completion of this review and using the results of the Westinghouse experimental programs discussed below, it was concluded that the approach defined by Langer-O'Donnel would be retained and the empirical factors of their correlation modified in order to conservatively bound the results of the Westinghouse testing program.[12]

The Langer-O'Donnel empirical correlation has the following form:

$$Sa = \frac{E}{4\sqrt{N_f}} \text{ Ln } \left\{\frac{100}{100 - RA}\right\} + S_e \qquad (3.2\text{-}1)$$

Where: Sa = 1/2 E

$\Delta\varepsilon_t$ = pseudo - stress amplitude which causes failure in N_t cycles (lb/in^2)

$\Delta\varepsilon_t$ = total strain range (in/in)

E = Young's Modulus (lb/in^2)

N_f = number of cycles to failure

RA = reduction in area at fracture in an uniaxial tensile test (%)

S_e = endurance limit (lb/in^2)

Both RA and S_e are material constants which depend on the type of material, the temperature and the irradiation. The Westinghouse testing program was subdivided in the following sub-programs:

1. A rotating bend fatigue experiment on unirradiated Zircaloy-4 specimens at room temperature and at 725°F. Both hydrided and non-hydrided Zircaloy-4 cladding were tested.

2. A biaxial fatigue experiment in gas autoclave on unirradiated Zircaloy-4 cladding both hydrided and non-hydrided.

3. A fatigue test program on irradiated cladding from the CVTR and Yankee Core V conducted at Battelle Memorial Institute.

The results of these test programs provided information on different cladding conditions including the effect of irradiation, of hydrogen level, and of temperature.

The Westinghouse design equations followed the concept for the fatigue design criterion according to Section 3 of the ASME Boiler and Pressure Vessel code. Namely:

1. The calculated pseudo-stress amplitude (S_a) has to be multiplied by a factor of 2 in order to obtain the allowable number of cycles (N_f).

2. The allowable cycles for a given Sa is 5% of N_f, or a safety factor of 20 on cycles.

The lesser of the two allowable number cycles is selected. The cumulative fatigue life fraction is then computed as:

$$\sum_{\text{all } k} \frac{n_k}{N_{f,k}} \leq 1 \qquad (3.2\text{-}2)$$

Where: n_k = number of diurnal cycles of mode k.

The potential effects of operation with waterlogged fuel are discussed in Section 3.4.3.6. Waterlogging is not considered to be a concern during operational transients.

3.2.1.3.2 Fuel Assembly Structure

Stresses and Deflections

The potential sources of high stresses in the assembly are avoided by the design. For example, stresses in the fuel rod due to thermal expansion and zircaloy/ZIRLO™ irradiation growth are limited by the relative motion of the rod as it slips over the grid spring and dimple surfaces. Clearances between the fuel rod ends and nozzles are provided so that zircaloy/ZIRLO™ irradiation growth will not result in end interferences. As another example, stresses due to holddown springs in opposition to the hydraulic lift force are limited by the deflection characteristic of the springs. Stresses in the fuel assembly caused by tripping of the rod cluster control assembly have little influence on fatigue because of the small number of events during the life of an assembly. Welded joints in the fuel assembly structure are considered in the structural analysis of the assembly. Appropriate material properties of welds are used to insure the design bases are met.

Assembly components and prototype fuel assemblies made from production parts were subjected to structural tests to verify that the design bases requirements are met (see Section 1.5).

The fuel assembly design loads for shipping have been established at 6 g. Probes are permanently placed into the shipping cask to monitor and detect fuel assembly displacements that would result from loads in excess of the criteria. Past history and experience has indicated that loads which exceeded the allowable limits rarely occur. Exceeding the limits requires reinspection of the fuel assembly for damage. Tests on various fuel assembly components such as the grid assembly, sleeves, inserts and structure joints have been performed to assure that the shipping design limits do not result in impairment of fuel assembly function.

Seismic analysis of the fuel assembly is presented in Reference 14.

Dimensional Stability

A prototype fuel assembly was subjected to column loads in excess of those expected in normal service and faulted conditions (see Section 1.5).

The coolant flow channels are established and maintained by the structure composed of grids and guide thimbles. The lateral spacing between fuel rods is provided and controlled by the support dimples of adjacent grid cells. Contact of the fuel rods on the dimples is assured by the clamping force provided by the grid springs. Lateral motion of the fuel rods is opposed by the spring force and the internal moments generated between the spring and the support dimples. Grid testing is discussed in Section 1.5.

No interference with control rod insertion into thimble tubes will occur during a postulated LOCA transient due to fuel rod swelling, thermal expansion, or bowing. In the early phase of the transient following the coolant break the high axial loads which potentially could be generated by the difference in thermal expansion between fuel clad and thimbles are relieved by slippage of the fuel rods thru the grids. The relatively low drag force restraint on the fuel rods will only induce minor thermal bowing not sufficient to close the fuel rod-to-thimble tube gap. This rod-to-grid slip mechanism occurs simultaneously with control rod drop. Subsequent to the control rod insertion the transient temperature increase of the fuel rod clad can result in swelling sufficient to contact the thimbles.

Vibration and Wear

The effect of a flow induced vibration on the fuel assembly and individual fuel rods is minimal. The cyclic stress range associated with deflections of such small magnitude is insignificant and has no effect on the structural integrity of the fuel rod. This conclusion is based on test results and analysis documented in the Hydraulic Flow Test of the 17 x 17 Fuel Assembly report[13] which takes into consideration the conditions normally encountered in reactor operation.

The high cross flows which produced the fuel rod failures in the Jose de Cabrera plant were the result of a baffle leakage problem. To alleviate the problem in Jose de Cabrera, a baffle repair operation was instituted during the 1972 refueling. The success of the repair was confirmed by the absence of failed rods at the baffle locations as verified by inspection during the 1973 refueling.

The reaction on the grid support due to vibration motions is also correspondingly small and definitely much less than the spring preload. Firm contact is therefore maintained. No significant wear of the cladding or grid supports is expected during the life of the fuel assembly, as described in the following section.

3.2.1.3.3 Operational Experience

A discussion of recent fuel operating experience is given in Reference 31.

3.2.1.3.4 High Power Fuel Rod Development

Note: This section was current as of 1973 and has not been updated. It is retained in the Updated FSAR for historical understanding.

A high power fuel test program completed in 1974 defined failure limits for the combined effects of linear heat generation rate and burnup, providing increased assurance that operating plants have an adequate performance and design margin to failure threshold, and verified the adequacy of design methods and computer codes in use during the design of BVPS #1.

3.2.1.4 Tests and Inspections

3.2.1.4.1 Quality Assurance Program

The Quality Assurance Program Plan of the Westinghouse Nuclear Fuel Division, as summarized in Reference 7 and Appendix A, has been developed to serve the division in planning and monitoring its activities for the design and manufacture of nuclear fuel assemblies and associated components.

The program provides for control over all activities affecting product quality, commencing with design and development and continuing through procurement, materials handling, fabrication, testing and inspection, storage, and transportation. The program also provides for the indoctrination and training of personnel and for the auditing of activities affecting product quality through a formal auditing program.

3.2.1.4.2 Manufacturing

Quality Control philosophy is generally based on the following inspections being performed to a 95% confidence that at least 95% of the product meets specification, unless otherwise noted, using either a hypergeometric function with zero defectives for small lots or the latest revision of Mil-105D for large lots. This confidence level has been based on past experience gained during the manufacturing of uranium cores. The following inspections are included.

Component Parts

All parts received are inspected to a 95 x 95 confidence level. The characteristics inspected depend upon the component parts and include dimensional, visual, check audits of test reports, material certification and nondestructive testing such as X-ray and ultrasonic. Westinghouse materials process and components specifications specify in detail the inspection to be performed.

All material used in the manufacture of this core is accepted and released by Quality Control.

Pellets

Inspection is performed to a 95 x 95 confidence level for the dimensional characteristics such as diameter and density. Additional visual inspections are performed for cracks, chips and porosity according to standards established at the beginning of production. These standards are based upon standards used in previous cores which have in turn served as standards for over 125 million pellets manufactured and used in operating cores. Density is determined in terms of weight per unit length and is plotted on zone charts used in controlling the process. Chemical analyses are taken on a daily sample basis throughout pellet production.

Rod Inspection

Fuel rod, control rod, burnable poison, and secondary source rod inspection consists of the following nondestructive examination techniques and methods, as applicable.

1. LEAK TESTING: Each rod is tested, using a calibrated mass spectrometer, with helium being the detectable gas.

2. ENCLOSURE WELDS: Rod welds are inspected by ultrasonic test or X-ray in accordance with a qualified technique and Westinghouse specification.

3. DIMENSIONAL: All rods are dimensionally inspected prior to final release. The requirements include such items as length, camber, and visual appearance.

4. PLENUM DIMENSIONS: All fuel rods are inspected by gamma scanning or other approved methods to ensure proper plenum dimensions.

5. PELLET-TO-PELLET GAPS: All fuel rods are inspected by gamma scanning or other approved methods to ensure that no significant gaps exist between pellets.

6. GAMMA SCANNING: All fuel rods are active gamma scanned to verify enrichment control prior to acceptance for assembly loading.

7. TRACEABILITY: Traceability of rods and associated rod components is established by Quality Control.

Assembly

Inspection consists of 100 percent inspection for drawing requirements.

Other Inspection

The following inspections are performed as part of the routine inspection operation:

1. Measurements other than those specified above which are critical to thermal and hydraulic analyses are obtained to enable evaluation of manufacturing variations to a 95 percent confidence level.

2. Tool and gage inspection and control including standardization to primary and secondary working standards. Tool inspection is performed at prescribed intervals on all serialized tools. Complete records are kept of calibration and condition of tools.

3. Check audit inspection of all inspection activities and records to assure that prescribed methods are followed and that all records are correct and properly maintained.

4. Surveillance of outside contractors, including approval of standards and methods are performed where necessary. However, all final acceptance is based upon inspection performed by Westinghouse personnel.

Process Control

To prevent the possibility of mixing enrichments during fuel manufacture and assembly, strict enrichment segregation and meticulous process control are exercised.

The UO_2 powder is kept in sealed containers by blend. The contents are fully identified both by descriptive tagging and preselected color coding. A Westinghouse identification tag completely describing the contents is affixed to the containers before transfer to powder storage. Isotopic content is confirmed by sample isotopic analysis or 100 percent gamma scanning of the powder containers.

Powder withdrawal from storage can be made by only one authorized group, which directs the powder to the correct pellet production line. All pellet production lines are physically separated from each other and pellets of only a single enrichment and density are produced in a given production line.

Finished pellets are placed on trays having the same color code as the powder containers and transferred to segregated storage racks within the confines of the pelleting area. Samples from each pellet lot are tested for isotopic content and impurity prior to acceptance by Quality Control. Physical barriers prevent mixing of pellets of different densities and enrichments in this storage area. Unused powder and sub-standard pellets to be analyzed and reprocessed are returned to storage in the original color coded containers.

Loading of pellets into the cladding is performed in isolated production lines and again only one density and enrichment is loaded on a line at a time.

A serialized traceability sticker is placed on each fuel tube which identifies the contract and enrichment. The sticker is color coded to the original pellet tray code for visual identification. The end plugs are inserted, the bottom end plug is permanently identified to the contract and enrichment, and welded to seal the tube. The fuel tube remains color coded and traceability identified until just prior to installation in the fuel assembly. The color coding and end plug identification character and traceability stickers provide a cross reference of the fuel contained in the fuel rods. All fuel rods are gamma scanned over the full length for isotopic content prior to acceptance for loading.

At the time of installation into an assembly, the color coding and traceability stickers are removed and a matrix is generated to identify each rod in its position within a given assembly. An inspector verifies that all fuel rods in an assembly have the same end plug identification, and that the top nozzle to be used on the assembly carries the correct identification character describing the fuel enrichment and density for the core region being fabricated. The top nozzle identification then becomes the permanent description of the fuel contained in the assembly.

3.2.1.4.3 On-site Inspection

Surveillance of fuel and reactor performance is routinely conducted on Westinghouse reactors. Power distribution is monitored using the excore fixed and incore movable detectors. Coolant activity and chemistry are followed which permits early detection of any fuel clad defects.

Visual fuel inspection is routinely conducted during refueling. Additional fuel inspections are dependent on the results of the operational monitoring and the visual inspections.

The Reactor Containment Refueling Mast has been modified to allow for sipping of the fuel assembly while it is within the mast as a means of identifying damaged or leaking fuel assemblies.

The first available irradiated fuel assemblies and rods will undergo an extended surveillance program following each cycle of operation. On-site examinations will include fuel rod integrity, fuel rod and fuel assembly dimensions and alignment, and surface deposits.

3.2.2 Reactor Vessel Internals

3.2.2.1 Design Bases

The design bases for the mechanical design of the reactor vessel internal components are as follows:

1. The reactor internals, in conjunction with the fuel assemblies, shall direct reactor coolant through the core to achieve acceptable flow distribution and to restrict bypass flow so that the heat transfer performance requirements are met for all modes of operation. In addition, required cooling for the pressure vessel head shall be provided so that the temperature differences between the vessel flange and head do not result in leakage from the flange during reactor operation.

2. In addition to neutron shielding provided by the reactor coolant, a separate thermal shield is provided to limit the exposure of the pressure vessel in order to maintain the required ductility of the material for all modes of operation.

3. Provisions shall be made for installing in-core instrumentation useful for the plant operation and vessel material test specimens required for a pressure vessel irradiation surveillance program.

4. The core internals are designed to withstand mechanical loads arising from operating basis earthquake, design basis earthquake, and pipe ruptures and meet the requirements of 5 below.

5. The reactor shall have mechanical provisions which are sufficient to adequately support the core and internals and to assure that the core is intact with acceptable heat transfer geometry following transients arising from abnormal operating conditions.

6. Following the design basis accident, the plant shall be capable of being shut down and cooled in an orderly fashion so that fuel cladding temperature is kept within specified limits. This implies that the deformation of certain critical reactor internals must be kept sufficiently small to allow core cooling.

The functional limitations for the core structures during the design basis accident are shown in Table 3.2-1. To insure no column loading of rod cluster control guide tubes, the upper core plate deflection is limited not to exceed the value shown in Table 3.2-1.

Details of the dynamic analyses, input forcing functions, and response loadings are presented in Section 14.3.3 and B.3.

3.2.2.2 Description and Drawings

The reactor vessel internals are described as follows:

The components of the reactor internals consist of the lower core support structure (including the entire core barrel and thermal shield), the upper core support structure and the in-core instrumentation support structure. The reactor internals support the core, maintain fuel alignment, limit fuel assembly movement, maintain alignment between fuel assemblies and control rod drive mechanisms, direct coolant flow past the fuel elements, direct coolant flow to the pressure vessel head, provide gamma and neutron shielding, and provide guides for the in-core instrumentation. The coolant flows from the vessel inlet nozzles down the annulus between the core barrel and the vessel wall and then into a plenum at the bottom of the vessel. It then reverses and flows up through the core support and through the lower core plate. The lower core plate is sized to provide the desired inlet flow distribution to the core. After passing through the core, the coolant enters the region of the upper support structure and then flows radially to the core barrel outlet nozzles and directly through the vessel outlet nozzles. A small portion of the coolant flows between the baffle plates and the core barrel to provide additional cooling of the barrel. Similarly, a small amount of the entering flow is directed into the vessel head plenum and exits through the vessel outlet nozzles.

All the major material for the reactor internals is Type 304 or equivalent[23] stainless steel. Parts not fabricated from Type 304 stainless steel include bolts and dowel pins which are fabricated from Type 316 or equivalent[23] stainless steel. The radial support insert and bolts are fabricated of inconel or an equivalent[23] type material. The only stainless steel materials used in the reactor core support structures which have yield strengths greater than 90,000 psi are the Type 403 or equivalent[23] series used for holddown springs. The use of these materials is compatible with the reactor coolant and is acceptable based on the 1971 ASME Boiler and Pressure Vessel Code, Code Case Number 1337.

All reactor internals are removable from the vessel for the purpose of their inspection as well as the inspection of the vessel internal surface.

Lower Core Support Structure

The major containment and support member of the reactor internals is the lower core support structure, shown in Figure 3.2-6. This support structure assembly consists of the core barrel, the core baffle, the lower core plate and support columns, the thermal shield, and the core support which is welded to the core barrel. All the major material for this structure is Type 304 or equivalent[23] stainless steel. The lower core support structure is supported at its upper flange from a ledge in the reactor vessel and its lower end is restrained from transverse motion by a radial support system attached to the vessel wall. Within the core barrel are an axial baffle and a lower core plate, both of which are attached to the core barrel wall and form the enclosure periphery of the core. The lower core support structure and core barrel provide passageways and direct the coolant flow. The lower core plate is positioned at the bottom level of the core below the baffle plates and provides support and orientation for the fuel assemblies.

The lower core plate is a member through which the necessary flow distribution holes for each fuel assembly are machined. Fuel assembly locating pins (two for each assembly) are also inserted into this plate. Columns are placed between the lower core plate and the core support of the core barrel to provide stiffness and to transmit the core load to the core support. Adequate coolant distribution is obtained through the use of the lower core plate and core support.

The one piece thermal shield is fixed to the core barrel at the top with rigid bolted connections. The bottom of the thermal shield is connected to the core barrel by means of axial flexures. This bottom support allows for differential axial growth of the shield/core barrel but restricts radial or horizontal movement of the bottom of the shield. Rectangular specimen guides in which material samples can be inserted and irradiated during reactor operation are welded to the thermal shield and extended to the top of the thermal shield. These samples are held in the rectangular specimen guides by a preloaded spring device at the top and bottom.

Vertically downward loads from weight, fuel assembly preload, control rod dynamic loading, hydraulic loads and earthquake acceleration are carried by the lower core plate into the lower core plate support flange on the core barrel shell and through the lower support columns to the core support and thence through the core barrel shell to the core barrel flange supported by the vessel flange. Transverse loads from earthquake acceleration, coolant cross flow, and vibration are carried by the core barrel shell and distributed between the lower radial support to the vessel wall, and to the vessel flange. Transverse loads of the fuel assemblies are transmitted to the core plate to the barrel wall and by upper core plate alignment pins which are welded into the core barrel.

The radial support system of the core barrel is accomplished by "key" and "keyway" joints to the reactor vessel wall. At four equally spaced points around the circumference, an Inconel clevis block is welded to the vessel inner diameter. An Inconel insert block is bolted to each of these clevis blocks, and has a "keyway" geometry. Opposite each of these is a "key" which is welded to the lower core support. At assembly, as the internals are lowered into the vessel, the keys engage the keyways in the axial direction. With this design, the internals are provided with a support at the furthest extremity, and may be viewed as a beam fixed at the top and simple supported at the bottom.

Radial and axial expansions of the core barrel are accommodated, but transverse movement of the core barrel is restricted by this design. With this system, cyclic stresses in the internal structures are within the ASME Section III limits. In the event of an abnormal downward vertical displacement of the internals following a hypothetical failure, energy absorbing devices limit the displacement of the core after contacting the vessel bottom head. The load is then transferred through the energy absorbing devices of the lower internals to the vessel.

The energy absorbers are mounted on a base plate which is contoured on its bottom surface to the reactor vessel bottom internal geometry. Their number and design are determined so as to limit the stresses imposed on all components except the energy absorber to less than yield (ASME Code Section III values). Assuming a downward vertical displacement, the potential energy of the system is absorbed mostly by the strain energy of the energy absorbing devices.

Upper Core Support Assembly

The upper core support assembly, shown in Figures 3.2-7 and 3.2-8, consists of the upper support assembly and the upper core plate between which are contained support columns and guide tube assemblies. The support columns establish the spacing between the upper support assembly and the upper core plate and are fastened at top and bottom to these plates. The support columns transmit the mechanical loadings between the upper support and upper core plate.

The guide tube assemblies shield and guide the control rod drive shafts and control rods. They are fastened to the upper support and are guided by pins in the upper core plate for proper orientation and support. Additional guidance for the control rod drive shafts is provided by the upper guide tube which is attached to the upper support.

The upper core support assembly, which is removed as a unit during refueling operation, is positioned in its proper orientation with respect to the lower support structure by slots in the upper core plate which engage flat-sided upper core plate alignment pins which are welded into the core barrel. At an elevation in the core barrel where the upper core plate is positioned, the flat-sided pins are located at angular positions of 90 degrees from each other. As the upper support structure is lowered into the lower internals, the slots in the plate engage the flat-sided pins in the axial direction. Lateral displacement of the plate and of the upper support assembly is restricted by this design. Fuel assembly locating pins protrude from the bottom of the upper core plate and engage the fuel assemblies as the upper assembly is lowered into place. Proper alignment of the lower core support structure, the upper core support assembly, the fuel assemblies and control rods are thereby assured by this system of locating pins and guidance arrangement. The upper core support assembly is restrained from any axial movements by a large circumferential spring which rests between the upper barrel flange and the upper core support assembly. The spring is compressed when the reactor vessel head is installed on the pressure vessel.

Vertical loads from weight, earthquake acceleration, hydraulic loads and fuel assembly preload are transmitted through the upper core plate via the support columns to the upper support assembly and then into the reactor vessel head. Transverse loads from coolant cross flow, earthquake acceleration, and possible vibrations are distributed by the support columns to the upper support and upper core plate. The upper support plate is particularly stiff to minimize deflection.

In-Core Instrumentation Support Structures

The in-core instrumentation support structures consist of an upper system to convey and support thermocouples penetrating the vessel through the head and a lower system to convey and support flux thimbles penetrating the vessel through the bottom (Figure 7.7-8 shows the Basic Flux-Mapping System).

The upper system utilizes the reactor vessel head penetrations. Instrumentation port columns are slip-connected to in-line columns that are in turn fastened to the upper support plate. These port columns protrude through the head penetrations. The thermocouples are carried through these port columns and the upper support plate at positions above their readout locations. The thermocouple conduits are supported from the columns of the upper core support system. The thermocouple conduits are Type 304 or equivalent[23] stainless steel tubes.

In addition to the upper in-core instrumentation, there are reactor vessel bottom port columns which carry the retractable, cold worked stainless steel flux thimbles that are pushed upward into the reactor core. Conduits extend from the bottom of the reactor vessel down through the concrete shield area and up to a thimble seal line. The minimum bend radii are about 144 inches and the trailing ends of the thimbles (at the seal line) are extracted approximately 15 feet during refueling of the reactor in order to avoid interference within the core. The thimbles are closed at the leading ends and serve as the pressure barrier between the reactor pressurized water and the containment atmosphere.

Mechanical seals between the retractable thimbles and conduits are provided at the seal line. During normal operation, the retractable thimbles are stationary and move only during refueling or for maintenance, at which time a space of approximately 15 feet above the seal line is cleared for the retraction operation.

The in-core instrumentation support structure is designed for adequate support of instrumentation during reactor operation and is rugged enough to resist damage or distortion under the conditions imposed by handling during the refueling sequence. These are the only conditions which affect the in-core instrumentation support structure. Reactor vessel surveillance specimen capsules are covered in Section 4.5.1.2. That section covers all the necessary details with regard to irradiation surveillance, including a cross-section of the reactor showing the capsule identity and location.

3.2.2.3 Design Loading Conditions

The design loading conditions that provide the basis for the design of the reactor internals are:

1. Fuel assembly weight.
2. Fuel assembly spring forces.
3. Internals weight.
4. Control rod trip (equivalent static load).
5. Differential pressure.

6. Spring preloads.
7. Coolant flow forces (static).
8. Temperature gradients.
9. Differences in thermal expansion.
    a. Due to temperature differences.
    b. Due to expansion of different materials.
10. Interference between components.
11. Vibration (mechanically or hydraulically induced).
12. One or more loops out of service.
13. All operational transients listed in Table 4.1-10.
14. Pump overspeed.
15. Seismic loads (operation basis earthquake and design basis earthquake).
16. Blowdown forces (due to cold and hot leg break).

Combined seismic and blowdown forces are included in the stress analysis as a design loading condition by assuming the maximum amplitude of each force to act concurrently.

The main objectives of the design analysis are to satisfy allowable stress limits, to assure an adequate design margin, and to establish deformation limits which are concerned primarily with the functioning of the components. The stress limits are established not only to assure that peak stresses will not reach unacceptable values, but also limit the amplitude of the oscillatory stress component in consideration of fatigue characteristics of the materials. Both low and high cycle fatigue stresses are considered when the allowable amplitude of oscillation is established. Dynamic analysis on the reactor internals are provided in Section 14.3.3 and B.3.

The specific stress limits which were used in the design of the reactor vessel internals are as follows:

1. Maximum membrane $P_m = 2.4\ S_m = 39{,}000$ psi
2. Maximum total $P_m + P_b = 3.0\ S_m = 49{,}000$ psi

where: S_m (evaluated at 588 F) = 16,600 psi

The specific deformation limits used in the design of the reactor vessel internals are contained in Section 14.3.3.4.

As part of the evaluation of design loading conditions, extensive testing and inspections are performed from the initial selection of raw materials up to and including component installation and plant operation. Among these tests and inspections are those performed during component fabrication, plant construction, startup and checkout, and during plant operation.

3.2.2.4 Design Loading Categories

The combination of design loadings fit into either the normal, upset or faulted conditions as defined in the ASME Section III Code.

Loads and deflections imposed on components due to shock and vibration are determined analytically and experimentally in both scaled models and operating reactors. The cyclic stresses due to these dynamic loads and deflections are combined with the stresses imposed by loads from component weights, hydraulic forces and thermal gradients for the determination of the total stresses of the internals.

The reactor internals are designed to withstand stresses originating from various operating conditions as summarized in Table 4.1-10.

The scope of the stress analysis problem is very large, requiring many different techniques and methods, both static and dynamic. The analysis performed depends on the mode of operation under consideration.

Allowable Deflections

For normal operating conditions, downward vertical deflection of the lower core support is negligible.

For the loss of coolant accident plus the design basis earthquake condition, the deflection criteria of critical internal structures are the limiting values given in Table 3.2-1. The corresponding no loss of function limits are included in Table 3.2-1 for comparison purposes with the allowed criteria.

The criteria for the core drop accident are based upon analyses which have been performed to determine the total downward displacement of the internal structures following a hypothesized core drop resulting from loss of the normal core barrel supports. The initial clearance between the secondary core support structures and the reactor vessel lower head in the hot condition is approximately one half inch. An additional displacement of approximately 3/4 inch would occur due to strain of the energy absorbing devices of the secondary core support; thus the total drop distance is about 1-1/4 inches, which is insufficient to permit the tips of the rod cluster control assembly to come out of the guide thimble in the fuel assemblies.

Specifically, the secondary core support is a device which will never be used, except during a hypothetical accident of the core support (core barrel, barrel flange, etc.). There are 4 supports in each reactor. This device limits the fall of the core and absorbs the energy of the fall which otherwise would be imparted to the vessel. The energy of the fall is calculated assuming a complete and instantaneous failure of the primary core support and is absorbed during the plastic deformation of the controlled volume of stainless steel, loaded in tension. The maximum deformation of this austenitic stainless piece is limited to approximately 15 percent, after which a positive step is provided to ensure support.

For additional information on design loading categories, see Appendix B.3.

3.2.2.5 Design Criteria Basis

The basis for the design stress and deflection criteria is identified below:

Allowable Stress

For normal operating conditions, Section III of the ASME Boiler and Pressure Vessel Code is used as a basis for evaluating acceptability of calculated stresses. Both static and alternating stress intensities are considered. Under Code Case 1618 bolt material Type 316 stainless steel is now covered in ASME Section III and is so treated. It should be noted that the allowable stresses in Section III of the ASME code are based on unirradiated material properties. In view of the fact that irradiation increases the strength of the 304 stainless steel used for the internals, although decreasing its elongation, it is considered that use of the allowable stresses in Section III are appropriate and conservative for irradiated internal structures.

The allowable stress limits during the design basis accident used for the core support structures are based on the January, 1971 draft of the ASME Code for Core Support Structures, Subsection NG, and the Criteria for Faulted Conditions.

3.2.2.6 Prototype Internals Verification Program

Note: This section was current in 1973 and has not been updated. It is retained in the Updated FSAR for historical understanding.

The H. B. Robinson (Carolina Power and Light) reactor has been established as the prototype for the Westinghouse three-loop plant internals verification program.[15] Subsequent three-loop plants are similar in design. Past experience with other reactors indicates that plants of similar designs behave in a similar manner. For these reasons an instrumentation program was conducted on the H. B. Robinson Plant to confirm the behavior of the reactor components. The main objectives of this test were to increase confidence in the adequacy of the internals by determining stress or deflection levels at key locations.

The only significant difference between the BVPS-1 internals and the H. B. Robinson prototype internals is that 17 x 17 fuel assemblies are in BVPS-1 and the Robinson plant employs 15 x 15 fuel assemblies. This internals change is manifested only in the design of guide tubes located in the upper core support structure. The new 17 x 17 guide tubes are stronger and more rigid and therefore less susceptible to flow induced vibration. The Trojan Nuclear Plant of the Portland General Electric Company will be the first operational Westinghouse PWR to employ 17 x 17 fuel assemblies. Operation of this plant preceded BVPS-1. The 17 x 17 guide tube in the Trojan Plant will be instrumented and the vibration behavior confirmed in accordance with Regulatory Guide 1.20.[16] The instrumentation of the Trojan Plant will also suffice to confirm guide tube vibration behavior on the BVPS-1 in accordance with Regulatory Guide 1.20 and no additional instrumenting of the internals on BVPS-1 will be necessary.[17]

In the final analysis, the proof that the internals are adequate, free from harmful vibrations, and have performed as intended is through component observations and examinations during service. With this thought, H. B. Robinson, the three-loop prototype, was subjected to a thorough visual and dye penetrant examination by a qualified Westinghouse Quality Assurance Engineer before and after the hot functional test. This inspection was in addition to the normal inspection of the internals in the shop, and before and after shipment.

Also, for the particular case of the three-loop plants, the following operating experiences offer additional assurance of the adequacy of this design (as of October, 1973):

1. Southern California Edison, San Onofre plant (Unit 1) is a three loop plant with a slightly different design. This plant has been in operation since 1967 with no internals vibration problems. The internals have been inspected on various occasions.

2. Carolina Power and Light, H. B. Robinson (CPL) after completion of the hot functional inspection the plant has been at power operation since 1970 with no internals vibration problems.

3. Florida Power and Light (FPL) Turkey Point 3 successfully completed the post hot functional inspection with the results indicating no internals vibration problems.

4. Virginia Electric & Power Co. (VEPCO) (Surry 1) also successfully completed the post hot functional inspection with similar results.

The CPL, FPL, and VEPCO internals have the same configuration as the other three-loop plants, thus providing important evidence of the reliability of the internals.

NRC Regulatory Guide 1.20, Paragraph D "Regulations for Reactor Internals Similar to the Prototype Design," is satisfied for these three-loop plants in the following manner:

The internals will be subjected to a thorough examination prior to preoperational flow tests. This examination will include the 35 points shown on the referenced drawing. These 35 points include the following:

1. All major load bearing elements of the reactor internals relied upon to retain the core structure in place.

2. The lateral, vertical, and torsional restraints provided within the vessel.

3. Those locking and bolting devices whose failure could adversely affect the structural integrity of the internals.

4. Those other locations on the reactor internal components which were examined on the Prototype H. B. Robinson design.

The interior of the reactor vessel will also be examined for evidence of loose parts or foreign material.

Specifically, the inside of the vessel will be inspected before and after the hot functional test, with all the internals removed, to verify that no loose parts or foreign material are in evidence.

Lower Internals

A particularly close inspection will be made on the following items and areas, using a 5X or 10X magnifying glass or Penetrant Test where applicable:

1. Upper barrel flange and girth weld.

2. Upper barrel to lower barrel girth weld.

3. Upper core plate aligning pin -- Examine for any shadow marks, burnishing, buffing, or scoring. Check for the soundness of lockwelds.

4. Irradiation specimen basket welds.

5. Baffle assembly locking devices -- Check for lockweld integrity.

6. Lower barrel to core support girth weld.

7. The flexible tie connections (flexures) at the lower end of the Thermal Shield.

8. Radial support key welds to barrel.

9. Insert locking devices -- Examine soundness of lockwelds.

10. Core support columns and instrumentation guide tubes -- Check all the joints for tightness and soundness of the locking devices.

11. Secondary core support assembly welds.

12. Lower radial support lugs and inserts -- Examine for any shadow marks, burnishing, buffing, or scoring. Check the integrity of the lockwelds. These members supply the radial and torsion constraint of the internals at the bottom relative to the reactor vessel while permitting axial growth between the two. One would expect to see, on the bearing surfaces of the key and keyway, burnishing, buffing, or shadowing marks which would indicate pressure loading and relative motion between the two parts. Some scoring of engaging surfaces is also possible and acceptable.

13. Bearing surfaces of upper core plate radial support key.

14. Mounting blocks thermal shield to core barrel -- Examine the connections for evidence of change in tightness or lockweld integrity.

15. Gaps at baffle joints -- Check for gaps between baffle and top former and at baffle to baffle joints.

Upper Internals

A particularly close inspection will be made on the following items or areas, using a magnifying glass of 5X or 10X magnification where necessary:

1. Thermocouple conduits, clamps, and couplings.

2. Guide tube, support column, and thermocouple column assembly locking devices.

3. Support column and conduit assembly clamp welds.

4. Radial support keys and inserts between the upper core plate and upper core barrel -- Examine for any shadow marks, burnishing, buffing, or scoring. Check the integrity of lockwelds.

5. Connections of the support columns and guide tubes to the upper core plate -- Check for tightness.

6. Thermocouple conduit gusset and clamp welds.

7. Thermocouple end-plugs -- Check for tightness.

8. Guide tube closure welds, tube-transition plate welds and card welds.

Acceptance standards are the same as required in the shop by the original design drawings and specifications.

During the hot functional test, the internals will be subjected to a total operating time at greater than normal full flow conditions (three pumps operating) of at least 10 days or 240 hours. This provides a cyclic loading of approximately 1 x 107 cycles on the main structural elements of the internals. In addition there will be some operating time with only one, two, and three pumps operating.

Therefore, when no signs of abnormal wear are found or of harmful vibration being present in the core support structures, and with no apparent structural changes taking place, the three loop core support structures are considered adequate. They function as intended and are free from harmful vibrations.

Note: All analyses specified in Section 3.2.2.6 were completed in the course of licensing BVPS-1 or prior to January 22, 1982.

3.2.3 Reactivity Control System

3.2.3.1 Design Bases

Bases for temperature, stress on structural members, and material compatibility are imposed on the design of the reactivity control components.

3.2.3.1.1 Design Stresses

The reactivity control system is designed to withstand stresses originating from various operating conditions such as those summarized in Table 4.1-10, as well as from conditions which directly involve the components of the reactivity control system.

Allowable Stresses

For normal operating conditions Section III of the ASME Boiler and Pressure Code is used. All components are analyzed as Class I components under Article NB-3000.

Dynamic Analysis

The cyclic stresses due to dynamic loads and deflections are combined with the stresses imposed by loads from component weights, hydraulic forces and thermal gradients for the determination of the total stresses of the reactivity control system.

3.2.3.1.2 Material Compatibility

Materials are selected for compatibility in a pressurized water reactor environment, for adequate mechanical properties at room and operating temperature, for resistance to adverse property changes in a radioactive environment, and for compatibility with interfacing components.

3.2.3.1.3 Reactivity Control Components

The reactivity control components are subdivided into two categories:

1. Permanent devices used to control or monitor the core.

2. Temporary devices used to control or monitor the core.

The permanent type components are the full length rod cluster control assemblies, control rod drive assemblies, neutron source assemblies, hafnium part-length power suppression assemblies, vibration damping assemblies, and thimble plug assemblies. Although the thimble plug assembly does not directly contribute to the reactivity control of the reactor, it is presented as a reactivity control system component in this document because it may be used to restrict bypass flow through those thimbles not occupied by absorber, source or burnable poison rods. Certain core designs do not require the use of thimble plug assemblies.

The temporary component is the burnable absorber assembly which is normally used in the initial core and could be used for any reload as to optimize fuel loading. Burnable absorber assemblies described in Section 3.2.3 utilize borosilicate glass absorber material. Wet Annular Burnable Absorber (WABA) rods may be used instead of the standard borosilicate glass absorber rods. The WABA rod design consists of annular pellets of aluminum oxide-boron carbide (Al_2O_3-B_4C) burnable absorber material encapsulated within two concentric zircaloy tubings. The reactor coolant flows inside the inner tubing and outside the outer tubing of the annular rod. Details of the WABA design are described in Reference 19.

Power peaking may also be controlled using Integral Fuel Burnable Absorbers (IFBA's) which are made by depositing a thin zirconium diboride coating on a fuel pellet. Zirconium diboride was selected because of its compatibility with the existing fuel pellet and cladding. The coating's capacity to absorb neutrons is precisely limited by the cycle reload design and the rate of absorption is closely matched to the reactivity depletion of the fuel. Use of the IFBA coated fuel pellets provides flexibility in fuel reload design since these fuel pellets can be axially and

radially positioned to maximize margin to peaking factor limits while achieving efficient use of neutrons. The IFBA design is further described and evaluated in Reference 20. The design bases for the rest of the components mentioned above are described in the following paragraphs.

Absorber Rods

The following are considered design conditions under Article NB-3000 of the ASME Boiler and Pressure Vessel Code Section III. The control rod which is cold rolled 304 stainless is the only non code material used in the control rod assembly. The stress intensity limit Sm for this material is defined at 2/3 of the 0.2 percent offset yield stress.

1. The external pressure equal to the reactor coolant system operating pressure.
2. The wear allowance equivalent to 1,000 reactor trips.
3. Bending of the rod due to a misalignment in the guide tube.
4. Forces imposed on the rods during rod drop.
5. Loads caused by accelerations imposed by the control rod drive mechanism.
6. Radiation exposure for maximum core life.

The absorber material temperature shall not exceed its melting point, which is 1,470°F for Ag-In-Cd.[2]

Burnable Absorber Rods

The burnable absorber rod clad (304 ss for the borosilicate glass design and Zircaloy-4 for the WABA design) is designed as a Class 1 component under Article NB-3000 of the 1971 ASME Boiler and Pressure Vessel Code, Section III, For Conditions I and II. For abnormal loads during Conditions III and IV, code stresses are not considered limiting. Failures of the burnable absorber rods during these conditions must not interfere with reactor shutdown or emergency cooling of the fuel rods.

The burnable absorber material, borosilicate glass, is non-structural. The structural elements of the burnable absorber rod are designed to maintain the absorber geometry even if the absorber material is fractured. The rods are designed so that the borosilicate absorber material is below its softening temperature, 1,492°F for reference 12.5 weight percent (w/o) boron rods. In addition, the structural elements are designed to prevent excessive slumping. Borosilicate glass is accepted for use in burnable absorber rods if the softening temperature is 1,510 $\pm$ 18°F. The softening temperature is defined in ASTM C-338-73, test for the softening point of glass.

Neutron Source Rods

The neutron source rods are designed to withstand the following:

1. The external pressure equal to the reactor coolant system operating pressure.

2. An internal pressure equal to the pressure generated by released gases over the source rod life.

Thimble Plug Assembly

The thimble plug assemblies satisfy the following:

1. Accommodate the differential thermal expansion between the fuel assembly and the core internals.

2. Maintain positive contact with the fuel assembly and the core internals.

3. Be inserted into or withdrawn from the fuel assembly by a force not exceeding 25 pounds.

3.2.3.1.4 Control Rod Drive Mechanisms

The mechanisms are Class I components designed to meet the stress requirements for normal operating conditions of Section III of the ASME Boiler and Pressure Vessel Code. Both static and alternating stress intensities are considered. The stresses originating from the required design transients are included in the analysis.

A dynamic seismic analysis is required on the full length control rod drive mechanism when a seismic disturbance has been postulated to confirm the ability of the mechanism to meet ASME Core, Section III, allowable stresses and to confirm its ability to trip when subjected to the seismic disturbances.

The control rod drive mechanism (CRDM) design used for the 17 x 17 fuel assembly control rod is identical to the 15 x 15 control rod drive mechanism. The seismic analysis and response of the 17 x 17 control rod drive mechanism is identical to those of the 15 x 15 mechanism plants.

Full Length Control Rod Drive Mechanism Operational Requirements

The basic operational requirements for the full length control rod drive mechanisms are:

1. 5/8-inch step.

2. 144-inch travel.

3. 360-pound maximum load.

4. Step in or out at 45 inches/min (72 steps/min).

5. Power interruption shall initiate release of drive rod assembly.

6. Trip delay of less than 150 ms - free fall of drive rod assembly shall begin less than 150 ms after power interruption no matter what holding or stepping action is being executed with any load and coolant temperatures of 100°F to 550°F.

7. 40-year design life.

8. 28,000 complete travel excursions which is 13 X 10^6 steps with replacement of latch assembly internal parts subject to wear after 3,000,000 steps. Note: The original design limit of 3,000,000 steps for the CRDM latch assembly was based on plant operation with load-follow conditions. Therefore, CRDM installation in plants such as BVPS that operate primarily under base-load conditions are NOT expected to approach the operational life design limits, even for the most highly used CRDMs.

3.2.3.2 Design Description

Reactivity control is provided by neutron absorbing rods and a soluble chemical neutron absorber (boric acid). The boric acid concentration is varied to control long-term reactivity changes such as:

1. Fuel depletion and fission product buildup.

2. Cold to hot, zero power reactivity change.

3. Reactivity change produced by intermediate-term fission products such as xenon and samarium.

4. Burnable absorber depletion.

Chemical and volume control is covered in Section 9.1.

The rod cluster control assemblies provide reactivity control for:

1. Shutdown.

2. Reactivity changes due to coolant temperature changes in the power range.

3. Reactivity changes associated with the power coefficient of reactivity.

4. Reactivity changes due to void formation.

If soluble boron were the sole means of control, the moderator temperature coefficient would be more positive than the limits assumed in the safety analyses. At hot full power conditions it is necessary to maintain a non-positive moderator temperature coefficient throughout the entire cycle in order to reduce possible deleterious effects caused by a positive coefficient during a loss of coolant accident or events that result in an RCS heatup, e.g. loss of flow. This is accomplished by the use of burnable absorbers, soluble boron, and/or rod withdrawal limits.

The neutron source assemblies provide a means of monitoring the core during periods of low neutron activity.

The most effective reactivity control components are the full length rod cluster control assemblies and their corresponding drive rod assemblies which are the only kinetic parts in the reactor. Figure 3.2-9 identifies the full length rod cluster control and drive rod assembly, in addition to the arrangement of these components in the reactor relative to the interfacing fuel assembly, guide tubes, and control rod drive mechanism. In the following paragraphs, each reactivity control component is described in detail.

The guidance system for the full-length control rod cluster is provided by the guide tube as shown in Figure 3.2-9. The guide tube provides two regimes of guidance.

1. In the lower section a continuous guidance system provides support immediately above the core. This system protects the rod against excessive deformation and wear due to hydraulic loading.

2. The region above the continuous section provides support and guidance at uniformly spaced intervals.

The envelope of support is determined by the pattern of the control rod cluster as shown in Figure 3.2-10. The guide tube assures alignment and support of the control rods, spider body, and drive rod while maintaining trip times at or below required limits.

3.2.3.2.1 Reactivity Control Components

Full Length Rod Cluster Control Assembly

The full length rod cluster control assemblies are divided into two categories, control and shutdown. The control groups compensate for reactivity changes due to variations in operating conditions of the reactor, i.e., power and temperature variations. Two criteria have been employed for selection of the control groups. First the total reactivity worth must be adequate to meet the nuclear requirements of the reactor. Second, in view of the fact that some of these rods may be partially inserted at power operation, the total power peaking factor should be low enough to ensure that the power capability is met. The control and shutdown groups provide adequate shut-down margin which is defined as the amount by which the core would be subcritical at hot shutdown if all rod cluster control assemblies are tripped assuming that the highest worth assembly remains fully withdrawn and assuming no changes in xenon or boron concentration.

A rod cluster control assembly comprises a group of individual neutron absorber rods fastened at the top end to a common spider assembly, as illustrated in Figure 3.2-10.

The absorber material used in the control rods is silver-indium- cadmium alloy which is essentially "black" to thermal neutrons and has sufficient additional resonance absorption to significantly increase its worth. The alloy is in the form of extruded rods which are sealed in stainless steel tubes to prevent the rods from coming in direct contact with the coolant. In construction, the silver-indium-cadmium rods are inserted into cold-worked stainless steel tubing which is then sealed at the bottom and the top by welded end plugs as shown in Figure 3.2-11. The rodlet tubes include a hard chrome plating to provide additional wear resistance. Sufficient diametral and end clearance is provided to accommodate relative thermal expansions.

The bottom plugs are made bullet-nosed to reduce the hydraulic drag during reactor trip and to guide smoothly into the dashpot section of the fuel assembly guide thimbles. The upper plug is threaded for assembly to the spider and has a reduced end section to make the joint more flexible.

The spider assembly is in the form of a central hub with radial vanes containing cylindrical fingers from which the absorber rods are suspended. Handling detents and detents for connection to the drive rod assembly are machined into the upper end of the hub.

Nested coil springs inside the spider body absorbs the impact energy at the end of a trip insertion. The radial vanes are joined to the hub by tack welds and brazing and the fingers are joined to the vanes by furnace brazing. A centerpost which holds the spring and its retainer is threaded into the hub within the skirt and welded to prevent loosening in service. All components of the spider assembly are made from Type 304 stainless steel and 308 stainless steel welding material except for the retainer which is of 17-4 PH material and the springs which are Inconel 718 alloy.

The absorber rods are fastened securely to the spider to assure trouble free service. The rods are first threaded into the spider fingers and then pinned to maintain joint tightness, after which the pins are welded in place. The end plug below the pin position is designed with a reduced section to permit flexing of the rods to correct for small operating or assembly misalignments.

The overall length is such that when the assembly is withdrawn through its full travel the tips of the absorber rods remain engaged in the guide thimbles so that alignment between rods and thimbles is always maintained. Since the rods are long and slender, they are relatively free to conform to any small misalignments with the guide thimble.

Burnable Absorber Assembly

Each burnable absorber assembly consists of borosilicate or WABA burnable absorber rods attached to a hold down assembly. Burnable absorber assemblies containing borosilicate poison are shown in Figure 3.2-13. WABA rods may be used in place of the borosilicate absorber rods.

The borosilicate absorber rods consist of borosilicate glass tubes contained within Type 304 or equivalent[23] stainless steel tubular cladding which is plugged and seal welded at the ends to encapsulate the glass. The glass is also supported along the length of its inside diameter by a thin wall tubular inner liner of Type 304 or equivalent[23] stainless steel. The top end of the liner is open to permit the diffused helium to pass into the void volume and the liner overhangs the glass. The liner has an outward flange at the bottom end to maintain the position of the liner with the glass. A typical borosilicate burnable absorber rod is shown in longitudinal and transverse cross-sections in Figure 3.2-14.

A WABA rod consists of annular pellets of alumina-boron carbide (Al_2-0_3-B_4C) burnable absorber material contained within two concentric zircaloy tubes. These zircaloy tubes, which form the inner and outer clad for the WABA rod, are plugged and welded at each end to encapsulate the annular stack of absorber material. The assembled rod is then internally pressurized to about 650 psig and seal welded. The absorber stack lengths are positioned

axially within the WABA rods by the use of zircaloy bottom-end spacers. An annular plenum is provided within the rod to accommodate the helium gas released from absorber material depletion during irradiation. The reactor coolant flows inside the inner tube and outside the outer tube of the annular rod. Further design details are given in Section 3.0 of Reference 22.

The burnable absorber rods are statically suspended and positioned in selected guide thimbles within specified fuel assemblies; location of these assemblies is shown in the Unit 2 UFSAR Figure 5.3-5. The absorber rods in each assembly are attached together at the top end of the rods to a hold down assembly by a flat, perforated retaining plate which fits within the fuel assembly top nozzle and rests on the adapter plate. The absorber rod assembly is held down and restrained against vertical motion through a spring pack which is attached to the plate and is compressed by the upper core plate when the reactor upper internals assembly is lowered into the reactor. This arrangement assures that the absorber rods cannot be ejected from the core by flow forces. Each rod is permanently attached to the base plate by a nut which is locked into place.

The clad in the borsilicate absorber rod assemblies is 10 percent cold worked Type 304 or equivalent[23] stainless steel. The WABA rod clad is Zircaloy-4 or equivalent.[23] All other structural materials are 304 or 308 stainless steel or equivalent[23] except for the springs which are Inconel 718 or equivalent.[23] The borosilicate glass tube provides sufficient boron content to meet the criteria discussed in Section 3.3.1.2 and 3.3.1.5.

Neutron Source Assembly

The purpose of the neutron source assembly is to provide a base neutron level to insure that the detectors are operational and responding to core multiplication neutrons. Since there is very little neutron activity during loading, refueling, shutdown, and approach to criticality, a neutron source may be placed in the reactor to provide a positive neutron count of at least 2 counts per second on the source range detectors attributable to core neutrons. The detectors, called source range detectors, are used primarily when the core is subcritical and during special sub-critical modes of operations. An irradiated fuel assembly may be used in place of a neutron source assembly to provide the desired base neutron level.

The base neutron level permits detection of changes in the core multiplication factor during core loading, refueling, and approach to criticality. This can be done since the multiplication factor is related to an inverse function of the detector count rate. Therefore a change in the multiplication factor can be detected during addition of fuel assemblies while loading the core, a change in control rod positions, and changes in boron concentration.

Both primary and secondary neutron source rods were used in the initial core. The primary source rod, containing a radioactive material, spontaneously emits neutrons during initial core loading and reactor startup. After the primary source rod decays beyond the desired neutron flux level, neutrons are then supplied by the secondary source rod. The secondary source rod contains a stable material which must be activated by neutron bombardment during reactor operation. The activation results in the subsequent release of neutrons. This can then be used as a source of neutrons during periods of low neutron flux, such as during refueling and the subsequent startups.

The initial core employed four source assemblies; two primary source assemblies and two secondary source assemblies. Each primary source assembly contained one primary source rod and between zero and nineteen burnable poison rods. Each secondary source assembly contained a symmetrical grouping of four secondary source rods and between zero and sixteen burnable poison rods. Locations not filled with a source or burnable poison rod contain a thimble plug. Conceptual source assemblies are shown in Figures 3.2-15A and 3.2-15B.

The source assemblies were employed at diametrically opposite sides of the core. The assemblies were inserted into the rod cluster control guide thimbles in fuel assemblies at selected unrodded locations.

The source assemblies contain a holddown assembly identical to that of the burnable poison assembly.

The secondary source rods utilize the same cladding material as the absorber rods. The secondary source rods contain Sb-Be pellets stacked to a height of approximately 88 inches. The rods in each assembly are permanently fastened at the top end to a holddown assembly, which is identical to that of the burnable absorber assemblies.

The other structural members are constructed of Type 304 stainless steel except for the springs. The springs exposed to the reactor coolant are wound from an age hardened nickel base alloy for corrosion resistance and high strength. The springs, when contained within the rods where corrosion resistance is not necessary, are oil tempered carbon steel.

Thimble Plug Assembly

Thimble plug assemblies may be used to limit bypass flow through the rod cluster control guide thimbles in fuel assemblies which do not contain either control rods, source rods, or burnable absorber rods.

The thimble plug assemblies as shown in Figure 3.2-16 consist of a flat base plate with short rods suspended from the bottom surface and a spring pack assembly. The twenty-four short rods, called thimble plugs, project into the upper ends of the guide thimbles to reduce the bypass flow area. Similar short rods may also be used on the source assemblies and burnable poison assemblies to plug the ends of vacant fuel assembly guide thimbles. At installation in the core, the thimble plug assemblies interface with both the upper core plate and with the fuel assembly top nozzles by resting on the adaptor plate. The spring pack is compressed by the upper core plate when the upper internals assembly is lowered into place. Each thimble plug is permanently attached to the base plate by a nut which is locked to the threaded end of the plug by a small lock-bar welded to the nut.

All components in the thimble plug assembly, except for the springs, are constructed from Type 304 stainless steel or its equivalent.[23] The springs are wound from an aged hardened nickel base alloy for corrosion resistance and high strength.

Vantage 5H Fuel Vibration Damping Assemblies

The vibration damping assemblies are similar in design to the burnable absorber assemblies except that the rodlets are made of solid unclad Zircaloy-4 instead of containing burnable absorber material. They may be used as needed to add mass to dampen potential flow induced vibration of a fuel assembly along the periphery of the reactor core.

Power Suppression Assemblies

The hafnium part-length power suppression assemblies (PSAs) are also similar in design to the burnable absorber assemblies except for the rodlets; the bottom 72 inches of each rodlet is made of solid unclad hafnium that is threaded and welded into the upper part of the rodlet made from solid unclad Zircaloy-4. Figure 3.2-14A presents the unclad hafnium peripheral PSA rodlet design and Figure 3.2-14B shows the hafnium PSA.

3.2.3.2.2 Control Rod Drive Mechanism

All parts exposed to reactor coolant are made of metals which resist the corrosive action of the water. Three types of metals are used exclusively: stainless steels, Inconel-X and cobalt based alloys. Wherever magnetic flux is carried by parts exposed to the main coolant, 400 series stainless steel is used. Cobalt based alloys are used for the pins and latch tips. Inconel-X is used for the springs of both latch assemblies and 304 stainless steel is used for all pressure containing parts. Hard chrome plating provides wear surfaces on the sliding parts and prevents galling between mating parts.

A position indicator assembly slides over the full length control rod drive mechanism housing. It detects the drive rod assembly position by means of 42 discrete coils that magnetically sense the entry and presence of the rod drive line through its center line over the normal length of the drive rod travel.

Full Length Control Rod Drive Mechanism

Control rod drive mechanisms are located on the dome of the reactor vessel. They are coupled to rod control clusters which have absorber material over the entire length of the control rods and derive their name from this feature. The full length control rod drive mechanism is shown in Figure 3.2-17 and schematically in Figure 3.2-18.

The primary function of the full length control rod drive mechanism is to insert or withdraw rod control clusters within the core to control average core temperature and to shut down the reactor.

The full length control rod drive mechanism is a magnetically operated jack. A magnetic jack is an arrangement of three electromagnets which are energized in a controlled sequence by a power cycler to insert or withdraw rod control clusters in the reactor core in discrete steps.

The control rod drive mechanism consists of four separate sub- assemblies. They are the pressure vessel, coil stock assembly, the latch assembly, and the drive rod assembly, each of which are described below:

1. The pressure vessel is a one-piece housing which is connected to the reactor vessel head adapter of each CRDM by a threaded, seal welded, maintenance joint which facilitates replacement of the latch assembly.

The lower portion of the CRDM contains the latch assembly. The upper portion of the CRDM provides space for the drive rod during its upward movement as the control rods are withdrawn from the core.

2. The coil stack assembly includes the coil housings, an electrical conduit and connector, and three operating coils:

   a. the stationary gripper coil.

   b. the movable gripper coil.

   c. the lift coil.

   The coil stack assembly is a separate unit which is installed on the drive mechanism by sliding it over the outside of the CRDM housing. It rests on the base of the CRDM housing without mechanical attachment.

   Energizing of the operation coils causes movement of the pole pieces and latches in the latch assembly.

3. The latch assembly includes the guide tube, stationary pole pieces, movable pole pieces, and two sets of latches, the movable gripper latch and the stationary gripper latch.

   The latches engage grooves in the drive rod assembly. The movable gripper latches are moved up or down in 5/8 inch steps by the lift pole to raise or lower the drive rod. The stationary gripper latches hold the drive rod assembly while the movable gripper latches are repositioned for the next 5/8 inch step.

4. The drive rod assembly includes a flexible coupling, a drive rod, a disconnect button, a disconnect rod, and a locking button.

   The drive rod has 5/8 inch grooves which receive the latches during holding or moving of the drive rod. The flexible coupling is attached to the drive rod and produces the means for coupling to the rod control cluster assembly.

   The disconnect button, disconnect rod, and locking button provide positive locking of the coupling to the rod control cluster assembly and permits remote disconnection of the drive rod.

The control rod drive mechanism is a trip design. Tripping can occur during any part of the power cycler sequencing if power to the coils is interrupted.

The control rod drive mechanism is threaded and seal welded on an adaptor on top of the reactor vessel and is coupled to the rod control cluster assembly directly below.

The mechanism is capable of handling a 360 pound load, including the drive rod weight, at a rate of 45 inches/minute. Withdrawal of the rod control cluster is accomplished by magnetic forces while insertion is by gravity.

The mechanism internals are designed to operate in 650°F reactor coolant. The pressure vessel is designed to contain reactor coolant at 650°F and 2,500 psia. The three operating coils are designed to operate at 392°F with forced air cooling required to maintain that temperature.

The full length control rod drive mechanism shown schematically in Figure 3.2-18 withdraws and inserts its control rod as electrical pulses are received by the operator coils. An ON or OFF sequence, repeated by silicon controlled rectifiers in the power programmer, causes either withdrawal or insertion of the control rod. Position of the control rod is measured by 42 discrete coils mounted on the position indicator assembly surrounding the CRDM housing.

Each magnetically senses the entry and presence of the top of the ferro-magnetic drive rod assembly as it moves through the coil center line.

During plant operation the stationary gripper coil of the drive mechanism holds the control rod withdrawn from the core in a static position until the movable gripper coil is energized.

Rod Cluster Control Assembly (RCCA) Withdrawal

The control rod is withdrawn by repetition of the following sequence of events:

1. MOVABLE GRIPPER COIL (identified as B on Figure 3.2-18) - ON: The latch locking plunger raises and swings the movable gripper latches into the drive rod assembly groove. A 1/16 inch axial clearance exists between the latch teeth and the drive rod.

2. STATIONARY GRIPPER COIL (A) - OFF: The force of gravity, acting upon the drive rod assembly and attached control rod, causes the stationary gripper latches and plunger to move downward 1/16 inch until the load of the drive rod assembly and attached control rod is transferred to the movable gripper latches. The plunger continues to move downward and swings the stationary gripper latches out of the drive rod assembly groove.

3. LIFT COIL (C) - ON: The 5/8 inch gap between the movable gripper pole and the lift pole closes and the drive rod assembly raises one step length (5/8 inch).

4. STATIONARY GRIPPER COIL (A) - ON: The plunger raises and closes the gap below the stationary gripper pole. The three links, pinned to the plunger, swing and the stationary gripper latches into a drive rod assembly groove. The latches contact the drive rod assembly and lift it (and the attached control rod) 1/16 inch. The 1/16 inch vertical drive rod assembly movement transfers the drive rod assembly load from the movable gripper latches to the stationary gripper latches.

5. MOVABLE GRIPPER COIL (B) - OFF: The latch locking plunger separates from the movable gripper pole under the force of a spring and gravity. Three links, pinned to the plunger, swing the three movable gripper latches out of the drive rod assembly groove.

6. LIFT COIL (C) - OFF: The gap between the movable gripper pole and lift pole opens. The movable gripper latches drop 5/8 inch to a position adjacent to a drive rod assembly groove.

7. REPEAT STEP 1: The sequence described above (1 thru 6) is termed as one step or one cycle. The control rod moves 5/8 inch for each step or cycle. The sequence is repeated at a rate of up to 72 steps per minute and the drive rod assembly (which has a 5/8 inch groove pitch) is raised 72 grooves per minute. The control rod is thus withdrawn at a rate of up to 45 inches per minute.

Rod Cluster Control Assembly Insertion

The sequence for control rod insertion is similar to that for control rod withdrawal, except the timing of lift coil (C) ON and OFF is changed to permit lowering the control rod.

1. LIFT COIL (C) - ON: The 5/8 inch gap between the movable gripper and lift pole closes. The movable gripper latches are raised to a position adjacent to a drive rod assembly groove.

2. MOVABLE GRIPPER COIL (B) - ON: The latch locking plunger raises and swings the movable gripper latches into a drive rod assembly groove. A 1/16 inch axial clearance exists between the latch teeth and the drive rod assembly.

3. STATIONARY GRIPPER COIL (A) - OFF: The force of gravity, acting upon the drive rod assembly and attached control rod, causes the stationary gripper latches and plunger to move downward 1/16 inch until the load of the drive rod assembly and attached control rod is transferred to the movable gripper latches. The plunger continues to move downward and swings the stationary gripper latches out of the drive rod assembly groove.

4. LIFT COIL (C) - OFF: The force of gravity separates the movable gripper pole from the lift pole and the drive rod assembly and attached control rod drops down 5/8 inch.

5. STATIONARY GRIPPER (A) - ON: The plunger raises and closes the gap below the stationary gripper pole. The three links, pinned to the plunger, swing the three stationary gripper latches into a drive rod assembly groove. The latches contact the drive rod assembly and lift it (and the attached control rod) 1/16 inch. The 1/16 inch vertical drive rod assembly movement transfers the drive rod assembly load from the movable gripper latches to the stationary gripper latches.

6. MOVABLE GRIPPER COIL (B) - OFF: The latch locking plunger separates from the movable gripper pole under the force of a spring and gravity. Three links, pinned to the plunger, swing the three movable gripper latches out of the drive rod assembly groove.

7. REPEAT STEP 1: The sequence is repeated, as for control rod withdrawal, up to 72 times per minute which gives a control rod insertion rate of 45 inches per minute.

Holding and Tripping of the Control Rods

During most of the plant operating time, the control rod drive mechanisms hold the control rods withdrawn from the core in a static position. In the holding mode, only one coil, the stationary gripper coil (A), is energized on each mechanism. The drive rod assembly and attached control rod hang suspended from the three latches.

If power to the stationary gripper coil is cut off, the combined weight of the drive rod assembly and the rod cluster control assembly is sufficient to move latches out of the drive rod assembly groove. The control rod falls by gravity into the core. The trip occurs as the magnetic field, holding the stationary gripper plunger half against the stationary gripper pole, collapses and the stationary gripper plunger half is forced down by the weight acting upon the latches. After the drive rod assembly is released by the mechanism, it falls freely until the control rods enter the buffer section of their thimble tubes.

3.2.3.3 Design Evaluation

3.2.3.3.1 Reactivity Control Components

The components are analyzed for loads corresponding to normal, upset, emergency and faulted conditions. The analysis performed depends on the mode of operation under consideration.

The scope of the analysis requires many different techniques and methods, both static and dynamic.

Some of the loads that are considered on each component where applicable are as follows:

1. Control rod trip (equivalent static load).
2. Differential pressure.
3. Spring preloads.
4. Coolant flow forces (static).
5. Temperature gradients.
6. Differences in thermal expansion.
    a. Due to temperature differences.
    b. Due to expansion of different materials.
7. Interference between components.
8. Vibration (mechanically or hydraulically induced).
9. All operational transients listed in Table 5.2-2.
10. Pump overspeed.
11. Seismic loads (operation basis earthquake and design basis earthquake).

The main objective of the analysis is to satisfy allowable stress limits, to assure an adequate design margin, and to establish deformation limits which are concerned primarily with the functioning of the components. The stress limits are established not only to assure that peak stresses will not reach unacceptable values, but also limit the amplitude of the oscillatory stress component in consideration of fatigue characteristics of the materials. Standard methods of strength of materials are used to establish the stresses and deflections of these components. The dynamic behavior of the reactivity control components has been studied using experimental test data (D-Loop, Section 1.5) and experience from operating reactors.

The design of reactivity component rods provides a sufficient cold void volume within the burnable absorber and source rods to limit the internal pressures to a value which satisfies the criteria in Section 3.2.3.1. The void volume for the helium in the borosilicate glass burnable absorber rods is obtained through the use of glass in tubular form which provides a central void along the length of the rods. For the WABA rods, an annular void volume is provided between the two tubes at the top and along the length of each WABA rod. Helium gas is not released by the neutron absorber rod material, thus the absorber rod only sustains an external pressure during operating conditions. The internal pressure of source rods continues to increase from ambient until end of life at which time the internal pressure never exceeds that allowed by the criteria in Section 3.2.3.1. Except for the WABA rods, the stress analysis of reactivity component rods assumes 100 percent gas release to the rod void volume, considers the initial pressure within the rod, and assumes the pressure external to the component rod is zero. The stress analysis for the WABA rods assumed a maximum 30 percent gas release.

Based on available data for properties of the borosilicate glass and on nuclear and thermal calculations for these burnable absorber rods, gross swelling or cracking of the glass tubing is not expected during operation. Some minor creep of the glass at the hot spot on the inner surface of the tube could occur but would continue only until the glass came in contact with the inner liner. The wall thickness of the inner liner is sized to provide adequate support in the event of slumping and to collapse locally before rupture of the exterior cladding if unexpected large volume changes due to swelling or cracking should occur. The top of the inner liner is open to allow communication to the central void by the helium which diffuses out of the glass.

Sufficient diametral and end clearances have been provided in the neutron absorber, burnable poison, and source rods to accommodate the relative thermal expansions between the enclosed material and the surrounding clad and end plugs. There is no bending or warping induced in the rods although the clearance offered by the guide thimble would permit a postulated warpage to occur without restraint on the rods. Bending, therefore, is not considered in the analysis of the rods. The radial and axial temperature profiles have been determined by considering gap conductance, thermal expansion, and neutron and/or gamma heating of the contained material as well as gamma heating of the clad. The maximum neutron absorber material temperature was found to be less than 850°F which occurs axially at only the highest flux region. The maximum borosilicate glass temperature was calculated to be about 1,200°F and takes place following the initial rise to power. The glass temperature then decreased rapidly for the following reasons:

1. Reduction in power generation due to B10 depletion

2. Better gap conductance as the helium produced diffuses to the gap.

3. External gap reduction due to borosilicate glass creep. Rod, guide thimble, and dashpot flow analysis performed indicates that the flow is sufficient to prevent coolant boiling and maintain clad temperatures at which the clad material has adequate strength to resist coolant operating pressures and rod internal pressures.

Analysis on the full length rod cluster control spider indicates the spider is structurally adequate to withstand the various operating loads including the higher loads which occur during the drive mechanism stepping action and rod drop. Experimental verification of the spider structural capability was planned (see Section 1.5).

The materials selected are considered to be the best available from the standpoint of resistance to irradiation damage and compatibility to the reactor environment. The materials selected partially dictate the reactor environment (e.g., Cl^- control in the coolant). The current design type reactivity controls have been in service for as much as six years with no apparent degradation of construction materials.

With regard to the materials of construction exhibiting satisfactory resistance to adverse property changes in a radioactive environment, it should be noted that work on breeder reactors in current design, similar materials are being applied. At high fluences the austenitic materials increase in strength with a corresponding decreased ductility (as measured by tensile tests) but energy absorption (as measured by impact tests) remain quite high. Corrosion of the materials exposed to the coolant is quite low and proper control of Cl^- and O-2 in the coolant will prevent the occurrence of stress corrosion. All of the austenitic stainless steel base materials used are processed and fabricated to preclude sensitization. Although the control rod spiders are fabricated by furnace brazing, the procedure used requires that the pieces be rapidly cooled so that the time-at-temperature is minimized. The time that is spent by the control rod spiders in the sensitization range, 800-1,500°F, is not more than 0.2 hours, as a maximum, during fabrication to preclude sensitization. The 17-4 PH parts are all aged at the highest standard aging temperature of 1,100°F to avoid stress corrosion problems exhibited by aging at lower temperatures.

Analysis of the full length rod cluster control assemblies show that if the drive mechanism housing ruptures the rod cluster control assembly will be ejected from the core by pressure differential of the operating pressure and ambient pressure across the drive rod assembly. The ejection is also predicted on the failure of the drive mechanism to retain the drive rod/rod cluster control assembly position. It should be pointed out that a drive mechanism housing rupture will cause the ejection of only one rod cluster control assembly with the other assemblies remaining in the core. Analysis also showed that a pressure drop in excess of 4,000 psi must occur across a two-fingered vane to break the vane/spider body joint causing ejection of two neutron absorber rods from the core. Since the greatest pressure of the primary system coolant is only 2,250 psi, a pressure drop in excess of 4,000 psi could not be expected to occur. Thus, the ejection of the neutron absorber rods is not possible.

Ejection of a burnable absorber or thimble plug assembly is conceivable based on the postulation that the hold down bar fails and that the base plate and burnable absorber rods are severely deformed. In the unlikely event that failure of the hold down bar occurs, the upward displacement of the burnable absorber assembly only permits the base plate to contact the upper core plate. Since this displacement is small, the major portion of the burnable absorber remains positioned within the core. In the case of the thimble plug assembly, the thimble plugs will partially remain in the fuel assembly guide thimbles thus maintaining a majority of the desired flow impedance. Further displacement or complete ejection would necessitate the square base plate and burnable absorber rods be forced, thus plastically deformed, to fit up through a smaller diameter hole. It is expected that this condition requires a substantially higher force or pressure drop than that of the hold down bar failure.

Experience with control rods, burnable absorber rods, and source rods are discussed in Reference 8.

The mechanical design of the reactivity control components provides for the protection of the active elements to prevent the loss of control capability and functional failure of critical components. The components have been reviewed for potential failure and consequences of a functional failure of critical parts. The results of the review are summarized below.

Full Length Rod Cluster Control Assembly

The basic absorbing material is sealed from contact with the primary coolant and the fuel assembly and guidance surfaces by a high quality stainless steel clad. Potential loss of absorber mass or reduction in reactivity control material due to mechanical or chemical erosion or wear is therefore reliably prevented.

A breach of the cladding for any postulated reason does not result in serious consequences. The absorber material silver-indium-cadmium is relatively inert and would still remain remote from high coolant velocity regions. Rapid loss of material resulting in significant loss of reactivity control material would not occur.

The individually clad absorber rods are doubly secured to the retaining spider vane by a threaded joint and a welded lock pin. No failure of this joint has ever been experienced in functional testing or in years of actual service in operating plants such as San Onofre, Connecticut Yankee, Jose de Cabbera, Besnau No. 1, Robert Emmett Ginna, etc.

It should also be noted that in several instances of control rod jamming caused by foreign particles, the individual rods at the site of the jam have borne the full capacity of the control rod drive mechanism and higher impact loads to dislodge the jam without failure. The guide tube card/guide thimble arrangement is such that large loads are required to buckle individual control rods. The conclusion to be drawn from this experience is that this joint is extremely insensitive to potential mechanical damage. A failure of the joint would result in the insertion of the individual rod into the core. This results in reduced reactivity which is a fail safe condition.

The spider finger braze joint by which the individual rods are fastened to the vanes has also experienced the service described above and been subjected to the same jam freeing procedures also without failure. A failure of this joint would also result in insertion of the individual rod into the core.

The radial vanes are attached to the spider body, again by a brazed joint. The joints are designed to a theoretical strength in excess of that of the components joined.

It is a feature of the design that the guidance of the rod cluster control is accomplished by the inner fingers of these vanes. They are therefore the most susceptible to mechanical damage. Since the vanes carry two rods, failure of the vane-to-hub joint such as the isolated incidents at Connecticut-Yankee does not prevent the free insertion of the rod pair.[8] Neither does such a failure interfere with the continuous free operation of the drive line, also as experienced at Connecticut-Yankee.[8]

Failure of the vane-to-hub joint of a single rod vane could potentially result in failure of the separated vane and rod to insert. This could occur only at withdrawal elevations where the spider is above the continuous guidance section of the guide tube (in the upper internals). A rotation of the disconnected vane could cause it to hang on one of the guide cards in the intermediate guide tube. Such an occurrence would be evident from the failure of the rod cluster control to insert below a certain elevation but with free motion above this point.

This possibility is considered extremely remote because the single rod vanes are subjected to only vertical loads and very light lateral reactions from the rods. The lateral loads are light even during a seismic event because tube/guide thimble arrangement allows very limited lateral motion. The consequences of such a failure are not considered critical since only one drive line of the reactivity control system would be involved. This condition is readily observed and can be cleared at shutdown.

The spider hub being of single unit cylindrical construction is very rugged and of extremely low potential for damage. It is difficult to postulate any condition to cause failure. Should some unforeseen event cause fracture of the hub above the vanes, the lower portion with the vanes and rods attached would insert by gravity into the core causing reactivity decrease. The rod could then not be removed by the drive line, again a fail safe condition. Fracture below the vanes cannot be postulated since all loads, including scram impact, are taken above the vane elevation.

The rod cluster control rods are provided a clear channel for insertion by the guide thimbles of the fuel assemblies. All fuel rod failures are protected against by providing this physical barrier between the fuel rod and the intended insertion channel. Distortion of the fuel rods by bending cannot apply sufficient force to damage or significantly distort the guide thimble. Fuel rod distortion by swelling, though precluded by design, would be terminated by fracture before contact with the guide thimble occurs. If such were not the case, it would be expected that a force reaction at the point of contact would cause a slight deflection of the guide thimble. The radius of curvature of the deflected shape of the guide thimbles would be sufficiently large to have a negligible influence on rod cluster control insertion.

Burnable Absorber Assemblies, Vibration Suppression Assemblies, and Power Suppression Assemblies

The burnable absorber assemblies, vibration suppression assemblies, and power suppression assemblies are static temporary reactivity control elements. The axial position is assured by the hold down assembly which bears against the upper core plate. Their lateral position is maintained by the guide thimbles of the fuel assemblies.

The individual rods are shouldered against the underside of the retainer plate and securely fastened at the top by a threaded nut which is then locked in place by a welded pin. The square dimension of the retainer plate is larger than the diameter of the flow holes through the core plate. Failure of the hold down bar or spring pack therefore does not result in ejection of the rods from the core.

The only incident that could potentially result in ejection of rods is a multiple fracture of the retainer plate. This is not considered credible because of the light loads borne by this component. During normal operation the loads borne by the plate are approximately 5 lb/rod or a total of 100 lb. distributed at the points of attachment. Even a multiple fracture of the retainer plate would result in jamming of the plate segments against the upper core plate, again preventing ejection. Excessive reactivity increase due to burnable poison ejection is therefore prevented.

Burnable absorber rods are clad with either stainless steel or Zircaloy-4. The burnable absorber is either a borosilicate glass tube whose position is maintained by a central hollow stainless steel tube or A1203-B4C annular pellets contained within two concentric zircaloy tubes. Burnable absorber rods are placed in static assemblies and are not subjected to motion that might damage the rods. Further, the guide thimble tubes of the fuel assembly afford additional protection from damage.

During the accumulated thousands of years of burnable absorber rodlet operating experience, only one instance of penetration of the stainless steel burnable absorber cladding has been observed. The consequences of clad breach are small. It is anticipated that upon clad breach, the B4C or borosilicate glass would be leached by the coolant water and that localized power peaking of a few percent would occur. However, no design criteria would be violated. Additional information on the consequences of postulated WABA rod failures is presented in Reference 22.

The vibration suppression assemblies are made of solid unclad Zircaloy-4 and the peripheral power suppression assemblies are made of solid unclad hafnium threaded and welded into the upper part of the rodlet made of solid Zircaloy-4. Zircaloy-4 and solid hafnium are not susceptible to release of contained materials.

Drive Rod Assemblies

All postulated failures of the drive rod assemblies either by fracture or uncoupling lead to the fail safe condition. If the drive rod assembly fractures at any elevation, that portion remaining coupled falls with, and is guided by the rod cluster control assembly. This always results in reactivity decrease for full length control rods.

3.2.3.3.2 Control Rod Drive Mechanism

Material Selection

All pressure containing materials comply with Section III of the ASME Boiler and Pressure Vessel Code and will be fabricated from Type 304 austenitic stainless steel or CF-8 stainless steel.

Magnetic pole pieces are fabricated from 410 stainless steel or equivalent.(23) All non-magnetic parts, except pins and springs, are fabricated from 304 stainless steel or its equivalent.(23) Haynes 25 or an equivalent(23) type material is used to fabricate link pins. Springs are made from Inconel-X or an equivalent(23) type material. Latch arm tips are clad with Stellite 6 or equivalent(23) hardfacing material to provide improved wearabilty. Hard chrome plate and Stellite 6 or equivalent(23) hardfacing material is used selectively for bearing and wear surfaces.

At the start to the development program, a survey was made to determine whether a material better than 410 stainless steel was available for the magnetic pole pieces. Ideal material requirements are as follows:

1. High magnetic saturation value.
2. High permeability.
3. Low coercive force.
4. High resistivity.
5. High curie temperature.
6. Corrosion resistant.
7. High impact strength.
8. Non-oriented.
9. High machinability.
10. Low susceptibility to radiation damage.

After a comprehensive material trade-off study was made it was decided that the 410 stainless steel was satisfactory for this application.

The cast coil housings require a magnetic material. Both low- carbon cast steel and ductile iron have been successfully tested for this application. The choice, made on the basis of cost, indicates that ductile iron will be specified on the control rod drive mechanism. The finished housings are zinc plated to provide corrosion resistance.

Coils are wound on bobbins of molded Dow Corning 302 material, with double glass-insulated copper wire. Coils are then vacuum impregnated with silicon varnish. A wrapping of mica sheet is secured to the coil outer surface. The result is a well-insulated coil capable of sustained operation at 200°C (392°F).

The drive shaft assembly utilizes a 410 stainless steel or equivalent[23] drive rod. The coupling is machined from 403 stainless steel or equivalent[23] type material. Other parts are 304 stainless steel or equivalent[23] with the exception of the springs which are Inconel-X or equivalent[23] and the locking button which is Haynes 25 or equivalent.[23]

Radiation Damage

As required by the equipment specification, the control rod drive mechanisms are designed to meet a radiation requirement of 10 Rad/hr. Materials have been selected to meet this requirement. The above radiation level which amounts to 1.753×10^6 Rads in twenty years will not limit control rod drive mechanism life.

Positioning Requirements

The mechanism has a step length of 5/8 inches which determines the positioning capabilities of the control rod drive mechanisms.

Note: Positioning requirements are determined by reactor physics.

Evaluation of Materials Adequacy

The ability of the pressure housing to perform throughout the design lifetime as defined in the equipment specification is confirmed by the stress analysis report required by the ASME Boiler and Pressure Vessel Code, Section III.

Due to the variations in expected seismic excitations from site to site, control rod drive mechanisms (CRDM) are dependent on an external seismic support system. This system is designed to assure that stress allowables are not exceeded in the CRDM for plant Upset or Faulted conditions. Stress limits for Upset and Faulted conditions are those defined in the ASME Boiler and Pressure Vessel Code, Section III.

Adequacy is demonstrated by analysis of the CRDM. The stress criteria are converted into the allowable seismic stresses in terms of bending moments in the structure. The CRDM is mathematically modeled as a system of lumped and distributed masses. The model is analyzed under appropriate seismic excitations and the resultant bending moments along the length of the CRDM are calculated. These values are then compared to the allowable seismic bending moments for the equipment, to assure adequacy of the design.

Internal components subjected to wear will withstand a minimum of 3,000,000 steps without refurbishment as confirmed by life tests.[34]

Results of Dimensional and Tolerance Analysis

With respect to the control rod drive mechanism systems as a whole, critical clearances are present in the following areas:

1. Latch assembly (Diametral clearances).
2. Latch arm-drive rod clearances.
3. Coil stack assembly-thermal clearances.
4. Coil fit in coil housing.

The following write-up defines clearances that are designed to provide reliable operation in the control rod drive mechanisms in these four critical areas. These clearances have been proven by life tests and actual field performance at operating plants.

Latch Assembly - Thermal Clearances

The magnetic jack has several clearances where parts made of 410 stainless steel fit over parts made from 304 stainless steel. Differential thermal expansion is therefore important. Minimum clearances of these parts at 68°F is 0.011 inches. At the maximum design temperature of 650°F minimum clearance is 0.0045 inches and at the maximum expected operating temperatures of 550°F is 0.0057 inches.

Latch Arm - Drive Rod Clearances

The control rod drive mechanism incorporates a load transfer action. The movable or stationary gripper latch are not under load during engagement, as previously explained, due to load transfer action. Figure 3.2-20 shows latch clearance variation with the drive rod as a result of minimum and maximum temperatures. Figure 3.2-21 shows clearance variations over design temperature range.

Coil Stack Assembly - Thermal Clearances

The assembly clearance of the coil stack assembly over the CRDM housing was selected so that the assembly could be removed under all anticipated conditions of thermal expansion.

At 70°F the inside diameter of the coil stack is 7.308/7.298 inches. The outside diameter of the CRDM housing is 7.260/7.270 inches.

Thermal expansion of the mechanism due to operating temperature of the control rod drive mechanism results in minimum inside diameter of the coil stack being 7.310 inches at 222°F and the maximum CRDM housing diameter being 7.302 inches at 532°F.

Under the extreme tolerance conditions listed above it is necessary to allow time for a 70°F coil housing to heat during a replacement operation.

Four coil stack assemblies were removed from four hot control rod drive mechanisms mounted on 11.035 inch centers on a 550°F test loop, allowed to cool, and then replaced without incident as a test to prove the preceding.

Coil Fit in Coil Housing

Control rod drive mechanism and coil housing clearances are selected so that coil heat up results in a close or tight fit. This is done to facilitate thermal transfer and coil cooling in a hot control rod drive mechanism.

3.2.3.4 Tests, Verification and Inspections

3.2.3.4.1 Reactivity Control Components

Tests and inspections are performed on each reactivity control component to verify the mechanical characteristics. In the case of the full length rod cluster control assembly, prototype testing has been conducted and both manufacturing test/inspections and functional testing at the plant site are performed.

During the component manufacturing phase, the following requirements apply to the reactivity control components to assure the proper functioning during reactor operation:

1. All materials are procured to specifications to attain the desired standard of quality.

2. A spider from each braze lot is proof tested by applying a 4,500 pound load to the spider body, so that approximately 187.5 lbs. is applied to each of the 24 fingers. This proof load provides a bending moment at the spider body approximately equivalent to the load caused by the acceleration imposed by the CRDM.

3. All clad/end plug welds are checked for integrity by visual inspection, X-ray, and are helium leak checked. All the seal welds in the neutron absorber rods, burnable poison rods and source rods are checked in this manner.

4. To assure proper fitup with the fuel assembly, the rod cluster control, burnable poison and source assemblies are installed in the fuel assembly without restriction or binding in the dry condition with a force not to exceed 15 pounds. Also a straightness of 0.010 inches/ft. is required on the entire inserted length of each rod assembly.

The full length rod cluster control assemblies were functionally tested, following cycle 1 core loading but prior to criticality to demonstrate reliable operation of the assemblies. Each assembly was operated (and tripped) one time at no flow/cold conditions and one time at full flow/hot conditions. In addition, selected assemblies, amounting to about 15 or 20 percent of the total assemblies were operated at no-flow/operating temperature conditions and full flow/ambient conditions. Also the slowest rod and the fastest rod were tripped 10 times at no-flow/ambient conditions and at full flow/operating temperature conditions. Thus each assembly was tested a minimum of 2 times or up to 14 times maximum to insure that the assemblies function properly. Ongoing testing is performed in accordance with Technical Specifications.

3.2.3.4.2 Control Rod Drive Mechanisms

Quality assurance procedures during production of control rod drive mechanisms include material selection, process control, mechanism components tests during production and hydrotests.

After all manufacturing procedures had been developed, several prototype control rod drive mechanisms and drive rod assemblies were life tested with the entire drive line under environmental conditions of temperature, pressure and flow. All acceptance tests were of duration equal to or greater than service required for the plant operation. All drive rod assemblies tested in this manner have shown minimal wear damage.

These tests include verification that the trip time achieved by the full length control rod drive mechanisms meet the design requirement measured from start of rod cluster control assembly motion to dashpot entry. This trip time requirement will be confirmed for each control rod drive mechanism prior to initial reactor operation and at periodic intervals after initial reactor operation. In addition, a Technical Specification has been set to ensure that the trip time requirement is met.

It is expected that all control rod drive mechanisms will meet specified operating requirements for the duration of plant life with normal refurbishment. However, a Technical Specification pertaining to an inoperable rod cluster control assembly has been set.

If a rod cluster control assembly cannot be moved by its mechanism, adjustments in the boron concentration ensure that adequate shutdown margin would be achieved following a trip. Thus, inability to move one rod cluster control assembly can be tolerated. More than one inoperable rod cluster control assembly could be tolerated, but would impose additional demands on the plant operator. Therefore, the number of inoperable rod cluster control assemblies has been limited to one.

In order to demonstrate continuous free movement of the full length rod cluster control assemblies and to ensure acceptable core power distributions during operation, partial-movement checks are performed on every full length rod cluster control assembly in accordance with Technical Specification requirements. In addition, periodic drop tests of the full length rod cluster control assemblies are performed at each refueling shutdown to demonstrate continued ability to meet trip time requirements, to ensure core subcriticality after reactor trip, and to limit potential reactivity insertions from a hypothetical rod cluster control assembly ejection.

Prior to initial startup, to confirm the mechanical adequacy of the fuel assembly and full length rod cluster control assembly, functional test programs have been conducted on a full scale control rod. The prototype assembly was tested under simulated conditions of reactor temperature, pressure, and flow for approximately 1,000 hours. The prototype mechanism accumulated about 3,000,000 steps and 600 trips. At the end of the test the control rod drive mechanism was still operating satisfactorily.

Prior to startup after 1R17, the replacement L106C control rod drive mechanisms (CRDM) were qualified with the completion of a life evaluation test. A new model L106C CRDM (similar to the original L-106A design) was exercised through 3,000,000 steps, with a rod drop every 300,000 steps. The test CRDM was subsequently dismantled and inspected for wear and damage. The results were documented in a report from the manufacturer to Westinghouse and FirstEnergy.(34)

All units are production tested prior to shipment to confirm ability of control rod drive mechanisms to meet design specification operational requirements.

3.2.3.5 Instrumentation Applications

Instrumentation for determining reactor coolant average temperature (Tavg) is provided to create demand signals for moving groups of full length rod cluster control assemblies to provide load follow (determined as a function of turbine first stage pressure) during normal operation and to counteract operational transients. The hot and cold leg resistance temperature detectors (RTD's) are described in Section 7.2. The location of the RTD's in each loop is shown on the flow diagrams in Section 4. The Reactor Control System which controls the reactor coolant average temperature by regulation of control rod bank position is described in Section 7.3.

Rod position indication instrumentation is provided to sense the actual position of each full length control rod so that the actual position of the individual rod may be displayed to the operator. Signals are also supplied by this system to the IPC (in-plant computer) as a secondary means of position indication. When the IPC is used as the primary means of rod position indication, administrative controls require the control room staff to continuously display the IPC computer point(s) in the control room. Signals are also supplied by this system as input to the rod deviation comparator. The rod position indication system is described in Section 7.

The reactor makeup control system, whose function is to permit adjustment of the reactor coolant boron concentration for reactivity control (as well as to maintain the desired operating fluid inventory in the volume control tank), consists of a group of instruments arranged to provide a manually preselected makeup composition that is borated or diluted as required to the charging pump suction header or the volume control tank. This system, as well as other systems including boron sampling provisions that are part of the Chemical and Volume Control System, are described in Section 9.1.

When the reactor is critical, the normal indication of reactivity status in the core is the position of the control bank in relation to reactor power (as indicated by the Reactor Coolant System loop T) and coolant average temperature. These parameters are used to calculate insertion limits for the control banks to give warning to the operator of excessive rod insertion. Monitoring of the neutron flux for various phases of reactor power operation as well as of core loading, shutdown, startup, and refueling is by means of the Nuclear Instrumentation System. The monitoring functions and readout and indication characteristics for the following means of monitoring reactivity are included in the discussion on safety related display instrumentation in Section 7.5:

1. Nuclear instrumentation system.
2. Temperature indicators.
    a. T average (Measured).
    b. ΔT (Measured).

c. Median T average.

d. T reference.

3. Demand position of rod cluster control assembly group.

4. Actual rod position indicators.

a. Analog rod position indicators.

b. In-plant computer points for rod position.

References for Section 3.2

1. J. A. Christensen, R. J. Allio and A. Biancheria, "Melting Point of Irradiated UO_2" WCAP-6065, Westinghouse Electric Corporation (February, 1965).

2. I. Cohen, "Development and Properties of Silver Base Alloys as Control Rod Materials for Pressurized Water Reactors," WAPD-214, Westinghouse Electric Corporation - Bettis Atomic Power Laboratory (December 1959).

3. Supplemental information on fuel design transmitted from R. Salvatori, Westinghouse NES, to D. Knuth, AEC, as attachments to letters NS-SL-518 (12/22/73), NS-SL-521 (12/29/72), NS-SL-524 (12/29/72) and NS-SL-543 (1/12/73), (Westinghouse Proprietary); and supplemental information on fuel design transmitted from R. Salvatori, Westinghouse NES, to D. Knuth, AEC, as attachments to letters NS-SL-527 (1/2/73) and NS-SL-544 (1/12/73).

4. J. Weisman, P. E. MacDonald, A. J. Miller and H. M. Ferrari, "Fission Gas Release from UO_2 Fuel Rods with Time Varying Power Histories," Trans. Am. Nucl. Soc. (12), (1969) pp. 900-901.

5. Deleted by Revision 16.

6. C. J. Kubit (Ed.), "Safety Related Research and Development for Westinghouse Pressurized Water Reactor - Program Summaries, Spring-Fall 1973," WCAP-8204, Westinghouse Electric Corporation (October, 1973).

7. W. J. Dollard, "Nuclear Fuel Division Quality Assurance Program Plan," WCAP-7800, Revision 3, Westinghouse Electric Corporation (April, 1974).

8. V. J. Plocido, R. E. Schreiber, J. Skaitka, "Operational Experience - Westinghouse Cores," WCAP-8183, Westinghouse Electric Corporation (October, 1973).

9. J. M. Hellman (Ed.), "Fuel Densification Experimental Results and Model for Reactor Operation," WCAP-8219, Westinghouse Electric Corporation (October, 1973).

10. B. Watkins and D. S. Wood, "The Significance of Irradiation - Induced Creep on Reactor Performance of a Zircaloy-2 Pressure Tube", Applications - Related Phenomena for Zirconium and its Alloys, ASTM STP 458, American Society for Testing and Materials (1969) pp. 226-240.

11. Deleted, Revision 0.

12. W. J. O'Donnell, B. F. Langer, "Fatigue Design Basis for Zircaloy Components", Nuclear Science and Engineering, 20, 1-12, (1964).

13. E. E. DeMario, S. Nakazato, "Hydraulic Flow Test of the 17 x 17 Fuel Assembly", WCAP-8279, Westinghouse Electric Corporation (February, 1974).

14. L. T. Gesinki, "Fuel Assembly Safety Analysis for Combined Seismic and Loss-of-Coolant Accident", WCAP-7950, Westinghouse Electric Corporation (July 1972).

References for Section 3.2 (CONT'D)

15. "Westinghouse PWR Internals Vibration Summary Three-Loop Internals Assurance", WCAP 7765-AR, Westinghouse Electric Corporation (November 1973).

16. Trojan Final Safety Analysis Report, Appendix A.12, Docket No. 50-344, Portland General Electric Company.

17. M. B. Aycock, "Internals Vibration Testing on Westinghouse 3 & 4 Loop Plants", AEC Meeting Summary for RESAR-3 (July 3, 1974).

18. Deleted by Revision 23

19. "Westinghouse Wet Annular Burnable Absorber Evaluation Report", WCAP-10021-P-A Revision 1, Westinghouse Electric Corporation (October 1983).

20. S. L. Davidson, (Ed.), et. al., "VANTAGE-5 Fuel Assembly, Reference Core Report," WCAP-10444-P-A, Westinghouse Electric Corporation (September 1985).

21. S. L. Davidson, (Ed.), et. al., "VANTAGE 5H Fuel Assembly," WCAP-10444-P-A, Addendum 2-A, Westinghouse Electric Corporation (February 1989).

22. J. Skaritka, (Ed.), "Westinghouse Wet Annular Burnable Absorber Evaluation Report," WCAP-10021-P-A, Revision 1, Westinghouse Electric Corporation (October 1983).

23. The term "equivalent" is described in UFSAR Section 1.8.2, "Equivalent Materials."

24. M. D. Beaumont, et. al., "Properties of Fuel and Core Component Materials," WCAP-9179, Revision 1 (Proprietary) and WCAP-9224 (Non-Proprietary), (July 1978).

25. M. D. Beaumont, et. al., "Properties of Fuel and Core Component Materials," WCAP-9179, Revision 1 (Proprietary) and WCAP-9224 (Non-Proprietary) Appendix A, "Hafnium" (October 1980).

26. S. L. Davidson, D. L. Nuhfer (Eds.), "VANTAGE+ Fuel Assembly Reference Core Report," WCAP-12610-P-A (April 1995).

27. S. L. Davidson (Ed.), "Westinghouse Fuel Criteria Evaluation Process," WCAP-12488-A (October 1994), and "Addendum to WCAP-12488-A Revision to Design Criteria," WCAP-12488-A, Addendum 1-A, Revision 1 (January 2002).

28. R. A. Weiner, et. al., "Improved Fuel Performance Models for Westinghouse Fuel Rod Designs and Safety Evaluations," WCAP-10851-P-A (Proprietary) and WCAP-11873-A (Non-Proprietary), (August 1988).

29. S. L. Davidson, (Ed.), et. al., "Extended Burnup Evaluation of Westinghouse Fuel," WCAP-10125-P-A (Proprietary) and WCAP-10126-A (Non-Proprietary), (December 1985).

30. P. J. Kersting, et. al., "Assessment of Clad Flattening and Densification Power Spike Factor Elimination in Westinghouse Nuclear Fuel," WCAP-13589-A (March 1995).

31. W. H. Slagle, "Operational Experience - Westinghouse Cores," WCAP-8183, Westinghouse Electric Corporation, (latest revision).

References for Section 3.2 (CONT'D)

32. W. J. Johnson (Westinghouse) letters to M. W. Hodges (NRC), NS-NRC-88-3319 (April 15, 1988) and NS-NRC-88-3363 (July 29, 1988).

33. J. P. Foster, S. Sidenor, "Westinghouse Improved Performance Analysis and Design Model (PAD 4.0)," WCAP-15063-P-A (Proprietary) and WCAP-15063-A (Non-Proprietary), Revision 1, with Errata (July 2000).

34. Curtiss-Wright Electro Mechanical Corporation, "Model L-106C CRDM Second Life Evaluation Test Disassembly & Examination," Engineering Memorandum 7159 Rev 1. Curtiss-Wright Electro Mechanical Corporation, "Results and Examination of the Model L-106C CRDM First and Second Life Evaluation Test," Engineering Memorandum 7158 Rev 1, Add 1.

35. P. Schueren & H.H. Shah, "Optimized ZIRLO™," WCAP-12610-P-A and CENPD-404-P-A, Addendum 1-A, Rev. 0, July 2006.

3.3 NUCLEAR DESIGN

3.3.1 Design Bases

This section describes the design bases and functional requirements used in the nuclear design of the fuel and reactivity control system and relates these design bases to the AEC General Design Criteria (GDC) of July 1971. Where appropriate, supplemental criteria such as the Final Acceptance Criteria for Emergency Core Cooling Systems are addressed. Before discussing the nuclear design bases, it is appropriate to briefly review the four major categories ascribed to conditions of plant operation.

The full spectrum of plant conditions is divided into four categories, in accordance with the anticipated frequency of occurrence and risk to the public:

1. Condition I - Normal Operation
2. Condition II - Incidents of Moderate Frequency
3. Condition III - Infrequent Faults
4. Condition IV - Limiting Faults

In general, the Condition I occurrences are accommodated with margin between any plant parameter and the value of that parameter which would require either automatic or manual protective action. Condition II incidents are accommodated with, at most, a shutdown of the reactor with the plant capable of returning to operation after corrective action. Fuel damage is not expected during Condition I and Condition II events. Fuel damage as used here is defined as penetration of the fission product barrier (i.e., the fuel rod clad). It is not possible, however, to preclude a very small number of rod failures. These are within the capability of the plant cleanup system and are consistent with the plant design basis.

Condition III incidents shall not cause more than a small fraction of the fuel elements in the reactor to be damaged, although sufficient fuel element damage might occur to preclude immediate resumption of operation. The release of radioactive material due to Condition III incidents should not be sufficient to interrupt or restrict public use of these areas beyond the exclusion radius. Furthermore, a Condition III incident shall not, by itself, generate a Condition IV fault or result in a consequential loss of function of the reactor coolant system or reactor containment barriers.

Condition IV occurrences are faults that are not expected to occur but are defined as limiting faults which must be designed against. Condition IV faults shall not cause a release of radioactive material that results in an undue risk to public health and safety.

The core design power distribution limits related to fuel integrity are met for Condition I occurrences through conservative design and maintained by the action of the Control System. The requirements for Condition II occurrences are met by providing an adequate protection system which monitors reactor parameters. The Control and Protection Systems are described in Section 7 and the consequences of Condition II, III, and IV occurrences are given in Section 14.

3.3.1.1 Fuel Burnup

Basis

The fuel rod design basis is described in Section 3.2. The nuclear design basis is described in Section 3.3.1.3. The above design basis satisfy GDC 10.

Discussion

Fuel burnup is a measure of fuel depletion which represents the integrated energy output of the fuel (MWD/MTU) and is a convenient means for quantifying fuel exposure criteria.

The core design lifetime or design discharge burnup is achieved by installing sufficient initial excess reactivity in each fuel region and by following a fuel replacement program (such as that described in Section 3.3.2) that meets all safety related criteria in each cycle of operation.

Initial excess reactivity installed in the fuel, although not a design basis, must be sufficient to maintain core criticality at full power operating conditions throughout cycle life with equilibrium xenon, samarium, and other fission products present. The end of design cycle life is defined to occur when the chemical shim concentration is essentially zero with control rods present to the degree necessary for operational requirements (e.g., the controlling bank at the "bite" position). In terms of chemical shim boron concentration, this represents approximately 10 ppm with no control rod insertion.

A limitation on initial installed excess reactivity is not required other than as is quantified in terms of other Design Bases such as core Negative Reactivity Feedback and Shutdown Margin discussed below.

3.3.1.2 Negative Reactivity Feedbacks (Reactivity Coefficient)

Basis

As the core power and temperature increase, the total reactivity defect is always negative, even when the moderator defect is positive as a result of implementing a positive moderator temperature coefficient limit below 100 percent power. Therefore, the cumulative reactivity feedback as the core power approaches 100 percent is always negative. The design basis meets GDC 11.

Discussion

When compensation for a rapid increase in reactivity is considered, there are two major effects. These are the resonance absorption effects (Doppler) associated with changing fuel temperature and the spectrum effect resulting from changing moderator density. These basic physics characteristics are often identified by reactivity coefficients. The use of slightly enriched uranium ensures that the Doppler coefficient of reactivity is negative. This coefficient provides the most rapid reactivity compensation. When the moderator temperature coefficient of reactivity is negative, it also provides reactivity compensation. At full power, the void content provides another, slower compensatory effect. The moderator temperature coefficient is maintained within the limits discussed in Section 3.3.2.3.2 through the use of burnable absorbers and/or control rods by limiting the reactivity held down by soluble boron.

3.3.1.3 Control of Power Distribution

Basis

The nuclear design bases are that, with at least a 95% confidence level:

1. The fuel will not be operated at greater than 13.74 kw/ft (based on F(Q) of 2.40) under normal operating conditions including an allowance of 0.6% for calorimetric error and not including a power spike factor due to densification.

2. Under abnormal conditions including the maximum overpower condition, the fuel peak power will not cause melting as defined in Section 3.4.1.2.

3. The fuel will not operate with a power distribution that violates the departure from nucleate boiling (DNB) design basis (i.e., the DNBR shall not be less than the safety analysis limit, as discussed in Section 3.4.1) under Condition I and II events including the maximum overpower condition.

4. Fuel management will be such as to produce rod powers and burnups consistent with the reload safety evaluation for each fuel cycle.

The above bases meet GDC 10.

Discussion

Calculation of extreme power shapes which affect fuel design limits is performed with proven methods and verified frequently with measurements from operating reactors. The conditions under which limiting power shapes are assumed to occur are chosen conservatively with regard to any permissible operating state.

Even though there is good agreement between measured peak power calculations and measurements, a nuclear uncertainty margin is applied to calculated peak local power. Such a margin is provided both for the analysis of normal operating states and for anticipated transients.

3.3.1.4 Maximum Controlled Reactivity Insertion Rate

Basis

The maximum reactivity insertion rate due to withdrawal of rod cluster control assemblies or by boron dilution is limited. This limit, expressed as a maximum reactivity change rate (75 pcm/sec) is set such that peak heat generation rate and DNBR do not exceed the maximum allowable at overpower conditions. (1 pcm = 10^{-5} ΔP, (See footnote Table 3.3-2). This satisfies GDC 25.

The maximum reactivity worth of control rods and the maximum rates of reactivity insertion employing control rods are limited so as to preclude rupture of the coolant pressure boundary or disruption of the core internals to a degree which would impair core cooling capacity due to a rod withdrawal or ejection accident (See Section 14).

Following any Condition IV event (rod ejection, steamline break, etc.) the reactor can be brought to the shutdown condition and the core will maintain acceptable heat transfer geometry. This satisfies GDC 28.

Discussion

Reactivity addition associated with an accidental withdrawal of a control bank (or banks) is limited by the maximum rod speed (or travel rate) and by the worth of the bank(s). For this reactor, the maximum control rod speed is 45 inches per minute and the maximum rate of reactivity change considering two control banks moving is less than 75 pcm/sec. During normal operation at power and with control rod overlap, the maximum reactivity change rate is less than 35 pcm/sec.

The reactivity change rates are conservatively calculated, assuming unfavorable axial power and xenon distributions. The peak xenon burnout rate is 25 pcm/min, which is lower than the maximum reactivity addition rate of 35 pcm/sec for normal operation and 75 pcm/sec for accidental withdrawal of two banks.

3.3.1.5 Shutdown Margins

Basis

Minimum shutdown margin as specified in the Technical Specifications are required at any power operating condition in the hot standby shutdown and in the cold shutdown conditions.

In all analyses involving reactor trip, the single, highest worth Rod Cluster Control Assembly is postulated to remain untripped in its full-out position (stuck rod criterion). This satisfies GDC 26.

Discussion

Two independent reactivity control systems are provided, namely control rods and soluble boron in the coolant. The control rod system can compensate for the reactivity effects of the fuel and water temperature changes accompanying power level changes over the range from full-load to no-load. In addition, the control rod system provides the minimum shutdown margin under Condition I events and is capable of making the core subcritical rapidly enough to prevent exceeding acceptable fuel damage limits assuming that the highest worth control rod is stuck out upon trip.

The boron system can compensate for all xenon burnout reactivity changes and will maintain the reactor in the cold shutdown. Thus, backup and emergency shutdown provisions are provided by a mechanical and a chemical shim control system which satisfies GDC 26.

Basis

When fuel assemblies are in the pressure vessel and the vessel lid is not in place, K_{eff} will be maintained at or below 0.95 with control rods and boron. Further, the fuel will be maintained sufficiently subcritical that removal of all Rod Cluster Control Assemblies will not result in criticality.

ANSI Standard N18.2, Nuclear Safety Criteria for the Design of Stationary Pressurized Water Reactor Plants, specified K_{eff} not to exceed 0.95 in spent fuel storage racks and transfer equipment flooded with pure water and K_{eff} not to exceed 0.98 in normally dry new fuel storage racks assuming optimum moderation. No criterion is given for the refueling operation, however a 5% margin, which is consistent with spent fuel storage and transfer and 3% below the new fuel storage, is adequate for the controlled and continuously monitored operations involved.

3.3.1.6 Stability

Basis

The core will be inherently stable to power oscillations of the fundamental mode. This satisfies GDC 12.

Discussion

Oscillations of the total power output of the core, from whatever cause, are readily detected by the loop temperature sensors and by the nuclear instrumentation. The core is protected by these systems and a reactor trip would occur if power increased unacceptably, preserving the design margins to fuel design limits. The stability of the turbine/steam generator/core systems and the reactor control system is such that total core power oscillations are not normally possible. The redundancy of the protection circuits ensures an extremely low probability of exceeding design power levels.

Basis

Spatial power oscillations within the core, with a constant core power output, should they occur can be reliably and readily detected and suppressed.

Discussion

The core is designed so that diametral and azimuthal oscillations due to spatial xenon effects are self-damping and no operator action or control action is required to suppress them. The stability to diametral oscillations is so great that this excitation is highly improbable. Convergent azimuthal oscillations can be excited by prohibited motion of individual control rods. Such oscillations are readily observable and alarmed, using the excore long ion chambers. Indications are also continuously available from incore thermocouples and loop temperature measurements. Movable incore detectors can be activated to provide more detailed information. In all presently proposed cores, these horizontal plane oscillations are self-damping by virtue of reactivity feedback effects designed into the core.

However, axial xenon spatial power oscillations may occur late in core life. The control bank and excore detectors are provided for control and monitoring of axial power distributions. Assurance that fuel design limits are not exceeded is provided by reactor overpower ΔT and overtemperature ΔT. Overtemperature ΔT trip functions use the measured axial power imbalance as an input.

The subject of xenon induced power oscillations is discussed fully in Section 3.3.2.8 and verifies that Westinghouse PWR cores are inherently stable to X-Y oscillations.

The potential source of power oscillation due to influences external to the core are prevented by the control system design. The control system, described in Section 7, is designed so as to provide stable operation with the appropriate setpoints.

3.3.1.7 Anticipated Transients Without Trip

The effects of anticipated transients with failure to trip are not considered in the Design Bases of the plant. Analysis has shown that the likelihood of such a hypothetical event is negligibly small.(1) Furthermore, analysis of the consequences of a hypothetical failure to trip following anticipated transients will be performed to show that no significant core damage would result and system peak pressures would be limited to acceptable values and no failure of the Reactor Coolant System would result. These analyses were in accordance with the AEC policy outlined in WASH-1270 "Technical Report on Anticipated Transients Without Scram for Water-Cooled Power Reactors," September, 1973.

3.3.2 Description

3.3.2.1 Nuclear Design Description

The reactor core consists of a specified number of fuel rods which are held in bundles by spacer grids and top and bottom fittings. The fuel rods are constructed of zircaloy, ZIRLO® or Optimized ZIRLO™ cylindrical tubes containing UO_2 fuel pellets. The bundles, known as fuel assemblies, are arranged in a pattern which approximates a right circular cylinder. Some fuel assemblies may contain non-fueled rods. For a description of non-fueled rods see Section 3.1.

Each fuel assembly contains a 17 x 17 rod array composed of 264 fuel rods, 24 rod cluster control (RCC) thimbles and an in-core instrumentation thimble. Figure 3.2-1 shows a cross sectional view of a 17 x 17 fuel assembly and the related RCC locations. Further details of the fuel assembly are given in Section 3.2.1.

The fuel rods within a given assembly have the same uranium enrichment in both the radial and axial planes with the exception of the 6 inches at the top and 6 inches at the bottom of the rod which may contain an axial blanket made of uranium with a lower enrichment than the rest of the rod. The fuel pellets used for the axial blankets may be formed with a central cylindrical void. The enrichments for the first core are shown in Table 3.3-1.

The reference reloading pattern is typically similar to Figure 3.3-1 with depleted fuel interspersed checkerboard style in the center and burned fuel on the periphery. The core will normally operate approximately eighteen months between refueling outages, accumulating 18,000 MWD/MTU, or more, per cycle. The exact reloading pattern, initial and final burnups of the assemblies, and the number of fresh assemblies and their placement are dependent on the energy requirement for the next cycle and burnup and power histories of the previous cycles.

The core average enrichment is determined by the amount of fissionable material required to provide the desired core lifetime and energy requirements. The physics of the burnout process is such that operation of the reactor depletes the amount of fuel available due to the absorption of neutrons by the U235 atoms and their subsequent fission. The rate of U235 depletion is directly proportional to the power level at which the reactor is operated. In addition, the fission process results in the formation of fission products, some of which readily absorb neutrons.

These effects, depletion and the buildup of fission products, are partially offset by the buildup of plutonium, shown in Figure 3.3-2 for the 17 x 17 fuel assembly, which occurs due to the non-fission absorption of neutrons in U-238. Therefore, at the beginning of any cycle a reactivity reserve equal to the depletion of the fissionable fuel and the buildup of fission product poisons over the specified cycle life must be "built" into the reactor. This excess reactivity is controlled by removable neutron absorbing material in the form of boron dissolved in the primary coolant, burnable absorber rods, or a boron-containing coating on the fuel pellets themselves.

The concentration of boric acid in the primary coolant is varied to provide control and to compensate for long-term reactivity requirements. The concentration of the soluble neutron absorber is varied to compensate for reactivity changes due to fuel burnup, fission product poisoning including xenon and samarium, burnable absorber depletion, and the cold-to-operating moderator temperature change. Using its normal makeup path, the Chemical and Volume Control System (CVCS) is capable of inserting negative reactivity at a rate of approximately 25 pcm/min when the reactor coolant boron concentration is 2000 ppm, approximately 30 pcm/min when the reactor coolant boron concentration is 1000 ppm and approximately 35 pcm/min when the reactor coolant boron concentration is 100 ppm.

If the emergency boration path is used, the CVCS is capable of inserting negative reactivity at a rate of approximately 55 pcm/min when the reactor coolant boron concentration is 2000 ppm, approximately 65 pcm/min when the reactor coolant boron concentration is 1000 ppm and approximately 75 pcm/min when the reactor coolant boron concentration is 100 ppm. The peak burnout rate of xenon is 25 pcm/min (Section 9.1 discusses the capability of the CVCS to counteract xenon decay). Rapid transient reactivity requirements and safety shutdown requirements are met with control rods.

As the boron concentration is increased, the moderator temperature coefficient becomes less negative. The use of soluble boron in the moderator alone would result in a moderator temperature coefficient more positive than that permitted by the Technical Specifications. Therefore, burnable absorber rods are used to reduce the soluble boron concentration sufficiently to insure that the moderator temperature coefficient remains more negative than the Technical Specification limit as a function of power level. The use of control rods may be required early in the cycle at low power to maintain the moderator temperature coefficient more negative than the Technical Specification limit. During operation, the boron content in these burnable absorbers is depleted, adding positive reactivity to offset some of the negative reactivity from fuel depletion and fission product buildup. The depletion rate of the burnable absorbers is not critical because chemical shim is always available and flexible enough to cover any possible deviations in the expected burnable absorber depletion rate. The Unit 2 UFSAR Figure 4.3-3 is a graph of typical core depletion with and without burnable absorber rods. Burnable absorbers, soluble boron, and/or rod withdrawal limits ensure that the moderator temperature coefficient in reload cores is within the limits discussed in Section 3.3.2.3.2.

In addition to reactivity control, the burnable absorber rods or Integral Fuel Burnable Absorbers (IFBAs) are strategically located to provide a favorable radial power distribution. The Unit 2 UFSAR Figures 4.3-4a through 4.3-4c show typical burnable absorber distributions within a fuel assembly for the several burnable absorber patterns used in a 17 x 17 array. A typical reload core integral burnable absorber loading pattern is shown in the Unit 2 UFSAR Figure 4.3-5.

Tables 3.3-1, 3.3-2 and 3.3-3 contain a summary of the reactor core design parameters, including reactivity coefficients, delayed neutron fraction and neutron lifetimes. Sufficient information is included to permit an independent calculation of the nuclear performance characteristics of the core.

3.3.2.2 Power Distributions

The accuracy of power distribution calculations has been confirmed through approximately one thousand flux maps during some twenty years of operation under conditions very similar to those expected from the plant described herein. Details of this confirmation are given in Reference 2 and in Section 3.3.2.2.6.

3.3.2.2.1 Definitions

Power distributions are quantified in terms of hot channel factors. These factors are a measure of the peak pellet power within the reactor core and the total energy produced in a coolant channel and are expressed in terms of quantities related to the nuclear or thermal design, namely:

Power density is the thermal power produced per unit volume of the core (kw/liter).

Linear power density is the thermal power produced per unit length of active fuel (kw/FT). Since fuel assembly geometry is standardized this is the unit of power density most commonly used. For all practical purposes it differs from kw/liter by a constant factor which includes geometry and the fraction of total thermal power which is generated in the fuel rod.

Average linear power density is the total thermal power produced in the fuel rods divided by the total active fuel length of all rods in the core.

Local heat flux is the heat flux at the surface of the cladding ($Btu\text{-}ft^{-2}\text{-}hr^{-1}$). For nominal power rod parameters this differs from linear power density by a constant factor.

Rod power or rod integral power is the length integrated linear power density in one rod (kw).

Average rod power is the total thermal power produced in the fuel rods divided by the number of fuel rods (assuming all rods have equal length).

The hot channel factors used in the discussion of power distributions in this section are defined as follows:

F(Q), Heat Flux Hot Channel Factor, is defined as the maximum local heat flux on the surface of a fuel rod divided by the average fuel rod heat flux, allowing for manufacturing tolerances on fuel pellets and rods.

F(N,Q), Nuclear Heat Flux Hot Channel Factor, is defined as the maximum local fuel rod linear power density divided by the average fuel rod linear power density, assuming nominal fuel pellet and rod parameters.

F(E,Q), Engineering Heat Flux Hot Channel Factor, is the allowance on heat flux required for manufacturing tolerances. The engineering factor allows for local variation in enrichment, pellet density and diameter, surface area of the fuel rod and eccentricity of the gap between pellet and clad.

Combined statistically the net effect is a factor of 1.03 to be applied to fuel rod surface heat flux.

F(N, ΔH), Nuclear Enthalpy Rise Hot Channel Factor, is defined as the ratio of the integral of linear power along the rod with the highest integrated power to the average rod power.

Manufacturing tolerances, hot channel power distribution and surrounding channel power distributions are treated explicitly in the calculation of DNB ratio described in Section 3.4.

It is convenient for the purposes of discussion to define subfactors of F(Q); however, design limits are set in terms of the total peaking factor.

F(Q) = Total peaking factor or heat flux hot-channel factor

$$= \frac{\text{Maximum kw/ft}}{\text{Average kw/ft}} \qquad (3.3\text{-}1)$$

without densification effects

$$F(Q) = F(N,Q) \times F(E,Q) \qquad (3.3\text{-}2)$$

$$= F(N,XY) \times F(N,Z) \times F(N,U) \times F(E,Q)$$

where:

F(N,Q) and F(E,Q) are defined above.

F(N,U) = factor for conservatism, assumed to be 1.05.

F(N,XY) = ratio of peak power density to average power density in the horizontal plane of peak local power.

F(N,Z) = ratio of the power per unit core height in the horizontal plane of peak local power to the average value of power per unit core height. If the plane of the peak local power coincides with the plane of maximum power per unit core height then F(N,Z) is the Core Average Axial Peaking Factor.

To include the allowances made for densification effects, which are height dependent, the following quantities are defined.

S(Z) = the allowance made for densification effects at height Z in the core. See Section 3.3.2.2.5.

P(Z) = ratio of power per unit core height in the horizontal plane at height Z to the average value of power per unit core height.

Then

$$F(Q) = \text{Total peaking factor}$$

$$= \frac{\text{Maximum kw/ft}}{\text{Average kw/ft}}$$

Including densification allowance

$$F(Q) = \max \{F(N,XY)\,(Z) \times P(Z) \times S(Z)\} \times F(N,U) \times F(E,Q) \qquad (3.3\text{-}3)$$

3.3.2.2.2 Radial Power Distributions

The power shape in horizontal sections of the core at full power is a function of the fuel and discrete and integral burnable absorbers loading patterns, and the presence or absence of a single bank of full length control rods. Thus, at any time in the cycle any horizontal section of the core can be characterized as (a) unrodded or (b) with group D control rods. These two situations combined with burnup effects determine the radial power shapes which can exist in the core at full power. The effect on radial power shapes of power level, xenon, samarium and moderator density effects are considered also but these are quite small. The effect of non-uniform flow distribution is negligible. While radial power distributions in various planes of the core are often illustrated, the core radial enthalpy rise distribution as determined by the integral of power up each channel is of greater interest. Figures 3.3-6, 3.3-7, 3.3-8, 3.3-10, and 3.3-11 show representative radial power distributions for one eighth of the core for representative operating conditions. These conditions are (1) Hot Full Power (HFP) at Beginning of Life (BOL) - unrodded - no xenon, (2) HFP at BOL - unrodded - equilibrium xenon, (3) HFP at BOL - Bank D partially in - equilibrium xenon, (4) HFP at Middle of Life - unrodded - equilibrium xenon, and (5) HFP at End of Life - unrodded - equilibrium xenon.

Since the position of the hot channel varies from time to time, a single reference radial design power distribution is selected for DNB calculations. This reference power distribution is chosen conservatively to concentrate power in one area of the core, minimizing the benefits of flow redistribution. Assembly powers are normalized to core average power.

3.3.2.2.3 Assembly Power Distributions

For the purpose of illustration, assembly power distributions from the BOL and EOL conditions corresponding to Figures 3.3-7 and 3.3-10, respectively, are given for the same assembly in Figures 3.3-12 and 3.3-13, respectively.

Since the detailed power distribution surrounding the hot channel varies from time to time, a conservatively flat assembly power distribution is assumed in the DNB analysis, described in Section 3.4, with the rod of maximum integrated power artificially raised to the design value of $F(N, \Delta H)$. Care is taken in the nuclear design of all fuel cycles and all operating conditions to ensure that a flatter assembly power distribution does not occur with limiting values of $F(N, \Delta H)$.

3.3.2.2.4 Axial Power Distributions

The shape of the power profile in the axial or vertical direction is largely under the control of the operator through the automatic (insertion) or manual (withdrawal) motion of full length rods responding to manual operation of the Chemical and Volume Control System. Nuclear effects which cause variations in the axial power shape include moderator density, Doppler effect on resonance absorption, spatial xenon and burnup. Automatically (insertion) or manual (withdrawal) controlled variations in total power output and full length rod motion are also important in determining the axial power shape at any time. Signals are available to the operator from the ex-core ion chambers which are long ion chambers outside the reactor vessel running parallel to the axis of the core. Separate signals are taken from the top and bottom halves of the chambers. The difference between top and bottom signals from each of four pairs of detectors is displayed on the control panel and called the Flux Difference, ΔI. Calculations of core average peaking factor for many plants and measurements from operating plants under many operating situations are associated with either ΔI or axial offset in such a way that an upper bound can be placed on the peaking factor. For these correlations axial offset is defined as:

$$\text{axial offset} = \frac{\theta_t - \theta_b}{\theta_t + \theta_b} \qquad (3.3\text{-}4)$$

Where θ_t and θ_b are the top and bottom detector readings, respectively.

The radial power distribution shown in Figure 3.3-8 and involving the partial insertion of control rods represents a synthesis of power shapes from the rodded and unrodded planes. The applicability of the separability assumption upon which this procedure is based is assured through extensive three-dimensional calculations of possible rodded conditions.

3.3.2.2.5 Local Power Peaking

Fuel densification, which has been observed to occur under irradiation in several operating reactors, causes the fuel pellets to shrink both axially and radially. The pellet shrinkage combined with random hang-up of fuel pellets results in gaps in the fuel column when the pellets below the hung-up pellet settle in the fuel rod. The gaps vary in length and location in the fuel rod. Because of decreased neutron absorption in the vicinity of the gap, power peaking occurs in the adjacent fuel rods resulting in an increased power peaking factor. A quantitative measure of this local power peaking is given by the power spike factor S(Z) where Z is the axial location in the core. The improved methodology described in Reference 52 shows that the penalty due to this is negligible. Results concerning the spike penalty in LOCA analysis show that the power spike penalty should not be included in the LOCA envelope.[28]

3.3.2.2.6 Limiting Power Distributions

According to the ANSI classification of plant conditions, Condition I occurrences are those which are expected frequently or regularly in the course of power operation, maintenance, or maneuvering of the plant. As such, Condition I occurrences are accommodated with margin

between any plant parameter and the value of that parameter which would require either automatic or manual protective action. Inasmuch as Condition I occurrences occur frequently or regularly, they must be considered from the point of view of affecting the consequences of fault conditions (Conditions II, III and IV). In this regard, analysis of each fault condition described is generally based on a conservative set of initial conditions corresponding to the most adverse set of conditions which can occur during Condition I operation.

The list of steady state and shutdown conditions, permissible deviations and operational transients is given in Section 14.D. Implicit in the definition of normal operation is proper and timely action by the reactor operator. That is, the operator follows recommended operating procedures for maintaining appropriate power distributions and takes any necessary remedial actions when alerted to do so by the plant instrumentation. Thus, as stated above, the worst or limiting power distribution which can occur during normal operation is to be considered at the starting point for analysis of ANSI Conditions II, III and IV events.

Improper procedural actions or errors by the operator are assumed in the design as occurrences of moderate frequency (ANSI Condition II). Some of the consequences which might result are listed in Section 14.1. Therefore, the limiting power shapes which result from such Condition II events, are those power shapes which deviate from the normal operating condition at the recommended axial offset band, e.g. due to lack of proper action by the operator during a xenon transient following a change in power level brought about by control rod motion. Power shapes which fall in this category are used for determination of the reactor protection system setpoints so as to maintain margin to overpower or DNB limits.

The means for maintaining power distributions within the required hot channel factor limits are described in the Technical Specifications. A complete discussion of power distribution control in Westinghouse PWRs is included in Reference 4. Detailed information on the design constraints on local power density in a Westinghouse PWR, on the defined operating procedures and on the measures taken to preclude exceeding design limits is presented in the Westinghouse Topical Reports and power distribution control and load following procedures.[29] The following paragraphs summarize these reports and describe the calculations used to establish the upper bound on peaking factors.

The calculations used to establish the upper bound on peaking factors, F(Q) and F(ΔH), include all of the nuclear effects which influence the radial and/or axial power distributions throughout core life for various modes of operation including load follow, reduced power operation, and axial xenon transients.

Radial power distributions are calculated for the full power condition and fuel and moderator temperature feedback effects are included for the average enthalpy plane of the reactor. The steady state nuclear design calculations are done for normal flow with the same mass flow in each channel and flow redistribution effects neglected. The effect of flow redistribution is calculated explicitly where it is important in the DNB analysis of accidents. The effect of xenon on radial power distribution is small (compare Figures 3.3-6 and 3.3-7) but is included as part of the normal design process. Radial power distributions are relatively fixed and easily bounded with upper limits.

The core average axial profile, however, can experience significant changes which can occur rapidly as a result of rod motion and load changes and more slowly due to xenon distribution.

For the study of points of closest approach to axial power distribution limits, several thousand cases are examined. Since the properties of the nuclear design dictate what axial shapes can occur, boundaries on the limits of interest can be set in terms of the parameters which are readily observed on the plant. Specifically, the nuclear design parameters which are significant to the axial power distribution analysis are:

1. core power level
2. core height
3. coolant temperature and flow
4. coolant temperature program as a function of reactor power
5. fuel cycle lifetimes
6. rod bank worths
7. rod bank overlaps.

Normal operation of the plant assumes compliance with the following conditions:

1. Control rods in a single bank move together with no individual rod insertion differing by more than 12 steps (indicated) from the bank demand position
2. Control banks are sequenced with overlapping banks
3. The control full length bank insertion limits are not violated
4. Axial power distribution procedures, which are given in terms of flux difference control and control bank position, are observed.

The axial power distribution procedures referred to above are part of the required operating procedures which are followed in normal operation.

Limits placed on the axial flux difference are designed to assure that the heat flux hot channel factor F_Q is maintained within acceptable limits. The constant axial offset control (CAOC) operating procedures described in reference 29 require control of the axial flux difference at all power levels within a permissible operating band about a target value corresponding to the equilibrium full power value. The Relaxed Axial Offset Control (RAOC) procedures to be implemented in Unit 1 Cycle 18 and beyond, described in Reference 53, were developed to provide wider control band widths and, consequently, more operating flexibility. These wider operating limits, particularly at lower power levels, can increase plant availability by allowing quicker plant startups and increased maneuvering flexibility.

Further operating flexibility is achieved by combining RAOC operation with an F_Q Surveillance Technical Specification. $F_{XY}(Z)$ Surveillance requires periodic plant surveillance on the height dependent radial peaking factor, $F_{XY}(Z)$, for partial verification that operation will not cause the $F_Q(Z)$ limit to be exceeded. In the F_Q Surveillance Technical Specification to be implemented in Unit 1 Cycle 18, $F_{XY}(Z)$ Surveillance will be replaced by $F_Q(Z)$ Surveillance. Monitoring $F_Q(Z)$ and increasing the measured value for expected plant maneuvers provides a more convenient

form of assuring plant operation below the $F_Q(Z)$ limit while retaining the intent of using a measured parameter to verify Technical Specification compliance.

In standard CAOC analysis described in Reference 29, the generation of the normal operation power distribution is constrained by the rod insertion limits (RIL) and the ΔI band limits. The purpose of RAOC is to find the widest permissible ΔI-Power operating space by analyzing a wide range of ΔI. Therefore, the generation of normal operation power distributions is constrained only by the RIL for RAOC.

For a CAOC analysis, load-follow simulations are performed covering the allowed CAOC operating space to generate a typical range of allowed axial xenon distributions, which in turn are used to calculate axial power distributions in both normal operation and Condition II accident conditions. For a RAOC analysis, however, a reconstruction model described in Reference 44 is used as a more practical method to create axial xenon distributions covering the wider ΔI-Power operating space allowed with RAOC operation. Each resulting power shape is analyzed to determine if LOCA constraints are met or exceeded. The total peaking factor, F^T_Q is determined using standard synthesis methods as described in Reference 29.

The envelope drawn over the calculated F(Q) points in Figure 3.3-21 represents an upper bound envelope on local power density versus elevation in the core. It should be emphasized that this envelope is a conservative representation of the bounding values of local power density. Expected values are considerably smaller and, in fact, less conservative bounding values may be justified with additional analysis or surveillance requirements. For example, Figure 3.3-21 bounds both BOL and EOL conditions but without consideration of radial power distribution flattening with burnup, i.e., both BOL and EOL points presume the same radial peaking factor. Inclusion of the burnup flattening effect would reduce the local power densities corresponding to EOL conditions which may be limiting at the higher core elevations. The calculated values have been increased by a factor of 1.05 for measurement error, a factor of 1.03 for the manufacturing tolerances.

Allowing for fuel densification effects the average kw/ft at 2900 MWt is 5.69 kw/ft. From Figure 3.3-21, the conservative upper bound value of normalized local power density, including uncertainty allowances is 2.40 corresponding to a peak local power density of 13.74 kw/ft at 100.6 percent power.

To determine reactor protection system set points, with respect to power distributions, three categories of events are considered, namely rod control equipment malfunctions, operator errors of commission and operator errors of omission.

The first category comprises uncontrolled rod withdrawal (with rods moving in the normal bank sequence) for full length banks. Also included are motions of the full length banks below their insertion limits, which could be caused, for example, by uncontrolled dilution or primary coolant cooldown. Power distributions were calculated throughout these occurrences assuming short term corrective action, that is no transient xenon effects were considered to result from the malfunction. The event was assumed to occur from typical normal operating situations which did include normal xenon transients. It was further assumed in determining the power distributions that total power level would be limited by reactor trip to below 118%. Since the

study is to determine protection limits with respect to power and axial offset, no credit was taken for trip set point reduction due to flux difference. The results are given in Figure 3.3-23 in units of kw/ft. The peak power density which can occur in such events, assuming reactor trip at or below 118%, is less than that required for center line melt, including uncertainties and densification effects.

The second category also appearing in Figure 3.3-23, assumes that the operator mis-positions the full length rod bank in violation of the insertion limits and creates short term conditions not included in normal operating conditions.

The third category assumes that the operator fails to take action to correct a flux difference violation. Figure 3.3-23A illustrates the behavior of the peak power under these conditions. The points represent the calculated F(Q) multiplied by 100% power plus the calorimetric error. The calorimetric error is 0.6% using a Leading Edge Flow Meter (LEFM) for calorimetric power. If the LEFM is unavailable, then the calorimetric error is 2%, with decreased RTP (Refer to Licensing Requirements Manual). The behavior of the peak power is essentially as illustrated, with the actual peak power values remaining below 20 kw/ft. The figure shows that, provided the assumed error in operation does not continue for a period which is long compared to the xenon time constant, the maximum local power does not exceed 20.0 kw/ft including the above factors. However, the Technical Specifications (COLR) restrict operation with F(Q) such that this peak linear power density is less than 22.4 kw/ft. These events are considered Condition II events.

It should be noted that a reactor overpower accident is not assumed to occur coincident with an independent operator error.

Analyses of possible operating power shapes for the reactor described herein show that the appropriate hot channel factors F(Q) and $F(N,\Delta H)$ for peak local power density and for DNB analysis at full power are described in the Beaver Valley Unit 1 Core Operating Limits Report (COLR).

F(Q) can be increased with decreasing power as shown in the Technical Specifications. Increasing $F(N,\Delta H)$ with decreasing power is permitted by the DNB protection set points and allows radial power shape changes with rod insertion to the insertion limits as described in Section 3.4.3.2. It has been determined that provided the above conditions 1 through 4 are observed, the Technical Specification limits are met.

When a situation is possible in normal operation which could result in local power densities in excess of those assumed as the pre-condition for a subsequent hypothetical accident, but which would not itself cause fuel failure, administrative controls and alarms are provided for returning the core to a safe condition. These alarms are described in detail in Sections 7.

3.3.2.2.7 Experimental Verification of Power Distribution Analysis

This subject is discussed in depth in Reference 2. A summary of this report is given here.

In a measurement of peak local power density, F(Q), with the movable detector system described in Section 7.7.1 and 3.4.5, the following uncertainties have to be considered:

1. reproducibility of the measured signal

2. errors in the calculated relationship between detector current and local flux

3. errors in the calculated relationship between detector flux and peak rod power some distance from the measurement thimble.

The appropriate allowance for (1) above has been quantified by repetitive measurements made with several intercalibrated detectors by using the common thimble features of the in-core detector system. This system allows more than one detector to access any thimble. Errors in category (2) above are quantified to the extent possible, by using the fluxes measured at one thimble location to predict fluxes at another location which is also measured. Local power distribution predictions are verified in critical experiments on arrays of rods with simulated guide thimbles, control rods, burnable poisons, etc. These critical experiments provide quantification of errors of types (2) and (3) above.

Reference 2 describes critical experiments performed at the Westinghouse Reactor Evaluation Center and measurement taken on two Westinghouse plants with in-core systems of the same type as used in the plant described herein. The report concludes that the uncertainty associated with the peak nuclear heat flux factor, F(Q) is 4.58% at the 95% confidence level with only 5% of the measurements greater than the inferred value. This is the equivalent of a 2 σ limit on a normal distribution and is the uncertainty to be associated with a full core flux map with movable detectors reduced with a reasonable set of input data incorporating the influence of burnup on the radial power distribution. The uncertainty is usually rounded up to 5%. An additional increase to the uncertainty of F_Q for reduced flux thimble availability is discussed in Sections 3.3.7 and 5.1.6 of the Licensing Requirements Manual.

In comparing measured power distributions (or detector currents) against the calculations for the same situation it is not possible to subtract out the detector reproducibility. Thus a comparison between measured and predicted power distributions has to include some measurement error. Such a comparison is given in Figure 3.3-24 for one of the maps used in Reference 2. Since the first publication of the report, hundreds of maps have been taken on these and other reactors. The results confirm the adequacy of the 5% uncertainty allowance on F(Q).

A similar analysis for the uncertainty in F(ΔH) (rod integral power) measurements results in an allowance of 3.65% at the equivalent of a 2 σ confidence level. For historical reasons, an 8% uncertainty factor is allowed in the nuclear design basis; that is, the predicted rod integral at full power must not exceed the design F(ΔH) less 8%. This 8% may be reduced in final design to 4% to allow a wider range of acceptable axial power distributions in the (Departure from Nucleate Boiling) analysis and still meet the design bases of Section 3.3.1.3. An additional increase to the uncertainty of $F^N_{\Delta H}$ for reduced flux thimble availability is discussed in Sections 3.3.7 and 5.1.7 of the Licensing Requirements Manual.

A measurement in the second cycle of a 121 assembly, 12 foot, core is compared with a simplified one dimensional core average axial calculation in Figure 3.3-25. This calculation does not give explicit representation to the fuel grids.

The accumulated data on power distributions in actual operation is basically of three types.

1. Much of the data is obtained in steady state operation at constant power in the normal operating configuration.

2. Data with unusual values of axial offset are obtained part of the ex-core detector calibration exercise which is performed monthly.

3. Special tests have been performed in the load follow and other transient xenon conditions which have yielded useful information on power distributions.

These data are presented in detail in Reference 5. Figure 3.3-26 contains a summary of measured values of F(Q) as a function of axial offset for five plants from the report.

3.3.2.2.8 Testing

A very extensive series of physics tests is performed on first cores. These tests and the criteria for satisfactory results are described in detail in Section 13. Since not all limiting situations can be created at beginning of life, the main purpose of the tests is to provide a check on the calculational methods used in the predictions for the conditions of the test. Tests are performed at the beginning of each reload cycle to verify that the physics models used to predict the core's behavior (power distributions, reactivity parameters, and kinetics parameters) are accurate and reflect the actual reload core characteristics.

3.3.2.2.9 Monitoring Instrumentation

The adequacy of instrument numbers, spatial deployment, required correlations between readings and peaking factors, calibration and errors are described in References 2, 4, and 5. The relevant conclusions are summarized here in Section 3.3.2.2.7 and 3.4.5.

Provided the limitations given in Section 3.3.2.2.6 on rod insertion and flux difference are observed, the ex-core detector system provides adequate monitoring of power distributions.

Further details of specific limits on the observed rod positions and flux difference are given in the Technical Specifications and the Licensing Requirements Manual, together with a discussion of their bases.

Limits for alarms, reactor trip, etc. are given in the Technical Specifications. Descriptions of the systems provided are given in Section 7.

3.3.2.3 Reactivity Coefficients

The kinetic characteristics of the reactor core determine the response of the core to changing plant conditions or to operator adjustments made during normal operation, as well as the core response during abnormal or accidental transients. These kinetic characteristics are quantified in reactivity coefficients. The reactivity coefficients reflect the changes in the neutron multiplication due to varying plant conditions such as power, moderator or fuel temperatures, or less significantly due to a change in pressure or void conditions. Since reactivity coefficients change during the life of the core, ranges of coefficients are employed in transient analysis to determine the response of the plant throughout life. The results of such simulations and the reactivity coefficients used are presented in Chapter 14. The analytical methods and calculational models used in calculating the reactivity coefficients are given in Section 3.3.3. These models have been confirmed through extensive testing of abnormal or accidental transients. These kinetic characteristics are quantified in reactivity coefficients. These models have been confirmed through extensive testing of more than thirty cores similar to the plant described herein; results of these tests are discussed in Section 3.3.3. Quantitative information for calculated reactivity coefficients, including fuel-Doppler coefficient, moderator coefficients (density, temperature, pressure, void) and power coefficient is given in the following sections.

3.3.2.3.1 Fuel Temperature (Doppler) Coefficient

The fuel temperature (Doppler) coefficient is defined as the change in reactivity per degree change in effective fuel temperature and is primarily a measure of the Doppler broadening of U-238 and Pu-240 resonance absorption peaks. Doppler broadening of other isotopes such as U-236, Np-237, etc., are also considered but their contributions to the Doppler effect are small. An increase in fuel temperature increases the effective resonance absorption cross sections of the fuel and produces a corresponding reduction in reactivity.

The fuel temperature coefficient is calculated by performing two- group two or three dimensional calculations using an updated version of the Advanced Nodal Code (ANC)[39]. Moderator temperature is held constant and the power level is varied. Spatial variation of fuel temperature is taken into account by calculating the effective fuel temperature as a function of power density as discussed in Section 3.3.3.1.

The Doppler temperature coefficient is shown as Figure 3.3-27 as a function of the effective fuel temperature (at beginning-of-life and end-of-life conditions). The effective fuel temperature is lower than the volume averaged fuel temperature since the neutron flux distribution is non-uniform through the pellet and gives preferential weight to the surface temperature. The Doppler-only contribution to the power coefficient, defined later, is shown in Figure 3.3-28 as a function of relative core power. The integral of the differential curve on Figure 3.3-28 is the Doppler contribution to the power defect and is shown in Figure 3.3-29 as a function of relative power. The Doppler coefficient becomes more negative as a function of life as the Pu-240 content increases, thus increasing the Pu-240 resonance absorption but less negative as the fuel temperature changes with burnup as described in Section 3.3.3.1. The upper and lower limits of Doppler coefficient used in accident analyses are given in Section 14.

3.3.2.3.2 Moderator Coefficients

The moderator coefficient is a measure of the change in reactivity due to a change in specific coolant parameters such as density, temperature, pressure or void. The coefficients so obtained are moderator density, temperature, pressure and void coefficients.

Moderator Density and Temperature Coefficients

The moderator temperature (density) coefficient is defined as the change in reactivity per degree change in the moderator temperature. Generally, the effect of the changes in moderator density as well as the temperature are considered together. A decrease in moderator density means less moderation which results in a negative moderator coefficient. An increase in coolant temperature, keeping the density constant, leads to a hardened neutron spectrum and results in an increase in resonance absorption in U-238, Pu-240 and other isotopes. The hardened spectrum also causes a decrease in the fission to capture ratio in U-235 and Pu-239. Both of these effects make the moderator coefficient more negative. Since water density changes more rapidly with temperature as temperature increases, the moderator temperature (density) coefficient becomes more negative with increasing temperature.

The soluble boron used in the reactor as a means of reactivity control also has an effect on moderator density coefficient since the soluble boron poison density as well as the water density is decreased when the coolant temperature rises. A decrease in the soluble poison concentration introduces a positive component in the moderator coefficient.

Thus if the concentration of soluble poison is large enough, the net value of the coefficients may be positive. With integral or discrete burnable absorbers present, however, the beginning of life hot boron concentration is sufficiently low that the moderator temperature coefficient is non-positive at 100 percent, less than +2.0 pcm/°F below 70 percent, and less than a linearly decreasing limit of +2.0 pcm/°F between 70 percent power to 100 percent power, respectively. The effect of control rods is to make the moderator coefficient more negative by increasing the "leakage" of the core.

With burnup, the moderator coefficient becomes more negative primarily as a result of boric acid dilution but also to a significant extent from the effects of the buildup of plutonium and fission products.

The moderator coefficient is calculated for the various plant conditions discussed above by performing two-group two or three dimensional calculations, varying the moderator temperature (and density) by about ±5°F about each of the mean temperatures. The moderator coefficient is shown as a function of core temperature and boron concentration for the unrodded and rodded core in Figures 3.3-30, 3.3-31, and 3.3-32. The temperature range covered is from cold (68°F) to about 600°F. The contribution due to Doppler coefficient (because of change in moderator temperature) has been subtracted from these results. Figure 3.3-33 shows the hot, full power moderator temperature coefficient plotted as a function of first cycle lifetime for the just critical boron concentration condition based on the design boron letdown condition.

The moderator coefficients presented here are calculated on corewise basis, since they are used to describe the core behavior in normal and accident situations when the moderator temperature changes can be considered to affect the whole core.

Moderator Pressure Coefficient

The moderator pressure coefficient relates the change in moderator density, resulting from a reactor coolant pressure change, to the corresponding effect on neutron production. This coefficient is of much less significance in comparison with the moderator temperature coefficient. A change of 50 psi in pressure has approximately the same effect on reactivity as a half-degree change in moderator temperature. This coefficient can be determined from the moderator temperature coefficient by relating change in pressure to the corresponding change in density. The moderator pressure coefficient is negative over a portion of the moderator temperature range at beginning of life (-0.004 pcm/psi, BOL) but is always positive at operating conditions and becomes more positive during life (+0.3 pcm/psi, EOL).

Moderator Void Coefficient

The moderator void coefficient relates the change in neutron multiplication to the presence of voids in the moderator. In a PWR this coefficient is not very significant because of the low void content in the coolant. The core void content is less than one-half of the one percent and is due to local or statistical boiling. The void coefficient varies from 50 pcm/% void at BOL and at low temperatures to -250 pcm/% void at EOL and at operating temperatures. The negative void coefficient at operating temperature becomes more negative with fuel burnup.

3.3.2.3.3 Power Coefficient

The combined effect of moderator temperature and fuel temperature change as the core power level changes is called the total power coefficient and is expressed in terms of reactivity change per percent power change. The power coefficient at BOL and EOL conditions is given in Figure 3.3-34.

It becomes more negative with burnup reflecting the combined effect of moderator and fuel temperature coefficients with burnup. The power defect (integral reactivity effect) at BOL and EOL is given in Figure 3.3-35.

3.3.2.3.4 Comparison of Calculated and Experimental Reactivity Coefficients

Section 3.3.3 describes the comparison of calculated and experimental reactivity coefficients in detail. Based on the data presented there, the accuracy of the current analytical model is:

1. $\pm$ .2%$\Delta\rho$ for Doppler and power defect
2. $\pm$ 2 pcm/°F for the moderator coefficient

Experimental evaluation of the calculated coefficients was done during the physics startup tests described in Section 13.

3.3.2.3.5 Reactivity Coefficients Used in Transient Analysis

Table 3.3-2 gives the representative ranges for the reactivity coefficients used in transient analysis. The exact values of the coefficient used in the analysis depend on whether the transient of interest is examined at the beginning or end of life, whether most negative or the most positive (least negative) coefficients are appropriate, and whether spatial nonuniformity must be considered in the analysis. Conservative values of coefficients, considering various aspects of analysis, are used in the transient analysis. The transient analyses are described in Section 14.

The values listed in Table 3.3-2 and illustrated in Figures 3.3-27, 3.3-28, 3.3-29, 3.3-30, 3.3-31, 3.3-32, 3.3-33, 3.3-34, and 3.3-35 apply to Cycle 1. The coefficients appropriate for use in subsequent cycles depend on the core operating history, the number and enrichment of fresh fuel assemblies, the loading pattern of burned and fresh fuel, the number and location of any integral or discrete burnable absorbers, etc. The need for a reevaluation of any accident in a subsequent cycle is contingent upon whether or not the coefficients for that cycle fall within the identified range used in the analysis presented in Section 14. Control rod requirements are given in Table 3.3-3 for Cycle 1 and for a hypothetical equilibrium cycle since these are markedly different. These latter numbers are provided for information only and their validity in a particular cycle would be an unexpected coincidence.

3.3.2.4 Control Requirements

To insure the shutdown margin stated in the Technical Specifications under conditions where a cooldown to ambient temperature is required, concentrated soluble boron is added to the coolant. Boron concentrations for several core conditions are listed in Table 3.3-2. For all core conditions including refueling, the boron concentration is well below the solubility limit. The rod cluster control assemblies are employed to bring the reactor to the hot shutdown condition. The minimum required shutdown margin is given in the Technical Specifications.

The ability to accomplish the shutdown for hot conditions is demonstrated in Table 3.3-3 by comparing the difference between the Rod Cluster Control Assembly reactivity available with an allowance for the worst stuck rod with that required for control and protection purposes. The shutdown margin includes an allowance of 10 percent for analytic uncertainties (see Section 3.3.2.4.9). The largest reactivity control requirement appears at the end-of-life (EOL) when the moderator temperature coefficient reaches its peak negative value as reflected in the larger power defect.

The control rods are required to provide sufficient reactivity to account for the power defect from full power to zero power and to provide the required shutdown margin. The reactivity addition resulting from power reduction consists of contributions from Doppler, variable average moderator temperature, flux redistribution, and reduction in void content as discussed below.

3.3.2.4.1 Doppler

The Doppler effect arises from the broadening of U-238 and Pu-240 resonance peaks with an increase in effective pellet temperature. This effect is most noticeable over the range of zero power to full power due to the large pellet temperature increase with power generation.

3.3.2.4.2 Variable Average Moderator Temperature

When the core is shutdown to the hot, zero power condition, the average moderator temperature changes from the equilibrium full load value determined by the steam generator and turbine characteristics (steam pressure, heat transfer, tube fouling, etc.) to the equilibrium no load value, which is based on the steam generator shell side design pressure. The design change in temperature is conservatively increased by 4°F to account for the control dead band and measurement errors.

Since the moderator coefficient is negative (except for early in core life), there is a reactivity addition with power reduction. The moderator coefficient becomes more negative as the fuel depletes because the boron concentration is reduced. This effect is the major contributor to the increased requirement at end of life.

3.3.2.4.3 Redistribution

During full power operation the coolant density decreases with core height. This, together with partial insertion of control rods, results in less fuel depletion near the top of the core. Under steady state conditions, the relative power distribution will be slightly asymmetric towards the bottom of the core. On the other hand, at hot zero power conditions, the coolant density is uniform up the core, and there is no flattening due to Doppler. The result will be a flux distribution which at zero power can be skewed toward the top of the core. The reactivity insertion due to the skewed distribution is calculated with an allowance for the most adverse effects of xenon distribution.

3.3.2.4.4 Void Content

A small void content in the core is due to nucleate boiling at full power. The void collapse coincident with power reduction makes a small reactivity contribution.

3.3.2.4.5 Rod Insertion Allowance

At full power, the control bank is operated within a prescribed band of travel to compensate for small periodic changes in boron concentration, changes in temperature and very small changes in the xenon concentration not compensated for by a change in boron concentration. When the control bank reaches either limit of this band, a change in boron concentration is required to compensate for additional reactivity changes. Since the insertion limit is set by a rod travel limit, a conservatively high calculation of the inserted worth is made which exceeds the normally inserted reactivity.

3.3.2.4.6 Installed Excess Reactivity for Depletion

Excess reactivity of 10% $\Delta\rho$ to 25%$\Delta\rho$ (hot) is installed at the beginning of each cycle to provide sufficient reactivity to compensate for fuel depletion and fission products throughout the cycle. This reactivity is controlled by the addition of soluble boron to the coolant and by burnable absorbers. The soluble boron concentration for several core configurations, the unit boron worth, and burnable absorber worth are given in Tables 3.3-1 and 3.3-2. Since the excess reactivity for burnup is controlled by soluble boron and/or burnable absorbers, it is not included in control rod requirements.

3.3.2.4.7 Xenon and Samarium Poisoning

Changes in xenon and samarium concentrations in the core occur at a sufficiently slow rate, even following rapid power level changes, that the resulting reactivity change is controlled by changing the soluble boron concentration.

3.3.2.4.8 pH Effects

Changes in reactivity due to a change in coolant pH, if any, are sufficiently small in magnitude and occur slowly enough to be controlled by the boron system. Further details are available in Reference 6.

3.3.2.4.9 Experimental Confirmation

Following a normal shutdown, the total core reactivity change during cooldown with a stuck rod has been measured on a 121 assembly, 10 ft high core and a 121 assembly, 12 ft high core. In each case, the core was allowed to cool down until it reaches criticality simulating the steamline break accident. For the ten foot core, the total reactivity change associated with the cooldown is overpredicted by about 0.3% with respect to the measured result. This represents an error of about 5% in the total reactivity change and is about half the uncertainty allowance for this quantity. For the 12 ft core, the difference between the measured and predicted reactivity change was an even smaller 0.2%$\Delta\rho$. These measurements and others demonstrate the ability of the methods described in Section 3.3.3 to accurately predict the total shutdown reactivity of the core.

3.3.2.5 Control

Core reactivity is controlled by means of a chemical poison dissolved in the coolant, Rod Cluster Control Assemblies, and integral and/or discrete burnable absorbers as described below.

3.3.2.5.1 Chemical Poison

Boron in solution as boric acid is used to control relatively slow reactivity changes associated with:

1. The moderator temperature defect in going from cold shutdown at ambient temperature to the hot operating temperature at zero power.

2. The transient xenon and samarium poisoning, such as that following power changes or changes in Rod Cluster Control position.

3. The excess reactivity required to compensate for the effects of fissile inventory depletion and buildup of long-life fission products.

4. The integral and/or discrete burnable absorber depletion.

The boron concentrations for various core conditions are presented in Table 3.3-2.

3.3.2.5.2 Rod Cluster Control Assemblies

The rod cluster control assemblies employed are full-length assemblies. The number of full-length assemblies are shown in Table 3.3-1. The full-length rod cluster control assemblies are used for shutdown and control purposes to offset fast reactivity changes associated with:

1. The required shutdown margin in the hot zero power, stuck rods condition

2. The reactivity compensation as a result of an increase in power above hot zero power (power defect including Doppler, and moderator reactivity changes)

3. Unprogrammed fluctuations in boron concentration, coolant temperature, or xenon concentration (with rods not exceeding the allowable rod insertion limits)

4. Reactivity ramp rates resulting from load changes.

The allowed full-length control bank reactivity insertion is limited at full power to maintain shutdown capability. As the power level is reduced, control rod reactivity requirements are also reduced and more rod insertion is allowed. The control bank position is monitored and the operator is notified by an alarm if the limit is approached. The determination of the insertion limit uses conservative xenon distributions. In addition, the rod cluster control assembly withdrawal pattern determined from these analyses is used in determining power distribution factors and in determining the maximum worth of an inserted rod cluster control assembly ejection accident. For further discussion, refer to the Technical Specifications on rod insertion limits.

Power distribution, rod ejection and rod misalignment analyses are based on the arrangement of the shutdown and control groups of the rod cluster control assemblies shown in Figure 3.3-36. All shutdown rod cluster control assemblies are withdrawn before withdrawal of the control banks is initiated. In going from zero to 100 percent power, control banks A, B, C and D are withdrawn sequentially. The limits of rod positions and further discussion on the basis for rod insertion limits are provided in the Technical Specifications.

3.3.2.5.3 Power Shaping With the Part-Length Control Rod Bank

Part-length rods are no longer permitted in the core and have been removed from the reactor vessel.

3.3.2.5.4 Integral and Discrete Burnable Absorbers

The integral and/or discrete burnable absorbers provide partial control of the excess reactivity available during the first fuel cycle and may be used for any reload to optimize fuel loading. In doing so, these absorbers ensure that the moderator temperature coefficient is within the limits discussed in Section 3.3.2.3.2. They perform this function by reducing the requirement for soluble boron in the moderator at the beginning of the first fuel cycle as described previously. For purposes of illustration, a typical burnable absorber pattern in the core is shown in the Unit 2 UFSAR Figure 4.3-5, while the arrangements within an assembly are displayed in the Unit 2 UFSAR Figure 4.3-4. The initial reactivity worth of these rods is shown in Table 3.3-1. The boron in the absorbers is depleted with burnup but at a sufficiently slow rate so that the resulting critical concentration of soluble boron concentration is such that the moderator temperature coefficient remains within the limits discussed in Section 3.3.2.3.2 at all times for power operating conditions.

3.3.2.5.5 Peak Xenon Startup

Compensation for the peak xenon buildup is accomplished using the boron control system. Startup from the peak xenon condition is accomplished with a combination of rod motion and boron dilution. The boron dilution may be made at any time, including during the shutdown period, provided the shutdown margin is maintained.

3.3.2.5.6 Load Follow Control and Xenon Control

During load follow maneuvers, power changes are accomplished using control rod motion and dilution or boration by the boron system as required. Control rod motion is limited by the control rod insertion limits on the full-length rods as provided in the Technical Specifications and discussed in Sections 3.3.2.5.2. Reactivity changes due to the changing xenon concentration can be controlled by rod motion and/or changes in the soluble boron concentration.

3.3.2.5.7 Burnup

Control of the excess reactivity for burnup is accomplished using soluble boron and/or burnable absorbers. The boron concentration must be limited during operating conditions to ensure the moderator temperature coefficient is within the limits discussed in Section 3.3.2.3.2. Sufficient burnable absorbers are installed at the beginning of a cycle to provide the desired cycle lifetime, and limit the boron concentration to ensure that the moderator temperature coefficient limits discussed in Section 3.3.2.3.2 are achieved. The practical minimum boron concentration is 10 ppm.

3.3.2.6 Control Rod Patterns and Reactivity Worth

The full-length Rod Cluster Control Assemblies are designated by function as the control groups and the shutdown groups. The terms "group" and "bank" are used synonymously throughout this report to describe a particular grouping of control assemblies. The Rod Cluster Assembly pattern is displayed in Figure 3.3-36 which is not expected to change during the life of the plant. The control banks are labeled A, B, C and D and the shutdown banks are labeled SA, SB, etc., as applicable. Each bank, although operated and controlled as a unit, is comprised of two subgroups. The axial position of the full-length Rod Cluster Control Assemblies may be controlled manually or automatically. These Rod Cluster Control Assemblies are all dropped into the core following actuation of reactor trip signals.

Two criteria have been employed for selection of the control groups. First, the total reactivity worth must be adequate to meet the requirements specified in Table 3.3-3. Second, in view of the fact that these rods may be partially inserted at power operation, the total power peaking factor should be low enough to ensure that the power capability requirements are met. Analyses indicate that the first requirement can be met either by a single group or by two or more banks whose total worth equals at least the required amount. The axial power shape would be more peaked following movement of a single group of rods worth three to four percent ΔP; therefore, four banks (described as A, B, C and D in Figure 3.3-36) each worth approximately one percent ΔP have been selected.

The position of control banks for criticality under any reactor condition is determined by the concentration of boron in the coolant. On an approach to criticality, boron is adjusted to ensure that criticality will be achieved with control rods above the insertion limit set by shutdown and other considerations (see the Technical Specifications). Early in the cycle there may also be a rod withdrawal limit at low power to maintain the moderator temperature coefficient within the limits discussed in Section 3.3.2.3.2. Usual practice is to adjust boron to ensure that the rod position lies within the so-called maneuvering band, that is, such that an escalation from zero power to full power does not require extensive adjustment of boron concentration.

Ejected rod worths are given in Section 14.2.6 for several different conditions. Experimental confirmation of these worths can be found by reference to startup test reports such as Reference 7.

Allowable deviations due to misaligned control rods are discussed in the Technical Specifications.

A representative calculation for two banks of control rods withdrawn simultaneously (rod withdrawal accident) is given in Figure 3.3-37.

Calculation of control rod reactivity worth versus time following reactor trip involves both control rod velocity and differential reactivity worth. The rod position versus time of travel after rod release assumed is given in Figure 14D-2. For nuclear design purposes, the reactivity worth versus rod position is calculated by a series of steady state calculations at various control rod positions assuming all rods out of the core as the initial position in order to minimize the initial reactivity insertion rate. Also, to be conservative, the rod of highest worth is assumed stuck out of the core and the flux distribution (and thus reactivity importance) is assumed to be skewed to the bottom of the core. The result of these calculations is shown on Figure 3.3-39.

The shutdown groups provide additional negative reactivity to assure an adequate shutdown margin. Shutdown margin is defined as the amount by which the core would be subcritical at hot shutdown if all Rod Cluster Assemblies are tripped, but assuming that the highest worth assembly remains fully withdrawn and no changes in xenon or boron concentration take place. The loss of control rod worth due to the material irradiation is negligible since only bank D may be in the core under normal operating conditions.

The values given in Table 3.3-3 show that the available reactivity in withdrawn Rod Cluster Control Assemblies provides the design bases minimum shutdown margin allowing for the highest worth cluster to be at its fully withdrawn position. An allowance for uncertainty in the calculated worth of N-1 rods is made before determination of the shutdown margin.

3.3.2.7 Criticality of Fuel Assemblies

Criticality of fuel assemblies outside the reactor is precluded by adequate design of fuel transfer, shipping and storage facilities, and by administrative control procedures. The three principal methods of preventing criticality are limiting the fuel assembly storage configuration, limiting assembly interaction by fixing the minimum separation between assemblies, and the installation of neutron absorbing material (Boral) in the high density spent fuel rack walls.

The design basis for preventing criticality outside the reactor is that, considering possible variations, there is a 95 percent probability at a 95 percent confidence level (95/95) that the effective multiplication factor (k_{eff}) of the fuel assembly array will be less than 0.95 as recommended in ANSI 57.2-1983, ANSI 57.3-1983 and Reference 33. For the case of low density optimum moderation or aqueous foam conditions (required for fresh fuel racks only), the 95/95 K_{eff} value will be less than 0.98 as recommended by NUREG-0800. The following are the conditions that are assumed in meeting this design basis:

1. The fuel assembly contains the highest enrichment authorized without any control rods or any noncontained burnable poison and is at its most reactive point in life.

2. For fully flooded conditions, the moderator is pure water at a density of 1.0 gm/cm^3 which conservatively bounds the normal range of spent fuel pool water temperatures and results in maximum spent fuel pool or fresh fuel rack reactivity.

3. For the low density optimum moderation (aqueous foam) analysis of the fresh fuel racks, a water density of 0.07 gm/cm^3 was assumed.

4. The array is either infinite in lateral extent or is surrounded by a conservatively chosen reflector, whichever is appropriate for the design.

5. Mechanical uncertainties are treated by either using "worst case" conditions or by performing sensitivity studies and obtaining appropriate uncertainties.

6. No credit is taken for any spacer grids or spacer sleeves.

7. No credit is taken for any U^{234} or U^{236} in the fuel.

8. Where borated water is present, credit for the dissolved boron is not taken, except under postulated accident conditions where the double contingency principle of ANSI N16.1-1975 is applied. This principle states that it shall require at least two unlikely, independent, and concurrent events to produce a criticality accident.

The design methods used conform with ANSI N18.2-1973, Nuclear Safety Criteria for the Design of Stationary Pressurized Water Reactor Plants, Section 5.7, Fuel Handling System; ANSI 57.2-1983, Design Objectives for LWR Spent Fuel Storage Facilities at Nuclear Power Stations, Section 6.4.2; ANSI N16.9-1975, Validation of Calculational Methods for Nuclear Criticality Safety; NRC Standard Review Plan, Section 9.1.2, Spent Fuel Storage; and the NRC guidance, NRC Position for Review and Acceptance of Spent Fuel Storage and Handling Applications; ANSI 57.3-1983, Design Requirements for New Fuel Storage Facilities at Light Water Reactor Plants.

3.3.2.7.1 New Fuel Storage

New fuel is generally stored in fuel storage facilities with no water present but which are designed so as to prevent accidental criticality even if unborated water is present.

The new fuel storage configuration consists of storage cells of one-eighth inch thick stainless steel with a 21-inch center-to-center spacing. The cells are arranged in a 5 x 14 array and fuel is stored dry in the cells. Under normal conditions (i.e., without moderator) and accident conditions (i.e., with moderator) fuel assemblies nominally enriched up to 5.0 weight percent may be safely stored in the array and will be maintained subcritical.

The design method[51] which ensures the criticality safety of fuel assemblies outside the reactor uses the AMPX system of codes[34,35] for cross-section generation and KENO-Va[44] for reactivity determination.

The 227 energy group cross-section library,[34] that is the common starting point for all cross-sections used for the benchmarks and the storage racks has been generated from ENDF/B-V data. The NITAWL program[35] includes in this library the self-shielded resonance cross-sections that are appropriate for each particular geometry. The Nordheim Integral Treatment is used. Energy and spatial weighting of cross-sections is performed by the XSDRNPM program,[35] which is a one-dimensional S_N transport theory code. These multi-group cross-section sets are then used as input to KENO-Va,[44] which is a three-dimensional Monte Carlo theory program designed for reactivity calculations.

A set of 32 low enriched, water moderated critical experiments has been analyzed using the above method to demonstrate its applicability to criticality analysis and to establish the method bias and variability. The experiments range from water moderated oxide fuel arrays separated by various materials that simulate LWR fuel shipping and storage conditions[37] to dry harder spectrum uranium metal cylinder arrays with various interspersed materials[38] that demonstrate the wide range of applicability of the method. Note that the 12 high enriched (93.2 w/o) uranium metal cylinder benchmarks[51] are not included in the determination of the method bias and variability since these cases are outside the normal range of applicability for commercial nuclear power plant applications.

The average k_{eff} of the 32 low enriched benchmarks is 0.993. Comparison with the average measured experimental K_{eff} of 1.0007 results in a method bias of 0.0077. The standard deviation of the bias value is 0.00136ΔK. The 95/95 one sided tolerance limit factor for 32 values is 2.20. There is thus a 95 percent probability with a 95 percent confidence level that the uncertainty in reactivity due to the method is not greater than 0.0030ΔK.

The following equation is used to develop the maximum k_{eff} for both the full water density case and the low density optimum moderation or aqueous foam case:

$$k_{eff} = k_{worst} + B_{method} + [(ks)^2_{worst} + (ks)^2_{method}]^{½}$$

where:

k_{worst} = worst case KENO k_{eff} that includes material tolerances, and mechanical tolerances which can result in spacings between assemblies less than nominal.

B_{method} = method bias determined from benchmark critical comparisons[51].

ks_{worst} = 95/95 uncertainty in the worst case KENO k_{eff}.

ks_{method} = 95/95 uncertainty in the method bias.

The criticality acceptance criteria is met when the effective multiplication factor (k_{eff}) including uncertainties at a 95/95 probability/confidence level is less than 0.95 under full density moderation conditions and less than 0.98 under low density optimum moderation or aqueous foam condition.

3.3.2.7.2 Spent Fuel Storage

The primary criticality analyses of the high density spent fuel storage racks were performed with a two-dimensional multi-group transport theory technique, using the CASMO-3 computer code.[43] Independent verification calculations were made with a Monte Carlo technique utilizing the KENO-5a computer code,[44] with the 27-group SCALE cross-section library[45] and the NITAWL routine for U-238 resonance shielding effects (Nordheim integral treatment). ("SCALE" is an acronym for Standardized Computer Analysis for Licensing Evaluation, a standard cross-section set developed by ORNL for the USNRC.) Benchmark calculations[50] were performed to determine the bias and uncertainty values associated with CASMO-3 and NITAWL-KENO, and applied to ensure that the k_{eff} limit of 0.95 was met.

CASMO-3 was also used both for burnup calculations and for evaluating small reactivity increments associated with manufacturing tolerances. In tracking long-term (30-year) reactivity effects of spent fuel stored in Region 2 of the fuel storage rack, CASMO calculations have confirmed a continuous reduction in reactivity with time (after Xe decay) due primarily to Pu-241 decay and Am-241 growth.

In the geometric model used in the calculations, each fuel rod and its cladding were described explicitly and reflecting boundary conditions (zero neutron current) were used in the axial direction and at the centerline of the water gap in Region 1 or the Boral and steel plates between storage cells for Region 2. These boundary conditions have the effect of creating an infinite array of storage cells in all directions.

KENO-5a Monte Carlo calculations inherently include a statistical uncertainty due to the random nature of neutron tracking. To minimize the statistical uncertainty of the KENO-calculated reactivity, a minimum of 500,000 neutron histories in 1000 generations of 500 neutrons each, are accumulated in each calculation.

CASMO-3 was used for burnup calculations during core operations. CASMO-3 has been extensively benchmarked[43, 46, 50] against cold, clean, critical experiments (including plutonium-bearing fuel), Monte Carlo calculations, reactor operations, and heavy-element concentrations in irradiated fuel. In particular, the analyses[46] of 11 critical experiments with plutonium-bearing fuel gave an average k_{eff} of 1.002 $\pm$ 0.011 (95%/95%), showing adequate treatment of the plutonium nuclides. In addition, Johansson[47] has obtained very good agreement in calculations of close-packed, high-plutonium-content, experimental configurations.

Since critical experiment data with spent fuel is not available for determining the uncertainty in burnup-dependent reactivity calculations, an allowance for uncertainty in reactivity was assigned based upon other considerations. Assuming the uncertainty in depletion calculations is less than 5% of the total reactivity decrement, a burnup dependent uncertainty in reactivity (only that portion of the uncertainty due to burnup; other uncertainties are accounted for elsewhere) may be assigned. For the Beaver Valley Unit 1 storage racks, at the design basis burnup the total reactivity decrease from beginning of life to 40,000 MWD/MTU is 0.2826 Δk and the reactivity allowance for uncertainty therefore is 0.0141Δk. The allowance for uncertainty in burnup calculations is believed to be a conservative estimate, particularly in view of the substantial reactivity decrease with aged fuel.

Initially, fuel loaded into the reactor will burn with a slightly skewed cosine power distribution. As burnup progresses, the burnup distribution will tend to flatten, becoming more highly burned in the central regions than in the upper and lower ends. This effect may be clearly seen in the curves compiled in Reference 48. At high burnup, the more reactive fuel near the ends of the fuel assembly (less than average burnup) occurs in regions of lower reactivity worth due to neutron leakage. Consequently, it would be expected that over most of the burnup history, distributed burnup fuel assemblies would exhibit a slightly lower reactivity than that calculated for the average burnup. As burnup progresses, the distribution, to some extent, tends to be self-regulating as controlled by the axial power distribution, precluding the existence of large regions of significantly reduced burnup.

Generic analytic results of the axial burnup effect have been provided by Turner[49] based upon calculated and measured axial burnup distributions. These analyses confirm the minor and generally negative reactivity effect of the axially distributed burnup, becoming positive at burnups greater than about 30,000 MWD/MTU. The trends observed[49] suggest the possibility of a small positive reactivity effect above 30,000 MWD/MTU increasing to slightly over 1% ΔK at 40,000 MWD/MTU.

Calculations for the Beaver Valley storage racks with fuel of an average burnup of 40,000 MWD/MTU were made using an axial burnup distribution representative of spent PWR fuel. (The axial burnup distribution measured on spent fuel from the Surry plant was used as representative of PWR fuel.) These calculations confirm a +0.0143 ΔK effect (at 40,000 MWD/MTU) due to the axial burnup distribution. At lower burnups, the reactivity increment is smaller, being zero at about 30,000 MWD/MTU and negative at lower burnups. No credit is taken for this negative reactivity effect at the lower burnups other than the suggestion of additional conservatism. Furthermore, the reactivity significantly decreases with time in storage providing a continuously increasing margin below the 0.95 limit.

On reactor shutdown, the reactivity of the fuel initially decreases due to the growth of Xe-135. Subsequently, the Xenon decays and the reactivity increases to a maximum at several hundred hours when the Xenon is gone. Over the next 30 years, the reactivity continuously decreases, due primarily to Pu-241 decay and Americium growth. At lower burnup, the reactivity decrease will be less pronounced since less Pu-241 would have been produced. No credit is taken for this long-term decrease in reactivity other than to indicate additional and increasing conservatism in the design criticality analysis.

Spent fuel storage is further described in section 9.12.

3.3.2.8 Stability

3.3.2.8.1 Introduction

The stability of the PWR cores against xenon-induced spatial oscillations and the control of such transients are discussed extensively in References 4, 8, 9 and 10. A summary of these reports is given in the following discussion and the design bases are given in Section 3.3.1.6.

In a large reactor core, xenon-induced oscillations can take place with no corresponding change in the total power of the core. The oscillation may be caused by a power shift in the core which occurs rapidly by comparison with the xenon-iodine time constants. Such a power shift occurs in the axial direction when a plant load change is made by control rod motion and results in a change in the moderator density and fuel temperature distributions. Such a power shift could occur in the diametral plane of the core as a result of abnormal control action.

For a discussion of the methods for detecting azimuthal or diametral induced power oscillations, see the discussions of measurements in the X-Y plane in Section 3.3.2.8.4 and the discussion of instrumentation applications in Section 3.4.5.

Operation with two loops does not have an effect on the xenon distribution since there is a plenum at the core inlet to mix the flow from all operating loops and distribute the flow across the core inlet. Since the core is open (uncanned assemblies) and provides for free cross flow, no gross asymmetry in flow, which could affect the xenon distribution, can exist for 2 or 3 loop operation.

Due to the negative power coefficient of reactivity, PWR cores are inherently stable to oscillations in total power. Protection against total power instabilities is provided by the Control and Protection System as described in Section 7.7. Hence, the discussion on the core stability will be limited here to xenon-induced spatial oscillations.

3.3.2.8.2 Stability Index

Power distributions, either in the axial direction or in the X-Y plane, can undergo oscillations due to perturbations introduced in the equilibrium distributions without changing the total core power. The xenon-induced oscillations are essentially limited to the first flux overtones in the current PWR's, and the stability of the core against xenon-induced oscillations can be determined in terms of the eigenvalues of the first flux overtones. Writing, either in the axial direction or in the X-Y plane, the eigenvalue ξ of the first flux harmonic as:

$$\xi = b + ic, \qquad (3.3\text{-}6)$$

then b is defined as the stability index and $T = 2^{\pi}/c$ as the oscillation period of the first harmonic. The time-dependence of the first harmonic $\delta\theta$ in the power distribution can now be represented as;

$$\delta\theta(t) = Ae\xi^{t} = ae^{bt}\cos(ct), \qquad (3.3\text{-}7)$$

where A and a are constants. The stability index can also be obtained approximately by:

$$b = \frac{1}{T} \ln \frac{A_{n+1}}{An} \qquad (3.3\text{-}8)$$

where: An and A_{n+1} are the successive peak amplitudes of the oscillation

T is the time period between the successive peaks.

3.3.2.8.3 Prediction of the Core Stability

The stability of the core described herein (i.e. with 17 x 17 fuel assemblies) against xenon-induced spatial oscillations is expected to be equal to or better than that of earlier designs. The prediction is based on a comparison of the parameters which are significant in determining the stability of the core against the xenon-induced oscillations, namely (a) the overall core size is unchanged and spatial power distributions will be similar, (b) the moderator temperature coefficient at 100 percent power is expected to be sufficiently negative, and (c) the Doppler coefficient of reactivity is expected to be equal to or slightly more negative at full power.

Analysis of both the axial and X-Y xenon transient tests, discussed in Section 3.3.2.8.5, shows that the calculational model is adequate for the prediction of core stability.

3.3.2.8.4 Stability Measurements

Axial Measurements

Two axial xenon transient tests conducted in a PWR with a core height of 12 feet and 121 fuel assemblies is reported in Reference 11 and will be briefly discussed here. The tests were performed at approximately 10% and 50% of cycle life.

Both a free-running oscillation test and a controlled test were performed during the first test. The second test at mid-cycle consisted of a free-running oscillation test only. In each of the free-running oscillation tests, a perturbation was introduced to the equilibrium power distribution through an impulse motion of the Control Bank D and the subsequent oscillation was monitored to measure the stability index and the oscillation period. The Axial Offset (AO) of power was obtained from the ex-core ion chamber readings (which had been calibrated against the in-core flux maps) as a function of time for both free-running tests as shown in Figure 3.3-40.

The total core power was maintained constant during these spatial xenon tests, and the stability index and the oscillation period were obtained from a least-square fit of the AO data in the form of Eq. (3.3-7). The AO of power is the quantity that properly represents the axial stability in the sense that it essentially eliminates any contribution from even order harmonics including the fundamental mode. The conclusions of the tests are:

1. The core was stable against induced axial xenon transients both at the core average burnups of 1550 MWD/MTU and 7700 MWD/MTU. The measured stability indices are -0.041 hr^{-1} for the first test (Curve 1 of Figure 3.3-40) and -0.014 hr^{-1} for the second test (Curve 2 of Figure 3.3-40). The corresponding oscillation periods are 32.4 hrs. and 27.2 hrs., respectively.

2. The reactor core becomes less stable as fuel burnup progresses and the axial stability index was essentially zero at 12,000 MWD/MTU.

Measurements in the X-Y Plane

Two X-Y xenon oscillation tests were performed at a PWR plant with a core height of 12 feet and 157 fuel assemblies. The first test was conducted at a core average burnup of 1540 MWD/MTU and the second at a core average burnup of 12,900 MWD/MTU. Both of the X-Y xenon tests show that the core was stable in the X-Y plane at both burnups. The second test shows that the core became more stable as the fuel burnup increased and all Westinghouse PWR's are expected to be stable throughout their burnup cycles.

In each of the two X-Y tests, a perturbation was introduced to the equilibrium power distribution through an impulse motion of one RCC unit located along the diagonal axis. Following the perturbation, the uncontrolled oscillation was monitored using the movable detector and thermocouple system and the ex-core power range detectors. The quadrant tilt difference is the quantity that properly represents the diametrical oscillation in the X-Y plane of the reactor core in that the differences of the quadrant average powers over two symmetrically opposite quadrants essentially eliminates the contribution to the oscillation from the azimuthal mode. The quadrant tilt difference (QTD) data were fitted in the form of Eq. (3.3-7) through a least-square method. A stability index of -0.076 hr^{-1} with a period of 29.6 hr was obtained from the thermocouple data shown in Figure 3.3-41.

It was observed in the second X-Y xenon test that the PWR core with 157 fuel assemblies had become more stable due to an increased fuel depletion and the stability index was not determined.

3.3.2.8.5 Comparison of Calculations With Measurements

The analysis of the axial xenon transient tests was performed in an axial slab geometry using a flux synthesis technique. The direct simulation of the AO data was carried out using the PANDA Code.[13] The analysis of the X-Y xenon transient tests was performed in an X-Y geometry using a modified TURTLE[14] code. Both the PANDA and TURTLE codes solve the two-group time-dependent neutron diffusion equation with time-dependent xenon and iodine concentrations. The fuel temperature and moderator density feedback is limited to a steady-state model. All the X-Y calculations were performed in an average enthalpy plane.

The basic nuclear cross-sections used in this study were generated from a unit cell depletion program which has evolved from the codes LEOPARD[15] and CINDER.[16] The detailed experimental data during the tests including the reactor power level, enthalpy rise and the impulse motion of the control rod assembly, as well as the plant follow burnup data were closely simulated in the study.

The results of the stability calculation for the axial tests are compared with the experimental data in Table 3.3-4. The calculations show conservative results for both the axial tests with a margin of approximately 0.01 hr^{-1}, in the stability index.

An analytical simulation of the first X-Y xenon oscillation test shows a calculated stability index of -0.081 hr^{-1}, in good agreement with the measured value of -0.076 hr^{-1}. As indicated earlier, the second X-Y xenon test showed that the core had become more stable compared to the first test and no evaluation of the stability index was attempted. This increase in the core stability in the X-Y plane due to increased fuel burnup is due mainly to the increased magnitude of the negative moderator temperature coefficient.

Previous studies of the physics of xenon oscillations, including three-dimensional analysis, are reported in the series of topical reports, References 8, 9, and 10. A more detailed description of the experimental results and analysis of the axial and X-Y xenon transient tests is presented in Reference 11 and Section 1 of Reference 12.

3.3.2.8.6 Stability Control and Protection

The ex-core detector system is utilized to provide indications of xenon-induced spatial oscillations. The readings from the ex-core detectors are available to the operator and also form part of the protection system.

Axial Power Distribution

For maintenance of proper axial power distributions, the operator is instructed to maintain an axial offset within a prescribed operating band, based on the ex-core detector readings. Should the axial offset be permitted to move far enough outside this band, the protection limit will be reached and the power will be automatically cut back.

Radial Power Distribution

The core described herein is calculated to be stable against X-Y xenon-induced oscillations at all times in life.

The X-Y stability of large PWR's were further verified as part of the startup physics test program at a PWR core with 193 fuel assemblies. The measured X-Y stability of the PWR core with 157 assemblies and the good agreement between the calculated and measured stability index for this core, as discussed in Sections 3.3.2.8.4 and 3.3.2.8.5, make it very unlikely that a sustained X-Y oscillation can occur in a core with 193 assemblies. As discussed in Section 3.3.2.8.2, the X-Y stability of the new model core (i.e., with 17 x 17 fuel assemblies) is expected to be equal to or better than the earlier PWR cores. However, in the unlikely event that X-Y oscillations occur, back-up actions are possible and would be implemented, if necessary, to increase the natural stability of the core until tests demonstrate a suitable stability. This is based on the fact that several actions could be taken to make the moderator temperature coefficient more negative, which will increase the stability of the core in the X-Y plane.

Provisions for protection against non-symmetric perturbations in the X-Y power distribution that could result from equipment malfunctions are made in the protection system design. This includes control rod drop, rod misalignment and asymmetric loss-of-coolant flow.

A more detailed discussion of the power distribution control in PWR cores is presented in Reference 4.

3.3.2.9 Vessel Irradiation

It is beyond the scope of this section to present methods and analyses used in determination of neutron and gamma flux attenuation between the core and the pressure vessel other than a brief review given below. A more complete discussion on the pressure vessel irradiation and surveillance program is given in Section 4.5.1.2.

The primary shielding material that serves to attenuate high energy neutron and gamma flux originating in the core consists primarily of the core baffle, core barrel, the neutron pads, and associated water annuli, all of which are within the region between the core and the pressure vessel.

In general, few group neutron diffusion theory codes are used to determine flux and fission power density distributions within the active core and the accuracy of these analyses is verified by in-core measurements on operating reactors. Outside the active core, methods such as those which use multigroup space dependent slowing down codes are used. Region-wise power sharing information from the core calculations is often used as reference source data for the multigroup codes.

The neutron flux distribution and spectrum in the various structural components varies significantly from the core to the pressure vessel. Representative values of the neutron flux distribution and spectrum are presented in Table 3.3-5. The values listed are based on equilibrium cycle reactor core parameters and power distributions, and thus, are suitable for long term nvt projections and for correlation with radiation damage estimates.

As discussed in Section 4.5.1.2, the irradiation surveillance program utilizes actual test samples to verify the accuracy of the calculated fluxes at the vessel.

3.3.3 Analytical Methods

Calculations required in nuclear design consist of three distinct types, which are performed in sequence:

1. determination of effective fuel temperatures.
2. generation of macroscopic few-group parameters.
3. space-dependent, few group diffusion calculations and space-dependent nodal calculations.

These calculations are carried out by computer codes which can be executed individually; however, at Westinghouse most of the codes required have been linked to form an automated design sequence which minimizes design time, avoids errors in transcription of data, and standardizes the design methods.

3.3.3.1 Fuel Temperature (Doppler) Calculations

Temperatures vary radially within the fuel rod, depending on the heat generation rate in the pellet, the conductivity of the materials in the pellet, gap and clad; and the temperature of the coolant.

The fuel temperatures for use in most nuclear design Doppler calculations are obtained from a simplified version of the Westinghouse fuel rod design model described in Section 3.2.1.3.1 which considers the effect of radial variation of pellet conductivity, expansion-coefficient and heat generation rate, elastic deflection of the clad, and a gap conductance which depends on the initial fill gas, the hot open gap dimension, and the fraction of the pellet over which the gap is closed. The fraction of the gap assumed closed represents an empirical adjustment used to produce good agreement with observed reactivity data at BOL. Further gap closure occurs with burnup and accounts for the decrease in Doppler defect with burnup which has been observed in operating plants.

Radial power distributions in the pellet as a function of burnup are obtained from LASER[17] calculations.

The effective U-238 temperature for resonance absorption is obtained from the radial temperature distribution by applying a radially dependent weighting function. The weighting function was determined from REPAD[18] Monte Carlo calculations of resonance escape probabilities in several steady state and transient temperature distributions. In each case a flat pellet temperature was determined which produced the same resonance escape probability as the actual distribution. The weighting function was empirically determined from these results.

The effective Pu-240 temperature for resonance absorption is determined by a convolution of the radial distribution of Pu-240 number densities from LASER burnup calculations and the radial weighting function. The resulting temperature is burnup dependent, but the difference between U-238 and Pu-240 temperatures, in terms of reactivity effects, is small.

The effective pellet temperature for pellet dimensional change is that value which produces the same outer pellet radius in a virgin pellet as that obtained from the temperature model. The effective clad temperature for dimensional change is its average value.

The temperature calculational model has been validated by plant Doppler defect data as shown in Table 3.3-6 and Doppler coefficient data as shown in Figure 3.3-42. Stability index measurements also provide a sensitive measure of the Doppler coefficient near full power (See Section 3.3.2.8). It can be seen that Doppler defect data is typically within 0.2% $\Delta\rho$ of prediction.

3.3.3.2 Macroscopic Group Constants

There are three lattice codes used for the generation of macroscopic group constants for use in the spatial few group diffusion codes. The first code is a linked version of LEOPARD[15] and CINDER[16], the second code is PHOENIX-P[40], and the third code is NEXUS/PARAGON[54, 55]. A description of each code follows.

Macroscopic few-group constants and analogous microscopic cross sections (needed for feedback and microscopic depletion calculations) may be generated for fuel cells by a Westinghouse version of the LEOPARD[15] and CINDER[16] Codes, which are linked internally and provide burnup dependent cross sections. Normally a simplified approximation of the main fuel chains is used; however, where needed, a complete solution for all the significant isotopes in the fuel chains from Th-232 to Cm-244 is available.[19] Fast and thermal cross section library tapes contain microscopic cross sections taken for the most part from the ENDF[20] library, with a few exceptions where other data provide better agreement with critical experiments, isotopic measurements, and plant critical boron values. The effect on the unit fuel cell of non-lattice components in the fuel assembly is obtained by supplying an appropriate volume fraction of these materials in an extra region which is homogenized with the unit cell in the fast (MUFT) and thermal (SOFOCATE) flux calculations. In the thermal calculation, the fuel rod, clad, and moderator are homogenized by energy-dependent disadvantage factors derived from an analytical fit to integral transport theory results.

Group constants for burnable poison cells, guide thimbles, instrument thimbles, and interassembly gaps are generated in a manner analogous to the fuel cell calculation. Reflector group constants are taken from infinite medium LEOPARD calculations. Baffle group constants are calculated from an average of core and radial reflector microscopic group constants for stainless steel.

Group constants for control rods are calculated in a linked version of the HAMMER[21] and AIM[22] codes to provide an improved treatment of self-shielding in the broad resonance structure of these isotopes at epithermal energies than is available in LEOPARD. The Doppler broadened cross sections of the control rod materials are represented as smooth cross sections in the 54-group LEOPARD fast group structure and in 30 thermal groups. The four-group constants in the rod cell and appropriate extra region are generated in the coupled space-energy transport HAMMER calculation. A corresponding AIM calculation of the homogenized

rod cell with extra region is used to adjust the absorption cross sections of the rod cell to match the reaction rates in HAMMER. These transport-equivalent group constants are reduced to two-group constants for use in space-dependent diffusion calculations. In discrete X-Y calculations only one mesh interval per cell is used, and the rod group constants are further adjusted for use in this standard mesh by reaction rate matching the standard mesh unit assembly to a fine-mesh unit assembly calculation.

Validation of the cross section method is based on analysis of critical experiments as shown in Table 3.3-7, isotopic data as shown in Table 3.3-8, plant critical boron (C) values at HZP, BOL, as shown in Table 3.3-9 and at HFP as a function of burnup as shown in Figures 3.3-43, 3.3-44, and 3.3-45. Control rod worth measurements are shown in Table 3.3-10.

Confirmatory critical experiments on burnable poisons are described in Reference 23.

The PHOENIX-P computer code is a two-dimensional, multigroup, transport based lattice code and is capable of providing all necessary data for PWR analysis. Being a dimensional lattice code, PHOENIX-P does not rely on pre-determined spatial/spectral interaction assumptions for a heterogeneous fuel lattice, hence, will provide a more accurate multi-group flux solution than versions of LEOPARD/CINDER. The PHOENIX-P computer code is approved by the USNRC as the lattice code for generating macroscopic and microscopic few group cross sections for PWR analysis.(40)

The solution for the detailed spatial flux and energy distribution is divided into two major steps in PHOENIX-P.(40, 41) In the first step, a two-dimensional fine energy group nodal solution is obtained which couples individual subcell regions (pellet, clad and moderator) as well as surrounding pins. PHOENIX-P uses a method based on the Carlvik's collision probability approach and heterogeneous response fluxes which preserves the heterogeneity of the pin cells and their surroundings. The nodal solution provides accurate and detailed local flux distribution which is then used to spatially homogenize the pin cells to fewer groups.

The second step in the solution process solves for the angular flux distribution using a standard S4 discrete ordinates calculation. This step is based on the group-collapsed and homogenized cross sections obtained from the first step of the solution. The S4 fluxes are then used to normalize the detailed spatial and energy nodal fluxes. The normalized nodal fluxes are used to compute reaction rates, power distribution and to deplete the fuel and burnable absorbers. A standard B1 calculation is employed to evaluate the fundamental mode critical spectrum and to provide an improved fast diffusion coefficient for the core spatial codes.

The PHOENIX-P code utilizes a cross section library designed to properly capture integral properties of the multi-group data during group collapse, and enabling proper modeling of important resonance parameters. The library contains all neutronic data necessary for modeling fuel, fission products, cladding and structural, coolant, and control/burnable absorber materials present in Light Water Reactor cores.

Group constants for burnable absorber cells, guide thimbles, instrument thimbles, control rod cells and other non-fuel cells can be obtained directly from PHOENIX-P without any adjustments such as those required in the cell or 1D lattice codes.

PARAGON has been approved by the NRC as the new generation of Westinghouse lattice code (Reference 54). PARAGON is a replacement for PHOENIX-P and its primary use will be to provide the same types of input data that PHOENIX-P generates for use in three dimensional

core simulator codes. This includes macroscopic cross sections, microscopic cross sections for feedback adjustments to the macroscopic cross sections, pin factors for pin power reconstruction calculations, discontinuity factors for a nodal method solution, and other data needed for safety analysis or other downstream applications.

PARAGON is based on collision probability – interface current cell coupling methods. PARAGON provides flexibility in modeling that was not available in PHOENIX-P including exact cell geometry representation instead of cylinderization, multiple rings and regions within the fuel pin and the moderator cell geometry, and variable cell pitch. The solution method permits flexibility in choosing the quality of the calculation through both increasing the number of regions modeled within the cell and the number of angular current directions tracked at the cell interfaces.

The calculation scheme in PARAGON is based on the conventional lattice modules: resonance calculation, flux solution, leakage correction and depletion. The detailed theory of these modules is described in Reference 54. The cross-section resonance calculation module is based on the space dependent Dancoff method; it is a generalization of the PHOENIX-P methodology that permits to subdivide the fuel pin into many rings and therefore generates space dependent self-shielded isotopic cross-sections. The flux solution module uses the interface current collision probability method and permits a detailed representation of the fuel cells. The other two modules (leakage and depletion) are similar to the ones used in PHOENIX-P.

The current PARAGON cross section library is a 70-group library, based on the ENDF/B basic nuclear data, with the same group structure as the library currently used with PHOENIX-P. The PARAGON qualification library has been improved through the addition of more explicit fission products and fission product chains. PARAGON is, however, designed to employ any number of energy groups.

The new NEXUS cross-section generation system uses PARAGON as the lattice code (Reference 55).

3.3.3.3 Spatial Few-Group Diffusion Calculations

Spatial few-group diffusion calculations have primarily consisted of two-group X-Y calculations using an updated version of the TURTLE code, and two-group axial calculations using an updated version of the PANDA[13] code, APOLLO[42]. However, with the advent of VANTAGE 5 fuel and, hence, axial features such as axial blankets and part length burnable absorbers, there will be a greater reliance on three dimensional nodal codes such as 3D ANC (Advanced Nodal Code).[39] The three dimensional nature of the nodal codes provides both the radial and axial power distributions.

Nodal three dimensional calculations are carried out to determine the critical boron concentrations and power distributions. The moderator coefficient is evaluated by varying the inlet temperature in the same calculations used for power distribution and reactivity predictions.

Validation of TURTLE reactivity calculations is associated with the validation of the group constants themselves, as discussed in Section 3.3.3.2. Validation of the Doppler calculation is associated with the fuel temperature validation discussed in Section 3.3.3.1. Validation of the moderator coefficient calculations is obtained by comparison with plant measurements at hot zero power conditions as shown in Table 3.3-11.

ANC is used in two-dimensional and three-dimensional calculations. ANC can be used for safety analyses and calculating critical boron concentrations, control rod worths, reactivity coefficients, etc.

Axial calculations are used to determine differential control rod worth curves (reactivity versus rod insertion) and axial power shapes during steady state and transient xenon conditions (flyspeck curve). Group constants and the radial buckling used in the axial calculation are obtained from three dimensional calculations (3-D TURTLE or ANC) from which group constants are homogenized by flux weighting.

Validation of the spatial codes for calculating power distributions involves the use of in-core and ex-core detectors and is discussed in Section 3.3.2.2.7.

Based on comparison with measured data it is estimated that the accuracy of current analytical methods is:

$\pm$0.1 percent $\Delta\rho$	for Doppler defect
$\pm 2 \times 10^{-5}$/°F	for moderator coefficient
$\pm$50 ppm	for critical boron concentration with depletion
$\pm$3 percent	for power distributions
$\pm$0.2 percent $\Delta\rho$	for rod bank worth
$\pm$4 pcm/step	for differential rod worth
$\pm$0.5 pcm/ppm	for boron worth
$\pm$0.1 percent $\Delta\rho$	for moderator defect

References for Section 3.3

1. "Anticipated Transients Without Reactor Trip in Westinghouse Pressurized Water Reactors," WCAP-8096, Westinghouse Electric Corporation (April, 1973).

2. F. L. Langford and R. J. Nath, Jr., "Evaluation of Nuclear Hot Channel Factor Uncertainties," WCAP-7308-L, (April, 1969) Westinghouse Electric Corporation (Proprietary) and WCAP-7810, Westinghouse Electric Corporation (December, 1971).

3. A. F. McFarlane, "Core Power Capability in Westinghouse PWRs," WCAP-7267-L, Westinghouse Electric Corporation (Proprietary) (October, 1969) and WCAP-7809, Westinghouse Electric Corporation (December, 1971).

4. J. S. Moore, "Power Distribution Control of Westinghouse Pressurizer Water Reactors," WCAP-7208, Westinghouse Electric Corporation (Proprietary) (September, 1968) and WCAP-7811, Westinghouse Electric Corporation (December, 1971).

5. A. F. McFarlane, "Power Peaking Factors," WCAP-791-L, Westinghouse Electric Corporation (Proprietary) (March, 1971), and WCAP-7912, Westinghouse Electric Corporation (March, 1972).

6. J. 0. Cermak, et. al., "Pressurized Water Reactor pH-Reactivity Effect," Final Report, WCAP-3696-8 (EUREAC-2074), Westinghouse Electric Corporation (October, 1968).

7. J. E. Outzs, "Plant Startup Test Report, H. B. Robinson Unit No. 2," WCAP-7844, Westinghouse Electric Corporation (January, 1972).

8. C. G. Poncelet and A. M. Christie, "Xenon-Induced Spatial Instabilities in Large PWRs," WCAP-3680-20, (EURAEC-1974), Westinghouse Electric Corporation (March, 1968).

9. F. B. Skogen and A. F. McFarlane, "Control Procedures for Xenon-Induced X-Y Instabilities in Large PWRs," WCAP-3680-21, (EURAEC-2111), Westinghouse Electric Corporation (February, 1969).

10. F. B. Shogen and A. F. McFarlane, "Xenon-Induced Spatial Instabilities in Three-Dimensions," WCAP-3680-22 (EURAEC-2116), Westinghouse Electric Corporation (September, 1969).

11. J. C. Lee, et. al., "Axial Xenon Transients Tests at the Rochester Gas and Electric Reactor," WCAP-7964, Westinghouse Electric Corporation (June, 1971).

12. C. J. Kubit, "Safety-Related Research and Development for Westinghouse Pressurized Water Reactors, Program Summaries, Spring-fall 1973," WCAP-8204, Westinghouse Electric Corporation (October, 1973).

13. R. F. Barry, et. al., "The PANDA Code," WCAP-7757, Westinghouse Electric Corporation (September, 1971).

14. S. Altomare and R. F. Barry, "The TURTLE 24.0 Diffusion Depletion Code," WCAP-7758, Westinghouse Electric Corporation (September, 1971).

References for Section 3.3 (CONT'D)

15. R. F. Barry, "LEOPARD - A Spectrum Dependent Non-Spatial Depletion Code for the IBM-7094," WCAP-3269-26, Westinghouse Electric Corporation (September, 1963).

16. T. R. England, "CINDER - A One-Point Depletion and Fission Product Program," WAPD-TM-334, Westinghouse Electric Corporation Bettis Atomic Power Laboratory (August, 1962).

17. C. G. Poncelet, "LASER - A Depletion Program for Lattice Calculations Based on MUFT and THERMOS," WCAP-607, Westinghouse Electric Corporation (April, 1966).

18. J. E. Olhoeft, "The Doppler Effect for a Non-Uniform Temperature Distribution in Reactor Fuel Elements," WCAP-2048, Westinghouse Electric Corporation (July, 1962).

19. R. J. Nodvik, et. al., "Supplementary Report on Evaluation of Mass Spectrometric and Radiochemical Analyses of Yankee Core I Spent Fuel, Including Isotopes of Elements Thorium Through Curium," WCAP-6086, Westinghouse Electric Corporation (August, 1969).

20. M. K. Drake, (Ed.), "Data Formats and Procedure for the ENDF Neutron Cross Section Library," BNL-50274, ENDF-102, Vol. I, Brookhaven National Laboratory (1970).

21. J. E. Suich and H. C. Honeck, "The HAMMER System, Heterogeneous Analysis by Multigroup Methods of Exponentials and Reactors," DP-1064, Savanah River Laboratory (January, 1967).

22. H. P. Flatt and D. C. Baller, "AIM-5, A Multigroup, One Dimensional Diffusion Equation Code," NAA-SR-4694, National Aeronautics and Space Administration (March, 1960).

23. J. S. Moore, "Nuclear Design of Westinghouse Pressurized Water Reactors with Burnable Poison Rods," WCAP-7806, Westinghouse Electric Corporation (December, 1971).

24. L. E. Strawbridge and R. F. Barry, "Criticality Calculation for Uniform Water-Moderated Lattices," Nuclear Science and Eng. 23, 58 (1965).

25. R. J. Nodvik, "Saxton Core II Fuel Performance Evaluation," WCAP-3385-56 Part II, "Evaluation of Mass Spectrometric and Radiochemical Analyses of Irradiated Saxton Plutonium Fuel" (July, 1970).

26. R. D. Leamer, et. al., "PU02-U02 Fueled Critical Experi-ments," WCAP-3726-1, Westinghouse Electric Corporation (July, 1967).

27. Deleted by Revision 16.

28. J. M. Hellman and J. W. Yang, "Effects of Fuel Densification Power Spikes on Clad Thermal Transients," WCAP-8359, Westinghouse Electric Corporation (July, 1974).

29. T. Morita, et. al., "Topical Report, Power Distribution Control and Load Following Procedures," WCAP-8385, Westinghouse Electric Corporation (September, 1974).

30. Deleted by Revision 23.

31. Deleted by Revision 8.

References for Section 3.3 (CONT'D)

32. Deleted by Revision 8.

33. Nuclear Regulatory Commission, Letter to All Power Reactor Licensees, from B. K. Grimes (April 14, 1978), "OT Position for Review and Acceptance of Spent Fuel Storage and Handling Applications."

34. W. E. Ford III, et. al., "CSRL-V: Processed ENDF/B-V 227-Neutron-Group and Pointwise Cross-Section Libraries for Criticality Safety, Reactor and Shielding Studies," ORNL/CSD/TM-160 (June, 1982).

35. N. M. Greene, et. al., "AMPX: A Modular Code System for Generating Coupled Multigroup Neutron-Gamma Libraries from ENDF/B," ORNL/TM-3706 (March, 1976).

36. L. M. Petrie and N. F. Cross, "KENO IV--An Improved Monte Carlo Criticality Program," ORNL-4938 (November, 1975).

37. M. N. Baldwin, et. al., "Critical Experiments Supporting Close Proximity Water Storage of Power Reactor Fuel," BAW-1484-7 (July, 1979).

38. J. T. Thomas, "Critical Three-Dimensional Arrays of U (93.2) -- Metal Cylinders," Nuclear Science and Engineering, Volume 52, pages 350-359 (1973).

39. Y. S. Liu, et. al., "ANC: A Westinghouse Advanced Nodal Computer Code," WCAP-10965-P-A, Westinghouse Electric Corporation (September, 1986).

40. T. Q. Nguyen, et. al., "Qualification of the PHOENIX-P/ANC Nuclear Design System for Pressurized Water Reactor Cores," WCAP-11596-P-A, Westinghouse Electric Corporation (June, 1988).

41. C. M. Mildrum, L. T. Mayhue, et. al., "Qualification of the PHOENIX/POLCA Nuclear Design and Analysis Program for Boiling Water Reactors," WCAP-10841 (Proprietary) and WCAP-10842 (Non-proprietary), Westinghouse Electric Corporation (June, 1985).

42. L. T. Mayhue and M. B. Yarbrough, "APOLLO - A One Dimensional Neutron Diffusion Theory Program," WCAP-13524, Westinghouse Electric Corporation (October, 1992).

43. A. Ahlin, M. Edenius, H. Haggblom, "CASMO - A Fuel Assembly Burnup Program," AE-RF-76-4158, Studsvik report (Proprietary).

A. Ahlin and M. Edenius, "CASMO - A Fast Transport Theory Depletion Code for LWR Analysis," ANS Transactions, Vol. 26, p. 604 (1977).

"CASMO-3 A Fuel Assembly Burnup Program, Users Manual," Studsvik/NFA-87/7, Studsvik Energitechnik AB (November 1986).

M. Edenius and A. Ahlin, "CASMO-3: New Features, Benchmarking, and Advanced Applications," Nuclear Science and Engineering, 100, 342-351 (1988).

References for Section 3.3 (CONT'D)

44. Green, Lucious, Petrie, Ford, White, Wright, "PSR-63/AMPX-1 (code package), AMPX Modular Code System for Generating Coupled Multigroup Neutron-Gamma Libraries from ENDF/B," ORNL-TM-3706, Oak Ridge National Laboratory (March 1976).

L. M. Petrie and N. F. Landers, "KENO V.a An Improved Monte Carlo Criticality Program with Supergrouping," Section F-11, Vol. 2, (NUREG CR-0200) ORNL/NUREG/CSD-2/VI/r2 (December 1984).

45. R. M. Westfall, et. al., "SCALE: A Modular Code System for Performing Standardized Computer Analyses for Licensing Evaluation," NUREG/CR-0200 (1979).

46. E. E. Pilat, "Methods for the Analysis of Boiling Water Reactors (Lattice Physics)," YAEC-1232, Yankee Atomic Electric Co. (December 1980).

47. E. Johansson, "Reactor Physics Calculations on Close-Packed Pressurized Water Reactor Lattices," Nuclear Technology, Vol. 68, pp. 263-268 (February 1985).

48. H. Richings, Some Notes on PWR (W) Power Distribution Probabilities for LOCA Probabilistic Analyses, Internal NRC Memorandum to P. S. Check (July 5, 1977).

49. S. E. Turner, "Uncertainty Analysis - Burnup Distributions," presented at the DOE/SANDIA Technical Meeting on Fuel Burnup Credit, Special Session, ANS/ENS Conference, Washington, D.C. (November 2, 1988).

50. S. E. Turner, Benchmark Calculations, App. A. to Section 4.0 of BV Unit 1 Spent Fuel Modification for Increased Storage Capacity, Holtec Report HI-92791 (April 1992), as supplemented by calculation 8700-DMC-3664, Rev. 0.

51. W. D. Newmyer, "Westinghouse Spent Fuel Rack Criticality Analysis Methodology," WCAP-14416-NP-A (November 1996).

52. P. J. Kersting, et. al., "Assessment of Clad Flattening and Densification Power Spike Elimination in Westinghouse Nuclear Fuel," WCAP-13589-A (March 1995).

53. Miller, R. W., et al., "Relaxation of Constant Axial Offset Control; Fq Surveillance Technical Specification," WCAP-10216-P-A Revision 1A (Proprietary), and WCAP-10217-A Revision 1A (Nonproprietary), February 1994.

54. Ouisloumen, M. et al., "Qualification of the Two-Dimensional Transport Code PARAGON," WCAP-16045-P-A, Westinghouse, 2004.

55. Zhang, B. et al., "Qualification of the NEXUS Nuclear Data Methodology," WCAP-16045-P-A, Addendum 1, Westinghouse 2005.

3.4 THERMAL AND HYDRAULIC DESIGN

3.4.1 Design Bases

The overall objective of the thermal and hydraulic design of the reactor core is to provide adequate heat transfer which is compatible with the heat generation distribution in the core such that heat removal by the Reactor Coolant System or the Emergency Core Cooling System (when applicable) assures that the following performance and safety criteria requirements are met:

1. Fuel damage, the penetration of the fission product barrier (i.e., the fuel rod clad), is not expected during normal operation and operational transients (Condition I) or any transient conditions arising from faults of moderate frequency (Condition II). It is not possible, however, to preclude a very small number of rod failures. These will be within the capability of the plant cleanup system and are consistent with the plant design bases.

2. The reactor can be brought to a safe state following a Condition III event with only a small fraction of fuel rods damaged although sufficient fuel damage might occur to preclude resumption of operation without considerable outage time.

3. The reactor can be brought to a safe state and the core can be kept subcritical with acceptable heat transfer geometry following transients arising from Condition IV events.

In order to satisfy the above criteria the following design bases have been established for the thermal and hydraulic design of the reactor core.

3.4.1.1 Departure from Nucleate Boiling Design Basis

Basis

There will be at least a 95 percent probability that departure from nucleate boiling (DNB) will not occur on the limiting fuel rods during normal operation, operational transients, or during transient conditions arising from faults of moderate frequency (Condition I and II events), at a 95 percent confidence level.

Discussion

By preventing departure from nucleate boiling, adequate heat transfer is assured between the fuel clad and the reactor coolant, thereby preventing clad damage as a result of inadequate cooling. Maximum fuel rod surface temperature is not a design basis as it will be within a few degrees of coolant temperature during operation in the nucleate boiling region. Limits provided by the nuclear control and protection systems are such that this design basis will be met for transients associated with Condition II events including overpower transients. There is an additional large DNBR margin at rated power operation and during normal operating transients.

Historically, the DNBR limit has been 1.30 for Westinghouse applications. In this application, the WRB-2M[104] and the WRB-1 correlation[37] are used. With the significant improvement in the accuracy of the critical heat flux prediction by using this correlation instead of the previous correlation, DNBR correlation limits of 1.14 and 1.17 apply, respectively, to WRB-2M and WRB-1.

The design method used to meet the DNB design basis is the Revised Thermal Design Procedure[82]. With the RTDP methodology[82], uncertainties in plant operating parameters[107], nuclear and thermal parameters, fuel fabrication parameters, computer codes, and DNB correlation predictions are considered statistically to obtain DNB uncertainty factors. Based on the DNB uncertainty factors, RTDP design limit DNBR values are determined such that there is at least a 95 percent probability at a 95 percent confidence level that DNB will not occur on the most limiting fuel rod during normal operation and operational transients and during transient conditions arising from faults of moderate frequency (Condition I and II events as defined in ANSI N18.2).

In the RTDP method, the following uncertainties are statistically combined with the DNB correlation uncertainties to obtain the overall DNBR uncertainty factor used to define the design limit DNBR:

- Plant operating parameters (vessel coolant flow, core power, coolant temperature, system pressure, effective core flow fraction)
- Nuclear and thermal parameter $(F^{N}_{\Delta H})$
- Fuel fabrication parameters $(F^{E}_{\Delta H,1})$
- VIPRE and transient codes

The uncertainty factor obtained is used to define the design limit DNBR which satisfies the DNB design criterion. The DNB design criterion is that the probability that DNB will not occur on the most limiting fuel rod is at least 95 percent at a 95 percent confidence level during normal operation and operational transients (Condition I events) and during transient conditions arising from faults of moderate frequency (Condition II events).

The RTDP design limit DNBR value is 1.22 for both the typical and thimble cells for the Robust Fuel Assembly (RFA). For the V5H Fuel Assemblies, the RTDP design limit DNBR values for the typical and thimble cells are 1.23 and 1.22, respectively.

In addition to the considerations above, a specific plant allowance has been considered in the present analysis. For the RFA, a DNBR safety limit value of 1.55 for typical and thimble cells has been used in the safety analyses for the plant. For the V5H Fuel Assemblies, DNBR safety limit values of 1.33 and 1.32 for typical and thimble cells, respectively, have been used in the safety analyses for the plant. The difference between the DNBR value used in the safety analyses and the design DNBR values provides plant-specific DNB margin to offset the rod bow penalty and other DNB penalties that may occur. This DNB margin may also be used for flexibility in the design, operation or analysis of the plant.

The standard thermal design procedure (STDP) is used for those analyses where RTDP is not applicable. In the STDP method, the parameters used in the analysis are treated in a conservative way from a DNBR standpoint. The parameter uncertainties are applied directly to the plant safety analyses input values to give the lowest minimum DNBR. The DNBR limit for STDP is the appropriate DNB correlation limit increased by sufficient margin to offset the applicable DNBR penalties.

For conditions outside the range of parameters for the WRB-1 and WRB-2M correlations (refer to Section 3.4.2.3.1), the W-3 correlation is used with a DNBR correlation limit of 1.30 for pressure equal to or greater than 1000 psia. For low pressure applications (500-1000 psia), the W-3 DNBR correlation limit is 1.45 (Reference 99).

A full region of Robust Fuel Assemblies (RFA/RFA-2) will be used starting with Cycle 15. The thermal – hydraulically equivalent RFA-2 design was used starting in Cycle 17. The RFA/RFA-2 has a mixing vane grid design that is different from the current VANTAGE 5H and VANTAGE+ mixing vane grids. In addition, the RFA/RFA-2 has Intermediate Flow Mixing (IFM) grids located between the top three mid-grid spans. The WRB-2M DNB correlation is applicable to the DNB analysis of the RFA/RFA-2. This correlation is described in Section 3.4.2.3.1.

Tests and analyses have confirmed that the RFA/RFA-2 is hydraulically compatible with the V5H/VANTAGE+ fuel assemblies, References 100, 101, and 102. The NRC-approved Fuel Criteria Evaluation Process, Reference 103, was used to address the design modifications for the 17x17 RFA, References 100 and 111. The modification for RFA-2 was addressed in Reference 112.

3.4.1.2 Fuel Temperature Design Basis

Basis

During modes of operation associated with Condition I and Condition II events, the maximum fuel temperature shall be less than the melting temperature of UO_2. The UO_2 melting temperature for at least 95% of the peak power fuel rods will not be exceeded at the 95% confidence level. The melting temperature of UO_2 is taken as 5080°F[(1)] unirradiated and is considered to decline 58°F per 10,000 MWD/MTU. By precluding UO_2 melting, the fuel geometry is preserved and possible adverse effects of molten UO_2 on the cladding are eliminated. To preclude center melting and as a basis for overpower protection system setpoints, a calculated centerline fuel temperature of 4700°F has been selected as the overpower limit. This provides sufficient margin for uncertainties in the thermal evaluations as described in Section 3.4.2.10.1.

Discussion

Fuel rod thermal evaluations are performed at rated power, maximum overpower and during transients at various burnups. These analyses assure that this design basis as well as the fuel integrity design bases given in Section 3.2 are met. They also provide input for the evaluation of Condition III and IV faults given in Chapter 14.

3.4.1.3 Core Flow Design Basis

Basis

A minimum of 93.5% of the thermal flow rate will pass through the fuel rod region of the core and be effective for fuel rod cooling. Coolant flow through the thimble tubes as well as the leakage from the core barrier-baffle region into the core are not considered effective for heat removal.

Discussion

Core cooling evaluations are based on the thermal flow rate (minimum flow) entering the reactor vessel. A maximum of 6.5% of this value is allotted as bypass flow. This includes RCC guide thimble cooling flow, head cooling flow, baffle leakage, and leakage to the vessel outlet nozzle.

3.4.1.4 Hydrodynamic Stability Design Bases

Modes of operation associated with Condition I and II events shall not lead to hydrodynamic instability.

3.4.1.5 Other Considerations

The above design bases together with the fuel clad and fuel assembly design bases given in Section 3.2.1.1 are sufficiently comprehensive so additional limits are not required. Fuel rod diametral gap characteristics, moderator-coolant flow velocity and distribution, and moderator void are not inherently limiting. Each of these parameters is incorporated into the thermal and hydraulic models used to ensure the above mentioned design criteria are met. For instance, the fuel rod diametral gap characteristics change with time (see Section 3.2.1.3.1) and the fuel rod integrity is evaluated on that basis. The effect of the moderator flow velocity and distribution (see Section 3.4.2.3) and moderator void distribution (see Section 3.4.2.5) are included in the core thermal (VIPRE) evaluation and thus affect the design bases.

Meeting the fuel clad integrity criteria covers possible effects of clad temperature limitations. As noted in Section 3.2.1.3.1, the fuel rod conditions change with time. A single clad temperature limit for Condition I or Condition II events is not appropriate since of necessity it would be overly conservative. A clad temperature limit is applied to the loss-of-coolant accident (Section 14.3.1), and control rod ejection accident.[2]

3.4.2 Description

3.4.2.1 Summary

The reactor is designed to meet the DNB design criteria of Section 3.4.1.1 as well as no fuel centerline melting during normal operation, operational transients and faults of moderate frequency.

3.4.2.2 Fuel and Cladding Temperatures (Including Densification)

Consistent with the thermal-hydraulic design bases described in Section 3.4.1, the following discussion pertains mainly to fuel pellet temperature evaluation. A discussion of fuel clad integrity is presented in Section 3.2.1.3.1. The thermal-hydraulic design assures that the maximum fuel temperature is below the melting point of UO (melting point of 5080°F[1] unirradiated and reducing by 58°F per 10,000 MWD/MTU). To preclude center melting and as a basis for overpower protection system setpoints, a calculated centerline fuel temperature of 4700°F has been selected as the overpower limit. This provides sufficient margin for uncertainties in the thermal evaluations as described in Section 3.4.2.10.1. The temperature distribution within the fuel pellet is predominantly a function of the local power density and the UO thermal conductivity. However, the computation of radial fuel temperature distributions combines crud, oxide, clad, gap and pellet conductances. The factors which influence these conductances, such as gap size (or contact pressure), internal gas pressure, gas composition, pellet density, and radial power distribution within the pellet, etc., have been combined into a semiempirical thermal model (see Section 3.2.1.3.1) with the model modifications for time dependent fuel densification given in Reference 93. This thermal model enables the determination of these factors and their net effects on temperature profiles. The temperature predictions have been compared to inpile fuel temperature measurements[9] and melt radius data[10][11] with good results.

Effect of Fuel Densification on Fuel Rod Temperatures

Fuel densification results in fuel pellet shrinkage. This affects the fuel temperatures in the following ways:

1. Pellet radial shrinkage increased the pellet diametral gap which results in increased thermal resistance of the gap, and thus, higher fuel temperatures (see Section 3.2.1.3.1).

2. Pellet axial shrinkage may produce pellet to pellet gaps which results in local power spikes, described in Section 3.3.2.2.5. The improved methodology described in Reference 91 shows that the penalty due to this is negligible.

3. Pellet axial shrinkage will result in a fuel stack height reduction and an increased linear power generation rate (kW/ft) for a constant core power level. Using the methods described in Section 5.3 of Reference 91, the increase in linear power for the fuel rod specifications listed in Table 3.3-1 is 0.2%.

As described in References 93 and 119, fuel rod thermal evaluations (fuel centerline, average and surface temperatures) are determined throughout the fuel rod lifetime with consideration of time dependent densification. Maximum fuel average and surface temperatures, shown in Figure 3.4-1 as a function of the LHGR, are peak values attained during the fuel lifetime. Figure 3.4-2 presents the peak value of fuel centerline temperature versus linear power density which is attained during the fuel lifetime.

The maximum pellet temperatures at the hot spot during transients is 4700°F. The principal factors which are employed in the determination of the fuel temperature are discussed below.

3.4.2.2.1 UO_2 Thermal Conductivity

The thermal conductivity of uranium dioxide was evaluated from data reported by References 12, 13, 14, 15, 16, 17, 18, 19, 7, 22, 23, and 24.

At the higher temperatures, thermal conductivity is best obtained by utilizing the integral conductivity method to melt which can be determined with more certainty. The equation for this method is of the form:

$$\int_0^{Tm} K dT$$

where Tm is the melting temperature of UO_2. From a determination of the data, it has been concluded that the best estimate for the value of this integral when Tm=2800°C (5072°F) is 93 watts/cm. This conclusion is based on the integral values reported by References 24, 25, 26, 10, 27 and 28.

The design curve for the thermal conductivity is shown in Figure 3.4-3. The section of the curve at temperatures between 0°C and 1300°C is in excellent agreement with the recommendation of the IAEA panel[29]. The Section of the curve above 1300°C is derived for an integral value of 93 watts/cm[10][24][28].

Thermal conductivity (K) for UO_2 at 95 percent theoretical density can be represented best by the following equation:

$$K = \frac{1}{11.8+0.0238T} + 8.775 \times 10^{-13} T^3 \qquad (3.4\text{-}2)$$

where K = watts/cm-°C
T = °C

3.4.2.2.2 Radial Power Distribution in UO_2 Fuel Rods

An accurate description of the radial power distribution as a function of burnup is needed for determining the power level for incipient fuel melting and other important performance parameters such as pellet thermal expansion, fuel swelling and fission gas rates.

This information on radial power distributions in UO fuel rods is determined with the neutron transport theory code, LASER. The LASER code has been validated by comparing the code predictions on radial burnup and isotopic distributions with measured radial microdrill data[30][31]. A "radial power depression factor", f, is determined using radial power distributions predicted by LASER. The factor f enters into the determination of the pellet centerline temperature, T_c, relative to the pellet surface temperature, T_s, through the expression:

$$\int_{Ts}^{T_c} K(T)\, dT = \frac{g'f}{4\pi} \qquad (3.4\text{-}3)$$

where

K(T) = the thermal conductivity for UO_2 with a uniform density distribution

g' = the linear power generation rate.

3.4.2.2.3 Gap Conductance (h)

The temperature drop across the pellet-clad gap is a function of the gap size and the thermal conductivity of the gas in the gap. The gap conductance model is selected such that when combined with the UO_2 thermal conductivity model, the calculated fuel centerline temperatures reflect the inpile temperature measurements.

The temperature drop across the gap is calculated by assuming an annular gap conductance model of the following form:

$$h = \frac{K_{gas}}{\frac{\delta}{2} + 14.4 \times 10^{-6}} \qquad (3.4\text{-}4)$$

or an empirical correlation derived from thermocouple and melt radius data:

$$h = 1500 K_{gas} + \frac{4.0}{0.006 + 12\delta} \qquad (3.4\text{-}4a)$$

where

K_{gas} = thermal conductivity of the gas mixture including a correction factor[10] for the accommodation coefficient for light gases (e.g. helium), Btu/hr-ft-°F

δ = diametral gap size, ft.

The larger gap conductance value from these two equations is used to calculate the temperature drop across the gap for finite gaps.

For evaluations in which the pellet-clad gap is closed, a contact conductance is calculated. The contact conductance between UO and zircaloy/ZIRLO™ has been measured and found to be dependent on the contact pressure, composition of the gas at the interface and the surface roughness of the fuel and cladding.[10][33] This information together with the surface roughness found in the fuel and clad installed in Westinghouse reactors leads to the following correlation:

$$h = 0.6p + \frac{K_{gas}}{14.4 \times 10^{-6}} \qquad (3.4\text{-}4)$$

where

h = contact conductance, Btu/hr-ft^2-°F

p = fuel clad contact pressure, psi

3.4.2.2.4 Surface Heat Transfer Coefficients

The fuel rod surface heat transfer coefficients during subcooled forced convection and nucleate boiling are presented in Section 3.4.2.8.1.

3.4.2.2.5 Fuel Clad Temperatures

The outer surface of the fuel rod clad at the hot spot operates at a temperature of approximately 660°F for steady state operation at rated power throughout core life due to the onset of nucleate boiling. Initially (beginning-of-life) this temperature is that of the clad metal outer surface.

During operation over the life of the core, the buildup of oxides and crud on the fuel rod surface causes the clad surface temperature to increase. Allowance is made in the fuel center melt evaluation for this temperature rise. Since the thermal-hydraulic design limits DNB, adequate heat transfer is provided between the fuel clad and the reactor coolant so that the core thermal output is not limited by considerations of the clad temperature. Figure 3.4-4 shows the axial variation of average clad temperature for the average power rod both at beginning and end-of-life.

3.4.2.2.6 Treatment of Peaking Factors

The total heat flux hot channel factor, F(Q), is defined by the ratio of the maximum to core average heat flux. The peak local power at full power conditions is given in Table 3.4-1 and is based on the design value of F(Q) for normal operation. As described in Section 3.3.2.2.6 the peak local power at the maximum overpower trip point is 22.4 kW/ft. The centerline temperature at this power level must be below the UO_2 melt temperature over the lifetime of the rod, including allowances for uncertainties. The melt temperature of unirradiated UO_2 is 5080°F[1] and is assumed to decrease by 58°F per 10,000 MWD/MTU. From Figure 3.4-2, it is evident that the centerline temperature at the maximum overpower trip point is far below that required to produce melting.

3.4.2.3 Critical Heat Flux Ratio and Departure from Nucleate Boiling Ratio and Mixing Technology

The minimum DNBR's for nominal conditions and design transients are given in Table 3.4-1. The core average DNBR is not a safety related item as it is not directly related to the minimum DNBR in the core, which occurs at some elevation in the limiting flow channel. Similarly, the DNBR at the hot spot is not directly safety related. The minimum DNBR in the limiting flow channel will be downstream of the peak heat flux location (hot spot) due to the increased downstream enthalpy rise.

DNBRs are calculated by using the correlation and definitions described in the following Sections 3.4.2.3.1 and 3.4.2.3.2. The VIPRE-01 computer code (discussed in Section 3.4.3.4.1) is used to determine the flow distribution in the core and the local conditions in the hot channel for use in the DNB correlation. The use of hot channel factors is discussed in Section 3.4.3.2.1 (nuclear hot channel factors) and in Section 3.4.2.3.4 (engineering hot channel factors).

3.4.2.3.1 Departure from Nucleate Boiling (DNB) Technology

Early experimental studies of DNB were conducted with fluid flowing inside single heated tubes or channels and with single annulus configurations with one or both walls heated. The results of the experiments were analyzed using many different physical models for describing the DNB phenomenon, but all resultant correlations are highly empirical in nature. The evolution of these correlations is given by Tong[34][40] including the W-3 correlation which is in wide use in the pressurized water reactor industry.

As testing methods progressed to the use of rod bundles, instead of single channels, it became apparent that the bundles average flow conditions cannot be used in DNB correlations. As outlined by Tong[35] test results showed that correlations based on average conditions were not accurate predictors of DNB heat flux. This indicated that a knowledge of the local subchannel conditions within the bundle is necessary.

The VIPRE-01 computer code (References 113 and 114) is used to determine coolant density, mass velocity, enthalpy, vapor void, static pressure, and DNBR distributions along parallel flow channels within a reactor core under expected steady state operating conditions. VIPRE-01, which replaces the THINC-IV computer code, has had extensive experimental verification and comparison with other licensed codes, and is considered a best estimate code. The DNBR predictions are very close to those predicted by THINC-IV. VIPRE-01 is licensed with the NRC as an acceptable model for performing thermal-hydraulic calculations. The W-3 correlation, developed from single channel data, can be applied to rod bundles by using the subchannel local fluid conditions calculated by the VIPRE-01 code.

It was shown by Tong[35] that the above approach yielded conservative predictions particularly in rod bundles with mixing vane grid spacers.

The WRB-1 DNB correlation (Reference 37) was developed based exclusively on the large bank of mixing vane grid rod bundle CHF data (over 1100 points) that Westinghouse has collected. The WRB-1 correlation, based on local fluid conditions, represents the rod bundle data with better accuracy over a wide range of variables than the previous correlation used in design. This correlation accounts directly for both typical and thimble cold wall cell effects, uniform and non-uniform heat flux profiles and variations in rod heated length and grid spacing. The WRB-1 correlation is applicable to the 17 x 17 STD, VANTAGE 5H fuel, and the Robust Fuel Assembly (RFA) (Reference 115).

The applicable range of variables is:

Pressure	:	$1440 \leq P \leq 2490$ psia
Local Mass Velocity	:	$0.9 \leq G_{loc}/10^6 \leq 3.7$ lb/ft^2-hr
Local Quality	:	$-0.2 \leq X_{loc} \leq 0.3$
Heated length, Inlet to CHF Location	:	$L_h \leq 14$ feet
Grid Spacing	:	$13 \leq g_{sp} \leq 32$ inches
Equivalent Hydraulic Diameter	:	$0.37 \leq d_e \leq 0.60$ inches
Equivalent Heated Hydraulic Diameter	:	$0.46 \leq d_h \leq 0.68$ inches

Figure 3.4-5 shows the measured critical heat flux plotted against predicted critical heat flux using the WRB-1 correlation.

In order to meet the design criterion that DNB will not occur at a 95 percent probability with a 95 percent confidence level, a limiting value of DNBR is determined by the method of Owen (Reference 89). Owen has prepared tables which give values of K such that "at least a proportion P of the population is greater than $\overline{M/P} - K_p s$ with confidence γ," where $\overline{M/P}$ and s are the sample mean and standard deviation. When this method was carried out using the data on Figure 3.4-5, the results indicated that a reactor core with these fuel geometries may operate with a minimum DNBR of 1.17 with the WRB-1 correlation and 1.14 with the WRB-2M correlation and satisfy the design criterion.

The WRB-2M DNB correlation, Reference 104, was developed to take advantage of the benefit seen in DNB test data of the mixing vane grids and Intermediate Flow Mixers (IFM) associated with the Robust Fuel Assembly (RFA/RFA-2). This correlation is based on 241 data points and local fluid conditions and is applicable to both typical and thimble cells, non-uniform heat flux profiles and variation in rod heated length and grid spacing. The DNB correlation limit for the WRB-2M DNB correlation is 1.14 compared to the value of 1.17 for the WRB-1 correlation. The WRB-2, References 105 and 106, or the W-3 DNB correlation is used wherever the WRB-2M correlation is not applicable. The applicable range of variables for the WRB-2M correlation is:

Pressure	$1495 \leq P \leq 2425$ psia
Local mass velocity	$0.97 \leq G_{loc}/10^6 \leq 3.1$ lb/ft^2-hr

Local Quality	$-0.1 \leq X_{loc} \leq 0.29$
Heated length, inlet to CHF Location	$L_h \leq 14$ feet
Grid spacing	$10 \leq g_{sp} \leq 20.6$ inch
Equivalent hydraulic diameter	$0.37 \leq d_e \leq 0.46$ inch
Equivalent heated diameter	$0.46 \leq d_h \leq 0.54$ inch

Effects of Fuel Densification on DNB
Effect of Heat Flux Spikes

As discussed in Section 3.3.2.2 and Reference 80 a gap or combination of gaps results in a heat flux spike on the individual or adjacent fuel rods. Westinghouse high pressure DNB Water Tests[81] on a 14 foot axially non-uniformly heated 4 x 4 rod bundle were carried out to measure the effect of heat flux spikes. The rod bundle incorporated mixing vane grids on a 26 inch spacing. A 20% heat flux spike was placed on three adjacent rods at the axial location where DNB is most likely to occur. This test series was run at the same conditions as those of two earlier test series which had unspiked rods so that a comparison of spiked and unspiked data could be made and the spike effects isolated. Figure 3.4-23 shows the relative positions of the three spiked rods. Figure 3.4-24 shows the heat flux profile of the spiked rods.

The test facilities consisted of a high pressure loop capable of supplying water at pressures up to 2400 psia with flow rates up to 400 GPM and inlet temperatures in excess of 600°F. The power supply was capable of delivering up to 4.5 MW.

Using these test facilities, a 14 foot, 16 rod test section can be operated over a wide range of test parameters. For the present tests, these ranges were:

1. Pressure 1500-2400 psia
2. Inlet temperature 401-569°F
3. Mass velocity $1.5\text{-}3.5 \times 10^6$ lb/hr-ft^2

The results of the spike test series indicated that the spike effect on DNB is so small that it lies within the repeatability of DNB measurements. The spike geometry modeled in the above rod bundle experiment was also more severe than that presently ascribed to fuel densification effects, and hence, the absence of a spike effect indicated that a special spike factor in DNB need not be incorporated into the BVPS-1 reactor design.

Effects of Pellet Eccentricity and Clad Ovality on DNB

Individual fuel pellets can be eccentrically located in the clad at BOL. The clad may also assume an oval shape at some later time in life. Both of these cases will produce azimuthal variation of the pellet clad gap. However, these local heat flux peaks will have limited axial lengths at any azimuthal angle.

For the eccentric case the local heat flux peak at a given azimuthal angle will have a maximum length equal to several pellet lengths. This is due to the randomness of the angle of contact of the pellets in the rod at BOL. The randomness has been verified by observation of radiographs of Beznau 1 fuel rods and is due in part to the variation in pellet diameter.

For the clad ovality case, the local heat flux peak also has a maximum length equal to several pellets at a given azimuthal angle. This is due to the randomness of the azimuthal location of the cracked pellet fragments in the axial direction.

The spike DNB tests[81] described previously indicate that for 360° circumferential heat flux spikes at 20% magnitude and 6" long, a special spike factor on DNB need not be incorporated into Westinghouse reactor designs which incorporate the Westinghouse type mixing vane grids. Since the 6 inch length is equivalent to 10" pellet lengths, no reduction in DNBR due to pellet eccentricity or clad ovality is applied in DNB evaluations. Similarly, the heat flux engineering hot channel factor, F(E,Q) of 1.03 which allowed for variations in manufacturing tolerances and was used to determine the local maximum linear heat generation rate at a point, the "hot spot", is no longer considered in DNB evaluations. This subfactor was determined by statistically combining the tolerances for the fuel pellet diameter, density, enrichment, eccentricity and the fuel rod diameter. F(E,Q) continues to be applied in determining the peak power and in fuel pellet temperature evaluations.

The effect of manufacturing tolerances which affect the integrated values along a channel, i.e., enthalpy rise engineering hot channel subfactor corresponding to pellet diameter, density and enrichment, and fuel rod diameter, pitch and bowing, are still considered in all DNB evaluations as described in Section 3.4.2.3.4.

3.4.2.3.2 Definition of DNB Heat Flux Ratio (DNBR)

The DNB heat flux ratio as applied to this design when all flow cell walls are heated is:

$$DNBR = \frac{q''(DNB), N}{q''(loc)} \qquad (3.4\text{-}9)$$

where q"(DNB), N is the heat flux predicted by the applicable DNB correlation for the W-3 correlation

$$q''(DNB), N = \frac{q''(DNB), EU}{F} \qquad (3.4\text{-}10)$$

and q"(DNB),EU is the uniform DNB heat flux as predicted by the W-3 DNB correlation[39] when all flow cell walls are heated.

F is the flux factor to account for non-uniform axial heat flux distributions[39] with the "C" term modified as in Reference 40.

q"(loc) is the actual local heat flux.

The DNB heat flux ratio as applied to this design when a cold wall is present is:

$$DNBR = \frac{q''(DNB), N, CW}{q''(loc)} \quad (3.4\text{-}11)$$

where

$$q''DNB, N, CW = \frac{q''(DNB), EU, Dh \times CWF}{F} \quad (3.4\text{-}12)$$

where

q"(DNB),EU,Dh is the uniform DNB heat flux as predicted by the W-3 cold wall DNB correlation[40] when not all flow cell walls are heated (thimble cold wall cell).

$$CWF^{40} = 1.0\text{-}Ru\left[13.76\text{-}1.372e^{1.78x}\text{-}4.732\left(\frac{G}{10^6}\right)^{-0.0535}\text{-}0.0619\left(\frac{P}{1000}\right)^{.14}\text{-}8.509Dh^{0.107}\right] \quad (3.4\text{-}13)$$

and Ru = 1 - De/Dh

For the WRB-1 and WRB-2M correlations,

$$q''(DNB), N = \frac{q'' WRB\text{-}1}{F} \quad \text{or} \quad q''(DNB), N = \frac{q'' WRB\text{-}2M}{F}$$

where F is the same flux shape factor that is used with the W-3 correlation. The CWF is built into the WRB-1 and the WRB-2M correlations.

3.4.2.3.3 Mixing Technology

The rate of heat exchange by mixing between flow channels is proportional to the difference in the local mean fluid enthalpy of the respective channels, the local fluid density and flow velocity. The proportionality is expressed by the dimensionless thermal diffusion coefficient, TDC, which is defined as:

$$TDC = \frac{W'}{\rho Va} \quad (3.4\text{-}14)$$

where:

W' = flow exchange rate per unit length, lbs/ft-sec
ρ = fluid density, lbm/ft^3
V = fluid velocity, ft/sec
a = lateral flow area between channels per unit length, ft^2/ft

The application of the TDC in the THINC analysis for determining the overall mixing effect or heat exchange rate is presented in Reference 36. The application of the TDC in the VIPRE-01 analysis is presented in Reference 114.

As a part of an ongoing R&D program Westinghouse has sponsored and directed mixing tests at Columbia University[41]. These series of tests, using the "R" mixing vane grid design on 13, 26 and 32 inch grid spacing, were conducted in pressurized water loops at Reynolds numbers similar to that of a PWR core under the following single and two phase (subcooled boiling) flow conditions:

1.	Pressure	1500 to 2400 psia
2.	Inlet temperature	332 to 642°F
3.	Mass velocity	1.0 to 3.5 x 10^6 lbm/hr ft^2
4.	Reynolds number	1.34 to 7.45 x 10^5
5.	Bulk outlet quality	-52.1 to -13.5%.

TDC is determined by comparing the THINC code predictions with the measured subchannel exit temperatures. Data for 26 inch axial grid spacing are presented in Figure 3.4-8 where the thermal diffusion coefficient is plotted versus the Reynolds number. TDC is found to be independent of Reynolds number, mass velocity, pressure and quality over the ranges tested. The two phase data (local, subcooled boiling) fell within the scatter of the single phase data. The effect of two-phase flow on the value of TDC has been demonstrated by References 41, 77, 78, and 79. In the subcooled boiling region the values of TDC were indistinguishable from the single phase values. In the quality region, References 77 and 78 show that in the case with rod spacing similar to that in PWR reactor core geometry, the value of TDC increased with quality to a point and then decreased, but never below the single phase value. Reference 79 showed that the mixing coefficient increased as the void fraction increased.

The data from these tests on the "R" grid showed that a design TDC value of 0.038 (for 26 inch grid spacing) can be used in determining the effect of coolant mixing in the THINC or VIPRE-01 analyses.

A mixing test program similar to the one described above was conducted at Columbia University for the 17 x 17 geometry and mixing vane grids on 26 inch spacing[84]. The mean value of TDC obtained from these tests was 0.051, and all data was well above the current design value of 0.038.

Since the actual reactor grid spacing is approximately 20 inches, the use of a TDC value of 0.038 is conservative for this design, as the value of TDC increased as grid spacing decreased.[41]

3.4.2.3.4 Hot Channel Factors

The total hot-channel factors for heat flux and enthalpy rise are defined as the maximum-to-core average ratios of these quantities. The heat flux hot-channel factor considers the local maximum linear heat generation rate at a point (the "hot spot"), and the enthalpy rise hot-channel factor involves the maximum integrated value along a channel (the "hot-channel").

Each of the total hot-channel factors considers a nuclear hot-channel factor (see Section 3.4.3.2) describing the neutron power distribution and an engineering hot-channel factor, which allows for variations in flow conditions and fabrication tolerances. The engineering hot-channel factors are made up of subfactors which account for the influence of the variations of fuel pellet diameter, density, enrichment and eccentricity; fuel rod diameter pitch and bowing; inlet flow distribution; flow redistribution; and flow mixing.

Engineering Heat Flux Hot-Channel Factor, F(E,Q)

The engineering heat flux hot channel factor is used to evaluate the maximum heat flux linear heat generation rate in the core. This subfactor is determined by statistically combining pellet to pellet variations and regionwise deviations in enrichment, density and burnable absorber (IFBA), and has a value of 1.03 at the 95% probability level, with a 95% confidence. As shown in Reference 113, no DNB penalty need be taken for the relatively low intensity heat flux spikes caused by variations in the above parameters, as well as fuel pellet eccentricity and variations in fuel rod diameter.

Enthalpy Rise Engineering Hot-Channel Factor, F(E, ΔH)

The effect of variations in flow conditions and fabrication tolerances on the hot-channel enthalpy rise is directly considered in the VIPRE-01 core thermal subchannel analysis (see Section 3.4.3.4.1) under any reactor operating condition. The items considered contributing to the enthalpy rise engineering hot-channel factor are discussed below:

1. Rod to Rod Variations in Enrichment, Density and Burnable Absorber (F (E, ΔH, I)):

   F (E, ΔH, I) is similar to F (E, Q) except it covers the effect of rod to rod variations. Rod to rod variations are less than pellet to pellet variations and F (E, ΔH, I) will therefore be less than F (E, Q).

2. Inlet Flow Maldistribution:

   The consideration of inlet flow maldistribution in core thermal performances is discussed in Section 3.4.3.1.2. A design basis of 5% reduction in coolant flow to the hot assembly is used in the VIPRE-01 analysis.

3. Flow Redistribution:

   The flow redistribution accounts for the reduction in flow in the hot channel resulting from the high flow resistance in the channel due to the local or bulk boiling. The effect of the non-uniform power distribution is inherently considered in the VIPRE-01 analysis for every operating condition which is evaluated.

4. Flow Mixing:

   The subchannel mixing model incorporated in the VIPRE-01 Code and used in reactor design is based on experimental data[42] discussed in Section 3.4.3.4.1. The mixing vanes incorporated in the spacer grid design induce additional flow mixing between the various flow channels in a fuel assembly as well as between adjacent assemblies. This mixing reduces the enthalpy rise in the hot channel resulting from local power peaking or unfavorable mechanical tolerances.

3.4.2.3.5 Effects of Rod Bow on DNBR

The phenomenon of fuel rod bowing, as described in Reference 86 must be accounted for in the DNBR safety analysis of Condition I and Condition II events for each plant application.

The safety analysis for BVPS-1 maintained sufficient margin, as discussed in Section 3.4.1.1, to accommodate full and low flow DNBR penalties identified in References 86 and 87 (<1.3 percent for the worst case which occurs at a burnup of 24,000 MWD/MTU).

For the upper assembly spans of the RFA, however, where additional restraint is provided with the Intermediate Flow Mixer (IFM) grids, the grid-to-grid spacing in DNB limiting space is approximately 10 inches compared to the 20 inches in the V5H fuel assemblies. The use of the rod bow topical methods (Reference 86), and scaling with the NRC-approved factor, results in predicted channel closure in the 10 inch spans of less than 50 percent. Therefore, no rod bow DNBR penalty is required in the 10 inch spans in the RFA safety analysis.

The maximum rod bow penalties accounted for in the design safety analysis are based on an assembly average burnup of 24,000 MWD/MTU. At burnups greater than 24,000 MWD/MTU, credit is taken for the effect of F(N, ΔH) burndown due to the decrease in fissionable isotopes and the buildup of fission product inventory, and no additional rod bow penalty is required[89].

3.4.2.3.6 Transition Core

The original Westinghouse transition core DNB methodology is given in References 116 and 117, and was approved by the NRC in Reference 118. An extension of this methodology was approved in Reference 99. Using this methodology, transition cores are analyzed as if they were full cores of one assembly type (i.e., full V5H, or full RFA), and applying the appropriate transition core penalties. The penalties are included in the safety analysis limit DNBRs, such that sufficient margin over the design limit DNBRs exists to accommodate the transition core penalty and other applicable penalties.

3.4.2.4 Flux Tilt Considerations

Significant quadrant power tilts are not anticipated during normal operation since this phenomenon is caused by some asymmetric perturbation. A dropped or misaligned RCCA could cause changes in hot-channel factors; however, these events are analyzed separately in Chapter 14. This discussion will be confined to flux tilts caused by X-Y xenon transients, inlet temperature mismatches, enrichment variations within tolerances and so forth.

The design value of the enthalpy rise hot-channel factor F(N, ΔH) which includes an 8% uncertainty (as discussed in Section 3.3.2.2.7), is assumed to be sufficiently conservative that flux tilts up to and including the alarm point will not result in values of F(N, ΔH) greater than that assumed in this submittal (alarm criteria described in the Technical Specifications and Licensing Requirements Manual). The design value of F(Q) does not include a specific allowance for quadrant flux tilts.

3.4.2.5 Void Fraction Distribution

The calculated core average and the hot subchannel maximum and average void fractions are presented in Table 3.4-3 for operation at full power with design hot-channel factors. The void fraction distribution in the core at various radial and axial locations based on THINC-IV predications is presented in Reference 43. The void models used in the VIPRE-01 computer code are described in Section 3.4.2.8.3.

Since void formation due to subcooled boiling is an important promoter of interassembly flow redistribution, a sensitivity study was performed with THINC-IV using the void model reference above.(43)

The results of this study showed that because of the realistic crossflow model used in THINC-IV, the minimum DNBR in the hot channel is relatively insensitive to variations in this model. The range of variations considered in this sensitivity study covered the maximum uncertainty range of the data used to develop each part of the void fraction correlation.

3.4.2.6 (Deleted)

3.4.2.7 Core Pressure Drops and Hydraulic Loads

3.4.2.7.1 Core Pressure Drops

The analytical model and experimental data used to calculate the pressure drops shown in Table 3.4-1 are described in Section 3.4.2.8. The full power operation pressure drop values shown in the Table are the unrecoverable pressure drops across the vessel, including the inlet and outlet nozzles, and across the core. These pressure drops are based on the best estimate flow (most likely value for actual plant operating conditions) as described in Section 4. Section 4 also defines and describes the Thermal design flow (minimum flow) which is the basis for reactor core thermal performance and the mechanical design flow (maximum flow) which is used in the mechanical design of the reactor vessel internals and fuel assemblies. Since the best estimate flow is that flow which is most likely to exist in an operating plant, the calculated core pressure drops in Table 3.4-1 will be greater than pressure drops previously quoted using the thermal design flow.

Uncertainties associated with the core pressure drop values are discussed in Section 3.4.2.10.2.

3.4.2.7.2 Hydraulic Loads

The fuel assembly hold down springs, Figure 3.2-2, are designed to keep the fuel assemblies resting on the lower core plate under transients associated with Condition I and II events. Maximum flow conditions are limiting because hydraulic loads are a maximum. The most adverse flow conditions occur during a LOCA. These conditions are presented in Section 14.3.1.

Hydraulic loads at normal operating conditions are calculated using best estimate flow and best estimate bypass flow. Core hydraulic loads at cold plant startup conditions are based on the cold zero power flow. Conservative core hydraulic loads for a pump overspeed transient, which creates flow rates 18% greater than the best estimate flow, are also evaluated.

Confirmatory experimental core hydraulic loads were obtained for the flow under the anticipated transient turbine overspeed conditions. Details of the hydraulic verification tests are discussed in Section 1.5 and Reference 83.

3.4.2.8 Correlation and Physical Data

3.4.2.8.1 Surface Heat Transfer Coefficients

Forced convection heat transfer coefficients are obtained from the familiar Dittus-Boelter correlation[44], with the properties evaluated at bulk fluid conditions:

$$\frac{hD(e)}{K} = 0.023\left[\frac{D(e)G}{\mu}\right]^{0.8}\left[\frac{c(p)\mu}{K}\right]^{0.4} \qquad (3.4\text{-}15)$$

where:

- h = heat transfer coefficient, Btu/hr-ft^2-°F
- D(e) = equivalent diameter, ft
- K = thermal conductivity, Btu/hr-ft-°F
- G = mass velocity, lb/hr-ft^2
- μ = dynamic viscosity, lb/ft-hr
- c(p) = heat capacity, Btu/lb-°F

This correlation has been shown to be conservative[45] for rod bundle geometries with pitch to diameter ratios in the range used by PWRs.

The onset of nucleate boiling occurs when the clad wall temperature reaches the amount of superheat predicted by Thom's[46] correlation. After this occurrence the outer clad wall temperature is determined by:

$$\Delta T(SAT) = [0.072 \exp(-P/1260)]\,(q'')^{0.5} \qquad (3.4\text{-}16)$$

where:

- ΔT(SAT) = wall superheat, T(W) - T(SAT), °F
- q" = wall heat flux, Btu/hr-ft^2
- p = pressure, psia
- T(W) = outer clad wall temperature, °F
- T(SAT) = saturation temperature of coolant at P, °F

3.4.2.8.2 Total Core and Vessel Pressure Drop

Unrecoverable pressure losses occur as a result of viscous drag (friction) and/or geometry changes (form) in the fluid flow path. The flow field is assumed to be incompressible, turbulent, single-phase water. These assumptions apply to the core and vessel pressure drop calculations for the purpose of establishing the primary loop flow rate. Two-phase considerations are neglected in the vessel pressure drop evaluation because the core average void is negligible (see Section 3.4.2.5 and Table 3.4-3). Two-phase flow considerations in the core thermal subchannel analyses are considered and the models are discussed in Section 3.4.3.1.3. Core and vessel pressure losses are calculated by equations of the form:

$$\Delta P(L) = (K + F\frac{L}{De})\frac{\rho V^2}{2g(c)(144)} \qquad (3.4\text{-}17)$$

$\Delta P(L)$ = Unrecoverable pressure drop, lb/in^2
ρ = fluid density, lbm/ft^3
L = length, ft.
D(e) = equivalent diameter, ft
V = fluid velocity, ft/sec
g(c) = 32.174 $\frac{\text{lbm-ft}}{\text{lb-sec}^2}$
K = form loss coefficient, dimensionless
F = friction loss coefficient, dimensionless

Fluid density is assumed to be constant at the appropriate value for each component in the core and vessel. Because of the complex core and vessel flow geometry, precise analytical values for the form and friction loss coefficients are not available. Therefore, experimental values for these coefficients are obtained from geometrically similar models.

Values are quoted in Table 3.4-1 for unrecoverable pressure loss across the reactor vessel, including the inlet and outlet nozzles, and across the core. The results of full scale tests of core components and fuel assemblies were utilized in developing the core pressure loss characteristic. The pressure drop for the vessel was obtained by combining the core loss with correlation of 1/7th scale model hydraulic test data on a number of vessels[47][48] and form loss relationships[49]. Moody[50] curves were used to obtain the single phase friction factors.

3.4.2.8.3 Void Fraction Correlation

VIPRE-01 considers two-phase flow in two steps. First, a quality model is used to compute the flowing vapor mass fraction (true quality) including the effects of subcooled boiling. Then, given the true void quality, a bulk void model is applied to compute the vapor volume fraction (void fraction).

VIPRE-01 uses a profile fit model (Reference 114) for determining subcooled quality. It calculates the local vapor volumetric fraction in forced convection boiling by: (1) predicting the point of bubble departure from the heated surface; and, (2) postulating a relationship between the true local vapor fraction and the corresponding thermal equilibrium value.

The void fraction in the bulk boiling region is predicted by using homogeneous flow theory and assuming no slip. The void fraction in this region is therefore a function only of the thermodynamic quality.

3.4.2.9 Thermal Effects of Operational Transients

DNB core safety limits are generated as a function of coolant temperature, pressure, core power and axial power imbalance. Steady-state operation within these safety limits insures that the minimum DNBR is not less than the safety analysis limit DNBR. Figure 14D-1 shows the limit lines for DNBR's greater than or equal to the safety analysis DNBR limit and the resulting overtemperature Delta-T trip lines (which become part of the Technical Specifications) plotted as ΔT vs T-average for various pressures. This system provides adequate protection against anticipated operational transients that are slow with respect to fluid transport delays in the primary system. In addition, for fast transients, e.g., uncontrolled rod bank withdrawal at power incident (Section 14.1.2) specific protection functions are provided as described in Section 7.2 and the use of these protection functions are described in Chapter 14 (see Table 14D-2). The thermal response of the fuel rod is discussed in Section 3.4.3.7.

3.4.2.10 Uncertainties in Estimates

3.4.2.10.1 Uncertainties in Fuel and Clad Temperatures

As discussed in 3.4.2.2, the fuel temperature is a function of crud, oxide, clad, gap, and pellet conductances. Uncertainties in the fuel temperature calculation are essentially of two types: fabrication uncertainties such as variation in the pellet and clad dimensions and the pellet density; and model uncertainties such as variations in the pellet densification and the gap.

In addition to the temperature uncertainty described above, the measurement uncertainty in determining the local power, and the effect of density and enrichment variations on the local power are considered in establishing the heat flux hot channel factor. These uncertainties are described in Section 3.3.2.2.1.

Reactor trip setpoints as specified in the Technical Specifications include allowance for instrument and measurement uncertainties such as calorimetric error, instrument drift and channel reproducibility, temperature measurement uncertainties, noise, and heat capacity variations.

3.4.2.10.2 Uncertainties in Pressure Drops

Core and vessel pressure drops based on the best estimate flow, as described in Section 4, are quoted in Table 3.4-1. The uncertainties quoted are based on the uncertainties in both the test results and the analytical extension of these values to the reactor application. The magnitude of the uncertainties will be confirmed when the experimental data on the prototype fuel assembly (Section 1.5) is obtained.

A major use of the core and vessel pressure drops is to determine the primary system coolant flow rates as discussed in Section 4. In addition, as discussed in Section 3.4.4.1, tests on the primary system prior to initial criticality will be made to verify that a conservative primary system coolant flow rate has been used in the design and analyses of the plant.

3.4.2.10.3 Uncertainties Due to Inlet Flow Maldistributions

The effects of uncertainties in the inlet flow maldistribution criteria used in the core thermal analyses is discussed in Section 3.4.3.1.2.

3.4.2.10.4 Uncertainty in DNB Correlation

The uncertainty in the DNB correlation (Section 3.4.2.3) can be written as a statement on the probability of not being in DNB based on the statistics of the DNB data. This is discussed in Section 3.4.2.3.2.

3.4.2.10.5 Uncertainties in DNBR Calculations

The uncertainties in the DNBRs calculated by VIPRE-01 analysis (see Section 3.4.3.4.1) due to uncertainties in the nuclear peaking factors are accounted for by applying conservatively high values of the nuclear peaking factors and including measurement error allowances in the statistical evaluation of the limit DNBR (Section 3.4.1.1) using the Revised Thermal Design Procedure (Reference 82). In addition, conservative values for the engineering hot-channel factors are used as discussed in Section 3.4.2.3.4.

The ability of the VIPRE-01 computer code to accurately predict flow and enthalpy distributions in rod bundles is discussed in Section 3.4.3.4.1, and in Reference 114. Studies have been performed (Reference 114) to determine the sensitivity of the minimum DNBR to the void fraction correlation (see also Section 3.4.2.8.3), and the inlet flow distributions. The results of these studies show that the minimum DNBR is relatively insensitive to variations in these parameters. Furthermore, the VIPRE-01 flow field model for predicting conditions in the hot channels is consistent with that used in the derivation of the DNB correlation limits, including void/quality modeling, turbulent mixing and cross-flow and two-phase flow (Reference 114).

3.4.2.10.6 Uncertainties in Flow Rates

For core thermal performance evaluations, a Thermal Design Loop Flow is used which is less than the Best Estimate Loop Flow (by approximately 10%). In addition, another 6.5% of the Thermal Design Flow is assumed to be ineffective for core heat removal capability because it bypasses the core through the various available vessel flow paths described in Section 3.4.3.1.1.

3.4.2.10.7 Uncertainties in Hydraulic Loads

As discussed in Section 3.4.2.7.2, hydraulic loads on the fuel assembly are evaluated for a pump overspeed transient which creates flow rates 18% greater than the best estimate flow.

3.4.2.10.8 Uncertainty in Mixing Coefficient

The value of the mixing coefficient, TDC, used in THINC analyses for this application is 0.038. VIPRE-01 analyses use a value equivalent to the THINC value. The mean value of TDC obtained in the "R" grid mixing tests described in Section 3.4.2.3.1 was 0.042 (for 26 inch grid spacing). The value of 0.038 is one standard deviation below the mean value; 90% of the data gives values of TDC greater than 0.038[41].

The results of the mixing tests done on 17 x 17 geometry, as discussed in Section 3.4.2.3.3, had a mean of TDC of 0.059 and a standard deviation of σ = 0.007. Hence the current design value of TDC is almost 3 standard deviations below the mean for 26 inch grid spacing.

3.4.2.11 Plant Configuration Data

Plant configuration data for the thermal-hydraulic and fluid systems external to the core are provided in the appropriate Chapters 4, 6, and 9. Implementation of the Emergency Core Cooling System (ECCS) is discussed in Chapter 14. Some specific areas of interest are the following:

1. Total coolant flow rates for the Reactor Coolant System (RCS) is provided in Table 4.1-1. Flow rates employed in the evaluation of the core are presented in Section 3.4.

2. Total RCS volume including pressurizer and surge line, RCS liquid volume including pressurizer water at steady state power conditions are given in Table 4.1-1.

3. The flow path length through each volume may be calculated from physical data provided in the above reference tables.

4. The height of fluid in each component of the RCS may be determined from the physical data presented in Section 4.2. The components of the RCS are water filled during power operation with the pressurizer being approximately 60% water filled.

5. Components of the ECCS are to be located so as to meet the criteria for NPSH described in Section 6.3.

6. Line lengths and sizes for the safety injection system are determined so as to guarantee a total system resistance which will provide, as a minimum, the fluid delivery rates assumed in the safety analyses described in Chapter 14.

7. The minimum flow areas for components of the RCS are presented in Section 4.2, Component and Subsystems Design.

3.4.3 Evaluation

3.4.3.1 Core Hydraulics

3.4.3.1.1 Flow Paths Considered in Core Pressure Drop and Thermal Design

The following flow paths or core bypass flow are considered:

1. Flow through the spray nozzles into the upper head for head cooling purposes.
2. Flow entering into the RCC Guide thimbles to cool the control rods and other core components.
3. Leakage flow from the vessel inlet nozzle directly to the vessel outlet through the gap between the vessel and the barrel.
4. Flow introduced between the baffle and the barrel for the purpose of cooling these components and which is not considered available for core cooling.
5. Flow in the gaps between the fuel assemblies on the core periphery and the adjacent baffle wall.

The above contributions are evaluated to confirm that the design basis value of $\leq$6.5% core bypass flow is met. This design bypass value is also used in the evaluation of the core pressure drops quoted in Table 3.4-1, and the determination of reactor flow rates in Section 5.1.

Flow model test results for the flow path through the reactor are discussed in Section 3.4.2.8.2.

3.4.3.1.2 Inlet Flow Distributions

Data has been considered from several 1/7 scale hydraulic reactor model tests[47][48][55] in arriving at the core inlet flow maldistribution criteria to be used in the VIPRE-01 analyses (see Section 3.4.3.4.1). THINC-I analyses made using this data have indicated that a conservative design basis is to consider a 5 percent reduction in the flow to the hot assembly[56]. The same design basis of 5% reduction to the hot assembly inlet is used in VIPRE-01 analyses.

The experimental error estimated in the inlet velocity distribution has been considered as outlined in Reference 43 where the sensitivity of changes in inlet velocity distributions to hot channel thermal performance is shown to be small. Studies[43] made with a subchannel code show that it is adequate to use the 5% reduction in inlet flow to the hot assembly for a loop out of service based on the experimental data in References 47 and 48.

The effect of the total flow rate on the inlet velocity distribution was studied in the experiments of Reference 47. As was expected, on the basis of the theoretical analysis, no significant variation could be found in inlet velocity distribution with reduced flow rate.

No relative effects on the core inlet velocity distribution caused by the change from a 15 x 15 to 17 x 17 fuel assembly array are expected since the lower internals design will remain unchanged. The flow impedance of the lower core plant and fuel assembly nozzles is equal at all locations.

3.4.3.1.3 Empirical Friction Factor Correlations

Two empirical friction factor correlations are used in the VIPRE-01 computer code (described in Section 3.4.3.4.1).

The friction factor for VIPRE-01 in the axial direction, parallel to the fuel rod axis, is evaluated using a correlation for a smooth tube (Reference 114). The effect of two-phase flow on the friction loss is expressed in terms of the single-phase friction pressure drop, and a two-phase friction multiplier. The multiplier is calculated using the homogeneous equilibrium flow model.

The flow in the lateral directions, normal to the fuel rod axis, views the reactor core as a large tube bank. Thus, the lateral friction factor, F(L), proposed by Idel'chick[49] is applicable. This correlation is of the form:

$$F(L) = A\ Re(L)^{-0.2} \qquad (3.4\text{-}18)$$

where:

A is a function of the rod pitch and diameter as given in Reference 49.

Re(L) is the lateral Reynolds number based on the rod diameter.

Extensive comparisons of VIPRE-01 to THINC-IV predictions, which are given in Reference 114, verify the applicability of the VIPRE-01 correlations in PWR design.

3.4.3.2 Influence of Power Distribution

The core power distribution which is largely established at beginning-of-life by fuel enrichment, loading pattern, and core power level is also a function of variables such as control rod worth and position, and fuel depletion throughout lifetime. Radial power distributions in various planes of the core are often illustrated for general interest, however, the core radial enthalpy rise distribution as determined by the integral of power up each channel is of greater importance for DNB analyses. These radial power distributions, characterized by $F(N, \Delta H)$ (defined in Section 3.3.2.2.2) as well as axial heat flux profiles are discussed in the following two sections.

3.4.3.2.1 Nuclear Enthalpy Rise Hot-Channel Factor, $F(N, \Delta H)$

The Nuclear Enthalpy Rise Hot-Channel Factor, $F(N, \Delta H)$ is given by the equation:

$$F(N,\Delta H) = \frac{\text{hot rod power}}{\text{average rod power}} = \frac{\text{Max} \int_o^H q'(xo,yo,z)\,dz}{\frac{1}{N} \Sigma \int_o^H q\,(x,y,z)\,dz} \qquad (3.4\text{-}19)$$

Where: q'(x,y) is the local power density at a point x,y,z
N is the number of fuel rods
H is the total core height.

The way in which F(N, ΔH) is used in the DNB calculation is important. The location of minimum DNBR depends on the axial profile, and the value of DNBR depends on the enthalpy rise to that point. Basically, the maximum value of the rod integral is used to identify the most likely rod for minimum DNBR. An axial power profile is obtained which when normalized to the design value of F(N, ΔH), recreates the axial heat flux along the limiting rod. The surrounding rods are assumed to have the same axial profile with rod average powers which are typical of distributions found in hot assemblies. In this manner, worst case axial profiles can be combined with worst case radial distributions for reference DNB calculations.

It would be noted again that F(N, ΔH) is an integral and is used as such in the DNB calculations. Local heat fluxes are obtained by using hot channel and adjacent channel explicit power shapes which take into account variations in horizontal power shapes throughout the core.

For operation at a fraction of full power, P, the design F(N, ΔH) used is given by:

$$F(N, \Delta H) = 1.62 [1 + 0.3 (1-P)] \quad \text{for RFA} \qquad (3.4\text{-}20)$$

$$F(N, \Delta H) = 1.456 [1 + 0.3 (1-P)] \quad \text{for V5H}$$

The permitted relaxation of F(N, ΔH) is included in the DNB protection setpoints and allows radial power shape changes with rod insertion to the insertion limits[59], thus allowing greater flexibility in the nuclear design.

3.4.3.2.2 Axial Heat Flux Distributions

As discussed in Section 3.3.2.2.4, the axial heat flux distribution can vary as a result of rod motion, power change, or due to spatial xenon transients which may occur in the axial direction. Consequently, it is necessary to measure the axial power imbalance by means of the ex-core nuclear detectors (as discussed in Section 3.3.2.2.7) and protect the core from excessive axial power imbalance. The Reactor Trip System provides automatic reduction of the trip setpoint in the Overtemperature ΔT channels on excessive axial power imbalance; that is, when an extremely large axial offset corresponds to an axial shape which could lead to a DNBR which is less than that calculated for the reference DNB design axial shape.

The reference DNB design axial shape used in this analysis is a chopped cosine shape with a peak to average value of 1.55.

3.4.3.3 Core Thermal Response

A general summary of the steady-state thermal-hydraulic design parameters including thermal output, flow rates, etc., is provided in Table 3.4-1 for all loops in operation.

The design bases of the application are to prevent departure from nucleate boiling and to prevent fuel melting for Condition I and II events. The protective systems described in Section 7 (Instrumentation and Controls) are designed to meet these bases. The response of the core to Condition II transients is given in Section 14 (Safety Analysis).

3.4.3.4 Analytical Techniques

3.4.3.4.1 Core Analysis Techniques with VIPRE

The objective of reactor core thermal design is to determine the maximum heat removal capability in all flow subchannels, and to show that the core safety limits, as presented in the plant Technical Specifications are not exceeded while compounding engineering and nuclear effects. The thermal design takes into account local variations in dimensions, power generation, flow distribution, and mixing. VIPRE-01 is a three-dimensional subchannel code that has been developed to account for hydraulic and nuclear effects on the enthalpy rise in the core and hot channels (Reference 113). VIPRE-01 modeling of a PWR core is based on a one-pass modeling approach (Reference 114), wherein hot channels and their adjacent channels are modeled in detail, while the rest of the core is modeled simultaneously on a relatively coarse mesh. The behavior of the hot assembly is determined by superimposing the power distribution upon inlet flow distribution, while allowing for flow mixing and flow distribution between flow channels. Local variations in fuel rod power, fuel rod and pellet fabrication, and turbulent mixing are also considered in determining conditions in the hot channels. Conservation equations of mass, axial and lateral momentum, and energy are solved for the fluid enthalpy, axial flow rate, lateral flow and pressure drop.

Steady State Analysis

The VIPRE-01 core model, as approved by the NRC (Reference 114), is used with the applicable DNB correlations to determine DNBR distributions along the hot channels of the reactor core under all expected operating conditions. The VIPRE-01 code is described in detail in Reference 113, including discussions on code validation with experimental data. The VIPRE-01 modeling method is described in Reference 114, including the empirical models and correlations used. The effect of crud on the flow and enthalpy distribution in the core is not directly accounted for in the VIPRE-01 evaluations. However, conservative treatment by the VIPRE-01 modeling method has been demonstrated to bound this effect in DNBR calculations (Reference 114).

Estimates of uncertainties are discussed in Section 3.4.2.10.

Experimental Verification

Extensive experimental verification of VIPRE-01 is presented in Reference 113. The VIPRE-01 analysis is based on knowledge and understanding of the heat transfer and hydrodynamic behaviors of the coolant flow, and the mechanical characteristics of the fuel elements. The use of the VIPRE-01 analysis provides a realistic evaluation of the core performance, and is used in the thermal-hydraulic analysis, as described above.

Transient Analysis

VIPRE-01 is capable of transient DNB analysis. The conservation equations in the VIPRE-01 code contain the necessary accumulation terms for transient calculations. The input description can include one or more of the following time dependent arrays:

1) Inlet flow variation
2) Core heat flux variation
3) Core pressure variation
4) Inlet temperature or enthalpy variation

At the beginning of the transient, the calculation procedure is carried out as in the steady state analysis. The time is incremented by an amount determined by either the user or the time step control options in the code itself. At each new time step the calculations are carried out with the addition of the accumulation terms which are evaluated using the information from the previous time step. This procedure is continued until a preset maximum time is reached.

At time intervals selected by the user, a complete description of the coolant parameter distributions, as well as DNBR, is printed out. In this manner the variation of any parameter with time can be readily determined.

3.4.3.4.2 Fuel Temperatures

As discussed in 3.4.2.2, the fuel rod behavior is evaluated utilizing a semi-empirical thermal model which considers in addition to the thermal aspects such items as clad creep, fuel swelling, fission gas release, release of absorbed gases, cladding corrosion and elastic deflection, and helium solubility.

A detailed description of the thermal model can be found in References 92 and 93.

3.4.3.4.3 Hydrodynamic Instability

The analytical methods used to access hydraulic instability are discussed in Section 3.4.3.5.

3.4.3.5 Hydrodynamic and Flow Power Coupled Instability

Boiling flows may be susceptible to thermohydraulic instabilities[(64)]. These instabilities are undesirable in reactors because they may cause a change in thermohydraulic conditions that may lead to a reduction in the DNB heat flux relative to that observed during a steady flow condition or to undesired forced vibrations of core components. Therefore, a thermohydraulic design criterion was develope b d which states that modes of operation under Condition I and II events will not lead to thermohydrodynamic instabilities.

Two specific types of flow instabilities are considered for Westinghouse PWR operation. These are the Ledinegg or flow excursion type of static instability and the density wave type of dynamic instability.

A Ledinegg instability involves a sudden change in flow rate from one steady state to another. This instability occurs[64] when the slope of the Reactor Coolant System pressure drop-flow rate curve ($\partial\Delta P/\partial G$ internal) becomes algebraically smaller than the loop supply (pump head) pressure drop-flow rate curve ($\partial\Delta P/\partial G$ external). The criterion for stability is $\partial\Delta P/\partial G$ internal > $\partial\Delta P/\partial G$ external. The Westinghouse pump head curve has a negative slope ($\partial\Delta P/\partial G$ external < 0) whereas the Reactor Coolant System pressure drop-flow curve has a positive slope ($\partial\Delta P/\partial G$ internal > 0) over the Condition I and Condition II operational ranges. Thus, the Ledinegg instability will not occur.

The mechanism of density wave oscillations in a heated channel has been described by Reference 94. Briefly, an inlet flow fluctuation produces an enthalpy perturbation. This perturbs the length and the pressure drop of the single-phase region and causes quality or void perturbations in the two-phase regions which travel up the channel with the flow. The quality and length perturbations in the two-phase region create two-phase pressure drop perturbations. However, because the total pressure drop across the core is maintained by the characteristics of the fluid system external to the core, the two-phase pressure drop perturbation feeds back to the single phase region. These resulting perturbations can be either attenuated or self-sustained.

A simple method has been developed[95] for parallel closed channel systems to evaluate whether a given condition is stable with respect to the density wave type of dynamic instability. This method has been used to assess the stability of typical Westinghouse reactor designs under Condition I and II operation. The results indicate that a large margin to density wave instability exists; for example, increases on the order of 150 to 200 percent of rated reactor power would be required for the predicted inception of this type of instability.

The application of the Reference 95 method to Westinghouse reactor designs is conservative because of the parallel open channel feature of Westinghouse PWR cores. For such cores, there is little resistance to lateral flow leaving the flow channels of high power density. There is also energy transfer from high power density channels to lower power density channels. This coupling with cooler channels causes an open channel configuration to be more stable than the above closed channel configuration under the same boundary conditions. Flow stability tests[96,97] have been conducted in which the closed channel systems were shown to be less stable than when the same channels were cross-connected at several locations. The cross-connections were such that the resistance to channel-to-channel crossflow and enthalpy perturbations would be greater than that which would exist in a PWR core which has a relatively low resistance to crossflow.

Flow instabilities, which have been observed, have occurred almost exclusively in closed channel systems operating at low pressures relative to the Westinghouse PWR operating pressures. Reference 98 analyzed parallel closed channel stability experiments simulating a reactor core flow. These experiments were conducted at pressures up to 2200 psia. The results showed that for flow and power levels typical of power reactor conditions, no flow oscillations could be induced above 1200 psia.

Additional evidence that flow instabilities do not adversely affect thermal margin is provided by the data from the rod bundle DNB tests. Many Westinghouse rod bundles have been tested over wide ranges of operating conditions with no evidence of premature DNB or of inconsistent data which might indicate flow instabilities in the rod bundle.

In summary, it is concluded that thermohydrodynamic instabilities will not occur under Condition I and II modes of operation for Westinghouse PWR reactor designs. A large power margin, greater than doubling rated power, exists to predicted inception of such instabilities. Analysis has been performed which shows that minor plant-to-plant differences in Westinghouse reactor designs - such as fuel assembly arrays, core power to flow ratios, and fuel assembly length - will not result in gross deterioration of the above power margins.

3.4.3.6 Temperature Transient Effects Analysis

Waterlogging damage of a fuel rod could occur as a consequence of a power increase on a rod after water has entered the fuel rod through a clad defect. Water entry will continue until the fuel rod internal pressure is equal to the reactor coolant pressure. A subsequent power increase raises the temperature and, hence, could raise the pressure of the water contained within the fuel rod. The increase in hydrostatic pressure within the fuel rod then drives a portion of the water from the fuel rod through the water entry defect. Clad distortion and/or rupture can occur if the fuel rod internal pressure increase is excessive due to insufficient venting of water to the reactor coolant. This occurs when there is both a rapid increase in the temperature of the water within the fuel rod and a small defect. Zircaloy clad fuel rods which have failed due to water logging[70][72] indicate that very rapid power transients are required for fuel failure. Normal operational transients are limited to about 40 cal/gm-min peak rod while the Spert tests[70] indicate that 120 to 150 cal/gm is required to rupture the clad even with very short transients (5.5 msec. period). Release of the internal fuel rod pressure is expected to have a minimal effect on the reactor coolant system[70] and is not expected to result in failure of additional fuel rods[72]. Ejection of fuel pellet fragments into the coolant stream is not expected.[70][72] A clad breech due to waterlogging is thus expected to be similar to any fuel rod failure mechanism which exposes fuel pellets to the reactor coolant stream. Waterlogging has not been identified as the mechanism for clad distortion or perforation of any Westinghouse Zircaloy-4 or ZIRLO™ clad fuel rods.

An excessively high fuel rod internal gas pressure could cause clad failure. The two fuel rod design criteria/bases associated with rod internal pressure are as follows. The internal pressure of the lead rod in the reactor will be limited to a value below that which could cause the 1) diametral gap to increase due to outward cladding creep during steady-state operation or 2) for extensive DNB propagation to occur.

The first criterion precludes the outward clad creep rate from exceeding the fuel solid swelling rate, and therefore, ensures that during steady-state operation the fuel-clad diametral gap will not reopen following contact, or increase in size. Restricting the fuel-clad gap from opening will prevent accelerated fission gas release at high burnup and preclude high burnup fuel from becoming limiting from a LOCA standpoint. Presently, the limiting LOCA condition is calculated to occur at low burnups, near the point of maximum densification.

3.4.3.7 Potentially Damaging Temperature Effects During Transients

The fuel rod experiences many operational transients (intentional maneuvers) during its residence in the core. A number of thermal effects must be considered when analyzing the fuel rod performance.

The clad can be in contact with the fuel pellet at some time in the fuel lifetime. Clad-pellet interaction occurs if the fuel pellet temperature is increased after the clad is in contact with the pellet. Clad-pellet interaction is discussed in Section 3.2.1.3.1.

Increasing the fuel temperature results in an increased fuel rod internal pressure. One of the fuel rod design bases is that the fuel rod internal pressures do not exceed the nominal coolant pressure even at the overpower condition (Section 3.2.1.1.1).

The potential effects of operation with waterlogged fuel are discussed in Section 3.4.3.6 which concluded that waterlogging is not a concern during operational transients.

Clad flattening, as noted in Section 3.2.1.3.1, has been observed in some operating power reactors. Thermal expansion (axial) of the fuel rod stack against a flattened section of clad could cause failure of the clad. This is no longer a concern because clad flattening is precluded during the fuel residence in the core (see section 3.2.1.3.1).

There can be a differential thermal expansion between the fuel rods and the guide thimbles during a transient. Excessive bowing of the fuel rods could occur if the grid assemblies did not allow axial movement of the fuel rods relative to the grids. Thermal expansion of the fuel rods is considered in the grid design so that axial loads imposed on the fuel rods during a thermal transient will not result in excessively bowed fuel rods (see Section 3.2.1.2.2).

3.4.3.8 Energy Release During Fuel Element Burnout

As discussed in Section 3.4.3.3 the core is protected from going through DNB over the full range of possible operating conditions. In the extremely unlikely event that DNB should occur, the clad temperature will rise due to the steam blanketing at the rod surface and the consequent degradation in heat transfer. During this time there is a potential for a chemical reaction between the cladding and the coolant. However, because of the relatively good film boiling heat transfer following DNB, the energy release resulting from this reaction is insignificant compared to the power produced by the fuel.

DNB With Physical Burnout

Westinghouse[63] has conducted DNB tests in a 25-rod bundle where physical burnout occurred with one rod. After this occurrence, the 25 rod test section was used for several days to obtain more DNB data from the other rods in the bundle. The burnout and deformation of the rod did not affect the performance of neighboring rods in the test section during the burnout or the validity of the subsequent DNB data points as predicted by the W-3 correlation. No occurrences of flow instability or other abnormal operation were observed.

DNB With Return to Nucleate Boiling

Additional DNB tests have been conducted by Westinghouse[73] in 19 and 21 rod bundles. In these tests, DNB without physical burnout was experienced more than once on single rods in the bundles for short periods of time. Each time, a reduction in power of approximately 10 percent was sufficient to reestablish nucleate boiling on the surface of the rod. During these and subsequent tests, no adverse effects were observed on this rod or any other rod in the bundle as a consequence of operating in DNB.

3.4.3.9 Energy Release or Rupture of Waterlogged Fuel Elements

A full discussion of waterlogging including energy release is contained in Section 3.4.3.6. It is noted that the resulting energy release is not expected to affect neighboring fuel rods.

3.4.3.10 Fuel Rod Behavior Effects from Coolant Flow Blockage

Coolant flow blockages can occur within the coolant channels of a fuel assembly or external to the reactor core. The effects of fuel assembly blockage within the assembly on fuel rod behavior are more pronounced than external blockages of the same magnitude. In both cases the flow blockages cause local reductions in coolant flow. The amount of local flow reduction, where it occurs in the reactor, and how far along the flow stream the reduction persists are considerations which will influence the fuel rod behavior. The effects of coolant flow blockages in terms of maintaining rated core performance are determined both by analytical and experimental methods. The experimental data are usually used to augment analytical tools such as computer programs similar to the VIPRE-01 program. Inspection of the DNB correlation (Section 3.4.2.3 and Reference 39) shows that the predicted DNBR is dependent upon the local values of quality and mass velocity.

The VIPRE-01 code is capable of predicting the effects of local flow blockages on DNBR within the fuel assembly on a subchannel basis, regardless of where the flow blockage occurs. In Reference 114, it is shown that for a fuel assembly similar to the Westinghouse design, VIPRE-01 accurately predicts the flow distribution within the fuel assembly when the inlet nozzle is completely blocked. Full recovery of the flow was found to occur about 30 inches downstream of the blockage. With the reactor operating at the nominal full power conditions, the effects of an increase in enthalpy and decrease in mass velocity in the lower portion of the fuel assembly would not result in the reactor reaching a minimum DNBR below the safety limit value.

From a review of the open literature it is concluded that flow blockage in “open lattice cores” similar to the Westinghouse cores cause flow perturbations which are local to the blockage. For instance, A. Oktsubo, et. al.[74] show that the mean bundle velocity is approached asymptotically about 4 inches downstream from a flow blockage in a single flow cell. Similar results were also found for 2 and 3 cells completely blocked. Basmer, et al[75], tested an open lattice fuel assembly in which 41 percent of the subchannels were completely blocked in the center of the test bundle between spacer grids. Their results show the stagnant zone behind the flow blockage essentially disappears after 1.65 L/De or about 5 inches for their test bundle. They also found that leakage flow through the blockage tended to shorten the stagnant zone or in

essence the complete recovery length. Thus, local flow blockages within a fuel assembly have little effect on subchannel enthalpy rise. The reduction in local mass velocity is then the main parameter which affects the DNBR. If the BVPS 1 plant were operating at full power and nominal steady state conditions, a reduction in local mass velocity greater than 70 percent would be required to reduce the DNBR to the safety limit. The above mass velocity effect on the DNB correlation was based on the assumption of fully developed flow along the channel length. In reality, a local flow blockage is expected to promote turbulence and thus would likely not affect DNBR at all.

Coolant flow blockages induce local crossflows as well as promote turbulence. Fuel rod behavior is changed under the influence of a sufficiently high crossflow component. Fuel rod vibration could occur, caused by this crossflow component, through vortex shedding or turbulent mechanisms. If the crossflow velocity exceeds the limit established for fluidelastic stability, large amplitude whirling results. The limits for a controlled vibration mechanism are established from studies of vortex shedding and turbulent pressure fluctuations. Crossflow velocity above the established limits can lead to mechanical wear of the fuel rods at the grid support locations. Fuel rod wear due to flow induced vibration is considered in the fuel rod fretting evaluation (Section 3.2).

3.4.4 Testing and Verification

3.4.4.1 Tests Prior to Initial Criticality

A reactor coolant flow test, as noted in Item 8 of Table 13.1-2, is performed following fuel loading but prior to initial criticality. Coolant Loop pressure drop data is obtained in this test. This data in conjunction with coolant pump performance information allows determination of the coolant flow rates at reactor operating conditions. This test verifies that proper coolant flow rates have been used in the core thermal and hydraulic analysis.

3.4.4.2 Initial Power and Plant Operation

Core power distribution measurements are made at several core power levels (see Section 3.3.2.2.7). These tests are used to insure that conservative peaking factors are used in the core thermal and hydraulic analysis.

Additional demonstration of the overall conservatism of the THINC analysis was obtained by comparing THINC predictions to incore thermocouple measurements. These measurements were performed on the Zion reactor.[85] No further in-reactor testing is planned.

3.4.4.3 Component and Fuel Inspections

Inspections performed on the manufactured fuel are delineated in Section 3.2.1.4. Fabrication measurements critical to thermal and hydraulic analysis are obtained to verify that the engineering hot channel factors employed in the design analysis (Section 3.4.2.3.4) are met.

3.4.5 Instrumentation Application

3.4.5.1 Incore Instrumentation

Instrumentation is located in the core so that by correlating moveable neutron detector information with fixed thermocouple information radial, axial, and azimuthal core characteristics may be obtained for all core quadrants.

The incore instrumentation system is comprised of thermocouples, positioned to measure fuel assembly coolant outlet temperatures at preselected positions, and fission chamber detectors positioned in guide thimbles which run the length of selected fuel assemblies to measure the neutron flux distribution. Figure 3.4-22 shows the number and location of instrumented assemblies in the core.

The core-exit thermocouples provide a backup to the flux monitoring instrumentation for monitoring power distribution. The routine, systematic, collection of thermocouple readings by the operator provides a data base. From this data base, abnormally high or abnormally low readings, quadrant temperature tilts, or systematic departures from a prior reference map can be deduced.

The movable incore neutron detector system would be used for more detailed mapping if the thermocouple system were to indicate an abnormality. These two complementary systems are more useful when taken together than either system alone would be. The incore instrumentation system is described in more detail in Section 7.7.

The Incore Instrumentation is provided to obtain data from which fission power density distribution in the core, coolant enthalpy distribution in the core, and fuel burnup distribution may be determined.

3.4.5.2 Overtemperature and Overpower ΔT Instrumentation

The Overtemperature ΔT trip protects the core against low DNBR. The Overpower ΔT trip protects against excessive power (fuel rod rating protection).

As discussed in Section 7.2, factors included in establishing the Overtemperature ΔT and Overpower ΔT trip setpoints include the reactor coolant temperature in each loop. The axial distribution of core power (based on indicated difference between the two section excore neutron detectors) is also a factor in calculating the Overtemperature ΔT setpoint.

3.4.5.3 Instrumentation to Limit Maximum Power Output

The output of the three ranges (source, intermediate, and power) of detectors, with the electronics of the nuclear instruments, are used to limit the maximum power output of the reactor within their respective ranges.

Excluding spares, there are six radial locations containing a total of eight neutron flux detectors installed around the reactor in the neutron shield tank. Two proportional counters for the source range are installed on opposite “flat” portions of the core containing the primary startup sources at an elevation approximately one quarter of the core height. (At locations 90 degrees from the source range detectors, spare detectors may be provided, which can be connected to the source range circuits to provide equivalent functions in place of inoperable source range detectors.) Two compensated ionization chambers for the intermediate range, located in the same instrument wells and detector assemblies as the source range detectors, are positioned at an elevation corresponding to one half of the core height. Four dual-section uncompensated ionization chamber assemblies for the power range are installed vertically at the four corners of the core and located equidistant from the reactor vessel at all points and, to minimize neutron flux pattern distortions, within one foot of the reactor vessel. Each power range detector provides two signals corresponding to the neutron flux in the upper and in the lower sections of a core quadrant. The three ranges of detectors are used as inputs to monitor neutron flux from a completely shutdown condition to 120 percent of full power with the capability of recording overpower excursions up to 200 percent of full power.

The difference in neutron flux between the upper and lower sections of the power range detectors are used to limit the Overtemperature ΔT trip setpoint and to provide the operator with an indication of the core power axial offset. In addition, the output of the power range channels are used for:

1. The rod speed control function
2. To alert the operator to an excessive power unbalance between the quadrants
3. Protect the core against rod ejection accidents
4. Protect the core against adverse power distributions resulting from dropped rods.

Details of the neutron detectors and nuclear instrumentation design and the control and trip logic are given in Chapter 7. The limitations on neutron detector operation and trip setpoints are given in the Technical Specifications.

3.4.5.4 Reactor Vessel Level Instrumentation

The Reactor Vessel Level Instrumentation System (RVLIS) uses differential pressure measuring devices to measure the vessel fluid level or relative void content of the primary coolant. The fluid level or void information is displayed in the main control room for use by the operator as follows:

- Assist in detecting the presence of a gas bubble or void in the Reactor Vessel.
- Assist in detecting the approach of inadequate core cooling.
- Indicate the formation of a void in the RCS

The RVLIS is described in more detail in Section 7.8.4.

References for Section 3.4

1. J. A. Christensen, R. J. Allio and A. Biancheria, "Melting Point of Irradiated UO_2", WCAP-6065, Westinghouse Electric Corporation (February, 1965).

2. D. H. Risher, Jr., "An Evaluation of the Rod Ejection Accident in Westinghouse Pressurized Water Reactors Using Spatial Kinetics Methods", WCAP-7588, Revision 1, Westinghouse Electric Corporation (December, 1971).

3. G. Kjaerheim and E. Rolstad, "In-Pile Determination of UO_2 Thermal Conductivity, Density Effects and Gap Conductance", HPR-80, OECD Halden Project (Norway), (December, 1967).

4. G. Kjaerheim, "In-Pile Measurements of Centre Fuel Temperatures and Thermal Conductivity Determination of Oxide Fuels", paper IFA-175 presented at the European Atomic Energy Society Symposium on Performance Experience of Water-Cooled Power Reactor Fuel, Stockholm, Sweden (October 21-22, 1969).

5. I. Cohen, B. Lustman and J. D. Eichenberg, "Measurement of the Thermal Conductivity of Metal-Clad Uranium Oxide Rods during Irradiation", WAPD-228, Westinghouse Electric Corporation Bettis Atomic Power Laboratory (1960).

6. D. J. Clough and J. B. Sayers, "The Measurement of the Thermal Conductivity of UO under Irradiation in the Temperature Range 150°C - 1600°C", AERE-R-4690, United Kingdom Atomic Energy Authority Research Group, Harwell (December, 1964).

7. J. P. Stora, B. DeBernardy DeSigoyer, R. Delmas, P. Deschamps, C. Ringot and B. Lavaud, "Thermal Conductivity of Sintered Uranium Oxide under In-Pile Conditions", EURAEC-1095, European Atomic Energy Commission (1964).

8. I. Devold, "A Study of the Temperature Distribution in UO Reactor Fuel Elements", AE-318, Aktiebolaget Atomenergi, (Studsvik, Sweden), (1968).

9. M. G. Balfour, J. A. Christensen and H. M. Ferrari, "In-Pile Measurement of UO Thermal Conductivity", WCAP-2923, Westinghouse Electric Corporation (1966).

10. R. N. Duncan, "Rabbit Capsule Irradiation of UO_2", CVTR Project, CVNA-142, Westinghouse Electric Corporation (June, 1962).

11. R. C. Nelson, D. H. Coplin, M. F. Lyons and B. Weidenbaum, "Fission Gas Release from UO_2 Fuel Rods with Gross Central Melting", GEAP-4572, General Electric Corporation (July, 1964).

12. V. C. Howard and T. G. Gulvin, "Thermal Conductivity Determinations on Uranium Dioxide by a Radial Flow Method", United Kingdom Atomic Energy Authority IG-Report 51 (November, 1960).

13. C. F. Lucks and H. W. Deem, "Thermal Conductivity and Electrical Conductivity of UO_2", in Progress Reports Relating to Civilian Applications", BMI-1448 (Rev.) (June, 1960); BMI-1489 (Rev.) (December, 1960) and BMI-1518 (Rev.) Battelle Memorial Institute - Columbus (May, 1961).

References for Section 3.4 (CONT'D)

14. J. L. Daniel, J. Matolich, Jr., and H. W. Deem, "Thermal Conductivity of UO_2", HW-69945, General Electric Corporation, Henford Works (September, 1962).

15. A. D. Feith, "Thermal Conductivity of UO_2 by a Radial Heat Flow Method", TID-21668, U.S. Atomic Energy Commission (1962).

16. J. Vogt, L. Grandell and U. Runfors, "Determination of the Thermal Conductivity of Unirradiated Uranium Dioxide", AB Atomenergi Report RMB-527 (1964), Quoted by IAEA Technical Report Series No. 59, "Thermal Conductivity of Uranium Dioxide".

17. T. Nishijima, T. Kawada and A. Ishihata, "Thermal Conductivity of Sintered UO_2 and Al_2O_3 at High Temperatures", J. American Ceramic Society, 48, 31-34, (1965).

18. J. B. Ainscough and M. J. Wheeler, "The Thermal Diffusivity and Thermal Conductivity of Sintered Uranium Dioxide", in "Proceedings of the Seventh Conference on Thermal Conductivity", p. 467, National Bureau of Standards, Washington (1968).

19. T. G. Godfrey, W. Fulkerson, T. G. Killie, J. P. Moore and D. L. McElroy, "Thermal Conductivity of Uranium Dioxide and Armco Iron by an Improved Radial Heat Flow Technique", ORNL-3556, Oakridge National Laboratory (June, 1964).

20. Reference deleted, Revision 0.

21. A. J. Bush, "Apparatus for Measuring Thermal Conductivity to 2500°C", Westinghouse Research Laboratories Report 64-lP6-401-R3, Westinghouse Electric Corporation (Proprietary) (February, 1965).

22. R. R. Asamoto, F. L. Anselin and A. E. Conti, "The Effect of Density on the Thermal Conductivity of Uranium Dioxide", GEAP-5493, General Electric Corporation (April, 1968).

23. O. L. Kruger, "Heat Transfer Properties of Uranium and Plutonium Dioxide", Paper 11-N-68F presented at the Fall meeting of Nuclear Division of the American Ceramic Society, Pittsburgh (September, 1968).

24. J. A. Gyllander, "In-Pile Determination of the Thermal Conductivity of UO_2 in the Range 500-2500°C", AE-411, AB Atomenergi, (Studsvik, Sweden) (January, 1971).

25. M. F. Lyons, et al., "UO_2 Powder and Pellet Thermal Conductivity During Irradiation", GEAP-5100-1, General Electric Corporation (March, 1966).

26. D. H. Coplin, et al., "The Thermal Conductivity of UO_2 by Direct In-reactor Measurement", GEAP-5100-6, General Electric Corporation (March, 1968).

27. A. S. Bain, "The Heat Rating Required to Produce Center Melting in Various UO_2 Fuels," American Society for Testing Materials Special Technical Publication No. 306, pp. 30-46, Philadelphia (1962).

28. J. P. Stora, "In-Reactor Measurements of the Integrated Thermal Conductivity of UO_2 - Effect of Porosity", Trans. ANS, 13, 137-138 (1970).

References for Section 3.4 (CONT'D)

29. International Atomic Energy Agency, "Thermal Conductivity of Uranium Dioxide", Report of the Panel Held in Vienna, April, 1965, International Atomic Energy Authority Technical Reports Series, No. 59, Vienna, The Agency (1966).

30. C. G. Poncelet, "Burnup Physics of Heterogeneous Reactor Lattices", WCAP-6069, Westinghouse Electric Corporation (June, 1965).

31. R. J. Nodvick, "Saxton Core II Fuel Performance Evaluation", WCAP-3385-56, Part II, "Evaluation of Mass Spectrometic and Radiochemical Analyses of Irradiated Saxton Plutonium Fuel", Westinghouse Electric Corporation (July, 1970).

32. Reference deleted, Revision 0.

33. A. M. Ross and R. L. Stoute, "Heat Transfer Coefficient Between UO_2 and Zircaloy-2", AECL-1552, Atomic Energy of Canada, Ltd. (June, 1962).

34. L. S. Tong, Boiling Heat Transfer and Two-Phase Flow, John Wiley & Sons, New York (1965).

35. L. S. Tong, "Critical Heat Fluxes on Rod Bundles", in "Two-Phase Flow and Heat Transfer in Rod Bundles", 31-41, American Society of Mechanical Engineers, New York (1969).

36. H. Chelemer, J. Weisman and L. S. Tong, "Subchannel Thermal Analysis of Rod Bundle Cores", WCAP-7015, Revision 1, Westinghouse Electric Corporation (January 1969).

37. F. E. Motley, K. W. Hill, F. F. Cadek, and J. Shefchek, "New Westinghouse Correlation WRB-1 for Predicting Critical Heat Flux in Rod Bundles with Mixing Vane Grids," WCAP-8762-P-A, Westinghouse Electric Corporation (July 1984).

38. Deleted by Revision 20.

39. L. S. Tong, "Prediction of Departure from Nucleate Boiling for an Axially Non-Uniform Heat Flux Distribution", Journal of Nuclear Energy, 21, 241-248 (1967).

40. L. S. Tong, "Boiling Crisis and Critical Heat Flux", AEC Critical Review Series, TID-25887, U.S. Atomic Energy Commission (1972).

41. F. F. Cadek, F. E. Motley and D. P. Dominicis, "Effect of Axial Spacing on Interchannel Thermal Mixing with the "R" Mixing Vane Grid", WCAP-7941-L, (June, 1972), Westinghouse Electric Corporation (Proprietary), and WCAP-7959, Westinghouse Electric Corporation (October, 1972).

42. F. F. Cadek, "Interchannel Thermal Mixing with Mixing Vane Grids", WCAP-7667-L, (May, 1971), Westinghouse Electric Corporation (Proprietary), and WCAP-7755, Westinghouse Electric Corporation (September, 1971).

43. L. E. Hochreiter, "Application of the THINC-IV Program to PWR Design", WCAP-7956-A, Westinghouse Electric Corporation (February, 1989).

44. F. W. Dittus and L. M. K. Boelter, "Heat Transfer in Automobile Radiators of the Tubular Type", California University Publication in Eng., 2, No. 13, 443-461 (1930).

References for Section 3.4 (CONT'D)

45. J. Weisman, "Heat Transfer to Water Flowing Parallel to Tube Bundles", Nuclear Science and Engineering, Vol. 6, 78-79 (1959).

46. J. R. S. Thom, W. M. Walker, T. A. Fallon and G. F. S. Reising, "Boiling in Sub-cooled Water During Flowup Heated Tubes of Annuli," Proc. Instn. Mech. Engrs., 180, Pt. C, 4226-246 (1965-66).

47. G. Hetsroni, "Hydraulic Tests of the San Onofre Reactor Model", WCAP-3269-8, Westinghouse Electric Corporation (June, 1964).

48. G. Hetsroni, "Studies of the Connecticut-Yankee Hydraulic Model", NYO-3250-2, U.S. Atomic Energy Commission (June, 1965).

49. I. E. Idel'chik, "Handbook of Hydraulic Resistance," AEC-TR-6630, U.S. Atomic Energy Commission (1960).

50. L. F. Moody, "Friction Factors for Pipe Flow", Transactions of the American Society of Mechanical Engineers, 66, 671-684 (1944).

51. Deleted by Revision 23.

52. Deleted by Revision 23.

53. Deleted by Revision 23.

54. Deleted by Revision 23.

55. F. D. Carter, "Inlet Orificing of Open PWR Cores", WCAP-9004, (January, 1969), Westinghouse Electric Corporation (Proprietary), and WCAP-7836, Westinghouse Electric Corporation (January, 1972).

56. J. Shefcheck, "Application of the THINC Program to PWR Design", WCAP-7359-L, (August, 1969), Westinghouse Electric Corporation (Proprietary), and WCAP-7838, Westinghouse Electric Corporation (January, 1972).

57. Deleted by Revision 23.

58. Deleted by Revision 23.

59. A. F. McFarlane, "Power Peaking Factors", WCAP-7912-L, (March, 1972), Westinghouse Electric Corporation (Proprietary), and WCAP-7912, Westinghouse Electric Corporation (March, 1972).

60. Deleted by Revision 23.

61. Deleted by Revision 23.

References for Section 3.4 (CONT'D)

62. Deleted by Revision 23.

63. J. Weisman, A. J. Wenzel, L. S. Tong, D. Fitzsimmons, W. Thorne, and J. Batch, "Experimental Determination of the Departure for Nucleate Boiling in Large Rod Bundles at High Pressures", Chemical Engineering Program Symposium Ser. 64, No. 82, 114-125 (1968).

64. J. A. Boure, A. E. Bergles and L. S. Tong, "Review of Two-Phase Flow Instability", American Society of Mechanical Engineers Paper 71-HT-42 (August, 1971).

65. Deleted by Revision 16.

66. Deleted by Revision 16.

67. Deleted by Revision 16.

68. Deleted by Revision 16.

69. Deleted by Revision 16.

70. L. A. Stephen, "The Effects of Cladding Material and Heat Treatment on the Response of Waterlogged UO_2 Fuel Rods to Power Bursts", IN-ITR-111, Aeoject Nuclear, Idaho National Engineering Laboratory (January, 1970).

71. Reference deleted, Revision 0.

72. Western New York Nuclear Research Center Correspondence with the AEC on (February 11 and August 27, 1971), Docket 50-57.

73. L. S. Tong, et. al., "Critical Heat Flux (DNB) in Square and Triangular Array Rod Bundles", presented at the Japan Society of Mechanical Engineers Semi-International Symposium held at Tokyo, Japan, 25-34 (September 4-8, 1967).

74. A. Ohtsubo and S. Uruwashi, "Stagnant Fluid due to Local Flow Blockage", Journal of Nuclear Science and Technology 9, No. 7, 433-434 (1972).

75. P. Basmer, D. Kirsh, and G. F. Schultheiss, "Investigation of the Flow Pattern in the Recirculation Zone Downstream of Local Coolant Blockages in Pin Bundles", Atomwirtschaft, 17, No. 8, 416-417 (1972) (In German).

76. Supplemental information on fuel design transmitted from R. Salvatori, Westinghouse NES, to D. Knuth, AEC, as attachments to letters NS-SL-518 (12/22/72), NS-SL-521 (12/19/72), NS-SL-524 (12/29/72) and NS-SL-543 (1/12/73), (Westinghouse Proprietary), and supplemental information on fuel design transmitted from R. Salvatori, Westinghouse NES, to D. Knuth, AEC, as attachments to letters NS-SL-527 (1/2/73) and NS-SL-544 (1/12/73).

References for Section 3.4 (CONT'D)

77. D. S. Rowe, C. W. Angle, "Crossflow Mixing Between Parallel Flow Channels During Boiling, Part II Measurement of Flow and Enthalpy in Two Parallel Channels," BNWL-371, part 2, Battelle Pacific Northwest Laboratory (December, 1967).

78. D. S. Rowe, C. W. Angle, "Crossflow Mixing Between Parallel Flow Channels During Boiling, Part III Effect of Spacers on Mixing Between Two Channels," BNWL-371, part 3, Battelle Pacific Northwest Laboratory (January, 1969).

79. J. M. Gonzalez-Santalo and P. Griffith, "Two-Phase Flow Mixing in Rod Bundle Subchannels", American Society of Mechanical Engineers Paper 72-WA/NE-19.

80. J. M. Hellman (Ed.), "Fuel Densification Experimental Results and Model For Reactor Application", WCAP-8219, Westinghouse Electric Corporation (October, 1973).

81. K. W. Hill, F. E. Motley and F. F. Cadek, "Effect of Local Heat Flux Spikes on DNB in Non-Uniform Heated Rod Bundles", WCAP-8174, (August, 1973), Westinghouse Electric Corporation (Proprietary), and WCAP-8202 (August, 1973).

82. A. J. Friedland, and S. Ray, "Revised Thermal Design Procedure," WCAP-11397 (Proprietary), (February 1987) and Letter, A. C. Thadani (USNRC) to W. J. Johnson (Westinghouse), "Acceptance for Referencing of Licensing Topical Report WCAP-11397, Revised Thermal Design Procedure" (January 1989).

83. S. Nakazato, E. E. DeMario, "Hydraulic Flow Test of the 17 x 17 Fuel Assembly", WCAP-8279, Westinghouse Electric Corporation (February, 1974).

84. F. E. Motley, A. H. Wenzel, F. F. Cadek, "The Effect of 17 x 17 Fuel Assembly Geometry on Interchannel Thermal Mixing", WCAP-8299, Westinghouse Electric Corporation (March, 1974).

85. T. M. Burke, C. E. Meyer, and J. Shefcheck, "Analysis of Data from the Zion (Unit 1) THINC Verification Test", WCAP-8453, (December, 1974) (Proprietary) and WCAP-8454, Westinghouse Electric Corporation (December, 1974).

86. Skaritka, J. (Ed.) 1979. Fuel Rod Bow Evaluation. WCAP-8691, Revision 1 (Proprietary) and WCAP-8692, Revision 1 (Non-proprietary).

87. Westinghouse 1981 letter. E. P. Rahe, Jr. (Westinghouse) to J. R. Miller (USNRC), NS-EPR-2515, dated October 9, 1981, entitled: Partial Response to Request Number 1 for Additional Information on WCAP-8691, Revision 1, and letter, E. P. Rahe, Jr. (Westinghouse) to J. R. Miller (USNRC), NS-EPR-2572, dated March 16, 1982, entitled: Remaining Response to Request Number 1 for Additional Information on WCAP-8691, Revision 1.

88. Deleted by Revision 23.

References for Section 3.4 (CONT'D)

89. Letter from A. C. Thadani (USNRC) to W. J. Johnson (Westinghouse), "Acceptance for Referencing of Licensing Topical Report WCAP-9226-P/9227-NP, Reactor Core Response to Excessive Secondary Steam Releases" (January 31, 1989).

90. D. B. Owen, "Factors for One-Sided Tolerance Limits and for Variable Sampling Plans," SCR-607 (March 1963).

91. P. J. Kersting, et. al., "Assessment of Clad Flattening and Densification Power Spike Elimination in Westinghouse Nuclear Fuel," WCAP-13589-A (March 1995).

92. W. J. Leech, et. al., "Revised PAD Code Thermal Safety Model," WCAP-8720, Addendum 2 (October 1982).

93. R. A. Weiner, et. al., "Improved Fuel Performance Models for Westinghouse Fuel Rod Design and Safety Evaluations," WCAP-11873-A (August 1988).

94. R. T. Lahey and F. J. Moody, "The Thermal Hydraulics of a Boiling Water Reactor," American Nuclear Society (1977).

95. P. Saha, M. Ishii and N. Zuber, "An Experimental Investigation of the Thermally Induced Flow Oscillations in Two-Phase Systems," J. of Heat Transfer (November 1976) pp. 616-622.

96. S. Kakac, T. N. Veziroglu, K. Akyuzlu, O. Berkol, "Sustained and Transient Boiling Flow Instabilities in a Cross-Connected Four-Parallel-Channel Upflow System," Proceedings of 5th International Heat Transfer Conference, Tokyo (September 3-7, 1974).

97. R. Taleyarkhan, M. Podowski, R. T. Lahey, Jr., "An Analysis of Density - Wave Oscillations in Ventilated Channels," NUREG/CR-2972 (March 1983).

98. H. S. Kao, C. D. Morgan, and W. B. Parker, "Prediction of Flow Oscillation in Reactor Core Channel," Transactions of the ANS, Vol. 16, 1973, pp. 212-213.

99. Schueren, P. McAtee, K. R., "Extension of Methodology for Calculating Transition Core DNBR Penalties," WCAP-11837-P-A, January 1990.

100. Kitchen, T. J., "Generic Safety Evaluation for 17x17 Standard Robust Fuel Assembly (17x17 STD RFA)," SECL-98-056, Rev 0, September 30, 1998.

101. Liparulo, N. J. (Westinghouse) letter to Lyons, J. E. (NRC), "Transmittal of Response to NRC Request for Information on Wolf Creek Fuel Design Modifications," NSD-NRC-97-5189, June 30, 1997.

102. Liparulo, N. J. (Westinghouse) letter to Jones, R. C. (NRC), "Transmittal of Presentation Material from NRC/Westinghouse Meeting on April 15, 1996," NSD-NRC-96-4964, April 22, 1996.

References for Section 3.4 (CONT'D)

103. Davidson, S. L. (Editor), "Westinghouse Fuel Criteria Evaluation Process," WCAP-12488-A, October 1994.

104. Smith, L. D., et. al., "Modified WRB-2 Correlation, WRB-2M, for Predicting Critical Heat Flux in 17x17 Rod Bundles with Modified LPD Mixing Vane Grids," WCAP-15025-P-A, April 1999.

105. Davidson, S. L., (Editor), "Reference Core Report -- VANTAGE 5 Fuel Assembly," WCAP-10444-P-A, September 1985, "VANTAGE 5H Fuel Assembly," WCAP-10444-P-A, Addendum 2-A, April 1998.

106. Sepp, H. A. (Westinghouse) letter to T. E. Collins (NRC), "Fuel Criteria Evaluation Process Notice for 17x17 Robust Fuel Assembly with IFM Grid Design," October 13, 1998.

107. "Westinghouse Revised Thermal Design Procedure Instrument Uncertainty Methodology - Beaver Valley Power Station Unit 1," WCAP-15264, Revision 4.

108. Deleted by Revision 23.

109. Deleted by Revision 23.

110. Deleted by Revision 23.

111. T. J. Kitchen, "Beaver Valley Power Station Units 1 and 2 EVAL-03-61-RFA/RFA-2 Robust Fuel Assembly and IFM Implementation," Westinghouse Letter LTR-ESI-03-35, April 24, 2003.

112. "Implementation of Robust Fuel Assembly-2 (RFA-2) Design Changes," EVAL-01-066.

113. Stewart, C. W., et. Al., "VIPRE-01: A Thermal-Hydraulic Code for Reactor Cores," Volume 1-3 (Revision 3, August 1989), Volume 4 (April 1987), NP-2511-CCM-A, Electric Power Research Institute.

114. Sung, Y. X., et. al., "VIPRE-01 Modeling and Qualification for Pressurized Water Reactor Non-LOCA Thermal-Hydraulic Safety Analysis," WCAP-14565-P-A, and WCAP-15306-NP-A, October 1999.

115. Westinghouse Letter to NRC (Sepp, H. A. to Collins, T. E.), "Notification of FCEP Application for WRB-1 and WRB-2 Applicability to the 17 X 17 Modified LPD Grid Design for Robust Fuel Assembly Application," NSD-NRC-98-5722, March 25, 1998.

116. Davidson, S. L., Iorii, J. A., (Ed.), WCAP-9500-A, "Reference Core Report - 17 X 17 Optimized Fuel Assembly," May 1982.

117. Westinghouse Letter to NRC, NS-EPR-2573, (Rahe, E. P., to Miller), "WCAP-9500 and WCAPs-9401/9402, NRC SER Mixed Core Compatibility Items."

References for Section 3.4 (CONT'D)

118. NRC Letter to Westinghouse, (Thomas, C. O. to Rahe, E. P.), Supplemental Acceptance No. 2 for Referencing Topical Report, WCAP-9500," January 1983.

119. J. P. Foster, S. Sidenor, "Westinghouse Improved Performance Analysis and Design Model (PAD 4.0)," WCAP-15063-P-A (Proprietary) and WCAP-15063-A (Non-Proprietary), Revision 1, with Errata (July 2000).

BVPS UFSAR UNIT 1

TABLES FOR SECTION 3

Table 3.1-1

REACTOR DESIGN PARAMETERS

Thermal and Hydraulic Design Parameters	**Design Value**
Reactor Core Heat Output, MWt	2900
Reactor Core Heat Output, Btu/hr	9895×10^6
Heat Generated in Fuel, %	97.4
System Pressure, Nominal psia	2,250
Minimum DNBR for Design Transients, typical/thimble	1.22/1.22 (RFA)* 1.23/1.22 (V5H)*
Coolant Flow	
Total Thermal Flow Rate, lb/hr	99.3×10^6
Effective Flow Rate for Heat Transfer, lb/hr	92.8×10^6 (3)
Effective Flow Area for Heat Transfer, ft^2	41.5 (RFA) 41.7 (V-5H)
Average Velocity Along Fuel Rods, ft/sec	14.0 (RFA) 13.9 (V5H)
Average Mass Velocity, lb/-hr-ft^2	2.10×10^6 (RFA) 2.09×10^6 (V5H)
Coolant Temperature, °F	
Nominal Inlet	543.1(4)
Average Rise in Vessel	73.9(4)
Average Rise in Core	78.4(4)
Average in Core	584.6(4)
Average in Vessel	580.0(4)

*RTDP Design Limits

Table 3.1-1 (CONT'D)
REACTOR DESIGN PARAMETERS

Thermal and Hydraulic Design Parameters	**Design Value**
Heat Transfer	
Active Heat Transfer, Surface Area, ft^2	48,600
Average Heat Flux, Btu/hr-ft^2	198,300
Maximum Heat Flux for Normal Operation, Btu/hr-ft^2	499,700(1)
Average Thermal Output, kW/ft	5.69
Maximum Thermal Output for Normal Operation, kW/ft	14.3 (1)
Peak linear power for determination of protection set points, kW/ft	22.4 (2)
Heat Flux Hot Channel Factor F(Q)	2.52
Fuel Central Temperature, °F	
Peak at Maximum Thermal Output for Maximum Overpower Trip Point, °F	<4,700
Core Mechanical Design Parameters	
Fuel Assemblies	
Design	RCC Canless
Number of Fuel Assemblies	157
UO_2 Rods per Assembly	264
Rod Pitch, inches	0.496
Overall Dimensions, inches	8.426 x 8.426
Fuel Weight (as UO_2), pounds (Cycle 1)	181,205
Zircaloy/ZIRLO™ Weight, lbs.	38,230
Number of Grids per Assembly (17x17 STD, V5H, VANTAGE+)	2 - non-Mixing Vane 6 - Type R Mixing Vane 1 - Protective Bottom Grid (VANTAGE+ only)
Number of Grids per Assembly (Robust Fuel Assembly - RFA)	2 - non-Mixing Vane 6 - LPD Mixing Vane 3 - IFM 1 - Protective Bottom Grid
Loading Technique	Multi-Region Non-Uniform

Table 3.1-1 (CONT'D)
REACTOR DESIGN PARAMETERS

Core Mechanical Design Parameters	**Design Value**
Fuel Rods	
Number	41,448
Outside Diameter, inches	0.374
Diametral Gap, inches (Uncoated pellets)	0.0065
Clad Thickness, inches	0.0225
Clad Material	Zircaloy-4 / ZIRLO® Optimized ZIRLO™
Fuel Pellets	
Material	UO_2 Sintered
Density (% of Theoretical)	95
Diameter, inches, (Uncoated pellets)	0.3225
Solid - Enriched (typical) Length, inches	0.387
Solid - Blanket (typical) Length, inches	0.500
Annular - Blanket (typical) Length, inches	0.500
Diameter of annulus (inches)	0.155
Rod Cluster Control Assemblies	
Neutron Absorber	Ag-In-Cd
Cladding Material	Type 304SS Cold Worked
Clad Thickness, Inches	0.0185
Number of Clusters, Full Length	48
Number of Absorber Rods per Cluster	24
Core Barrel, I.D./O.D., inches	133.85/137.875
Thermal Shield, I.D./O.D., inches	143.63/148.000
Nuclear Design Parameters	
Structure Characteristics	
Core Diameter, inches (Equivalent)	119.7
Core Average Active Fuel Height, inches	144.0
Reflector Thickness and Composition	
Top - Water plus Steel, inches	~10

Table 3.1-1 (CONT'D)
REACTOR DESIGN PARAMETERS

Bottom - Water plus Steel, inches	~10
Side - Water plus Steel, inches	~15
H_2O/U, Cold Molecular Ratio (Lattice)	3.43 Volume 2.41 Molecular
Feed Enrichment, w/o (Cycle 1)	
Region 1	2.10
Region 2	2.60
Region 3	3.10

(1) This limit is associated with the value of F(Q)=2.52.

(2) See Section 3.3.2.2.6.

(3) Based on 6.5% core bypass flow.

(4) Based on high T_{avg} at 580.0°F.

Table 3.1-2

ANALYTIC TECHNIQUES IN CORE DESIGN

Analysis	Technique	Computer Code	Section Referenced
Mechanical Design or Core Internals			
Loads, Deflections and Stress Analysis	Static and Dynamic Modeling	MULTIFLEX code, FORCE, Finite element structural analysis code and others	14.3.3 B.3
Fuel Rod Design			
Fuel Performance Characteristics (temperature, internal pressure, clad stress, etc.)	Semi-empirical thermal model of fuel rod with consideration of fuel density changes, heat transfer, fission gas release, etc.	Westinghouse fuel rod design model	3.2.1.3.1 3.3.3.1
Nuclear Design			
1) Cross Sections and Group Constants	Microscopic data Macroscopic constants for homogenized core regions	Modified ENDF/B library PHOENIX-P, NEXUS/PARAGON	3.3.3.2 3.3.3 3.3.3.2
	Group constants for control rods with self-shielding	PHOENIX-P, NEXUS/PARAGON	3.3.3.2
2) X-Y Power Distributions, Fuel Depletion, Critical Boron Concentrations, x-y Xenon Distributions, Reactivity Coefficients and Control Rod Worths	2-D, 3-Group Diffusion Theory	ANC	3.3.3.3
3) X-Y-Z Power Distributions, Fuel Depletion, Critical Boron Concentrations, X-Y-Z Xenon Distributions, Reactivity Coefficients and Control Rod Worths	3-D, 2-Group Diffusion Theory	3D ANC	3.3.3.3
4) Axial Power Distributions, Control Rod Worths and Axial Xenon Distribution	1-D, 2-Group Diffusion Theory	PANDA/APOLLO	3.3.3 3.3.3.3

Table 3.1-2 (CONT'D)

ANALYTIC TECHNIQUES IN CORE DESIGN

5)	Fuel Rod Power	Integral Transport Theory	LASER	3.3.3.1
6)	Effective Resonance Temperature	Monte Carlo Weighting Function	REPAD	3.3.3.1
Thermal-Hydraulic Design				
1)	Steady-state	Subchannel analysis of local fluid conditions in rod bundles, including inertial and crossflow resistance terms, solution progresses from core-wide to hot assembly to hot channel	VIPRE-01	3.4.3.4.1
2)	Transient DNB Analysis	Subchannel analysis of local fluid conditions in rod bundles during transients by including accumulation terms in conservation equations; solution progresses from core wide to hot assembly to hot channel.	VIPRE-01	3.4.3.4.1

Table 3.1-3

DESIGN LOADING CONDITIONS FOR REACTOR CORE COMPONENTS

1. Fuel Assembly Weight
2. Fuel Assembly Spring Forces
3. Internals Weight
4. Control Rod Scram (equivalent static load)
5. Differential Pressure
6. Spring Preloads
7. Coolant Flow Forces (static)
8. Temperature Gradients
9. Differences in thermal expansion
    a. Due to temperature differences
    b. Due to expansion of different materials
10. Interference between components
11. Vibration (mechanically or hydraulically induced)
12. One or more loops out of service
13. All operational transients listed in Table 4.1-1
14. Pump overspeed
15. Seismic loads (operational basis earthquake and Safe Shutdown earthquake)
16. Blowdown forces (due to cold and hot leg break)

Table 3.2-1

Maximum Deflections Allowed for Reactor Internal Support Structures

Component	Allowable Deflections (inches)	No Loss-of-Function Deflections (inches)
Upper Barrel		
radial inward	4.38	8.77
radial outward	1.00	1.50
Upper Package	0.10	0.15
Rod Cluster Guide Tubes	1.00	1.75

Table 3.3-1

REACTOR CORE DESCRIPTION

Active Core	
Equivalent Diameter, inches	119.7
Core Avg. Active Fuel Hgt., inch	144.0
Height-to-Diameter Ratio	1.20
Total Cross-Section Area, ft^2	78.14
Reflector Thickness and Composition	
Top - Water plus Steel, inches	10
Bottom - Water plus Steel, inches	10
Side - Water plus Steel, inches	15
Fuel Assemblies	
Number	157
Rod Array	17 x 17
Rods per Assembly	264
Rod Pitch, inches	0.496
Overall Transverse Dimensions, inches	8.426 x 8.426
Fuel Weight (as UO_2), lbs (Cycle 1)	181,205
Zircaloy Weight, lbs (Cycle 1)	38,230
Number of Grids per Assembly (17x17 STD, V5H, VANTAGE+)	2 - non mixing vane 6 - Type R mixing vane 1 - Protective Bottom Grid (VANTAGE+ only)
Number of Grids per Assembly (Robust Fuel Assembly - RFA)	2 - non-Mixing Vane 6 - LPD Mixing Vane 3 - IFM 1 - Protective Bottom Grid

Table 3.3-1 (CONT'D)
REACTOR CORE DESCRIPTION

Fuel Assemblies (Cont'd)

Composition of Grids	Inconel 718 - Standard Zircaloy 4 - VANTAGE 5H ZIRLO® - VANTAGE+, RFA
Weight of Grids (Effective in Core) lbs (Cycle 1)	1,885
Number of Guide Thimbles per Assembly	24
Composition of Guide Thimbles	Zircaloy 4/ZIRLO®
Diameter of Guide Thimbles (upper part), inches	0.450 I.D. x 0.482 O.D. (Std) 0.442 I.D. x 0.474 O.D. (VANTAGE 5H/ VANTAGE+) 0.442 I.D. x 0.482 O.D. (RFA)
Diameter of Guide Thimbles (lower part), inches	0.397 I.D. x 0.430 O.D. (VANTAGE5H/VANTAGE+) 0.397 I.D. x 0.439 O.D. (RFA)
Diameter of Instrument Guide Thimbles, inches	0.450 I.D. x 0.482 O.D. (Std) 0.442 I.D. x 0.474 O.D. (VANTAGE 5H/ VANTAGE+) 0.442 I.D. x 0.482 O.D. (RFA)

Fuel Rods

Number	41,448
Outside Diameter, inches	0.374
Diameter Gap, inches (uncoated pellets)	0.0065
Clad Thickness, inches	0.0225
Clad Material	Zircaloy-4 / ZIRLO® / Optimized ZIRLO™

Table 3.3-1 (CONT'D)

REACTOR CORE DESCRIPTION

Fuel Pellets	
Material	UO_2 Sintered
Density (percent of Theoretical)	95
Fuel Enrichments w/o (Cycle 1)	
Region 1	2.10
Region 2	2.60
Region 3	3.10
Diameter, inches Regions 1,2,3	0.3225
Length, inches (Cycle 1)	0.530
Mass of UO_2 per Foot of Fuel Rod, lb/ft (Cycle 1)	0.364
Rod Cluster Control Assemblies	
Neutron Absorber	Ag-In-Cd
Composition	80%, 15%, 5%
Diameter, inches	0.341
Density, lbs/inches^3	0.367
Cladding Material	Type 304, Cold-Worked Stainless Steel
Clad Thickness, inches	0.0185
Number of Full Length Clusters	48
Number of Absorber Rods per Cluster	24
Full Length Assembly Weight (dry), lb.	149

Table 3.3-1 (CONT'D)

REACTOR CORE DESCRIPTION

Burnable Absorber Rods (Cycle 1)

Number	1,072
Material	Borosilicate Glass
Outside Diameter, inches	0.381
Inner Tube, O.D., inches	0.1815
Clad Material	Stainless Steel
Inner Tube Material	Stainless Steel
Boron Loading (w/o B_2O_3 in glass rod)	12.5
Weight of B^{10} per foot of rod, lb/ft	.000419
Initial Reactivity Worth, %	7.0 (hot), 5.5 (cold)

Excess Reactivity (Cycle 1)

Maximum Fuel Assembly k_∞ (Cold, Clean, Unborated Water)	<1.6
Maximum Core Reactivity (Cold, Zero Power, Beginning of Cycle 1)	1.25

Table 3.3-2

NUCLEAR DESIGN PARAMETERS

Core Average Linear Power, kW/ft, Including Densification Effects	5.69
Total Heat Flux Hot-Channel Factor	<2.40
Nuclear Enthalpy Rise Hot-Channel Factor, $F(N,\Delta H)$	1.62
Reactivity Coefficients (Cycle 1)	
Doppler Coefficient	See Figures 3.3-27 and 3.3-28
Moderator Temperature Coefficient at Operating Conditions, pcm/°F(1)	See Figures 3.3-30, 3.3-31, 3.3-32, and 3.3-33
Boron Coefficient in Primary Coolant pcm/ppm(1)	-16 to -8
Rodded Moderator Density Coefficient at Operating Conditions, pcm/gm/cc	$\leq$+0.43 x 10^5
Delayed Neutron Fraction and Lifetime (Cycle 1)	
β_{eff} BOL, (EOL)	0.0075 (0.0044)
ε^*, BOL, (EOL), μ sec	19.4 (18.1)
Control Rod Worths (Cycle 1)	
Rod Requirements	See Table 3.3-3
Maximum Bank Worth, pcm	<2,300
Maximum Ejected Rod Worth	See Technical Specifications

(1) NOTE: 1 pcm = (percent mille) 10^{-5} Δp where Δp is calculated from two statepoint values of k_{eff} by Ln (k_2/k_1).

Table 3.3-2 (CONT'D)

NUCLEAR DESIGN PARAMETERS

Boron Concentrations (Three Loop Operation, Cycle 1)

Refueling	
$k_{eff} \leq 0.95$, Cold, Rod Cluster	2000
Control Assemblies In	1196
Zero Power	
$k_{eff} = 0.99$, Cold, Rod Cluster	
Control Assemblies Out	1429
Zero Power	
$k_{eff} = 0.99$, Hot, Rod Cluster	
Control Assemblies Out	1419
Full Power, No Xenon, Beginning of Cycle $k_{eff} = 1.0$, Hot, Rod	
Cluster Control Assemblies Out	1195
Full Power, Equilibrium Xenon, $k_{eff} = 1.0$, Hot, Rod Cluster	
Control Assemblies Out	906
Reduction With Fuel Burnup	
First Cycle, ppm/GWD/MTU(2)	See Figure 4.3-3
Reload Cycle, ppm/GWD/MTU	~100

(2) Gigawatt Day (GWD) = 1,000 Megawatt Day (1,000 MWD). During the first cycle, fixed burnable poison rods were present which significantly reduce the boron depletion rate compared to reload cycles. The values quoted are representative of averages only.

Table 3.3-3

Reactivity requirements for Rod Cluster Control Assemblies

	Reactivity Effects, percent	Beginning of Life (First Cycle)	End of Life (First Cycle)	End of Life (Equilibrium Cycle) (Preliminary)
1.	Control requirements			
	Fuel temperature (Doppler), %Δρ	1.26(1)	1.05	1.30
	Moderator temperature, %Δρ	.21	.98	1.25
	Void, %Δρ	.05	.05	.05
	Redistribution, %Δρ	.50	.85	.85
	Rod Insertion Allowance, %Δρ	.50	.50	.50
2.	Total Control, %Δρ	2.52	3.43	3.95
3.	Estimated Rod Cluster Control Assembly Worth (48 Rods)			
	a. All full length assemblies inserted, %Δρ	9.88	9.57	8.50
	b. All but one (highest worth) assemblies inserted, %Δρ	7.85	7.81	6.64
4.	Estimated Rod Cluster Control Assembly credit with 10 percent adjustment to accommodate uncertainties (3b - 10 percent), %Δρ	7.06	7.03	5.97
5.	Shutdown margin available (4-2), %Δρ	4.54	3.60	2.02(1)

(1) The design basis minimum shutdown is 1.77%.

Table 3.3-4

AXIAL STABILITY INDEX

PWR CORE WITH A 12 FT HEIGHT

Burnup	F_Z	C_B	Stability Index (hr^{-1})	
(MWD/T)		(ppm)	Exp	Calc
1,550	1.34	1,065	-0.041	-0.032
7,700	1.27	700	-0.014	-0.006
		Difference:	+0.027	+0.026

Table 3.3-5

TYPICAL NEUTRON FLUX LEVELS (n/cm^2-sec) AT FULL POWER

(Three Loop)

	E>1.0 Mev	5.53 Kev<E ≤ 1.0 Mev	.625ev ≤E < 5.53 Kev	E < .625 ev $(n\mu)_o$
Core Center	6.51×10^{13}	1.12×10^{14}	8.50×10^{13}	3.00×10^{13}
Core Outer Radius at Midheight	3.23×10^{13}	5.74×10^{13}	4.63×10^{13}	8.60×10^{12}
Core Top, on Axis	1.53×10^{13}	2.42×10^{13}	2.10×10^{13}	1.63×10^{13}
Core Bottom, on Axis	2.36×10^{13}	3.94×10^{13}	3.50×10^{13}	1.46×10^{13}
Pressure Vessel Inner Wall, Azi-muthal Peak, Core Mid-height	2.77×10^{10}	5.75×10^{10}	6.03×10^{10}	8.38×10^{10}

Table 3.3-6

COMPARISON OF MEASURED AND CALCULATED DOPPLER DEFECTS

Plant	Fuel Type	Core Burnup (MWD/MTU)	Measured (pcm)[1]	Calculated (pcm)
1	Air-filled	1,800	1,700	1,710
2	Air-filled	7,700	1,300	1,440
3	Air- and helium-filled	8,460	1,200	1,210

[1] pcm = 10^5 x Ln (K_1/K_2)

Table 3.3-7

BENCHMARK CRITICAL EXPERIMENTS

Description of [1] Experiments	No. of Experiments	LEOPARD k_{eff} Using Experimental Bucklings
UO_2		
Al Clad	14	1.0012
SS Clad	19	0.9963
Borated H_2O	7	0.9989
Total	40	0.9985
U-Metal		
Al Clad	41	0.9995
Unclad	20	0.9990
Total	61	0.9993
Grand Total	101	0.9990

[1]Reported in Reference 24.

Table 3.3-8

SAXTON CORE II ISOTOPICS
ROD MY, AXIAL ZONE 6

Atom Ratio	Measured [1]	2σ Precision (%)	LEOPARD Calculation
U-234/U	4.65×10^{-5}	± 29	4.60×10^{-5}
U-235/U	5.74×10^{-3}	± 0.9	5.73×10^{-3}
U-236/U	3.55×10^{-4}	± 5.6	3.74×10^{-4}
U-238/U	0.99386	± 0.01	0.99385
Pu-238/Pu	1.32×10^{-3}	± 2.3	1.222×10^{-3}
Pu-239/Pu	0.73971	± 0.03	0.74497
Pu-240/Pu	0.19302	± 0.2	0.19102
Pu-241/Pu	6.014×10^{-2}	± 0.3	5.74×10^{-2}
Pu-242/Pu	5.81×10^{-3}	± 0.9	5.38×10^{-3}
Pu/U[2]	5.938×10^{-2}	± 0.7	5.970×10^{-2}
Np-237/U-238	1.14×10^{-4}	± 15	0.86×10^{-4}
Am-241/Pu-239	1.23×10^{-2}	± 15	1.08×10^{-2}
Cm-242/Pu-239	1.05×10^{-4}	± 10	1.11×10^{-4}
Cm-244/Pu-239	1.09×10^{-4}	± 20	0.98×10^{-4}

[1] Reported in Reference 25
[2] Weight Ratio

Table 3.3-9

CRITICAL BORON CONCENTRATIONS, HZP, BOL

Plant Type	Measured	Calculated
2-Loop, 121 Assemblies 10 foot core	1,583	1,589
2-Loop, 121 Assemblies 12 foot core	1,625	1,624
2-Loop, 121 Assemblies 12 foot core	1,517	1,517
3-Loop, 157 Assemblies 12 foot core	1,169	1,161

Table 3.3-10

COMPARISON OF MEASURED AND CALCULATED ROD WORTH

2-Loop Plant, 121 Assemblies, 10 foot core	Measured (pcm)	Calculated (pcm)
Group B	1,885	1,893
Group A	1,530	1,649
Shutdown group	3,050	2,917
ESADA Critical[1], 0.69 inch Pitch, 2 w/o PUO_2, 8% Pu^{240}, 9 Control Rods		
6.21 inch rod separation	2,250	2,250
2.07 inch rod separation	4,220	4,160
1.38 inch rod separation	4,100	4,010

[1] Reported in Reference 26.

Table 3.3-11

COMPARISON OF MEASURED AND CALCULATED MODERATOR COEFFICIENTS AT HZP, BOL

Plant Type/ Control Bank Configuration	Measured[1] (pcm/°F)	Calculated (pcm/°F)
3-Loop, 157 Assemblies, 12 foot core		
D at 160 steps	-0.50	-0.50
D in, C at 190 steps	-3.01	-2.75
D in, C at 28 steps	-7.67	-7.02
B, C and D in	-5.16	-4.45
2-Loop, 121 Assemblies 12 foot core		
D at 180 steps	+0.85	+1.02
D in, C at 180 steps	-2.40	-1.90
C and D in, B at 165 steps	-4.40	-5.58
B, C and D in, A at 174 steps	-8.70	-8.12

(1) Isothermal coefficients, which include the Doppler effect in the fuel.

$\alpha_{in} = 10^5 \quad \mathrm{Ln}\frac{k_2}{k_1} / \Delta T°F$

Table 3.4-1

REACTOR DESIGN PARAMETERS

Thermal and Hydraulic Design Parameters	Design Value
Reactor Core Heat Output, MWt	See Table 3.1-1
Reactor Core Heat Output, Btu/hr	See Table 3.1-1
Heat Generated in Fuel, %	See Table 3.1-1
System Pressure, Nominal psia	See Table 3.1-1
Minimum DNBR at Nominal Conditions	
Typical Flow Channel	2.83 (RFA) 2.56 (V5H)
Thimble (Cold Wall) Flow Channel	2.76 (RFA) 2.45 (V5H)
Minimum DNBR for Design Transients, typical/thimble	See Table 3.1-1
DNB Correlation	WRB-2M (RFA) WRB-1 (V5H)
Coolant Flow	
Total Thermal Design Flow Rate, lb/hr	See Table 3.1-1
Effective Flow Rate for Heat Transfer, lb/hr	See Table 3.1-1
Effective Flow Area for Heat Transfer, ft^2	See Table 3.1-1
Average Velocity Along Fuel	
Rods, ft/sec	See Table 3.1-1
Average Mass Velocity, lb/hr-ft^2	See Table 3.1-1

Table 3.4-1

REACTOR DESIGN PARAMETERS

Thermal and Hydraulic Design Parameters	Design Value
Coolant Temperature	
Nominal Inlet, °F	See Table 3.1-1
Average Rise in Vessel, °F	See Table 3.1-1
Average Rise in Core, °F	See Table 3.1-1
Average in Core, °F	See Table 3.1-1
Average in Vessel, °F	See Table 3.1-1
Heat Transfer	
Active Heat Transfer, Surface Area, ft^2	See Table 3.1-1
Average Heat Flux, $Btu/hr\text{-}ft^2$	See Table 3.1-1
Maximum Heat Flux, for normal operation $Btu/hr\text{-}ft^2$	See Table 3.1-1
Average Thermal Output, kw/ft	See Table 3.1-1
Maximum Thermal Output, for normal operation, kw/ft	See Table 3.1-1
Maximum Thermal Output at Maximum Overpower Trip Point, kw/ft	See Table 3.1-1
Fuel Central Temperature (BOL)	
Peak at linear power for prevention of centerline melt (°F)	4700
Pressure Drop	
Across Core, psi	22.3 ± 2.2 (RFA)(1) 20.25 ± 2.0 (V5H)(1)
Across Vessel, including nozzle psi	43.25 ± 4.3 (RFA) 41.2 ± 4.1 (V5H)

(1) Based on best estimate reactor flow rate as discussed in Section 4.1.

.

Table 3.4-3

VOID FRACTIONS AT NOMINAL REACTOR CONDITIONS
WITH DESIGN HOT-CHANNEL FACTORS

	Average	Maximum
Core	0.0%	--
Hot Subchannel	0.7%	3.6%

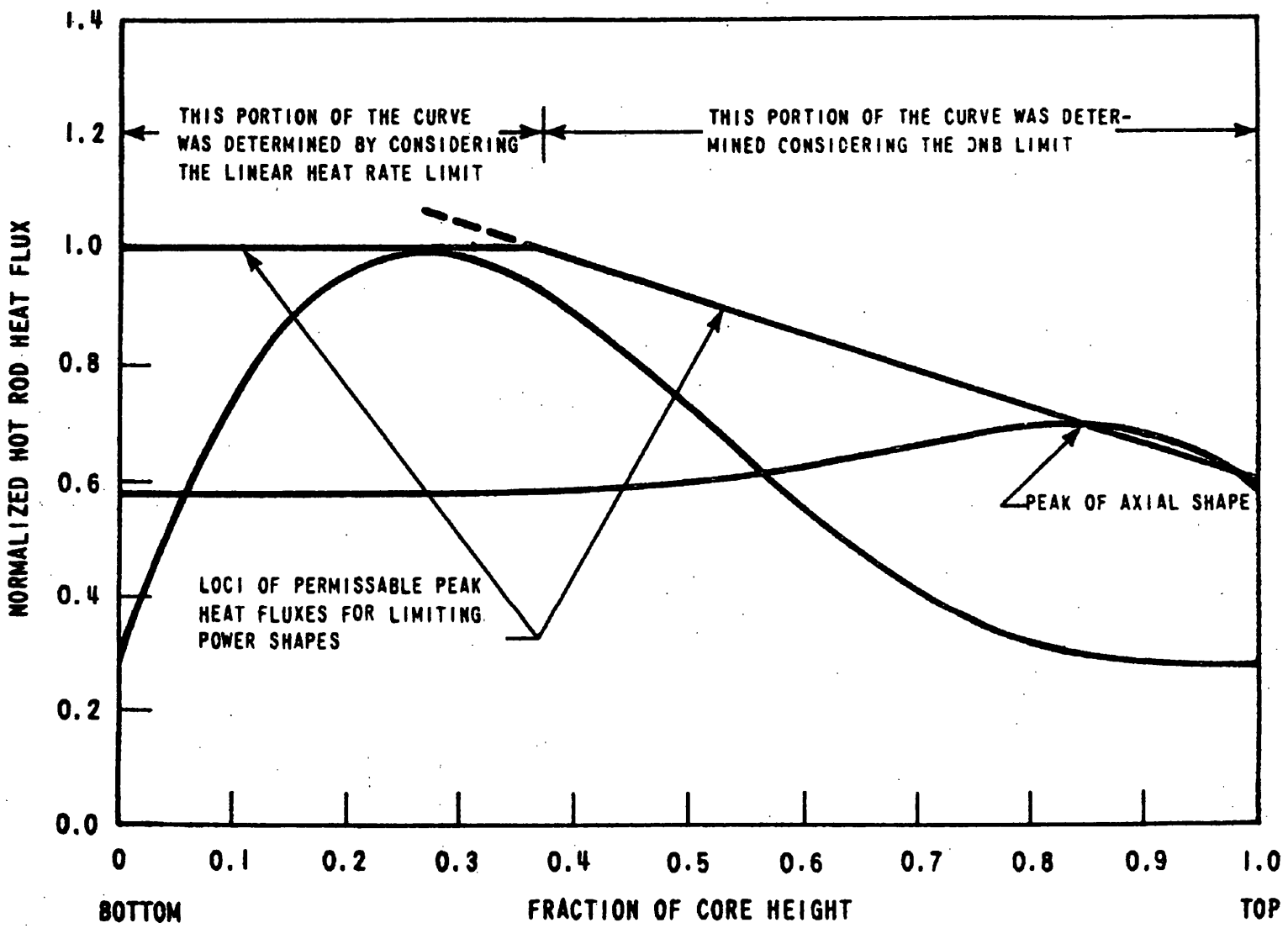

FIGURE 3.1-1
POWER DISTRIBUTION LIMITS
BEAVER VALLEY POWER STATION UNIT NO. 1
UPDATED FINAL SAFETY ANALYSIS REPORT

REV. 32

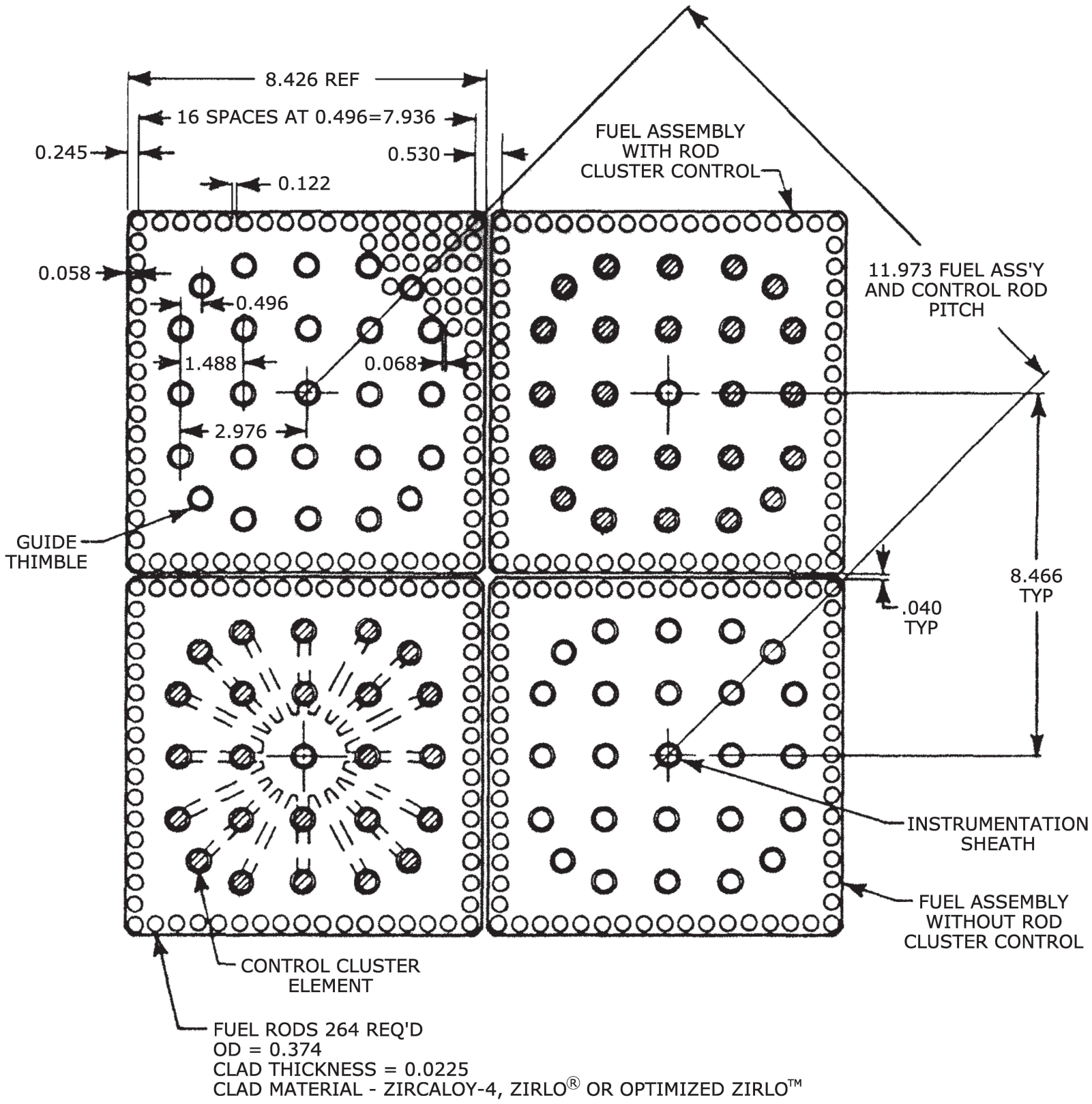

FIGURE 3.2-1

FUEL ASSEMBLY CROSS SECTION 17 x 17

BEAVER VALLEY POWER STATION UNIT NO. 1
UPDATED FINAL SAFETY ANALYSIS REPORT

M:\U1\USFAR\FIG 3.2 THRU 3.3\FIGURE 3.2-1.dgn

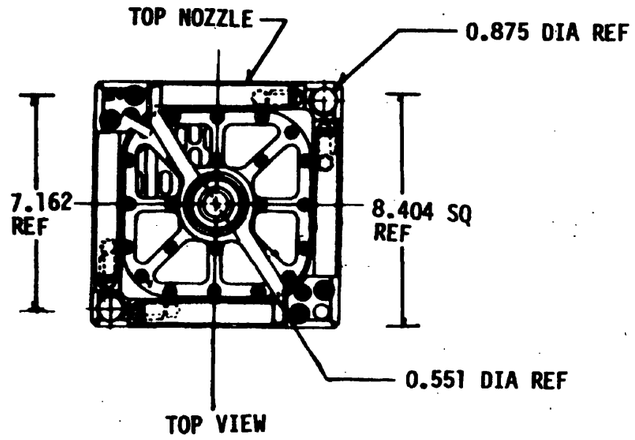

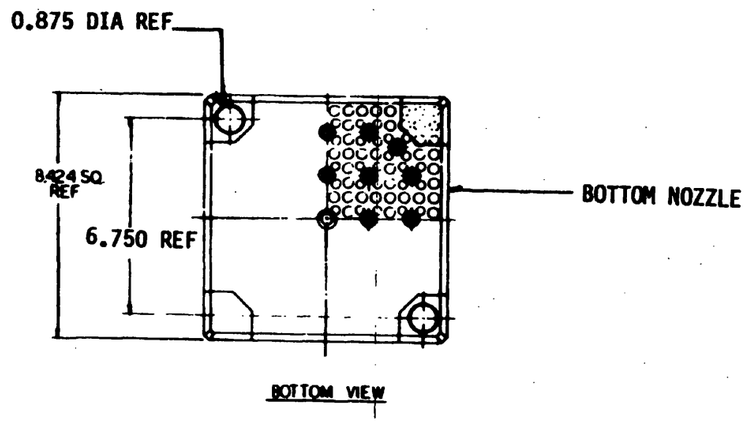

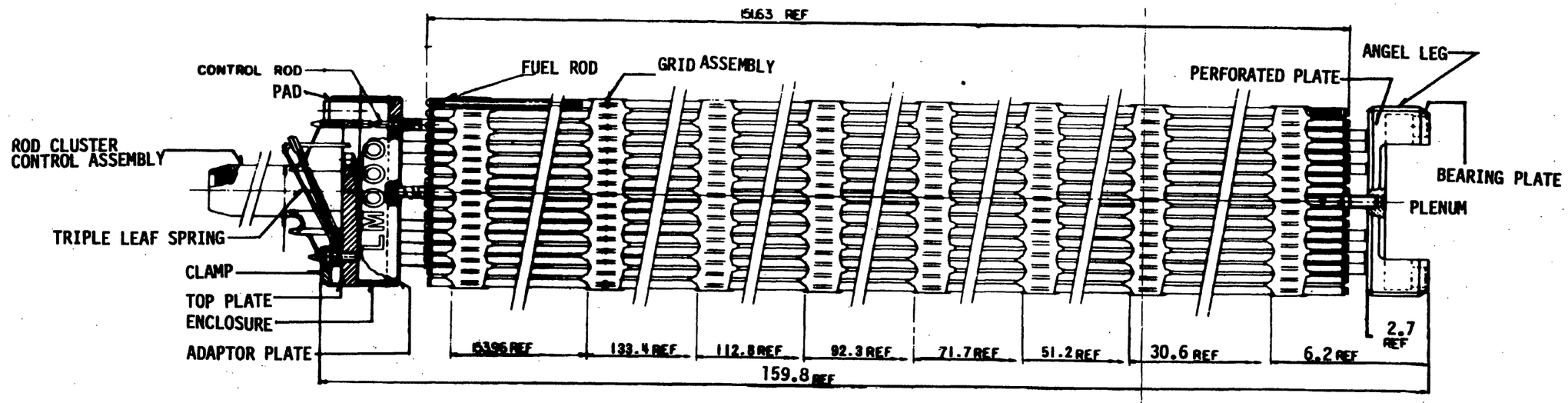

FIGURE 3.2-2
FUEL ASSEMBLY OUTLINE 17 X 17
BEAVER VALLEY POWER STATION UNIT NO. 1
UPDATED FINAL SAFETY ANALYSIS REPORT

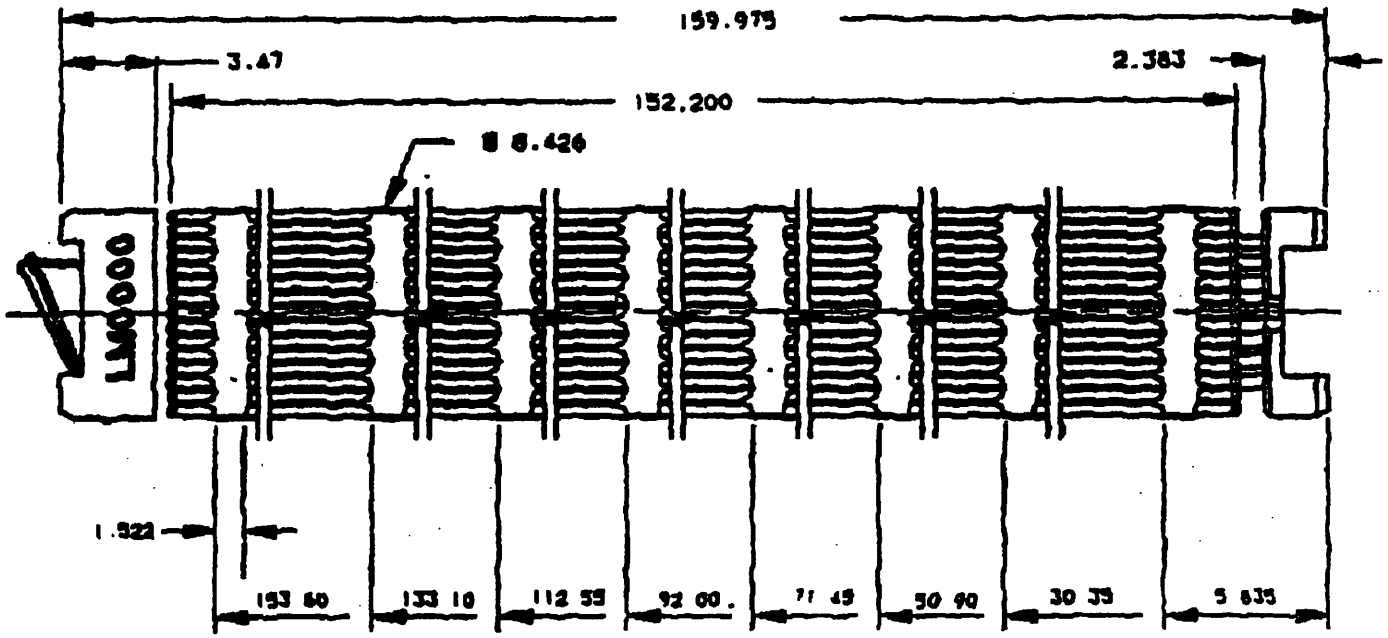

17X17 VANTAGE 5-H FUEL ASSEMBLY

FIGURE 3.2-2A

17 X 17 VANTAGE 5-H FUEL ASSEMBLY

BEAVER VALLEY POWER STATION UNIT 1
UPDATED FINAL SAFETY ANALYSIS REPORT

REV. 16

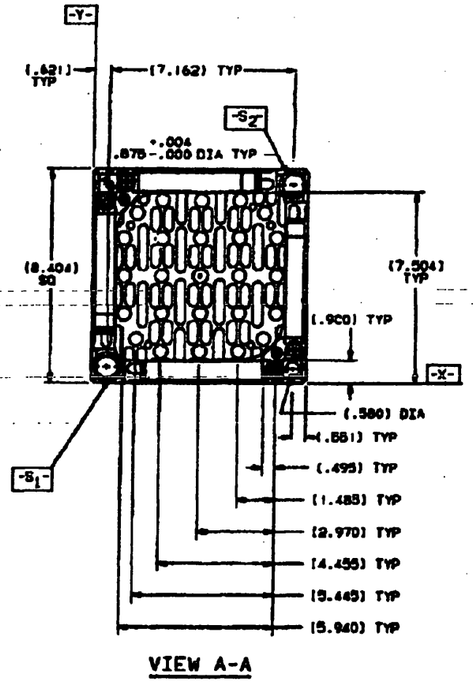

VIEW A-A

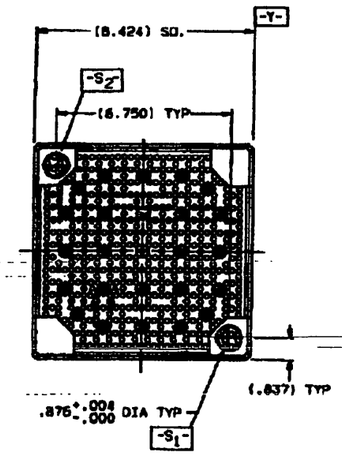

VIEW B-B

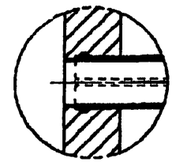

DETAIL "A"

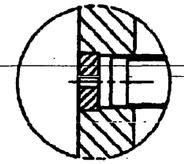

DETAIL "B"

				BILL OF MATERIAL	
REQ'D 01	ITEM	SERIES	PART NAME	SIZED REFERENCE DIFFERENTIATION	MAT'L SIZE CODE PART NUMBER OR REF DWG
1	01	-	BOTTOM NOZZLE, DEBRIS FILTER	STAINLESS STEEL	
1	02	-	TOP NOZZLE	STAINLESS STEEL	
4	03	-	NOZZLE SPRING SET	INCONEL	
24	04	-	GUIDE THIMBLE	ZIRLO	
2	05	-	GRID ASSEMBLY (TOP & BOTTOM)	INCONEL	
1	06	-	INSTRUMENT TUBE	ZIRLO	
6	07	-	GRID ASSEMBLY (MID)	ZIRLO	
1	08	-	PROTECTIVE GRID ASSEMBLY	INCONEL	

NOTES:

1. DIMENSIONS SHOWN ARE PRIOR TO IRRADIATION.
2. THESE FUEL ASSEMBLIES MAY CONTAIN INTEGRAL FUEL BURNABLE ABSORBER (IFBA) RODS. THESE FUEL RODS ARE IDENTICAL TO OTHER FUEL RODS EXCEPT FOR A THIN COATING OF ZrB_2 ON THE CIRCUMFERENTIAL SURFACE OF THE UO_2 PELLET. THE QUANTITY AND LOCATION OF IFBA RODS MAY VARY AMONG FUEL ASSEMBLIES.
3. THESE FUEL ASSEMBLIES MAY CONTAIN ROTATED MID-GRIDS. GRIDS 3, 5 AND 7 ARE ROTATED 90° CCW AS VIEWED FROM ABOVE.
4. .13 MIN ALLOWANCE REQUIRED ALL AROUND FOR PROTECTION COVER DURING DRY SHIPPING AND STORAGE.

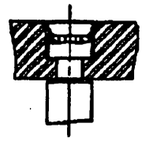

SECTION "A-A"

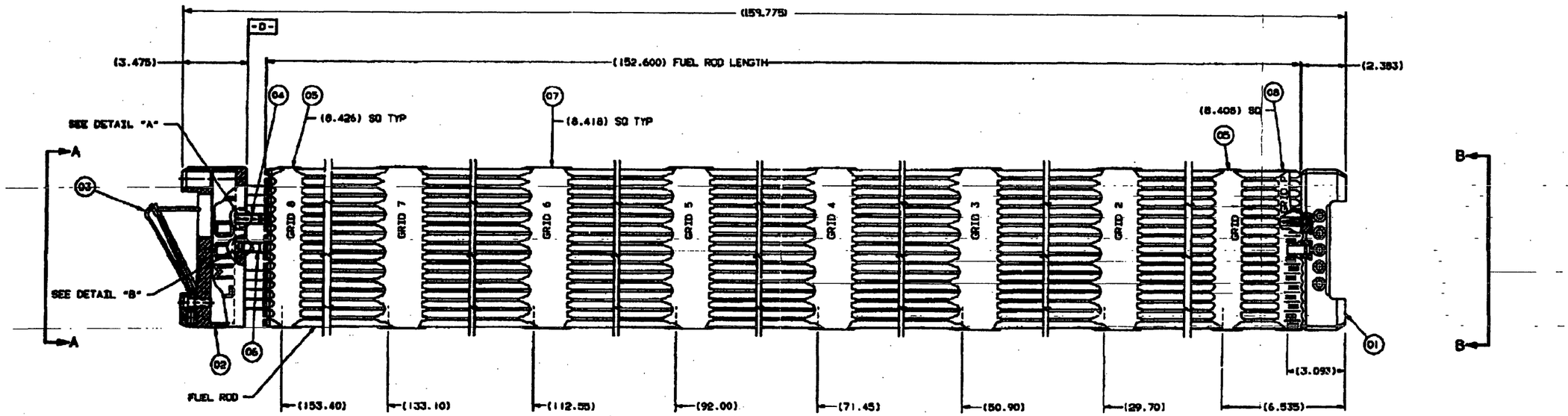

ESTIMATED WEIGHT OF MATERIALS IN FUEL ASSEMBLY:	
TOTAL	1436 LBS

FIGURE 3.2-2B
17 x 17 V5H + ZIRLO
FUEL ASSEMBLY OUTLINE

BEAVER VALLEY POWER STATION-UNIT 1
UPDATED FINAL SAFETY ANALYSIS REPORT

REV. 20

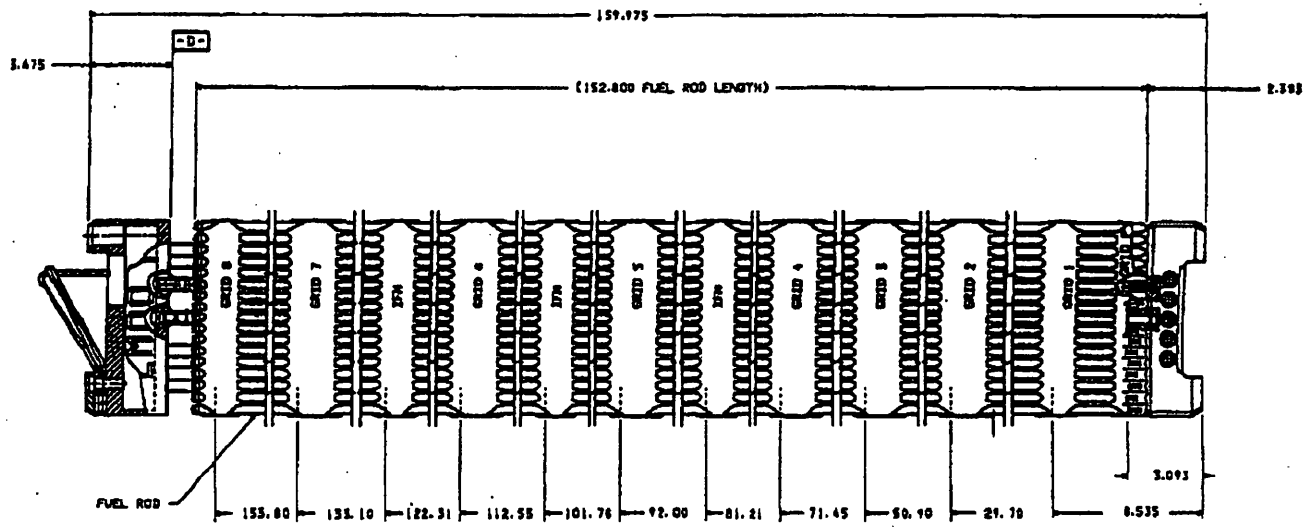

FIGURE 3.2-2C

17x17 ROBUST FUEL ASSEMBLY

BEAVER VALLY POWER STATION UNIT NO. 1
UPDATED FINAL SAFETY ANALYSIS REPORT

PREPARED ON THE CNSU CAEDDI SYSTEM

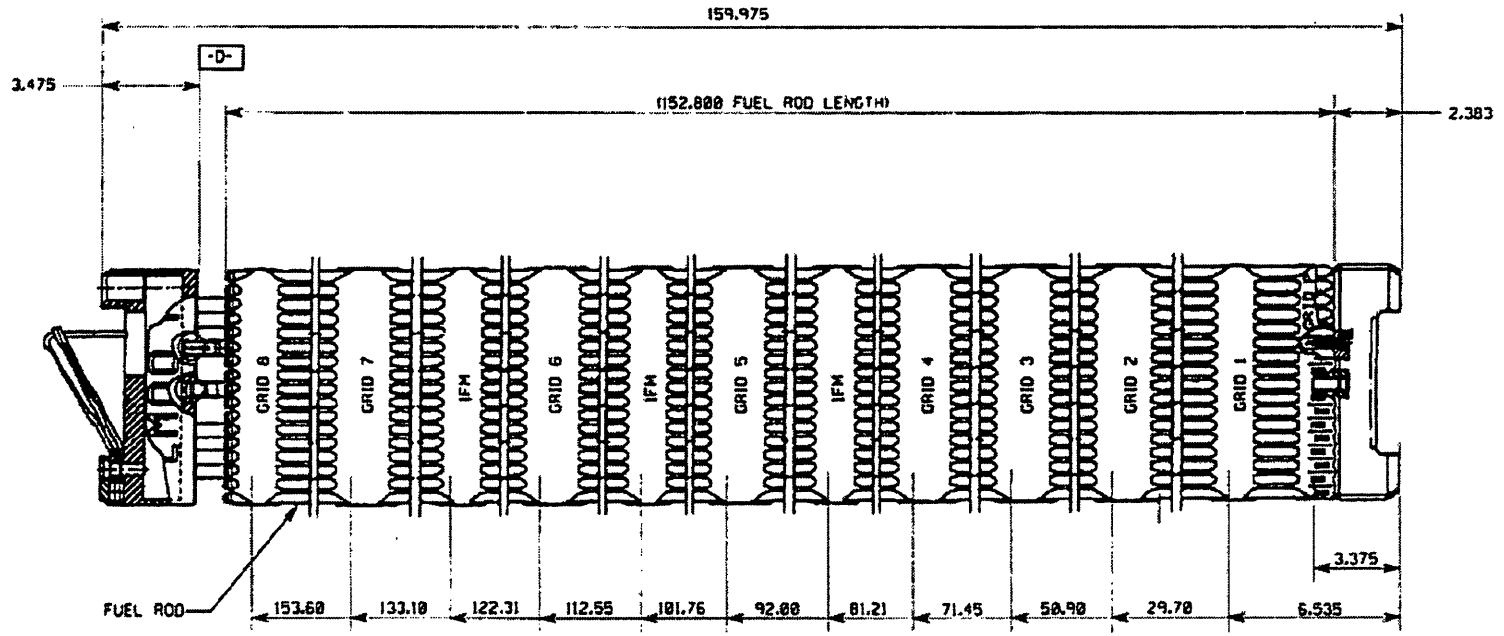

FIGURE 3.2-2D

17x17 ROBUST FUEL ASSEMBLY
WITH STANDARDIZED DEBRIS
FILTER BOTTOM NOZZLE AND
ROBUST PROTECTIVE GRID

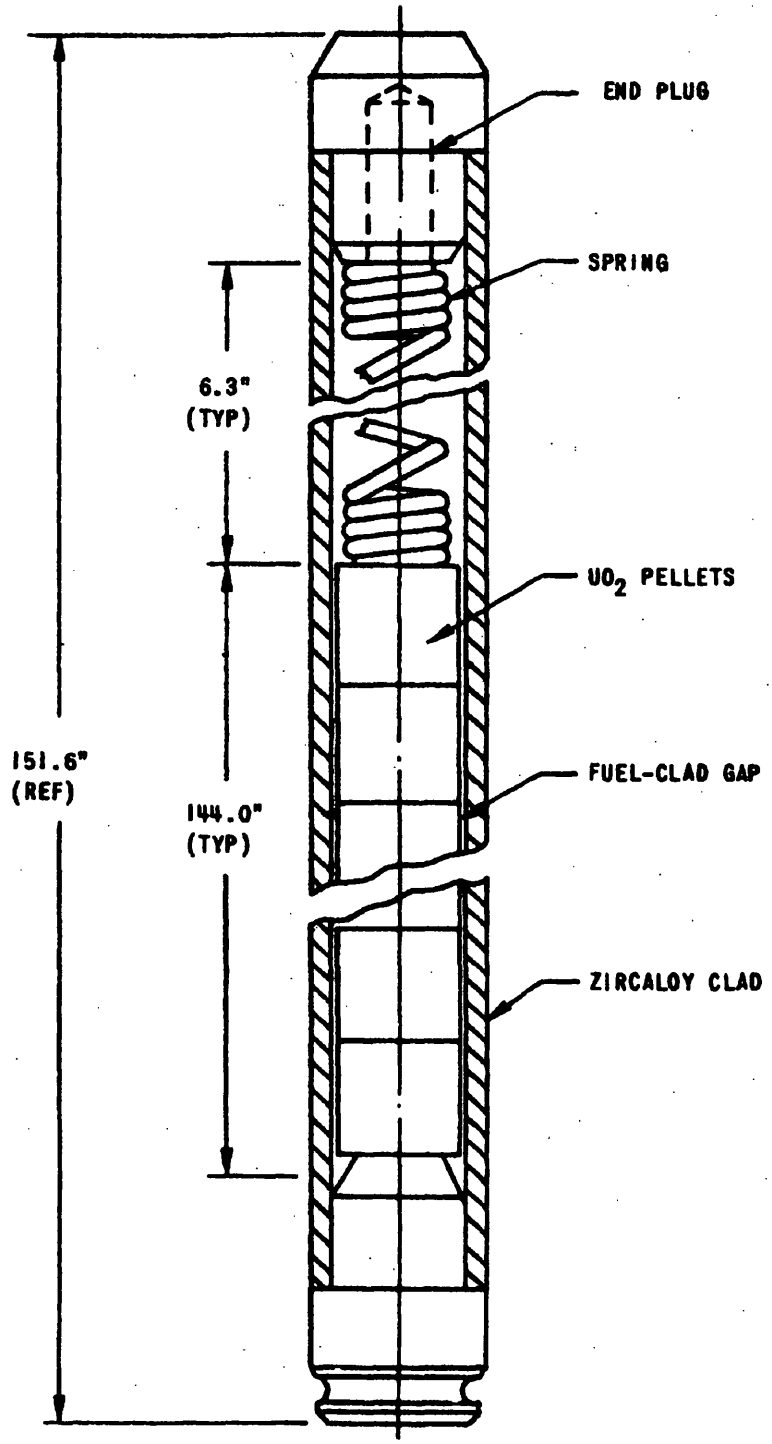

SPECIFIC DIMENSIONS DEPEND ON DESIGN VARIABLES SUCH AS PRE-PRESSURIZATION. POWER HISTORY. AND DISCHARGE BURNUP

FIGURE 3-2-3
FUEL ROD SCHEMATIC
BEAVER VALLEY POWER STATION UNIT NO. 1
UPDATED FINAL SAFETY ANALYSIS REPORT

DIM	17X17 V5-H
A	152.200
B	7.350
C	144.00
DIA D	.329
DIA E	.374

DIMENSIONS ARE IN INCHES

BOTTOM END PLUG SHOWS INTERNAL GRIP TYPE FOR V5-H FUEL RODS.

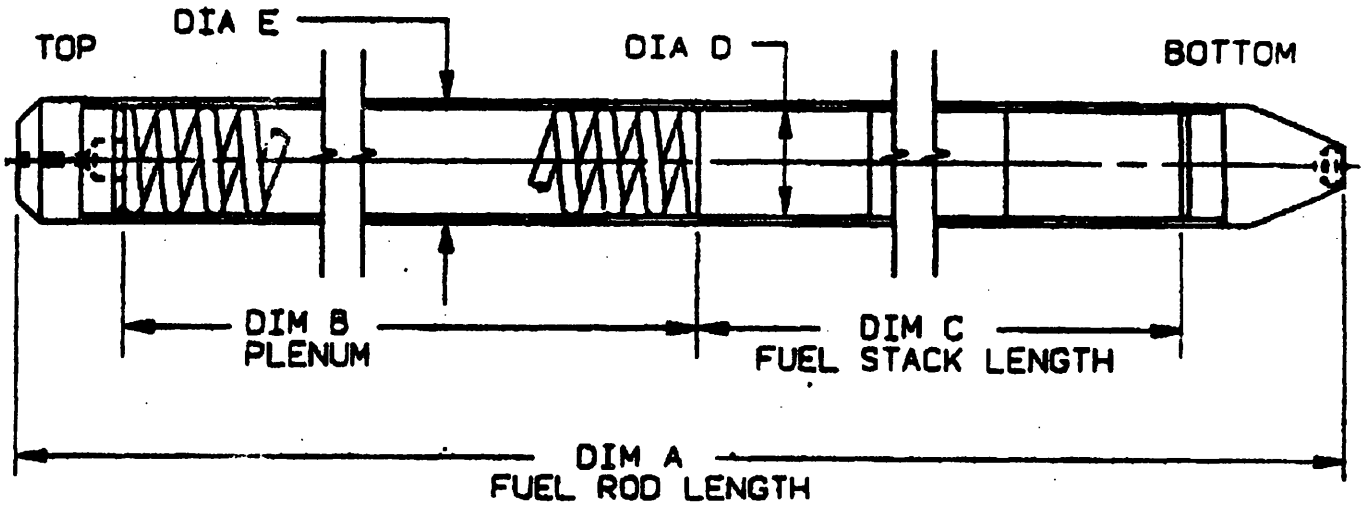

17X17 VANTAGE 5-H FUEL ROD

FIGURE 3.2-3A
BEAVER VALLEY UNIT 1
17 X 17 VANTAGE 5-H
FUEL ROD ASSEMBLY

REV. 16

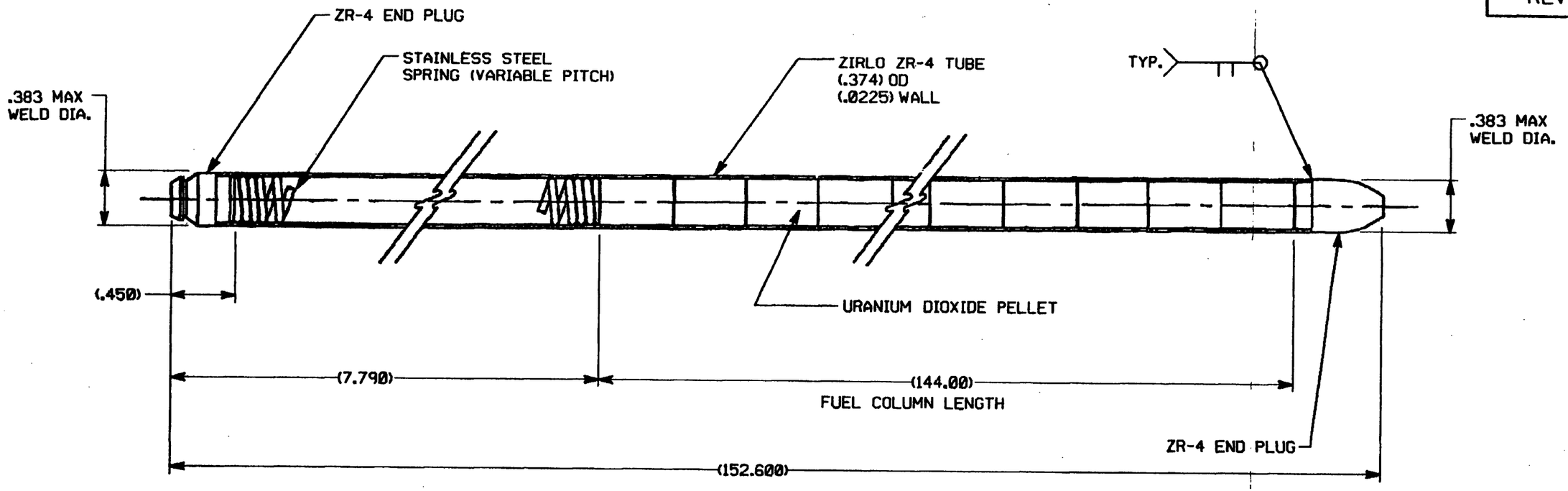

NOTES:

1. DIMENSIONS SHOWN ARE PRIOR TO IRRADIATION.
2. FUEL ROD ASSEMBLY IS PRESSURIZED.
3. SOME FUEL PELLETS MAY CONTAIN A THIN COATING OF NATURAL OR ENRICHED ZrB_2 ON THE CIRCUMFERENTIAL SURFACE OF THE PELLET.
4. THE FUEL ROD ASSEMBLIES MAY CONTAIN NATURAL OR ENRICHED UO_2 ANNULAR AXIAL BLANKET PELLETS AT THE TOP AND BOTTOM OF THE FUEL COLUMN LENGTH.
5. SOME FUEL RODS MAY CONTAIN THE DEBRIS RESISTANT OXIDE COATING.
6. THE ESTIMATED WEIGHT OF THE MATERIAL IN A FUEL ROD ASSEMBLY IN POUNDS IS:

ZIRLO	0.88
ZR-4	0.03
STAINLESS STEEL	0.01
URANIUM DIOXIDE	4.27
TOTAL	5.19

FIGURE 3.2-3B

17 x 17 V5H, ZIRLO
FUEL ROD ASSEMBLY OUTLINE

BEAVER VALLEY POWER STATION-UNIT 1
UPDATED FINAL SAFETY ANALYSIS REPORT

REV. 32

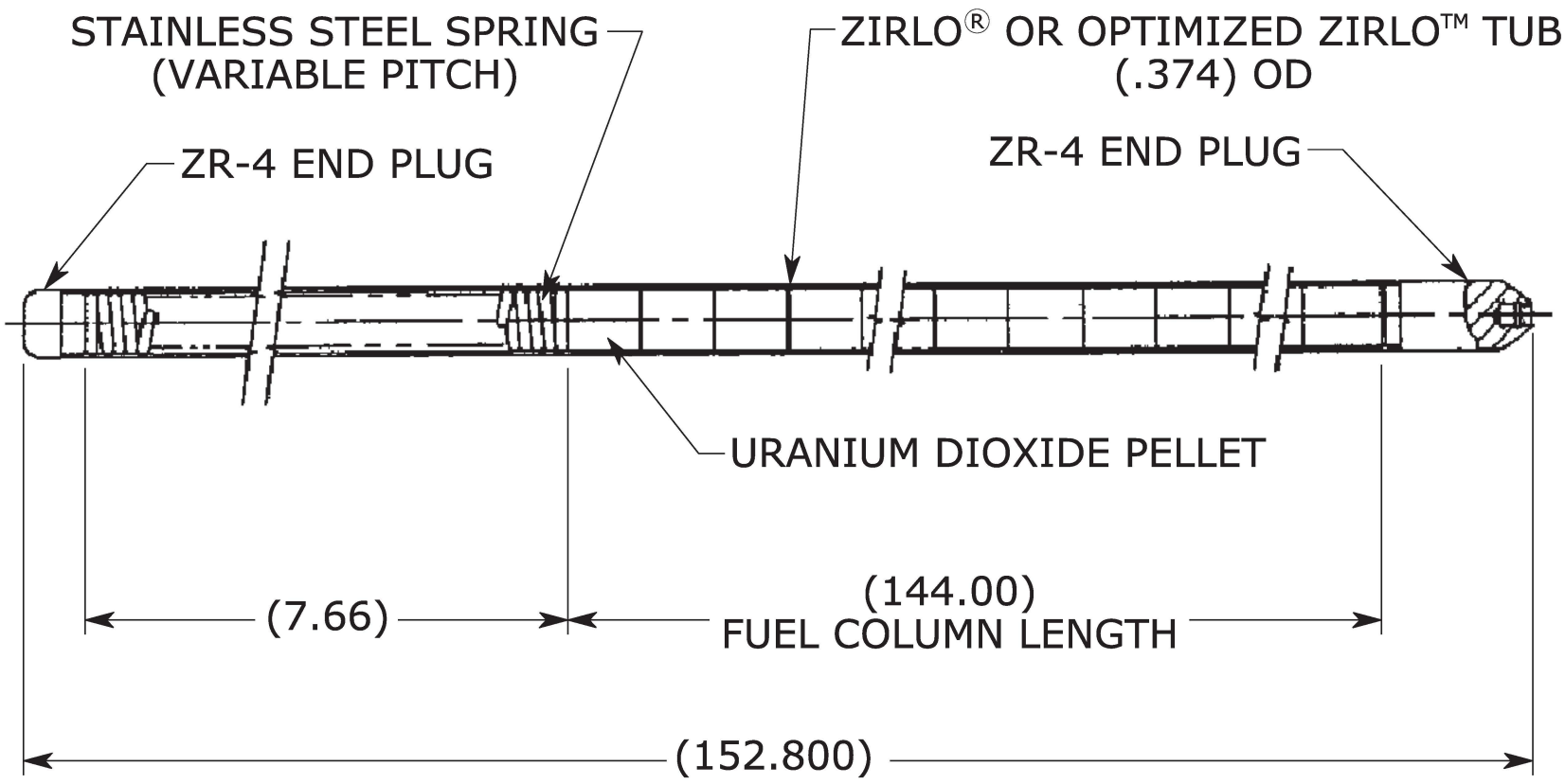

FIGURE 3.2-3C

17 x 17 ROBUST FUEL ROD ASSEMBLY

BEAVER VALLEY POWER STATION UNIT NO. 1
UPDATED FINAL SAFETY ANALYSIS REPORT

M:\U1\USFAR\FIG 3.2 THRU 3.3\FIGURE 3.2-3C.dgn

REV. 0 (1/82)

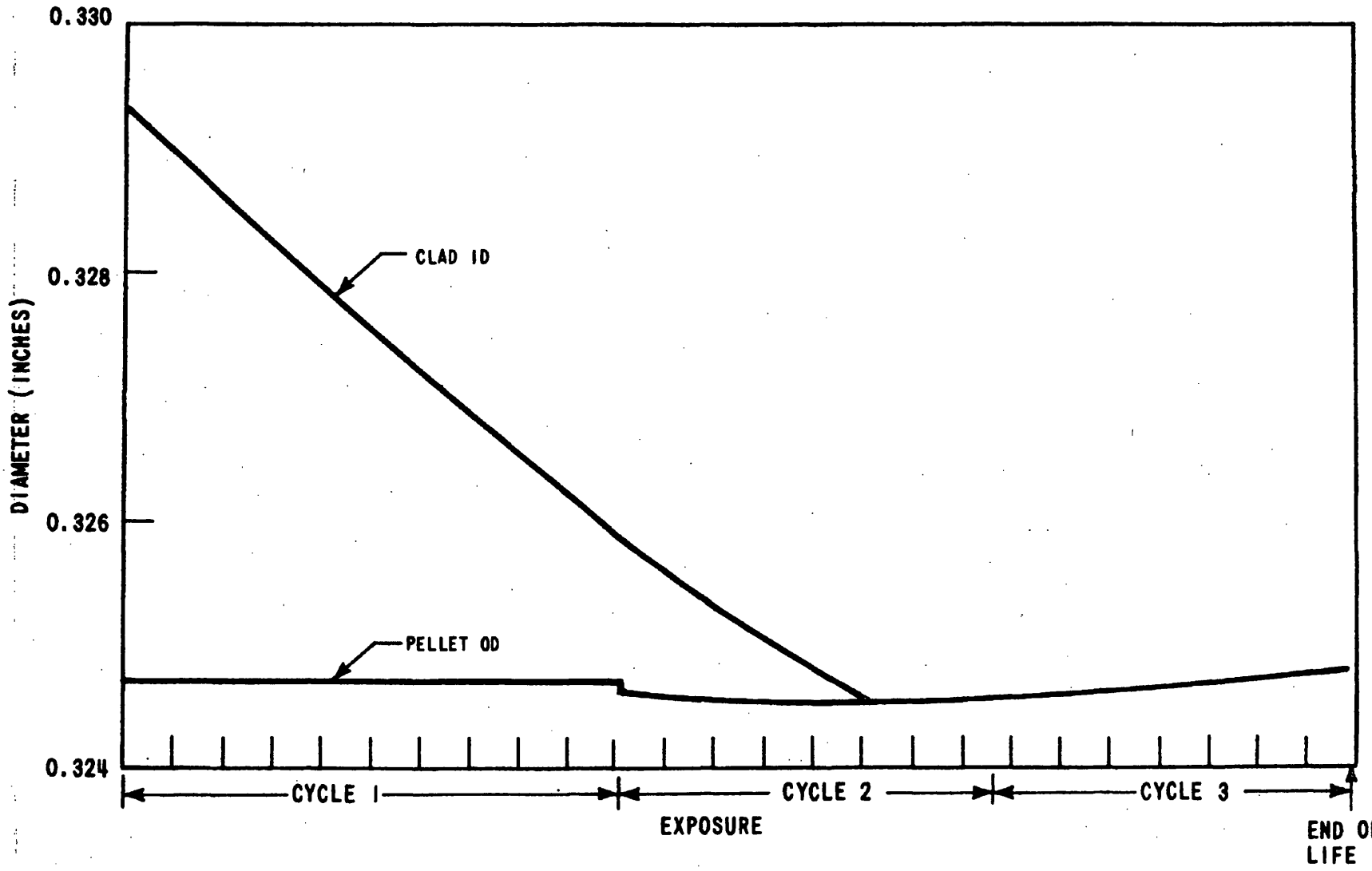

FIGURE 3.2-4
TYPICAL CLAD AND PELLET DIMENSIONS AS A FUNCTION OF EXPOSURE
BEAVER VALLEY POWER STATION UNIT NO. 1
UPDATED FINAL SAFETY ANALYSIS REPORT

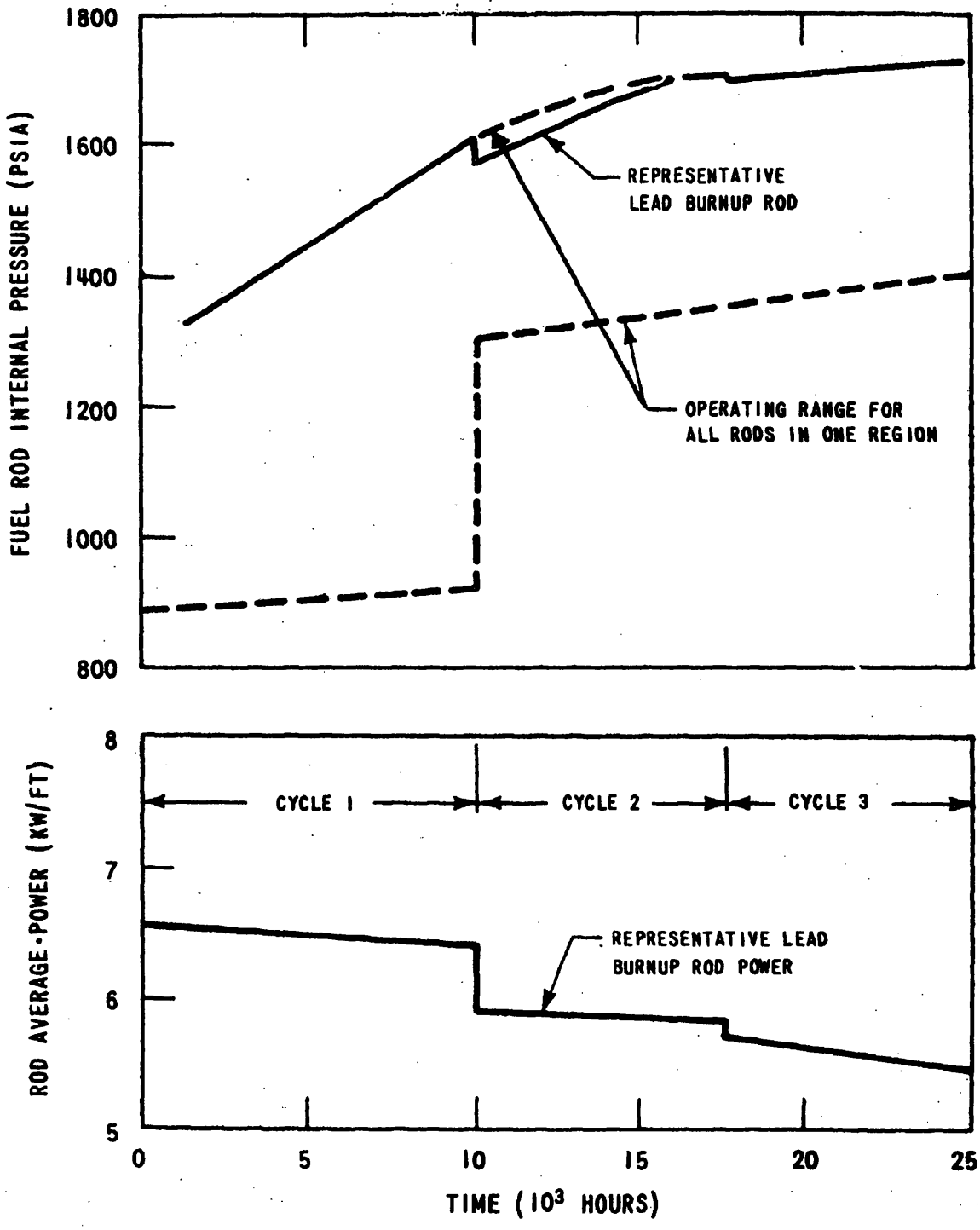

FIGURE 3.2-5
REPRESENTATIVE FUEL ROD INTERNAL PRESSURE AND LINEAR POWER DENSITY FOR THE LEAD BURNUP ROD AS A FUNCTION OF TIME

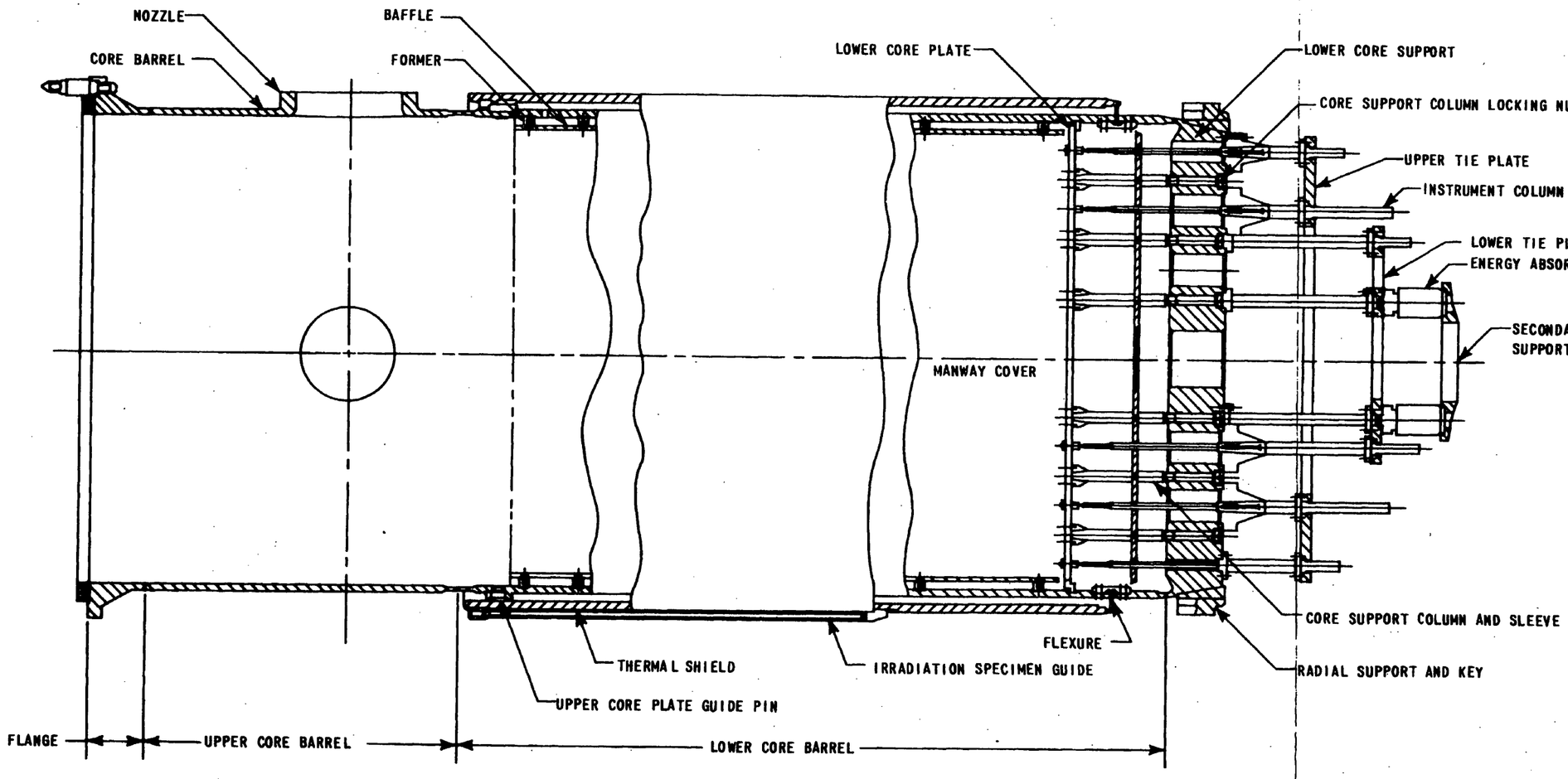

FIGURE 3.2-6
LOWER CORE SUPPORT ASSEMBLY
(CORE BARREL ASSEMBLY)
BEAVER VALLEY POWER STATION UNIT NO. 1
UPDATED FINAL SAFETY ANALYSIS REPORT

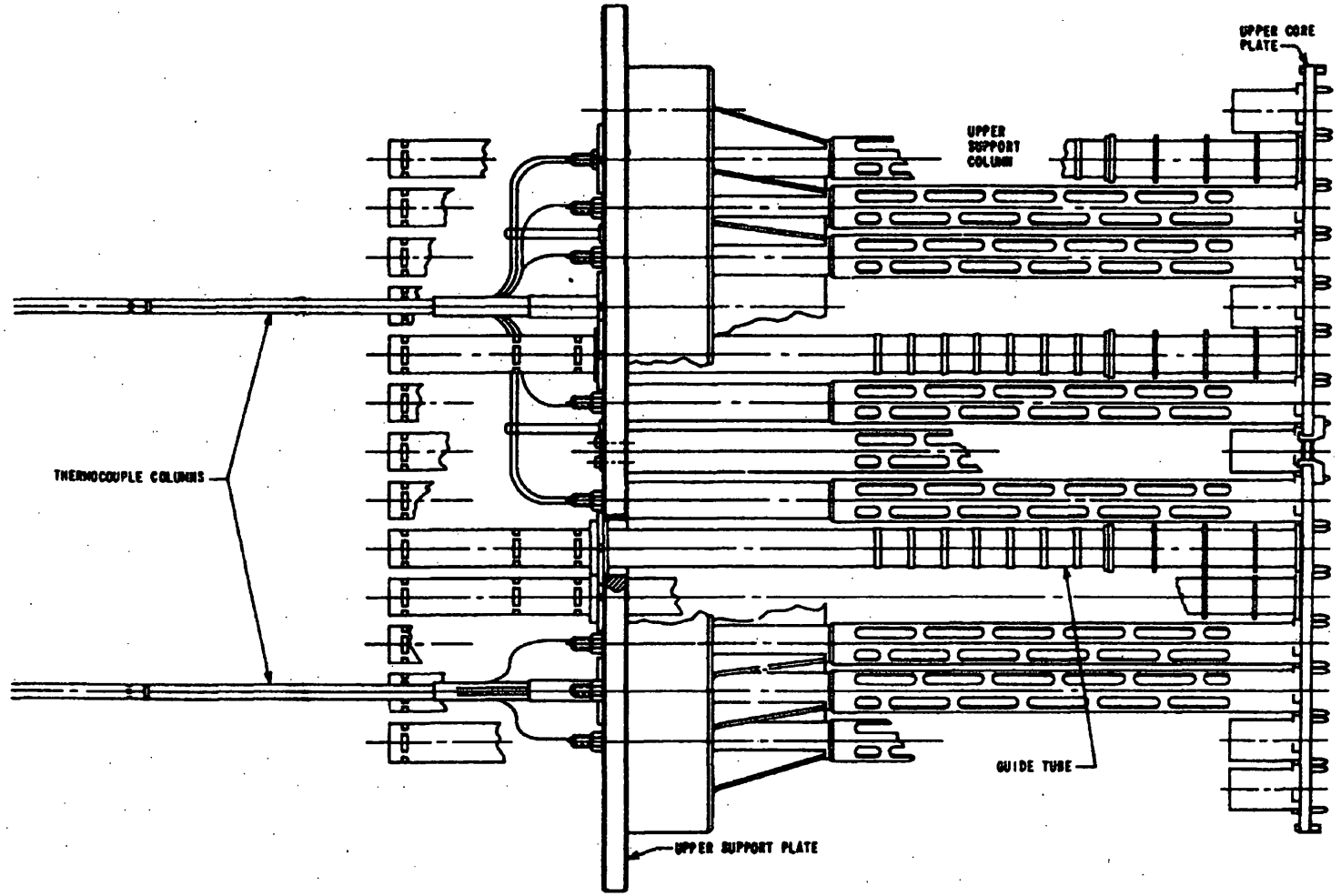

FIGURE 3.2-7
UPPER CORE SUPPORT ASSEMBLY
BEAVER VALLEY POWER STATION UNIT NO. 1
UPDATED FINAL SAFETY ANALYSIS REPORT

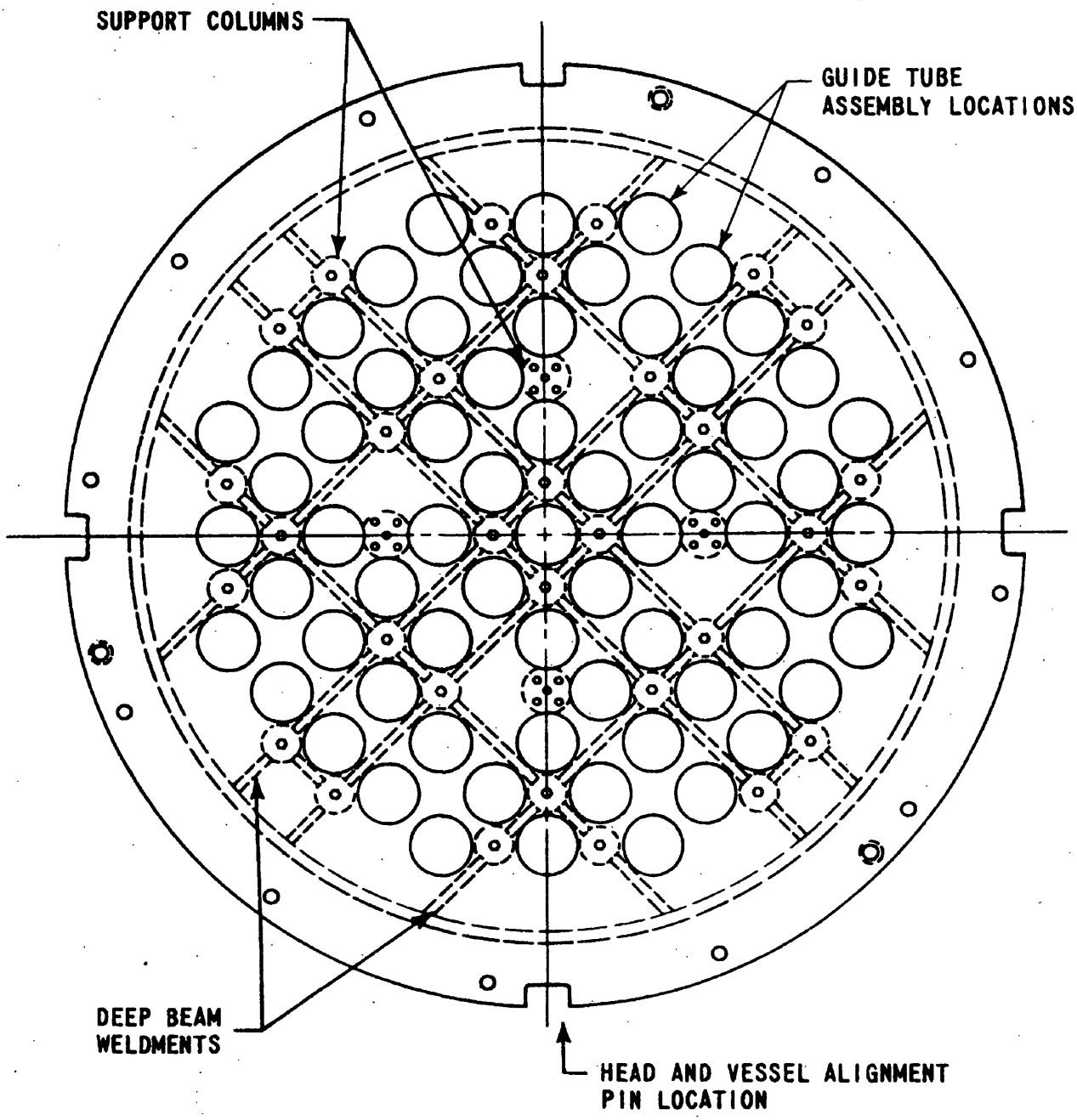

FIGURE 3.2-8
PLAN VIEW OF UPPER CORE SUPPORT STRUCTURE
BEAVER VALLEY POWER STATION UNIT NO. 1
UPDATED FINAL SAFETY ANALYSIS REPORT

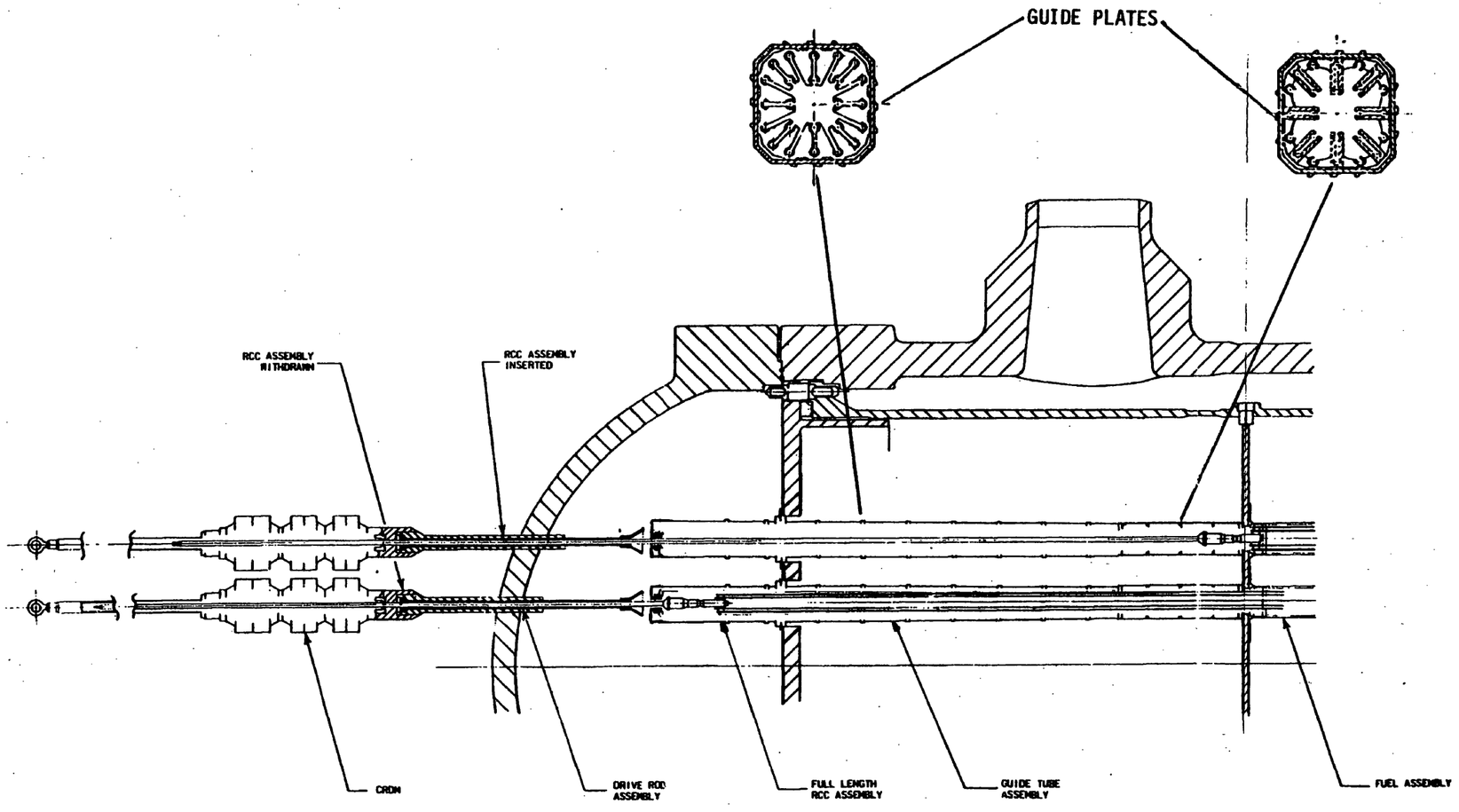

FIGURE 3.2-9
FULL LENGTH ROD CLUSTER CONTROL AND DRIVE ROD ASSEMBLY WITH INTERFACING COMPONENTS
BEAVER VALLEY POWER STATION UNIT NO. 1
UPDATED FINAL SAFETY ANALYSIS REPORT

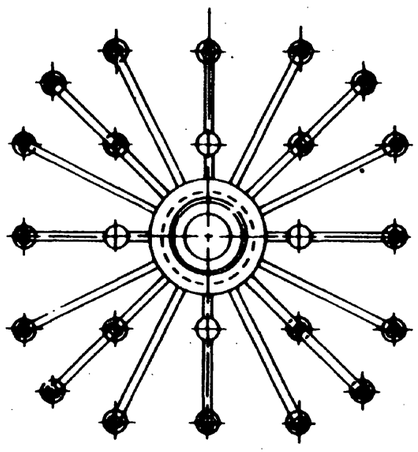

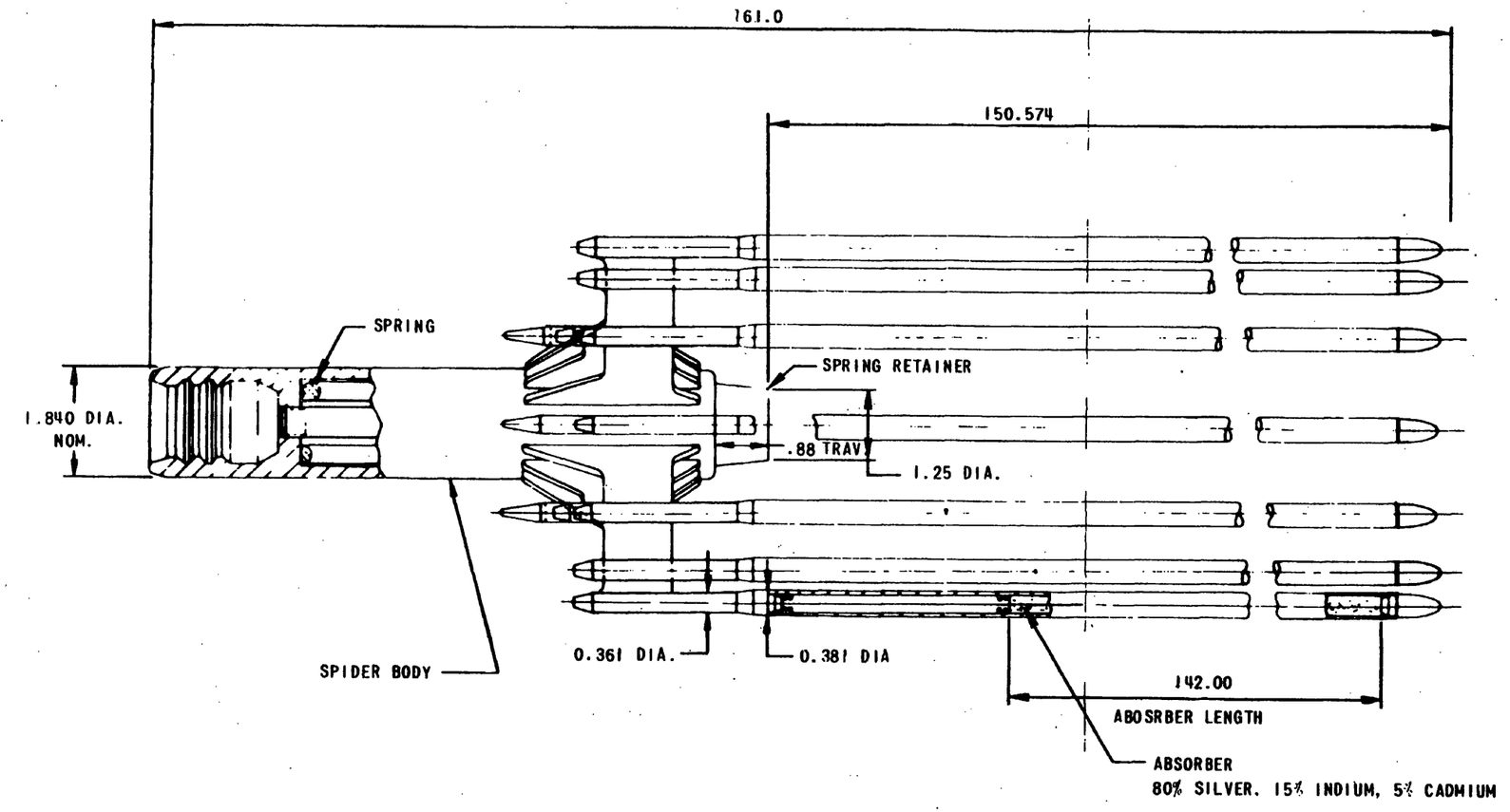

FIGURE 3.2-10
FULL LENGTH ROD CLUSTER
CONTROL ASSEMBLY OUTLINE
BEAVER VALLEY POWER STATION UNIT NO. 1
UPDATED FINAL SAFETY ANALYSIS REPORT

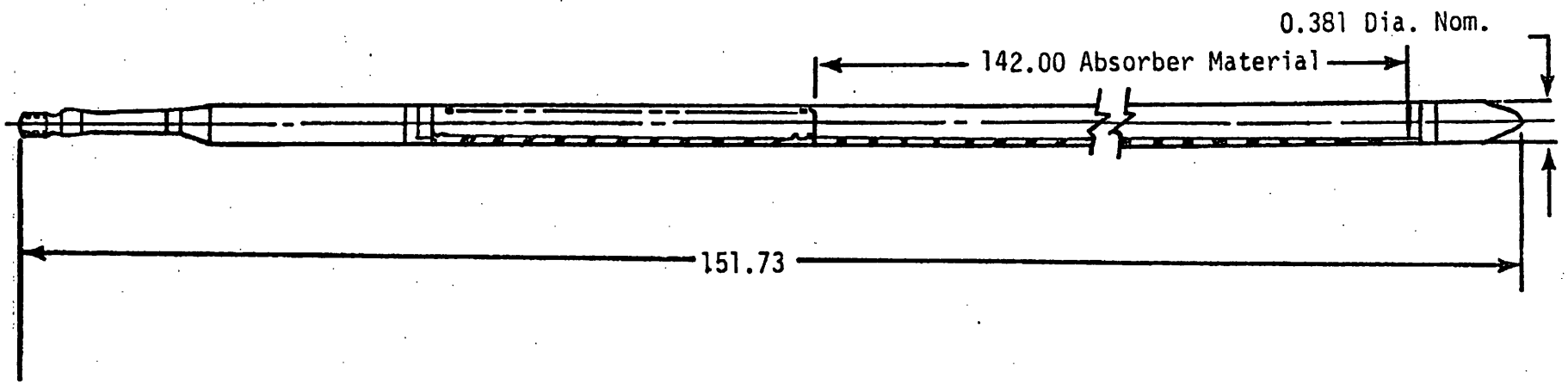

FIGURE 3.2-11
FULL LENGTH ABSORBER ROD
BEAVER VALLEY POWER STATION UNIT NO. 1
UPDATED FINAL SAFETY ANALYSIS REPORT

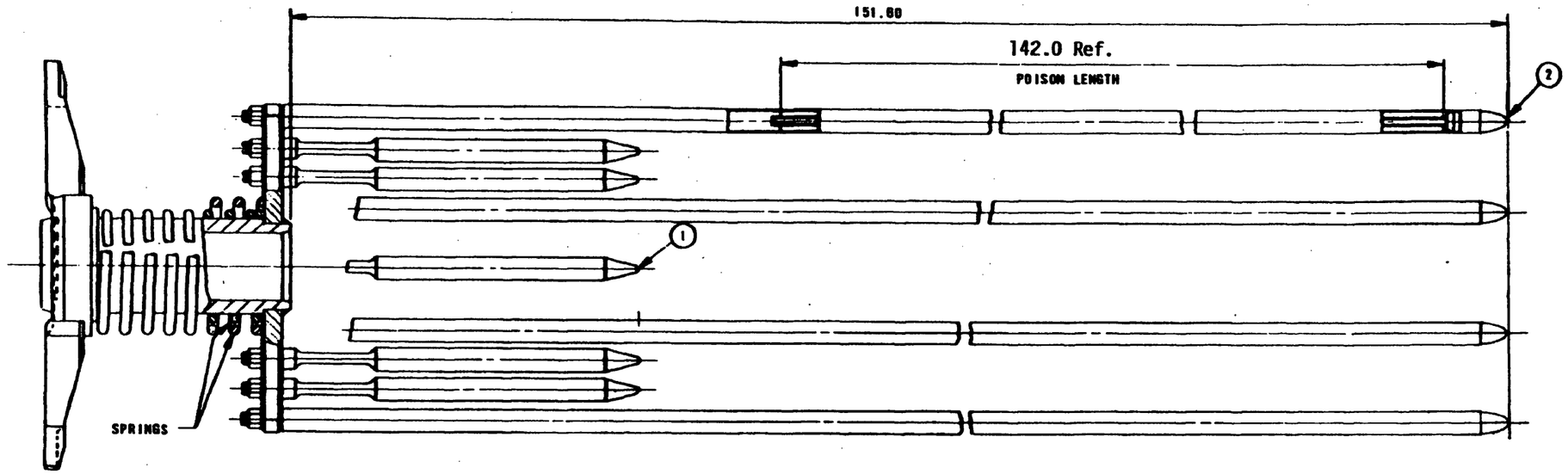

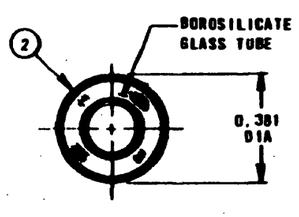

BURNABLE
POISON ROD

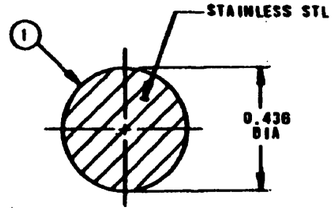

THIMBLE
PLUG

FIGURE 3.2-13
BURNABLE POISON ASSEMBLY (CONCEPTUAL)
BEAVER VALLEY POWER STATION UNIT NO. 1
UPDATED FINAL SAFETY ANALYSIS REPORT

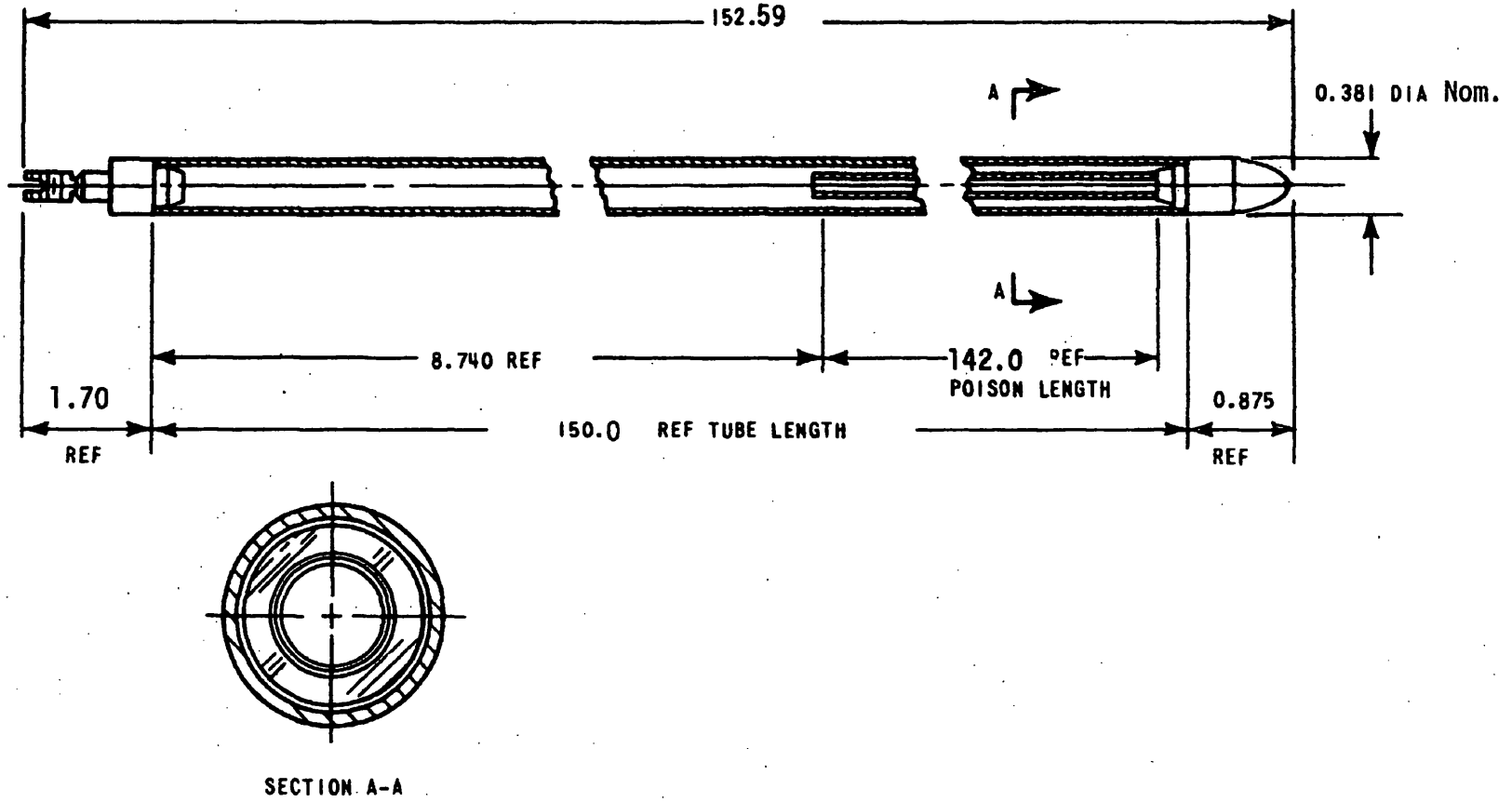

FIGURE 3.2-14
BURNABLE POISON ROD-CROSS SECTION
BEAVER VALLEY POWER STATION UNIT NO. 1
UPDATED FINAL SAFETY ANALYSIS REPORT

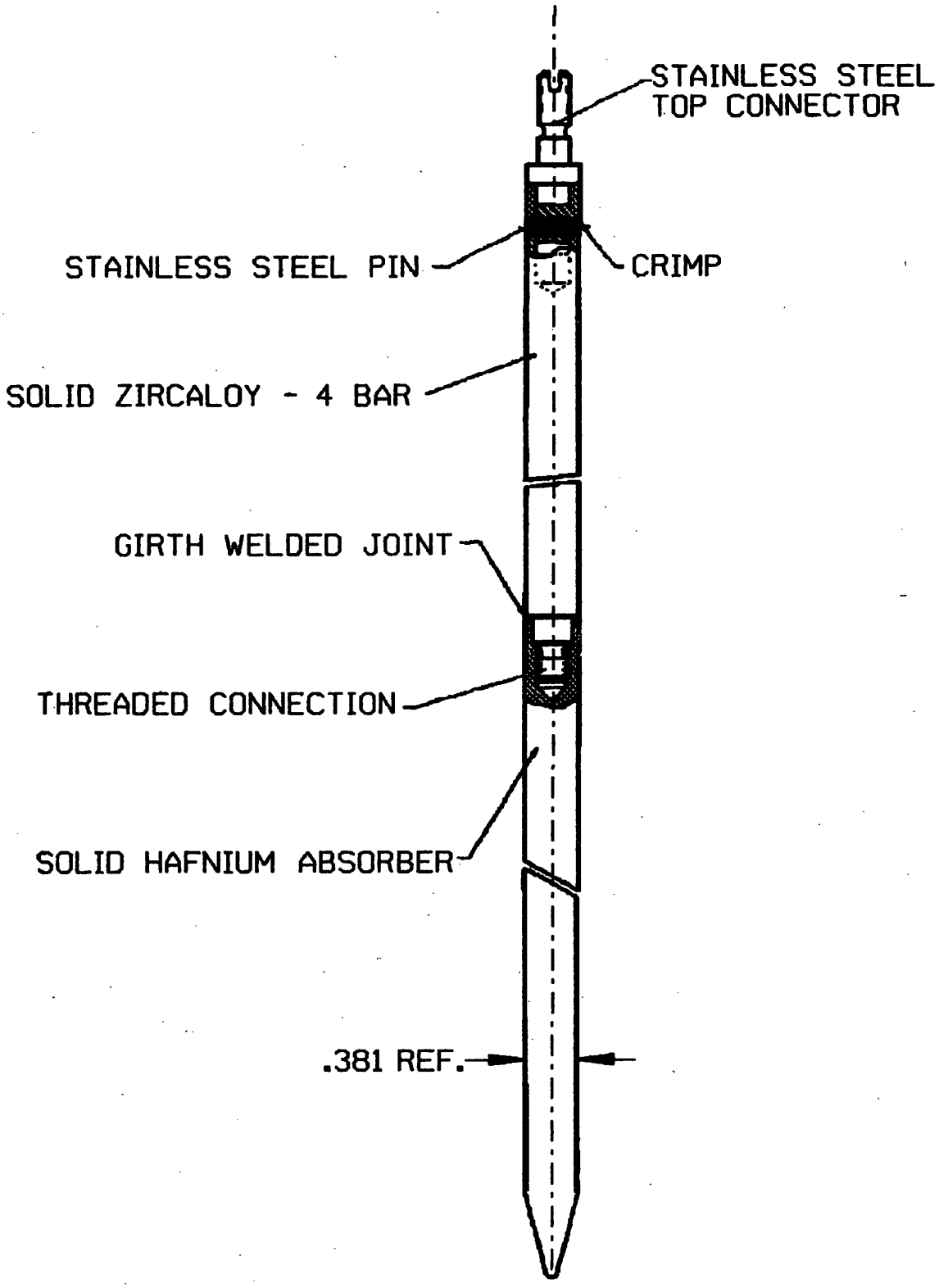

FIGURE 3.2-14A
UNCLAD HAFNIUM PSA RODLET
BEAVER VALLEY POWER STATION UNIT NO. 1
UPDATED FINAL SAFETY ANALYSIS REPORT

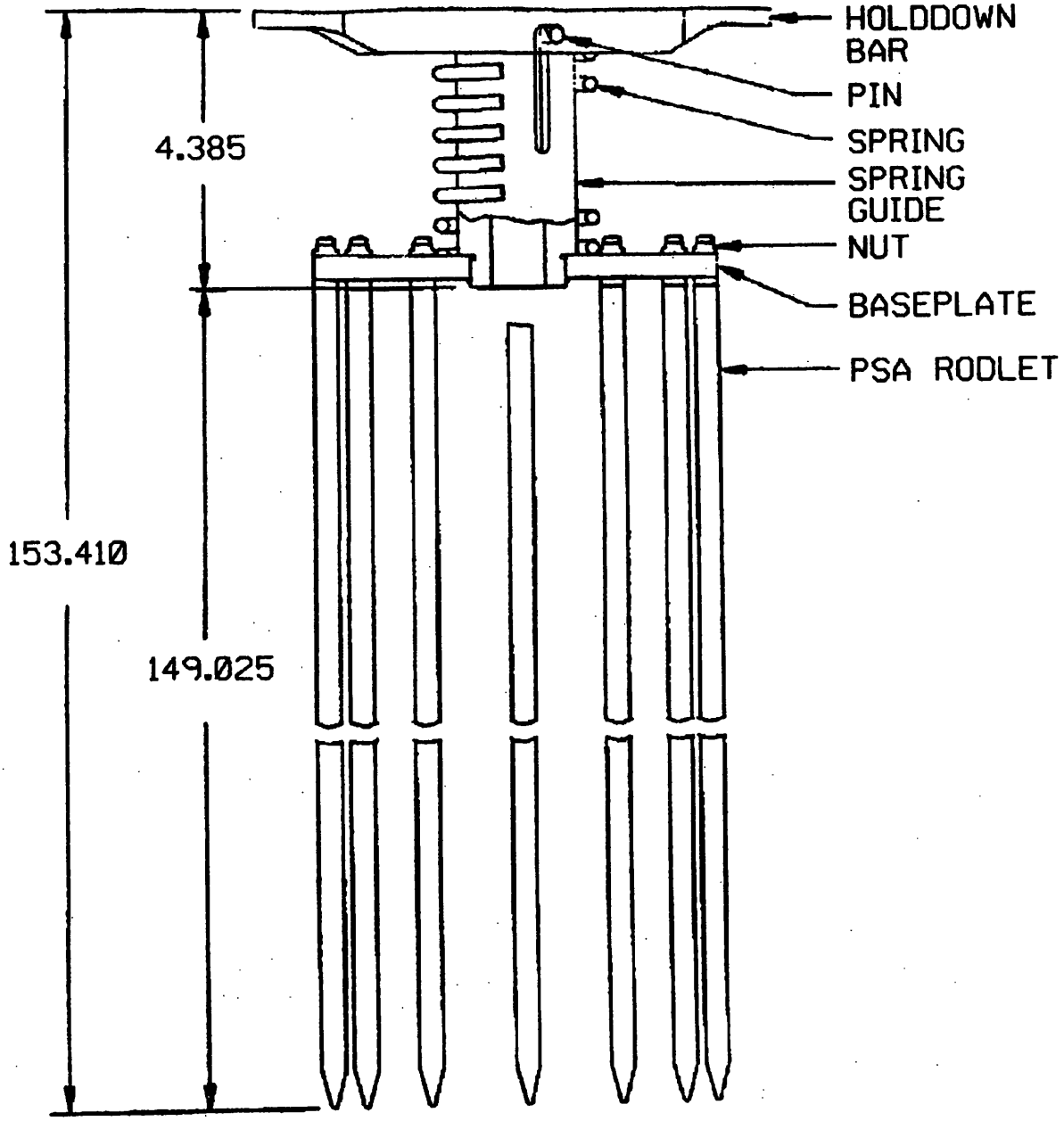

FIGURE 3.2-14B
HAFNIUM PSA
BEAVER VALLEY POWER STATION UNIT NO. 1
UPDATED FINAL SAFETY ANALYSIS REPORT

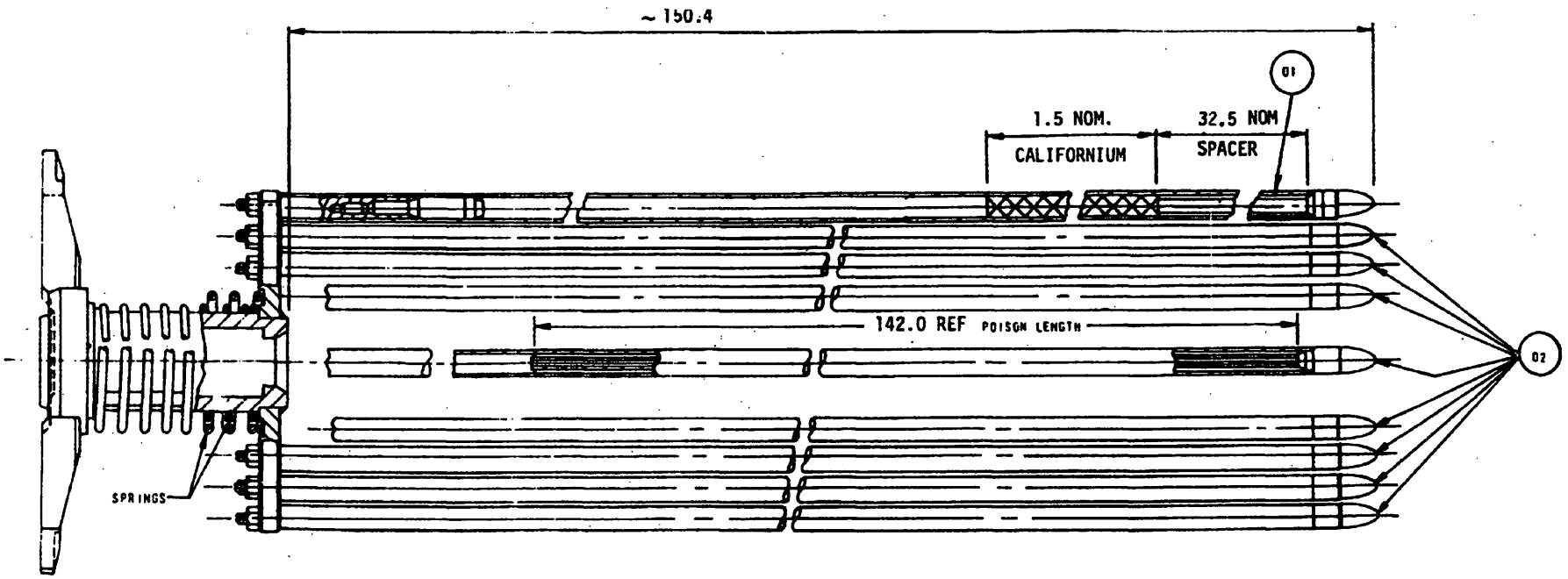

NOTE ALL DIMENSIONS ARE IN INCHES

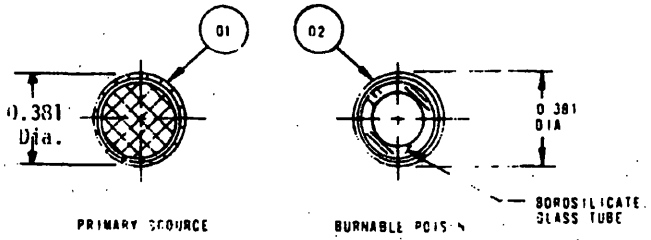

FIGURE 3.2-15A
PRIMARY SOURCE ASSEMBLY
BEAVER VALLEY POWER STATION UNIT NO. 1
UPDATED FINAL SAFETY ANALYSIS REPORT

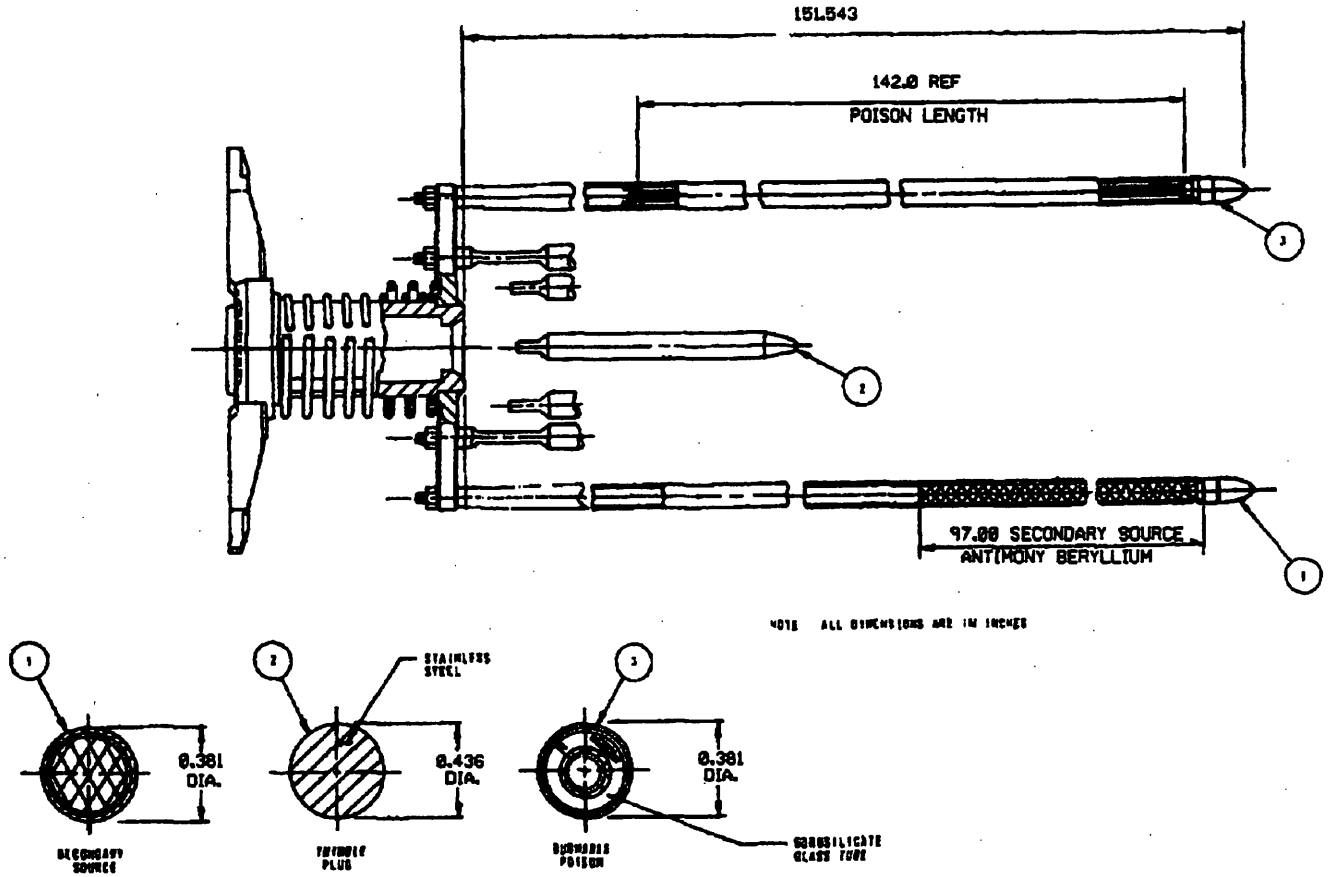

FIGURE 3.2-15B
SECONDARY SOURCE ASEMBLY
BEAVER VALLEY POWER STATION UNIT 1
UPDATED FINAL SAFETY ANALYSIS REPORT

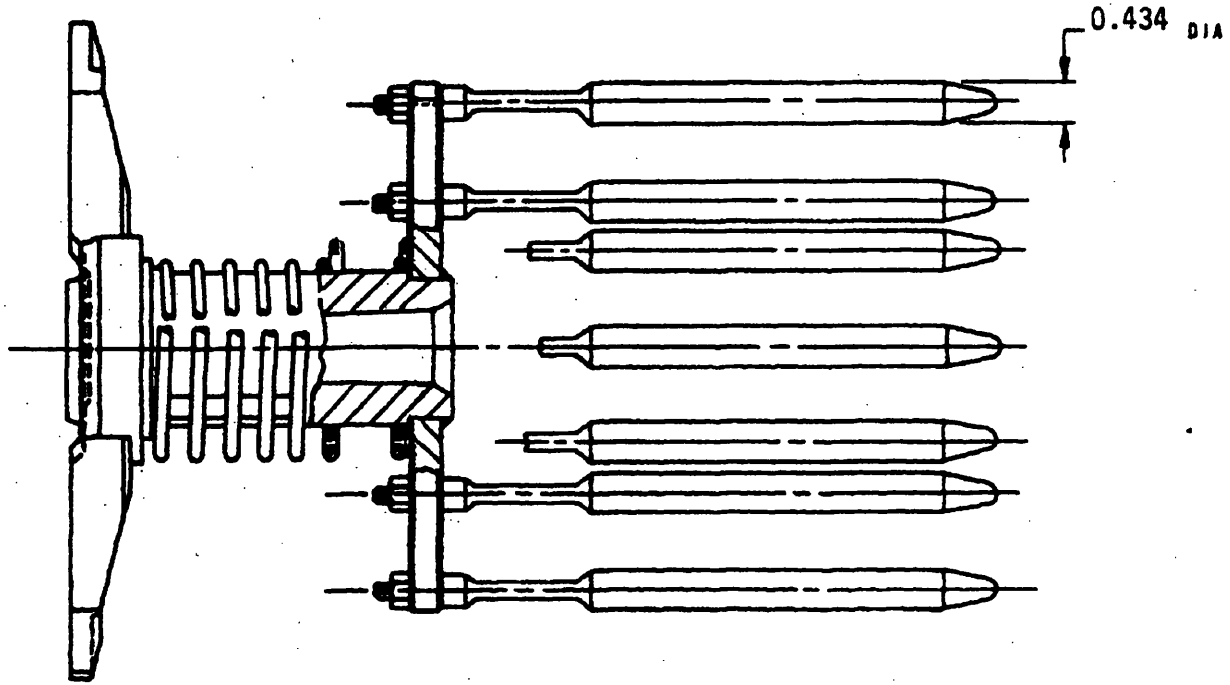

FIGURE 3.2-16
THIMBLE PLUG ASSEMBLY
BEAVER VALLEY POWER STATION UNIT NO. 1
UPDATED FINAL SAFETY ANALYSIS REPORT

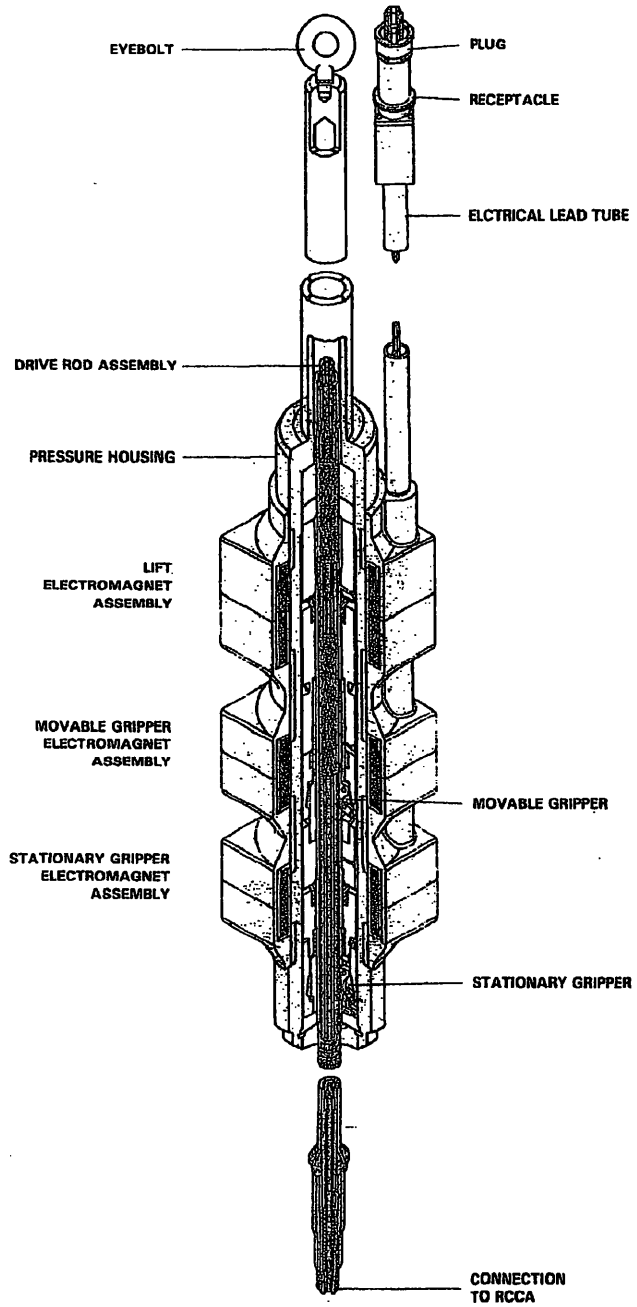

FIGURE 3.2-17

FULL LENGTH CONTROL ROD
DRIVE MECHANISM

BEAVER VALLEY POWER STATION UNIT NO. 1
UPDATED FINAL SAFETY ANALYSIS REPORT

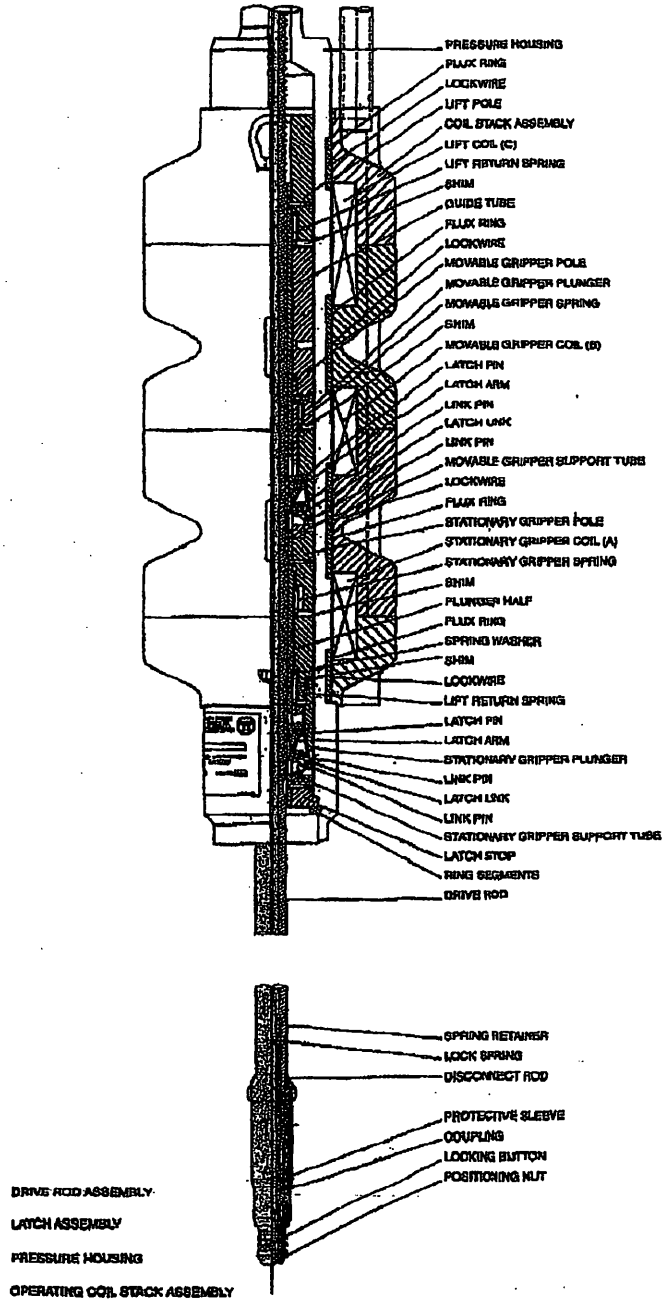

FIGURE 3.2-18

FULL LENGTH CONTROL ROD
DRIVE MECHANISM SCHEMATIC

BEAVER VALLEY POWER STATION UNIT NO. 1
UPDATED FINAL SAFETY ANALYSIS REPORT

BEFORE LOAD TRANSFER

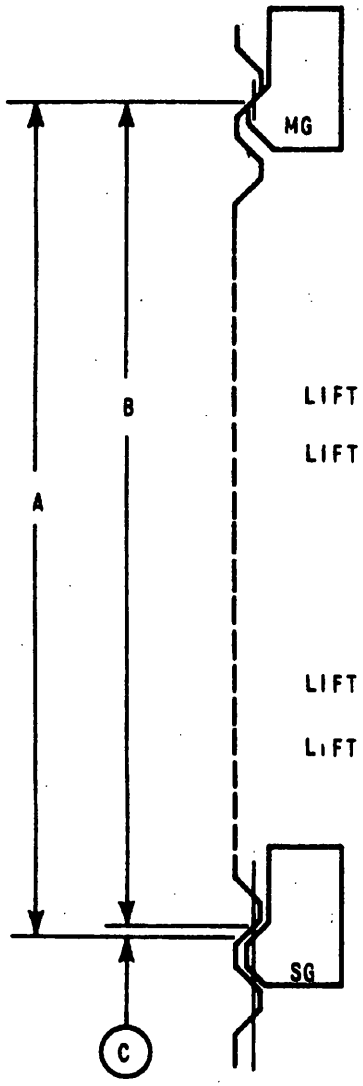

	AT 70°		
	A	B	C
LIFT COIL OFF	15.640	15.625	0.015
LIFT COIL ON	16.265	16.250	0.015

	AT 650°		
	A	B	C
LIFT COIL OFF	15.725	15.679	0.046
LIFT COIL ON	16.375	16.387	0.068

AFTER LOAD TRANSFER

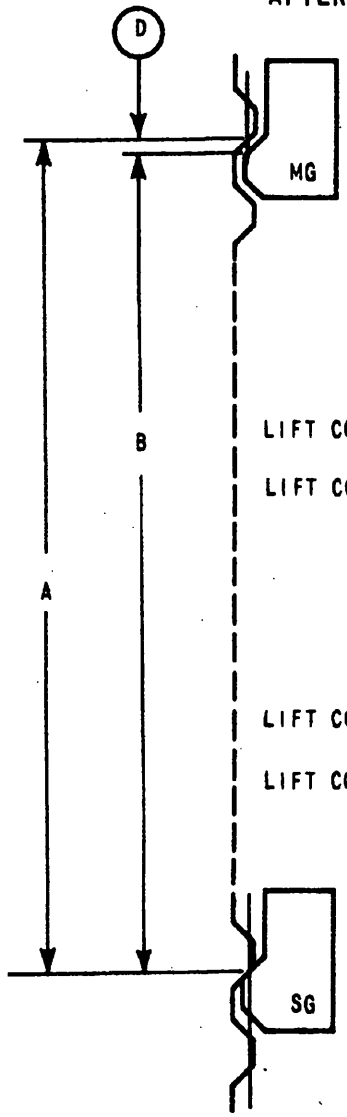

	AT 70°		
	A	B	D
LIFT COIL OFF	15.625	15.578	0.047
LIFT COIL ON	16.258	16.203	0.047

	AT 650°		
	A	B	D
LIFT COIL OFF	15.679	15.641	0.038
LIFT COIL ON	16.387	16.291	0.016

FIGURE 3.2-20
NOMINAL LATCH CLEARANCE AT MINIMUM AND MAXIMUM TEMPERATURE
BEAVER VALLEY POWER STATION UNIT NO. 1
UPDATED FINAL SAFETY ANALYSIS REPORT

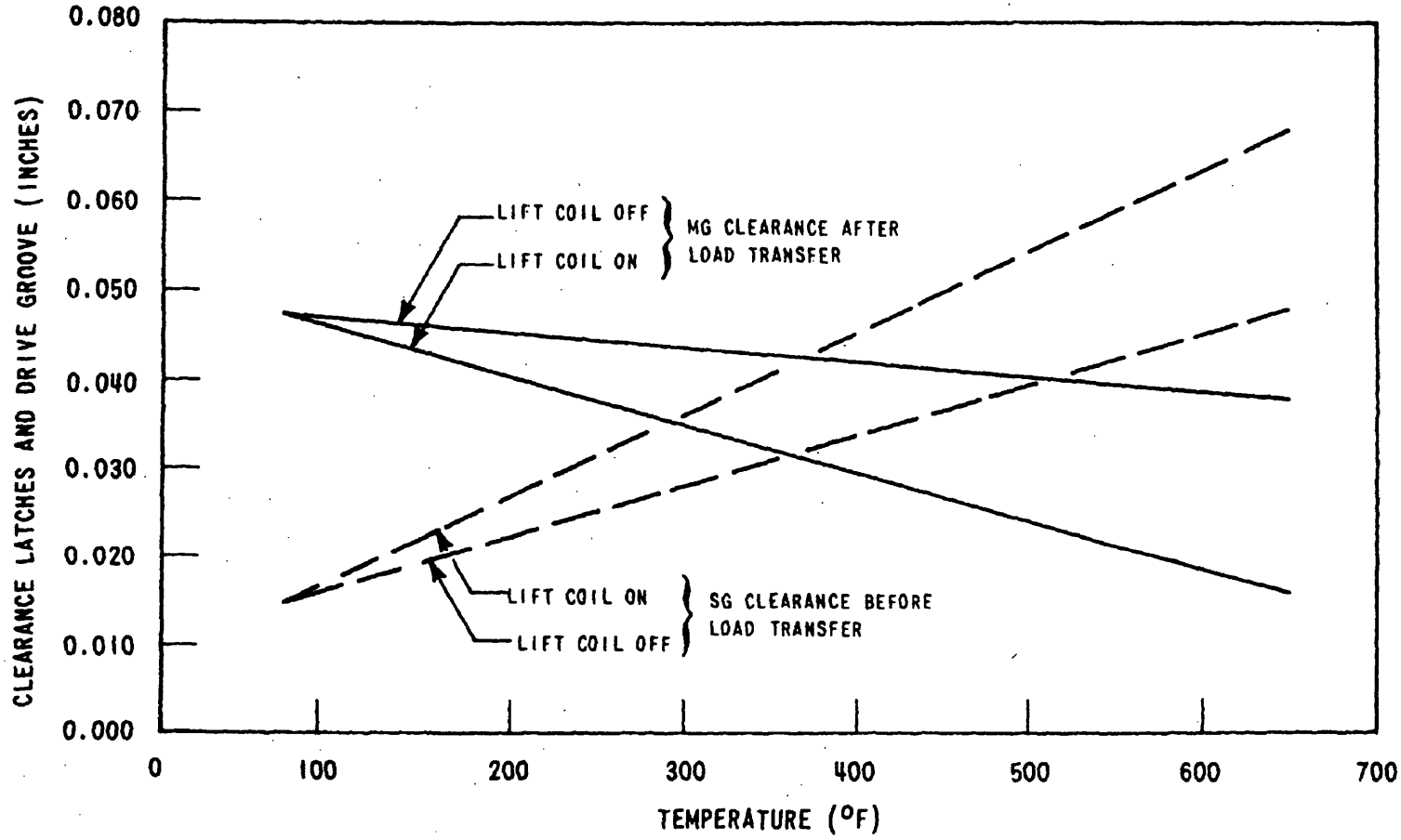

FIGURE 3.2-21
CONTROL ROD DRIVE MECHANISM
LATCH CLEARANCE THERMAL EFFECT
BEAVER VALLEY POWER STATION UNIT NO. 1
UPDATED FINAL SAFETY ANALYSIS REPORT

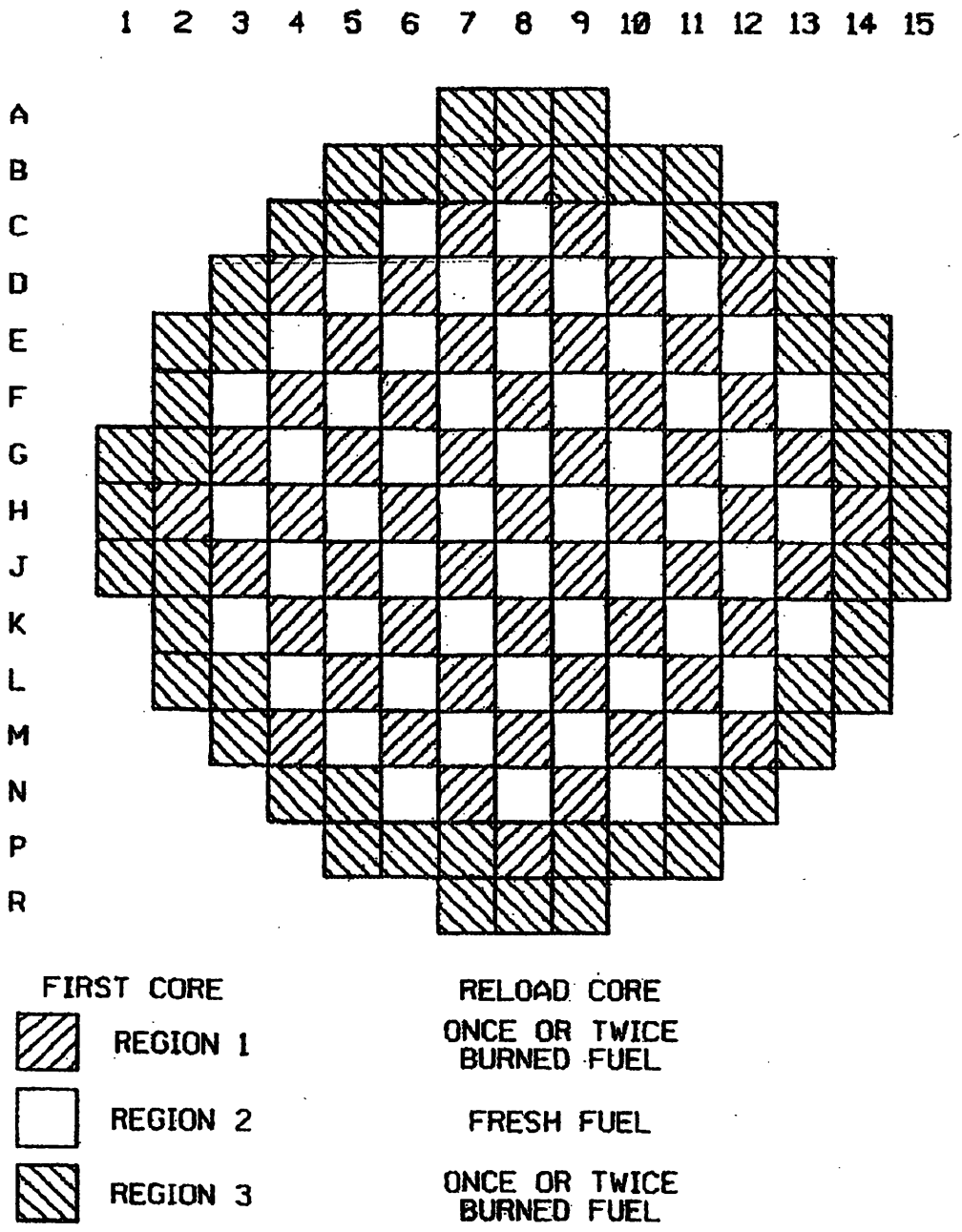

FIGURE 3.3-1

TYPICAL FUEL LOADING ARRANGEMENT

BEAVER VALLEY POWER STATION UNIT NO. 1
UPDATED FINAL SAFETY ANALYSIS REPORT

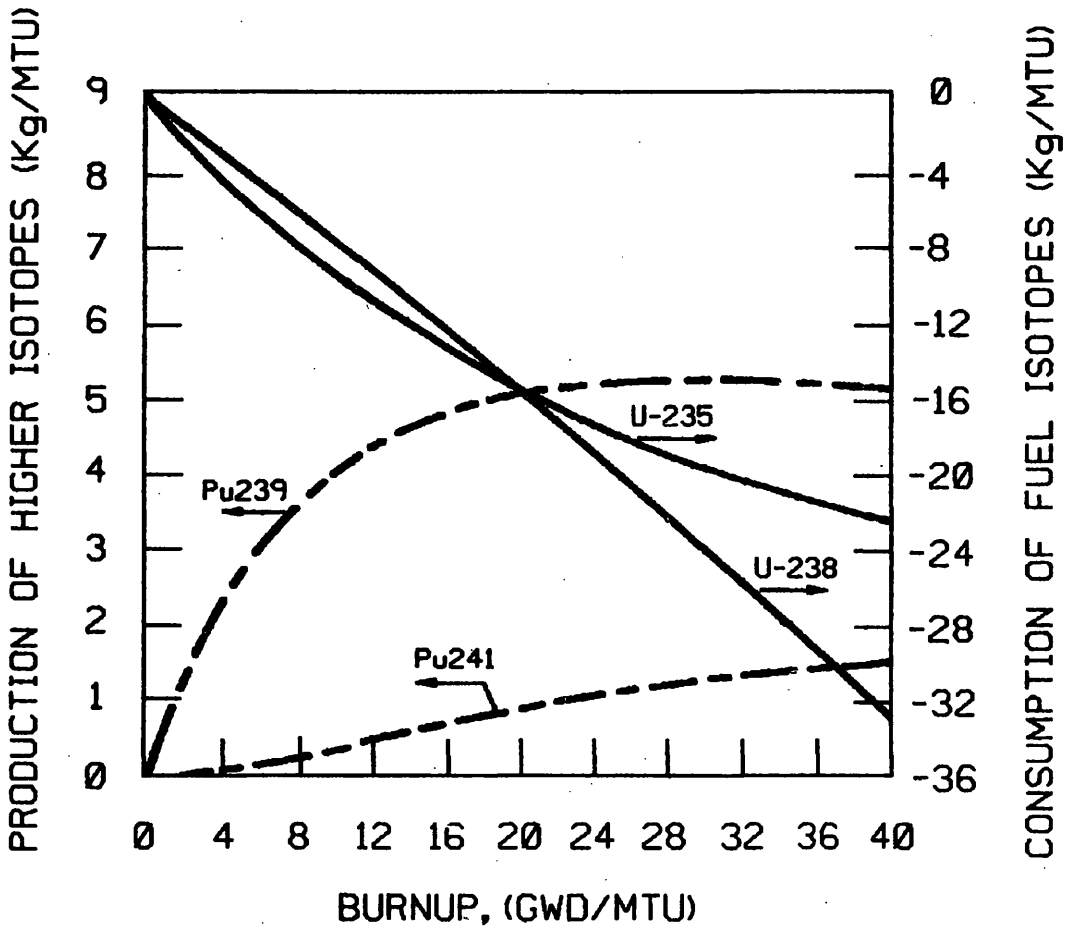

FIGURE 3.3-2

TYPICAL PRODUCTION AND CONSUMPTION OF HIGHER ISOTOPES

BEAVER VALLEY POWER STATION-UNIT 1
UPDATED FINAL SAFETY ANALYSIS REPORT

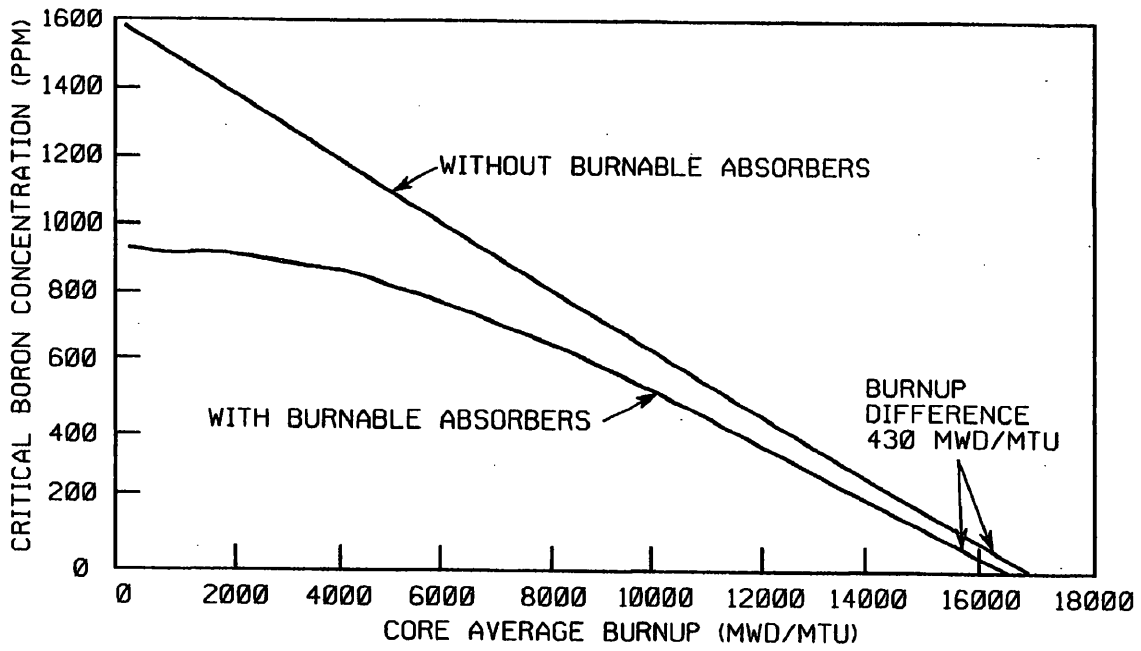

FIGURE 3.3-3

TYPICAL BORON CONCENTRATION
VERSUS FIRST CYCLE BURNUP WITH &
WITHOUT BURNABLE ABSORBER RODS

BEAVER VALLEY POWER STATION UNIT NO. 1
UPDATED FINAL SAFETY ANALYSIS REPORT

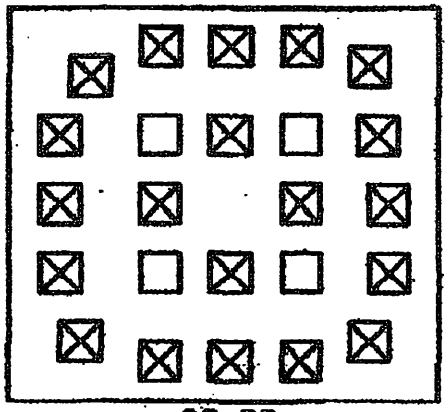

20 BP

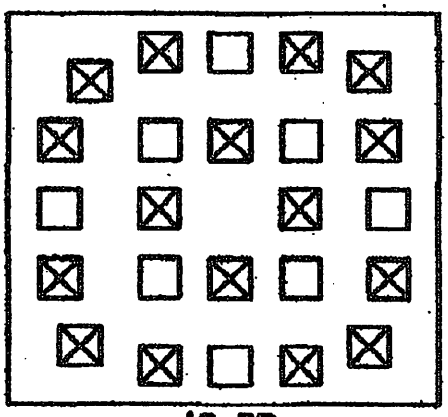

16 BP

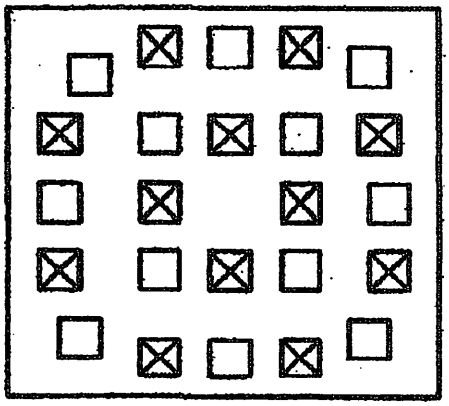

12 BP

FIGURE 3.3-4

TYPICAL BURNABLE ABSORBER ROD
ARRANGEMENT WITHIN AN ASSEMBLY

BEAVER VALLEY POWER STATION UNIT NO. 1
UPDATED FINAL SAFETY ANALYSIS REPORT

CONFIGURATION FOR 16 IFBA ROD ASSEMBLY (17x17)

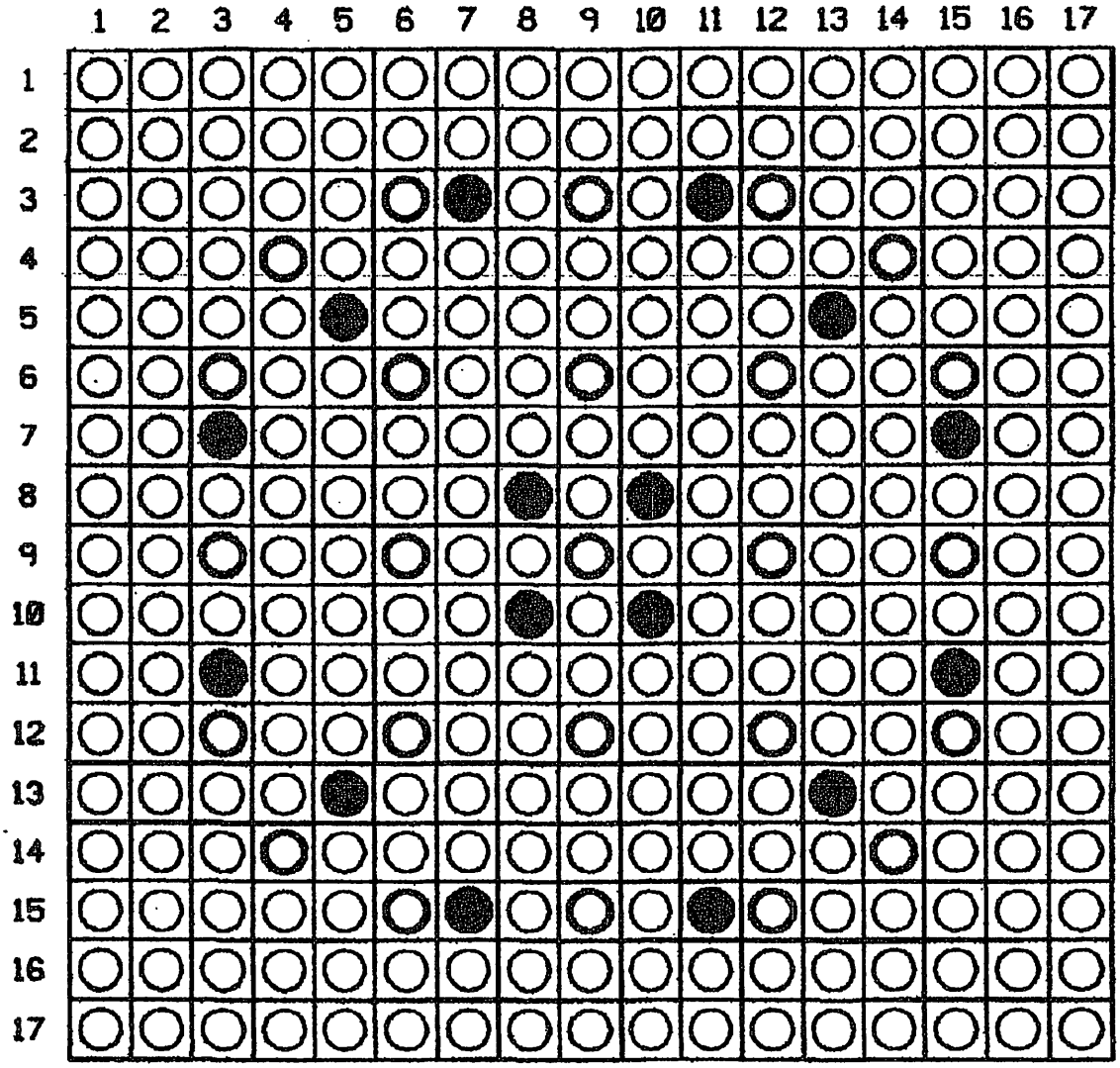

FUEL ROD

FUEL ROD WITH IFBA

GUIDE TUBE/INST TUBE

FIGURE 3.3-4A

TYPICAL BURNABLE ABSORBER ROD
ARRANGEMENT WITHIN AN ASSEMBLY

BEAVER VALLEY POWER STATION UNIT NO. 1
UPDATED FINAL SAFETY ANALYSIS REPORT

17x17 DEFAULT BURNABLE ABSORBER PATTERNS

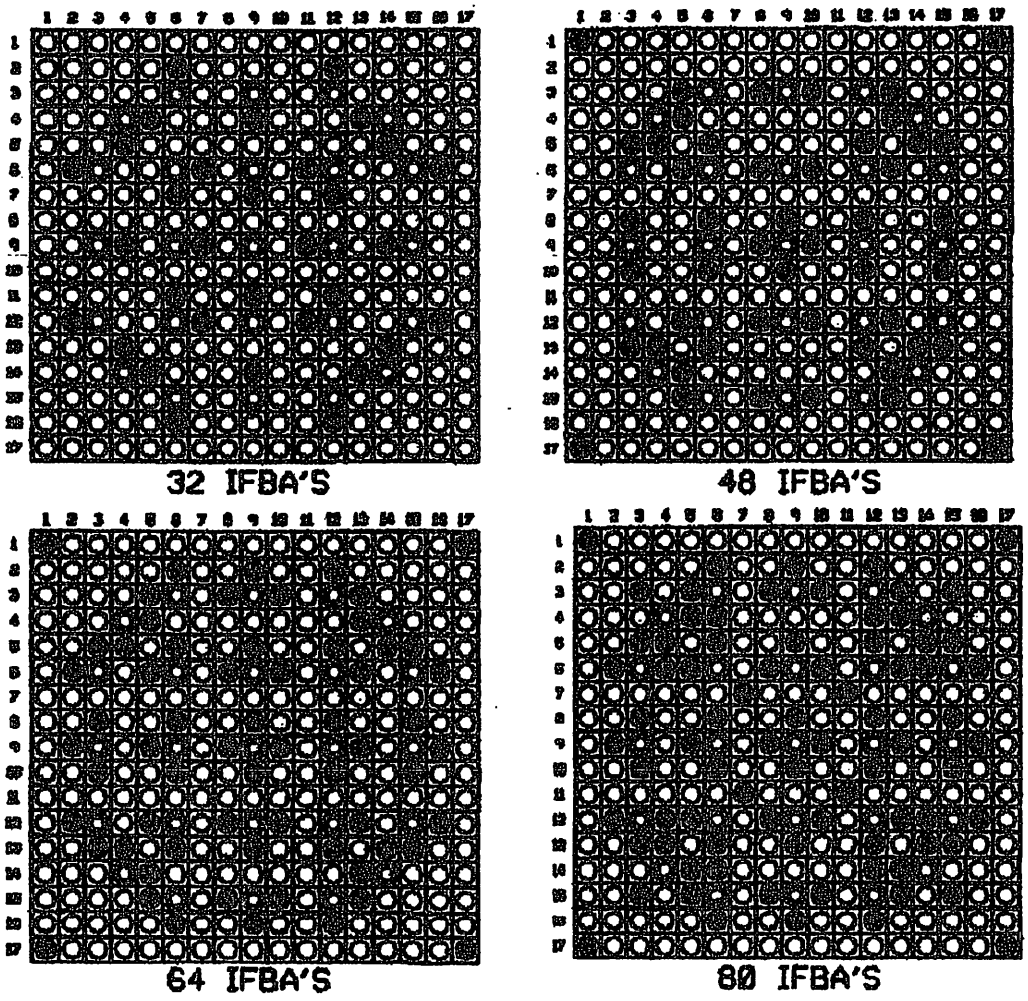

FUEL ROD

FUEL ROD WITH IFBA

GUIDE TUBE/INST TUBE

FIGURE 3.3-4B

TYPICAL BURNABLE ABSORBER ROD
ARRANGEMENT WITHIN AN ASSEMBLY

BEAVER VALLEY POWER STATION UNIT NO. 1
UPDATED FINAL SAFETY ANALYSIS REPORT

17x17 DEFAULT BURNABLE ABSORBER PATTERNS

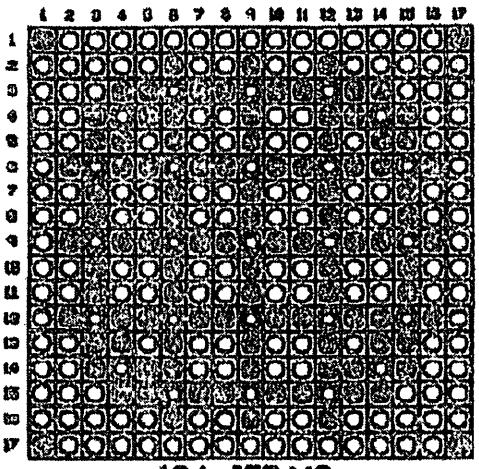

104 IFBA'S

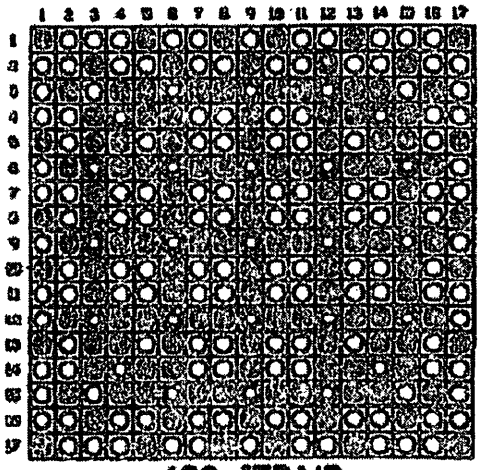

128 IFBA'S

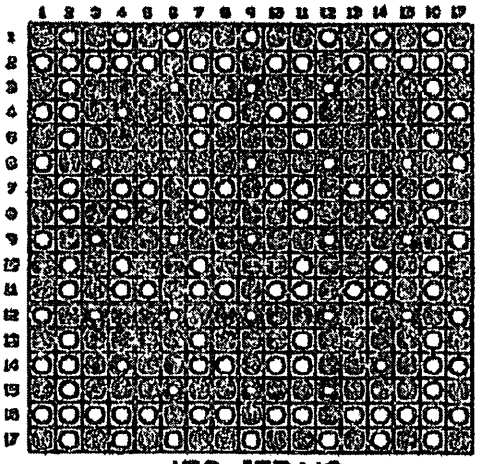

156 IFBA'S

FUEL ROD

FUEL ROD WITH IFBA

GUIDE TUBE/INST TUBE

FIGURE 3.3-4C

TYPICAL BURNABLE ABSORBER ROD
ARRANGEMENT WITHIN AN ASSEMBLY

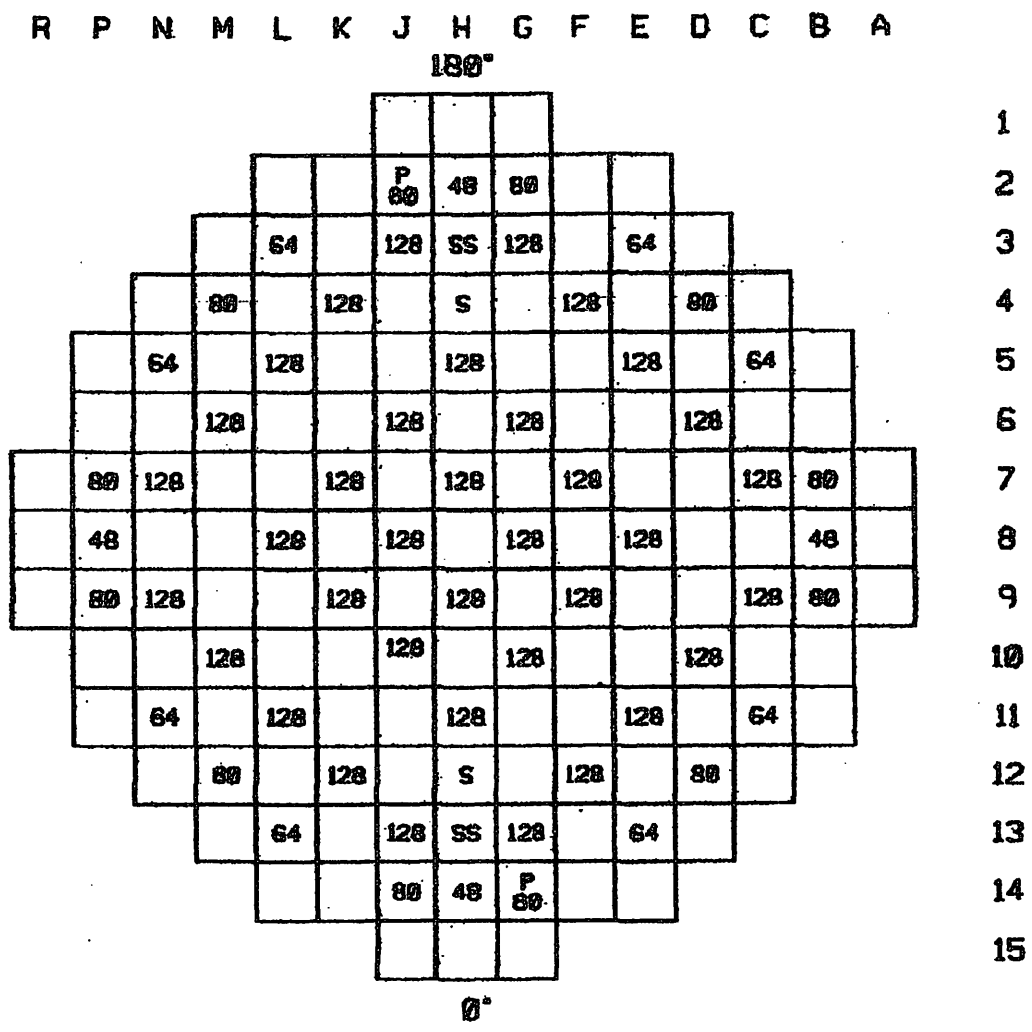

NUMBER INDICATES NUMBER OF IFBA RODS
S INDICATES SECONDARY SOURCE RODS } FIRST CORE ONLY
P INDICATES PRIMARY RODS
SS INDICATES SECONDARY SOURCE RODS
IN LATER CYCLES

FIGURE 3.3-5

TYPICAL INTEGRAL FUEL BURNABLE
ABSORBER LOADING PATTERN

BEAVER VALLEY POWER STATION UNIT NO. 1
UPDATED FINAL SAFETY ANALYSIS REPORT

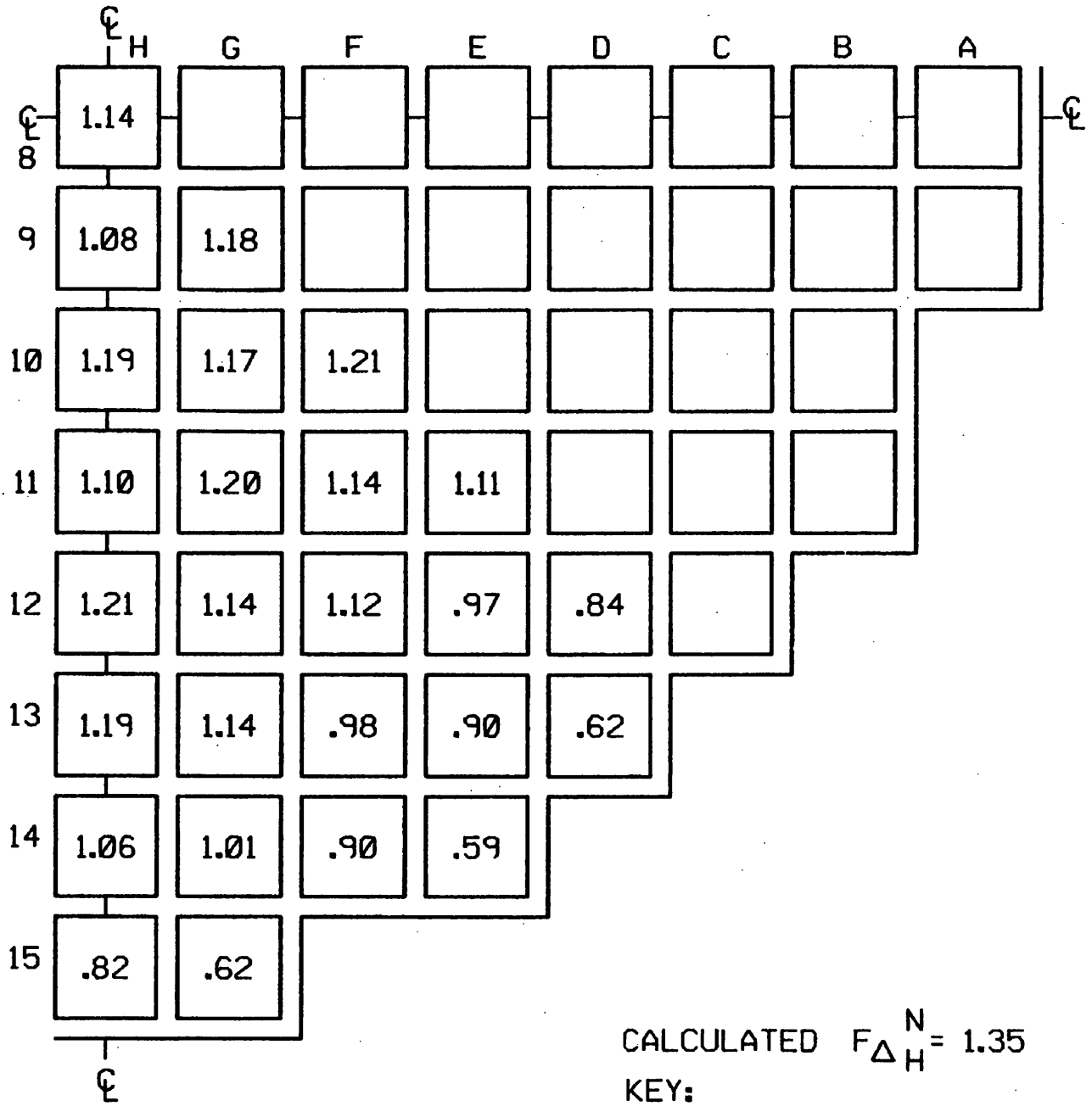

CALCULATED $F_{\Delta H}^{N}$ = 1.35

KEY:
VALUE REPRESENTS ASSEMBLY
RELATIVE POWER

FIGURE 3.3-6

TYPICAL NORMALIZED POWER DISTRIBUTION BEGINNING OF LIFE, ALL RODS OUT, HOT FULL POWER, NO XENON

BEAVER VALLEY POWER STATION-UNIT 1
UPDATED FINAL SAFETY ANALYSIS REPORT

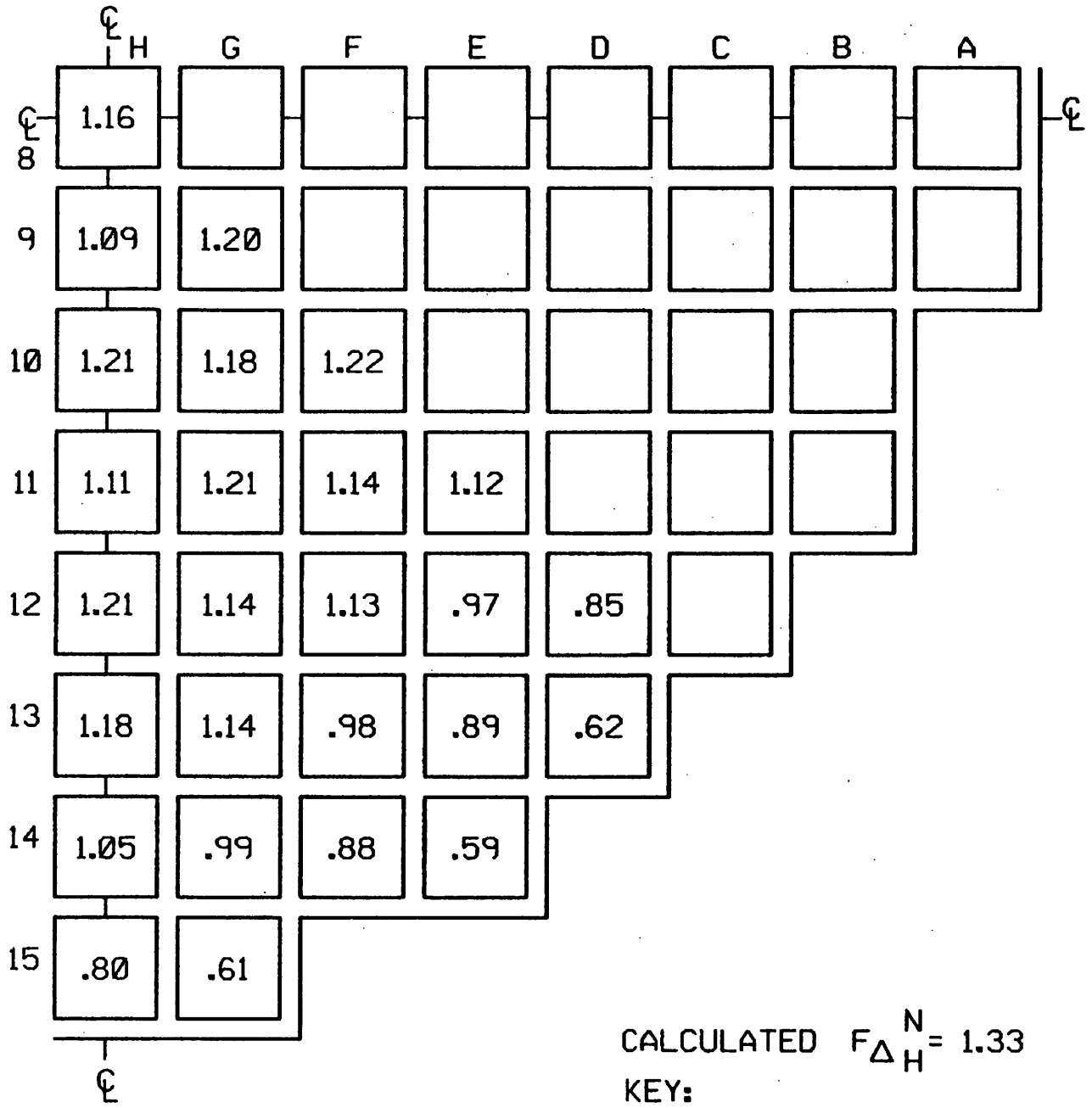

CALCULATED $F_{\Delta H}^{N}$ = 1.33

KEY:
VALUE REPRESENTS ASSEMBLY
RELATIVE POWER

FIGURE 3.3-7

TYPICAL NORMALIZED POWER DISTRIBUTION BEGINNING OF LIFE, ALL RODS OUT, HOT FULL POWER, EQUILIBRIUM XENON

BEAVER VALLEY POWER STATION-UNIT 1
UPDATED FINAL SAFETY ANALYSIS REPORT

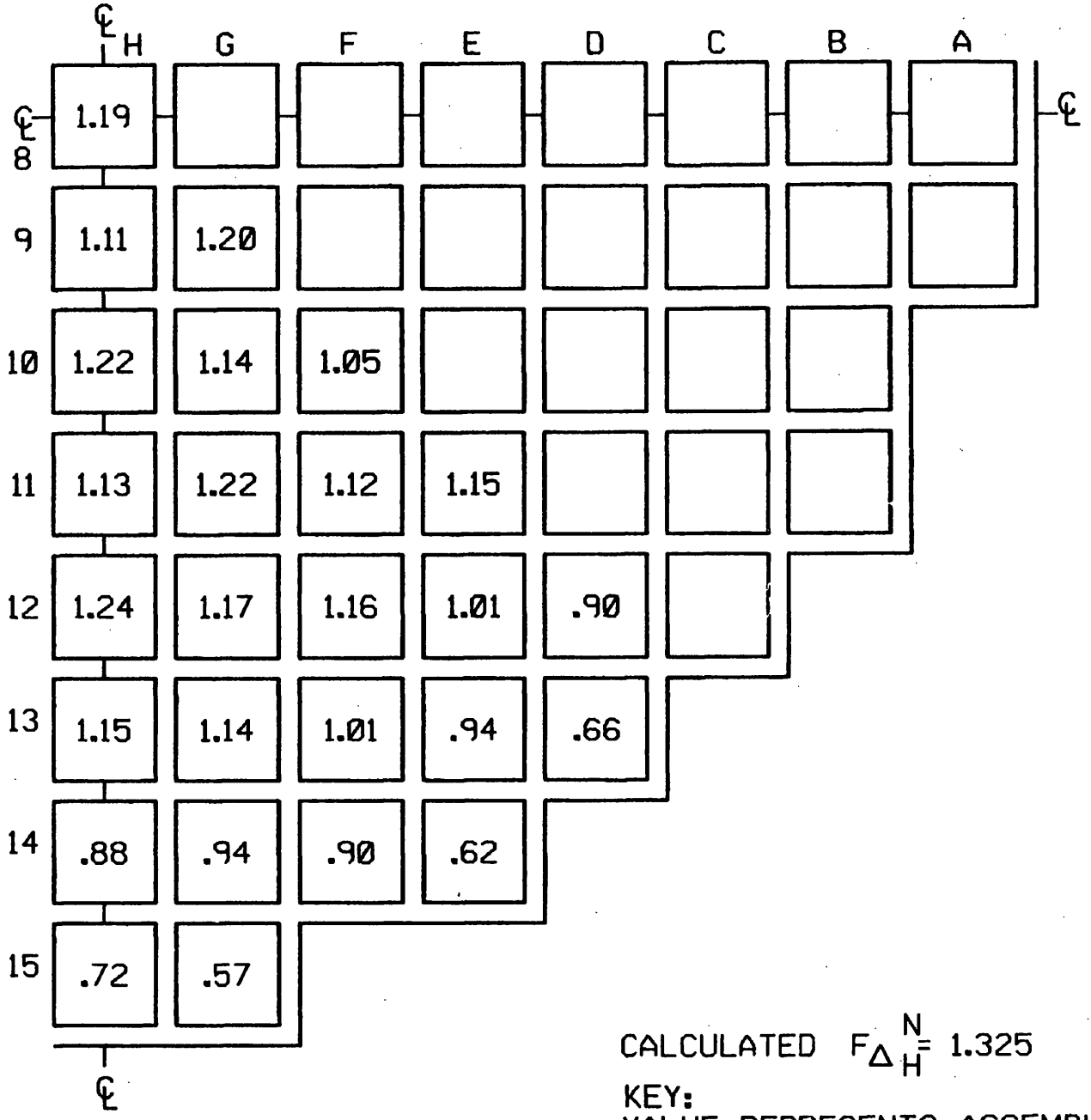

CALCULATED $F_{\Delta H}^{N} = 1.325$

KEY:
VALUE REPRESENTS ASSEMBLY
RELATIVE POWER

FIGURE 3.3-8

TYPICAL NORMALIZED POWER DISTRIBUTION BEGINNING OF LIFE, GROUP D INSERTED, HOT FULL POWER, EQUILIBRIUM XENON

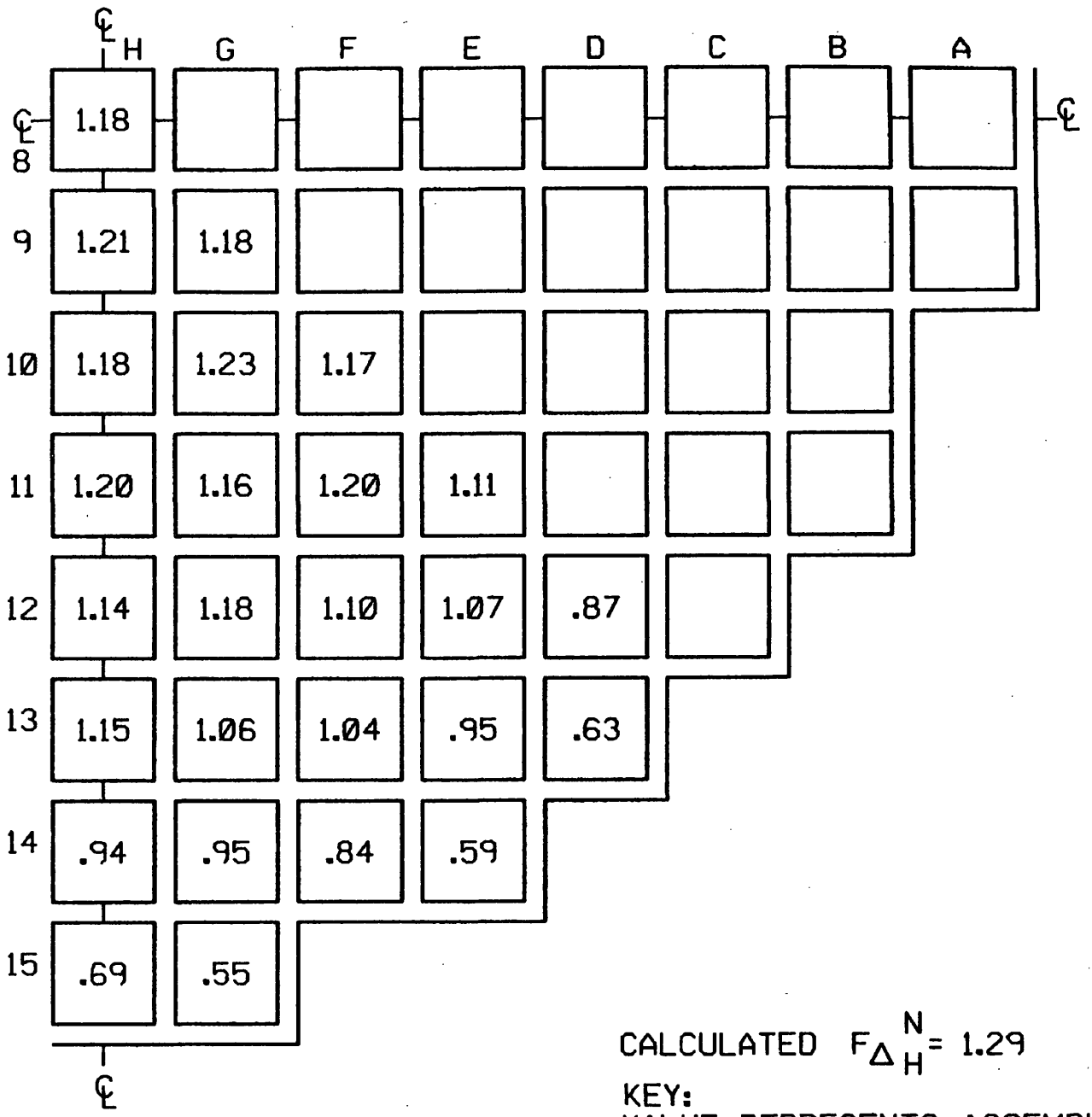

CALCULATED $F_{\Delta H}^{N}$ = 1.29

KEY:
VALUE REPRESENTS ASSEMBLY
RELATIVE POWER

FIGURE 3.3-10

TYPICAL NORMALIZED POWER DISTRIBUTION NEAR MIDDLE OF LIFE, ALL RODS OUT, HOT FULL POWER, EQUILIBRIUM XENON

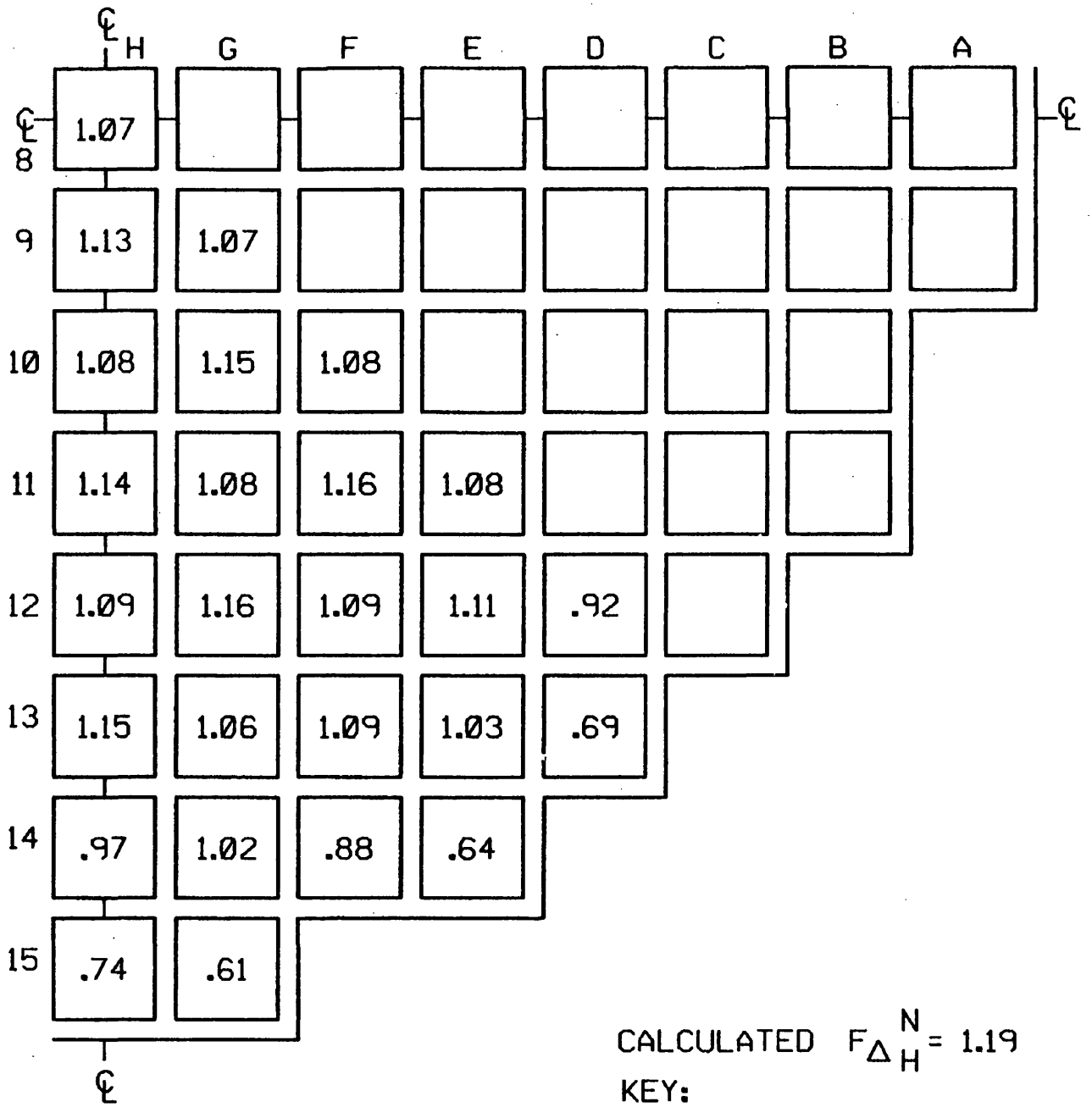

CALCULATED $F_{\Delta H}^{N}$ = 1.19

KEY:
VALUE REPRESENTS ASSEMBLY
RELATIVE POWER

FIGURE 3.3-11

TYPICAL NORMALIZED POWER DISTRIBUTION END OF LIFE, ALL RODS OUT, HOT FULL POWER, EQUILIBRIUM XENON

BEAVER VALLEY POWER STATION-UNIT 1
UPDATED FINAL SAFETY ANALYSIS REPORT

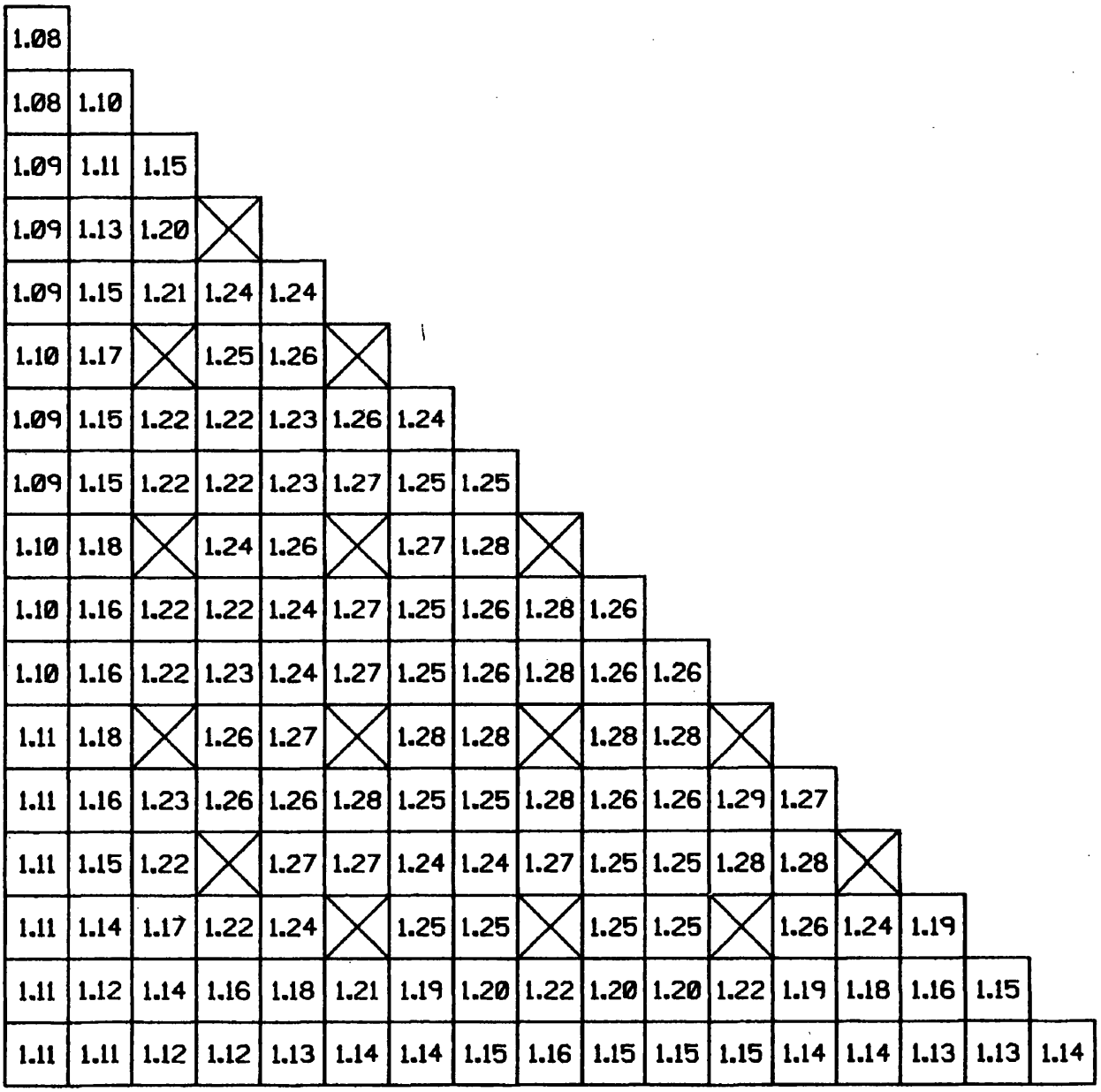

FIGURE 3.3-12

TYPICAL RODWISE POWER DISTRIBUTION IN A TYPICAL ASSEMBLY (ASSEMBLY G-9) NEAR BEGINNING OF LIFE, HOT FULL POWER, EQUILIBRIUM XENON, UNRODDED CORE

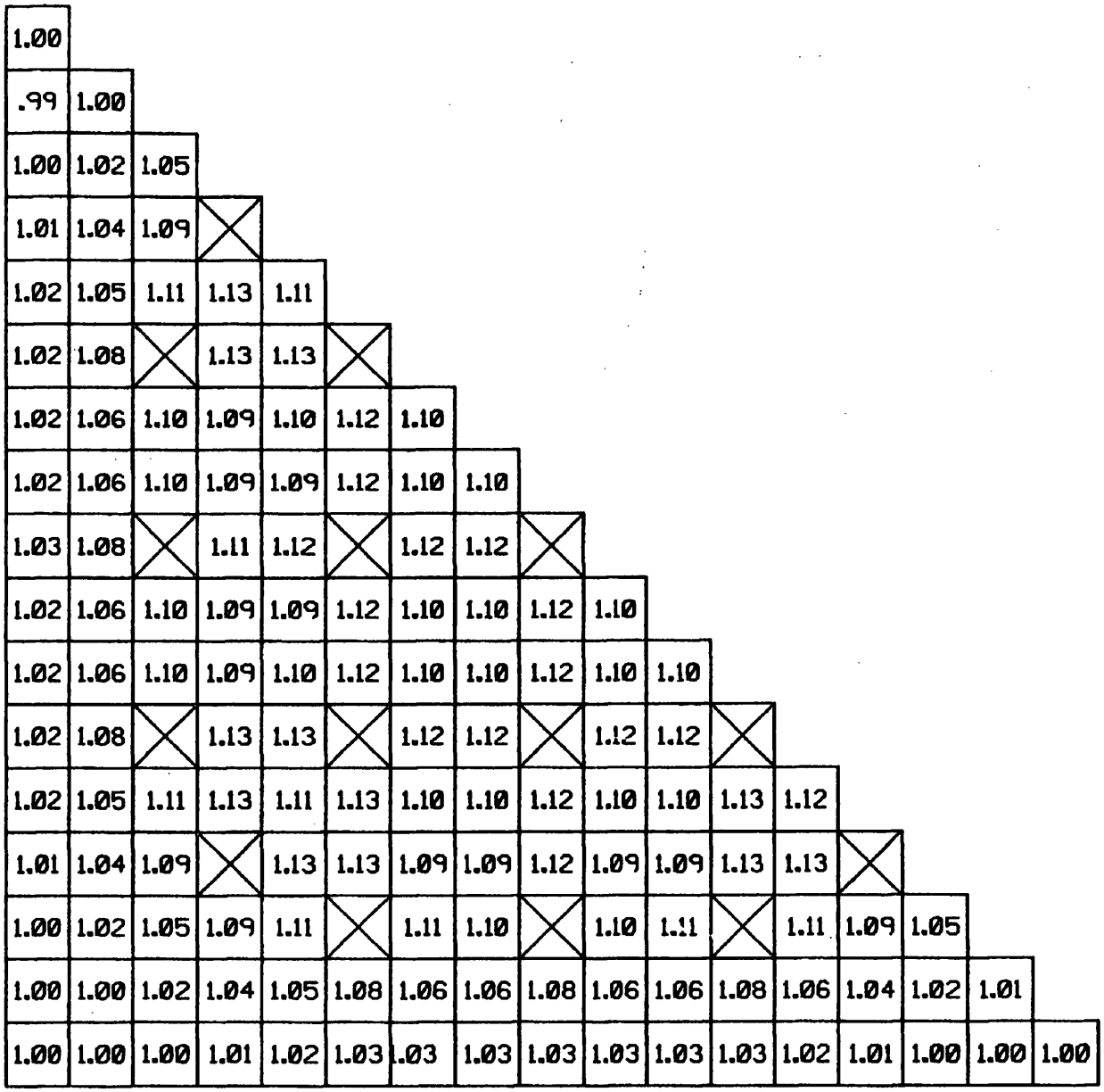

FIGURE 3.3-13

TYPICAL RODWISE POWER DISTRIBUTION IN A TYPICAL ASSEMBLY (ASSEMBLY G-9) NEAR END OF LIFE, HOT FULL POWER, EQUILIBRIUM XENON, UNRODDED CORE

BEAVER VALLEY POWER STATION-UNIT 1
UPDATED FINAL SAFETY ANALYSIS REPORT

WESTINGHOUSE PROPREITARY CLASS 2

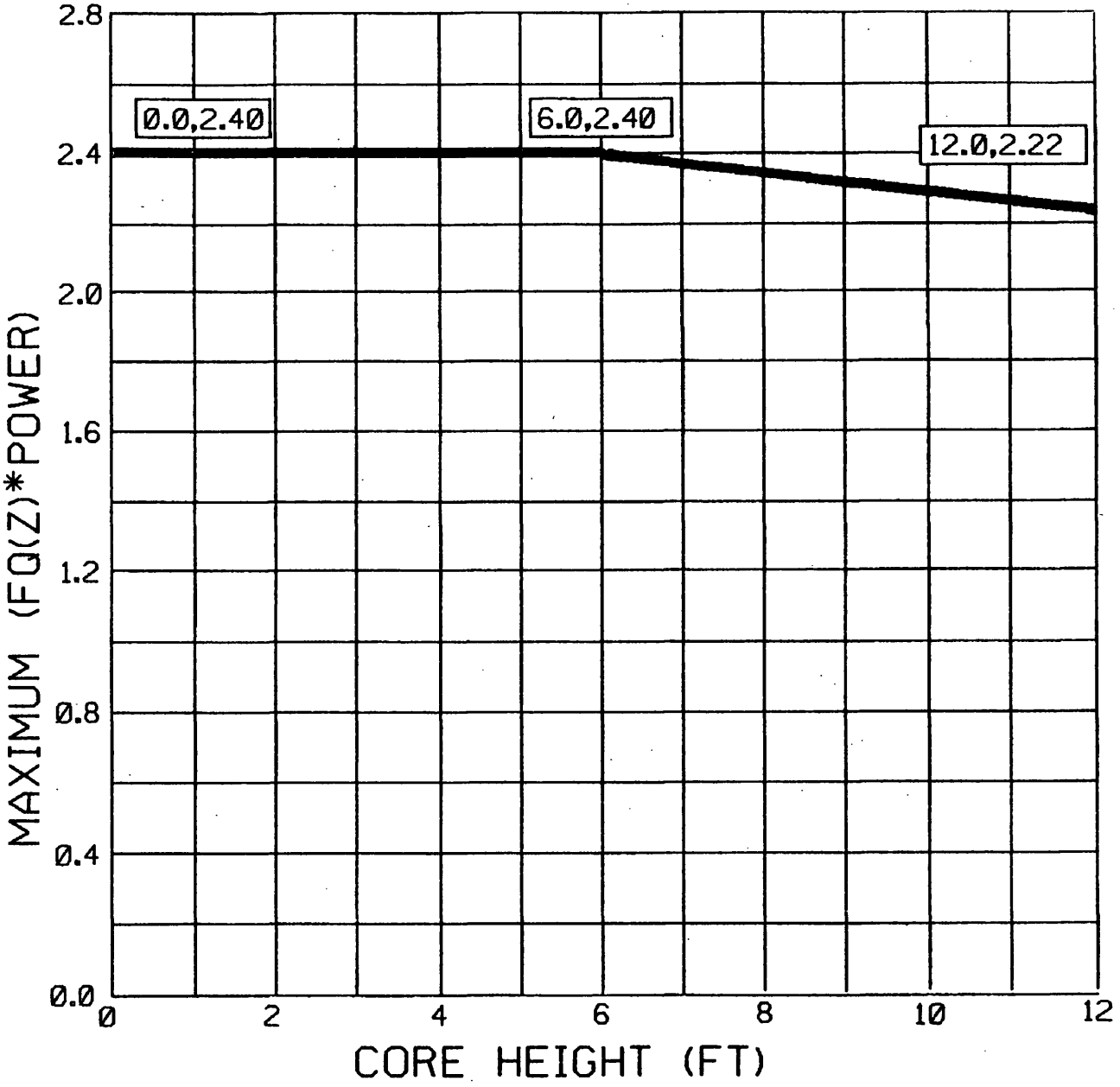

FIGURE 3.3-21

MAXIMUM FQ * POWER VS. AXIAL HEIGHT DURING NORMAL OPERATION

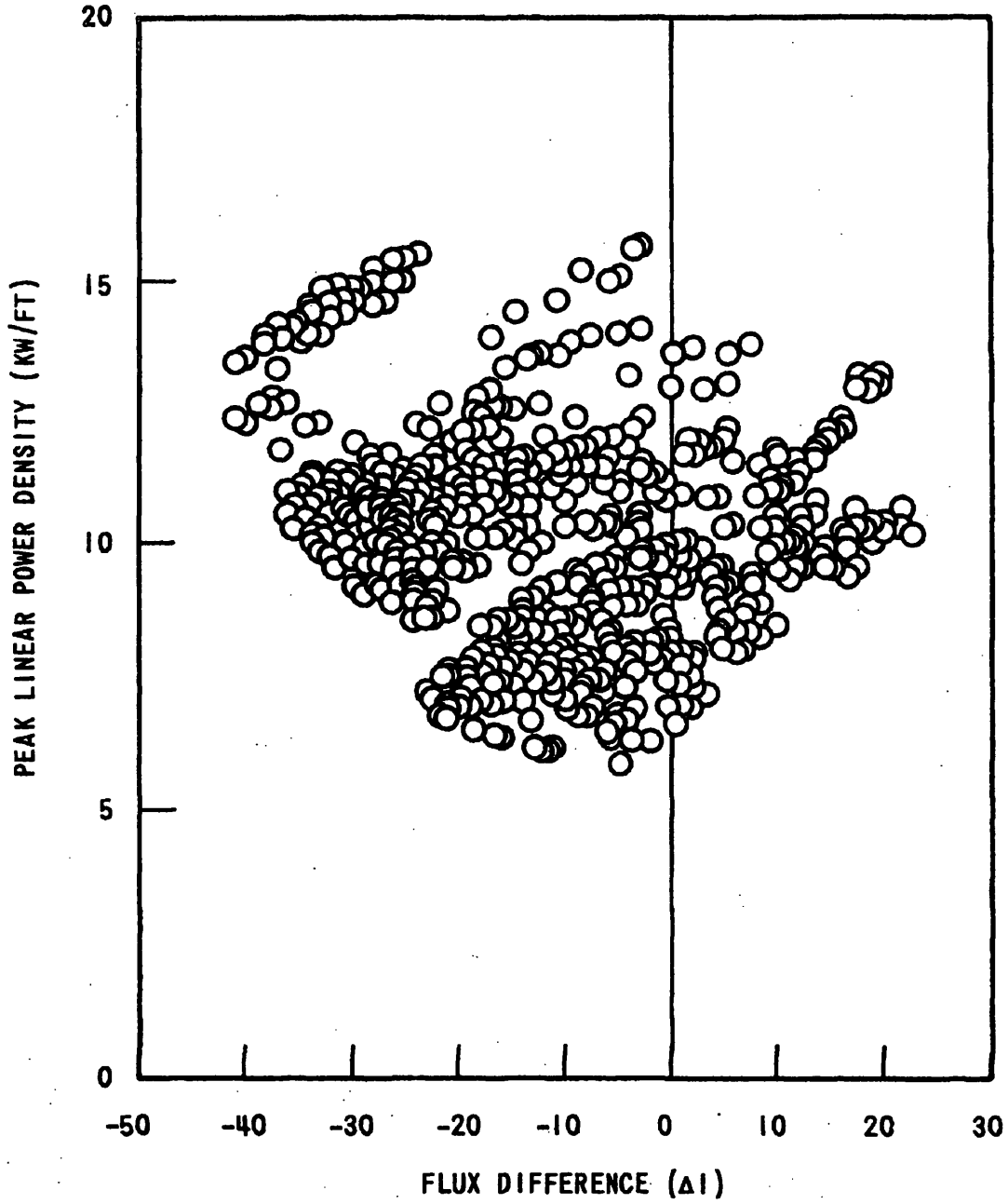

FIGURE 3.3-23
PEAK POWER DURING CONTROL ROD
MALFUNCTION OVERPOWER TRANSIENTS
BEAVER VALLEY POWER STATION UNIT NO. 1
UPDATED FINAL SAFETY ANALYSIS REPORT

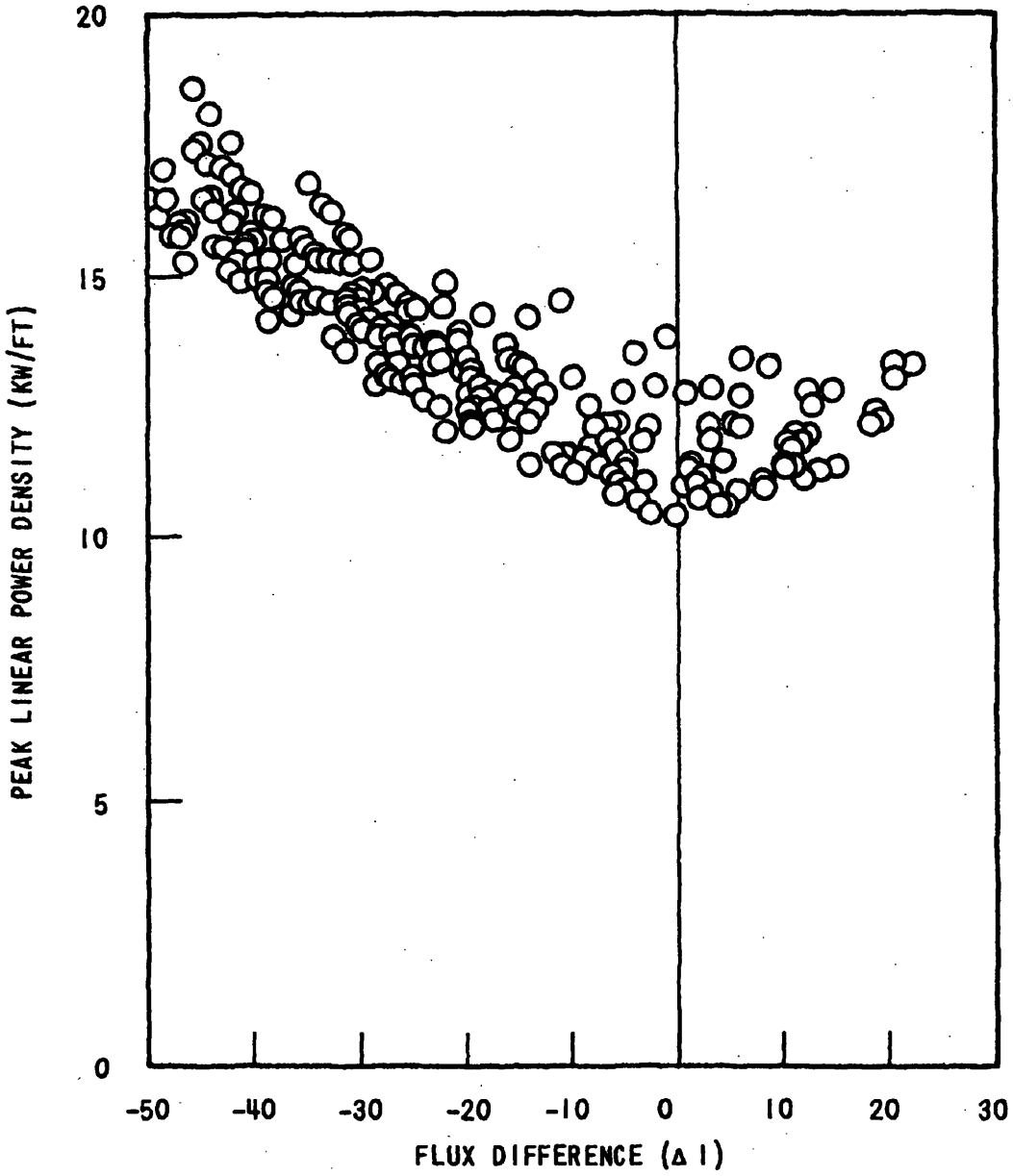

FIGURE 3.3-23A
PEAK POWER DURING BORATION/
DILUTION OVERPOWER TRANSIENTS
BEAVER VALLEY POWER STATION UNIT NO. 1
UPDATED FINAL SAFETY ANALYSIS REPORT

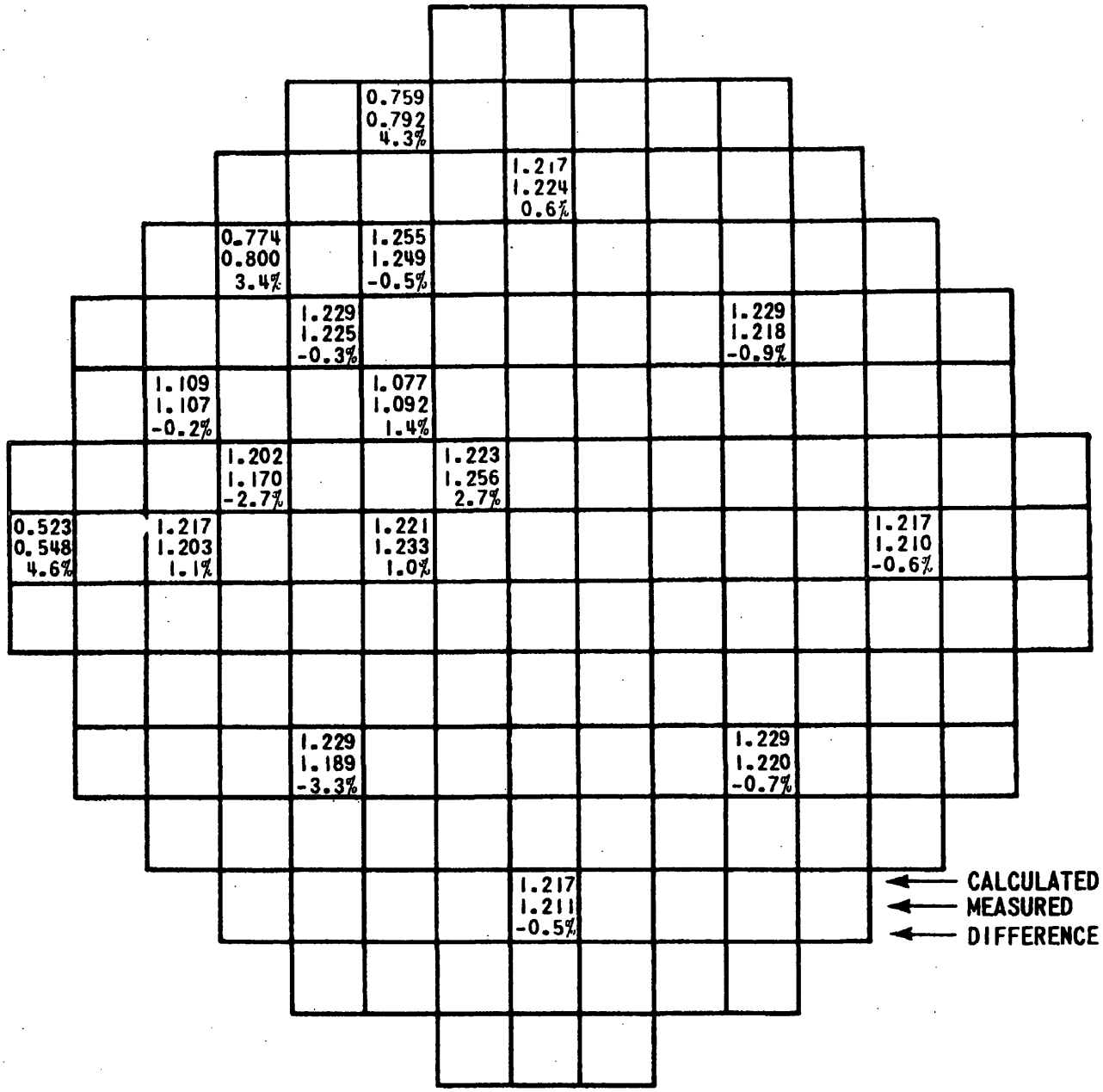

PEAKING FACTORS

$\bar{F}_z$ = 1.5

$F^N_{\Delta H}$ = 1.357

F^N_Q = 2.07 LOCATED AT M-8 SOUTH

FIGURE 3.3-24
COMPARISON BETWEEN CALCULATED AND MEASURED RELATIVE FUEL ASSEMBLY POWER DISTRIBUTION
BEAVER VALLEY POWER STATION UNIT NO. 1
UPDATED FINAL SAFETY ANALYSIS REPORT

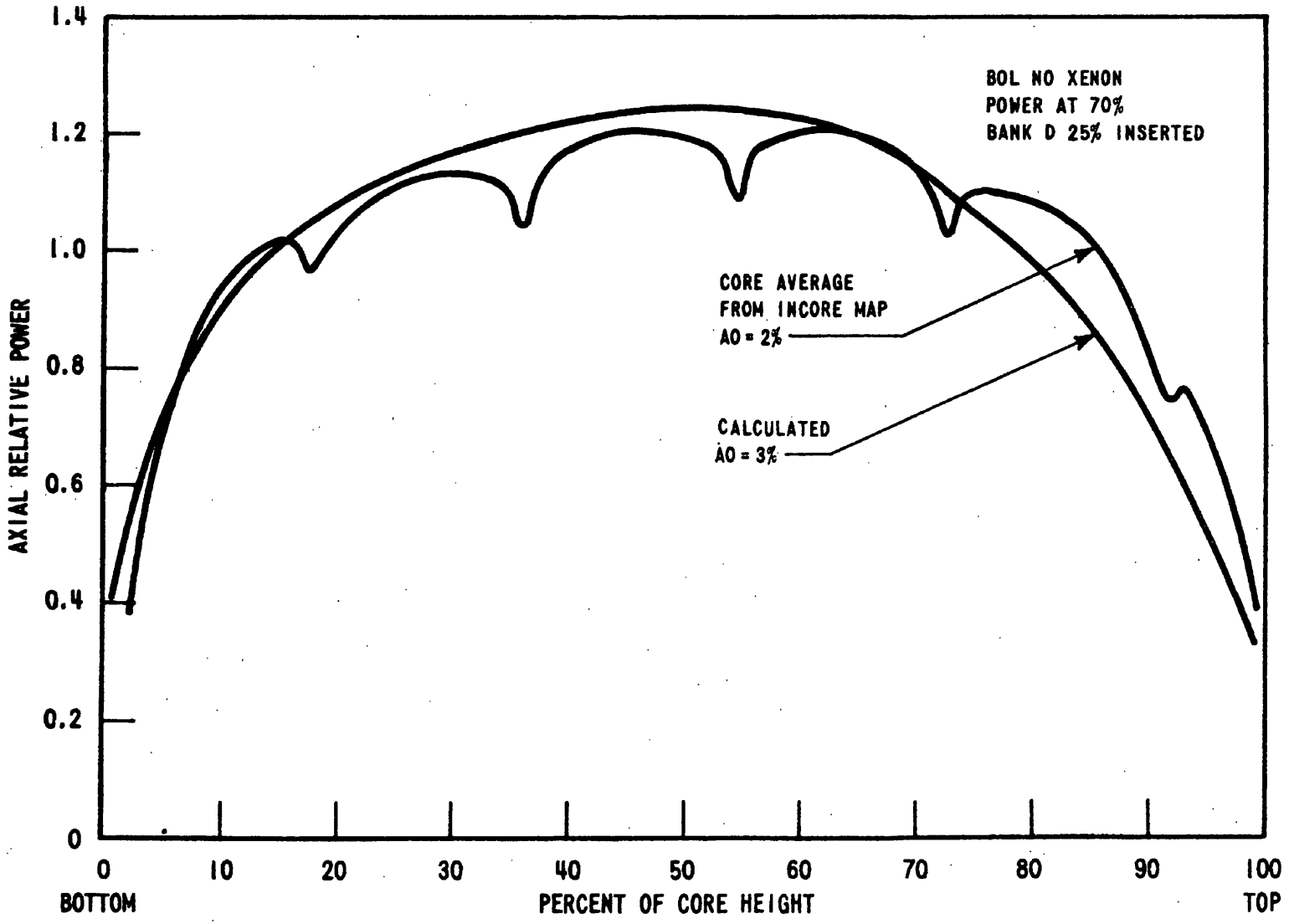

FIGURE 3.3-25
COMPARISON OF CALCULATED AND MEASURED AXIAL SHAPE
BEAVER VALLEY POWER STATION UNIT NO. 1
UPDATED FINAL SAFETY ANALYSIS REPORT

REV. 0 (1/82)

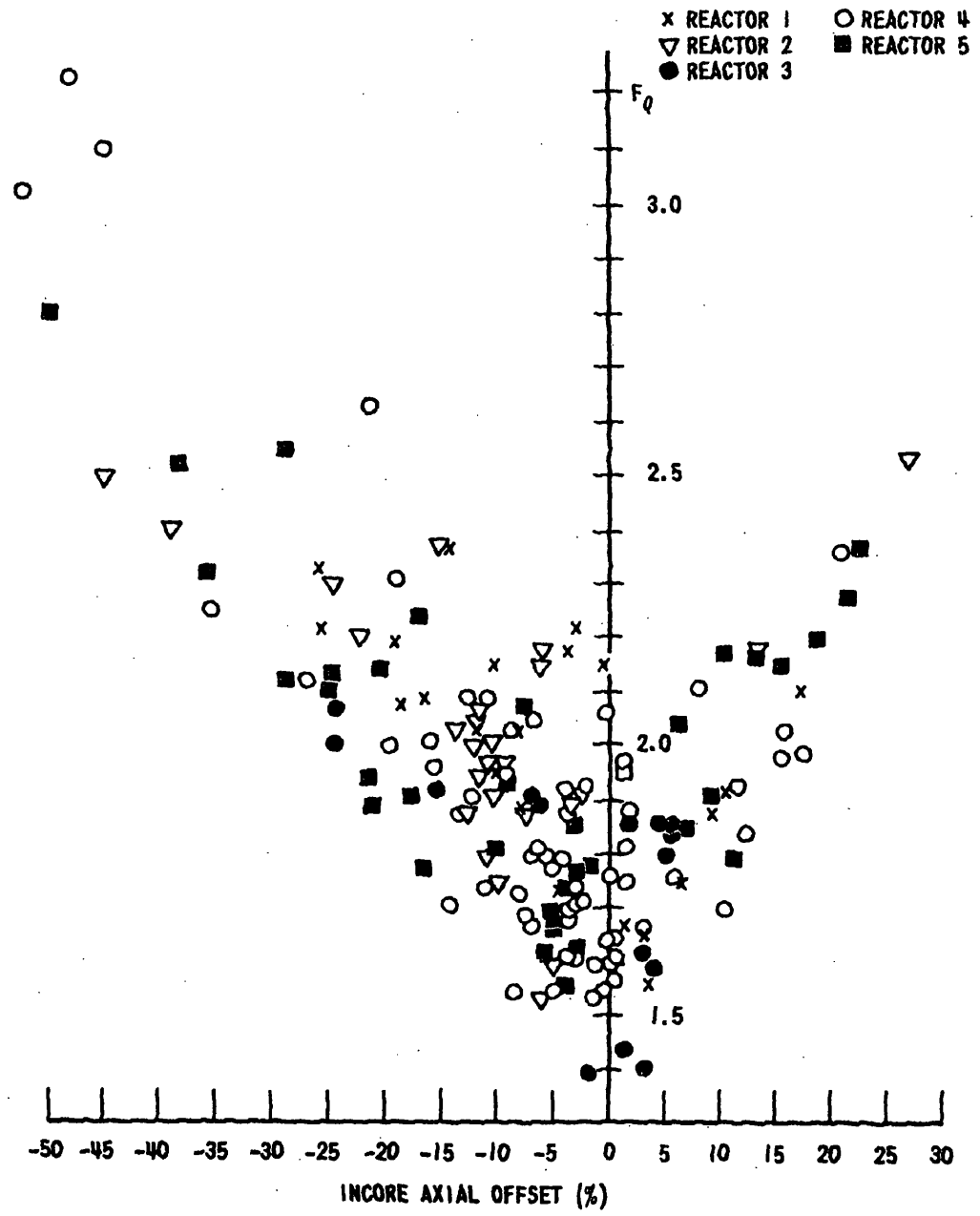

FIGURE 3-3-26
MEASURED VALUE OF F_Q FOR FULL POWER ROD CONFIGURATIONS
BEAVER VALLEY POWER STATION UNIT NO. 1
UPDATED FINAL SAFETY ANALYSIS REPORT

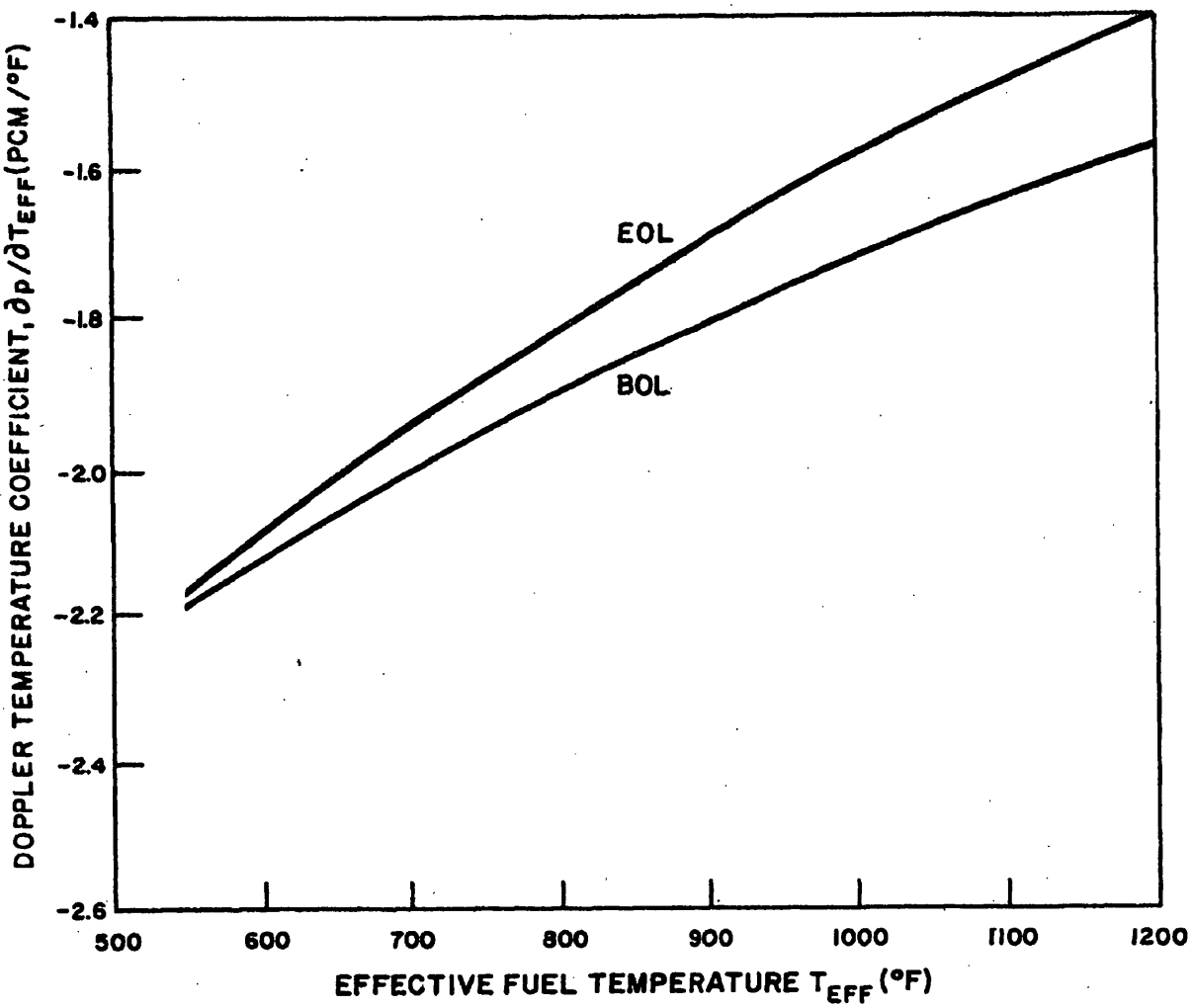

FIGURE 3.3-27
DOPPLER TEMPERATURE COEFFICIENT AT BOL AND EOL VS. T_{EFF} FOR CYCLE 1
BEAVER VALLEY POWER STATION UNIT NO. 1
UPDATED FINAL SAFETY ANALYSIS REPORT

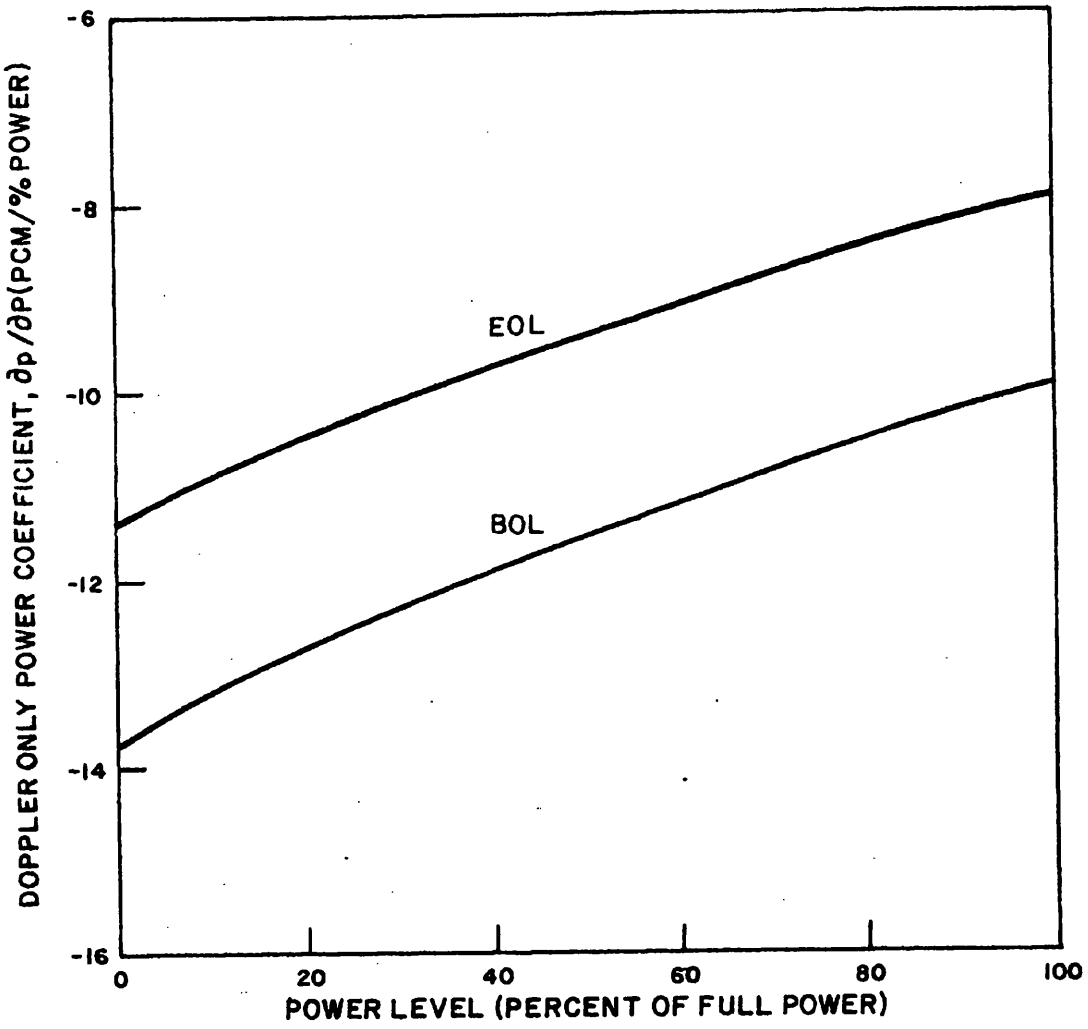

FIGURE 3.3-28
DOPPLER ONLY POWER COEFFICIENT VS POWER LEVEL AT BOL AND EOL, CYCLE 1
BEAVER VALLEY POWER STATION UNIT NO. 1
UPDATED FINAL SAFETY ANALYSIS REPORT

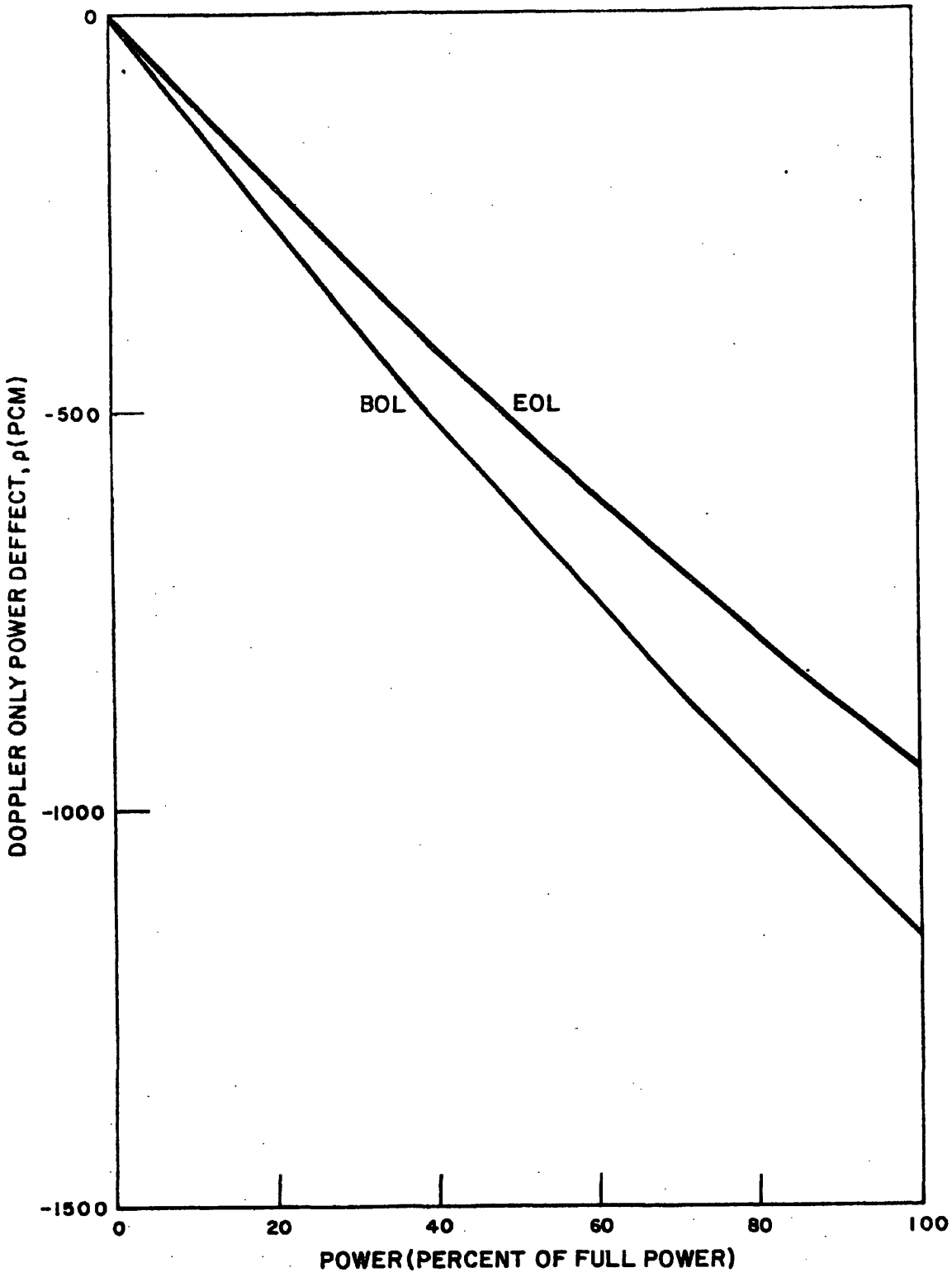

FIGURE 3.3-29
DOPPLER ONLY POWER DEFECT VERSUS PERCENT POWER, BOL AND EOL, CYCLE 1
BEAVER VALLEY POWER STATION UNIT NO. 1
UPDATED FINAL SAFETY ANALYSIS REPORT

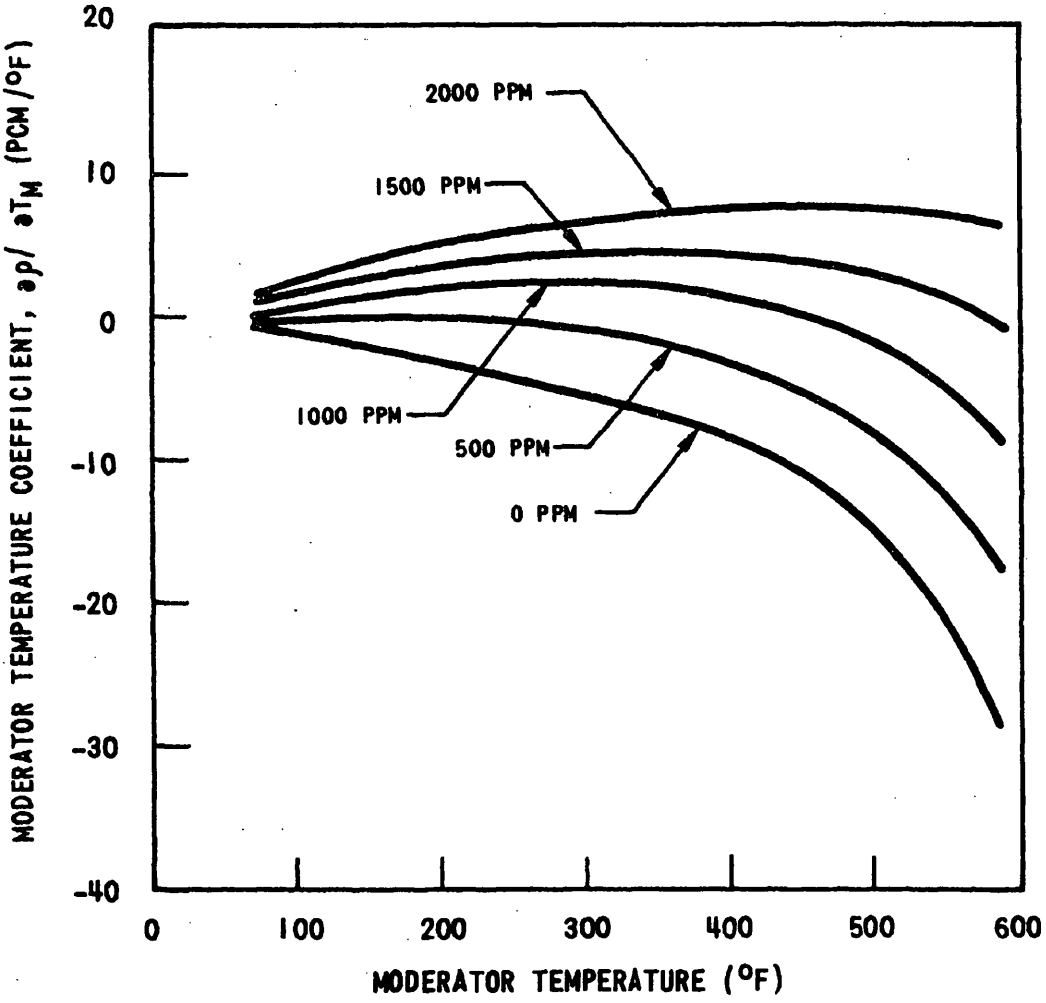

FIGURE 3.3-30
MODERATOR TEMPERATURE COEFFICIENT
BOL, CYCLE 1, NO RODS
BEAVER VALLEY POWER STATION UNIT NO. 1
UPDATED FINAL SAFETY ANALYSIS REPORT

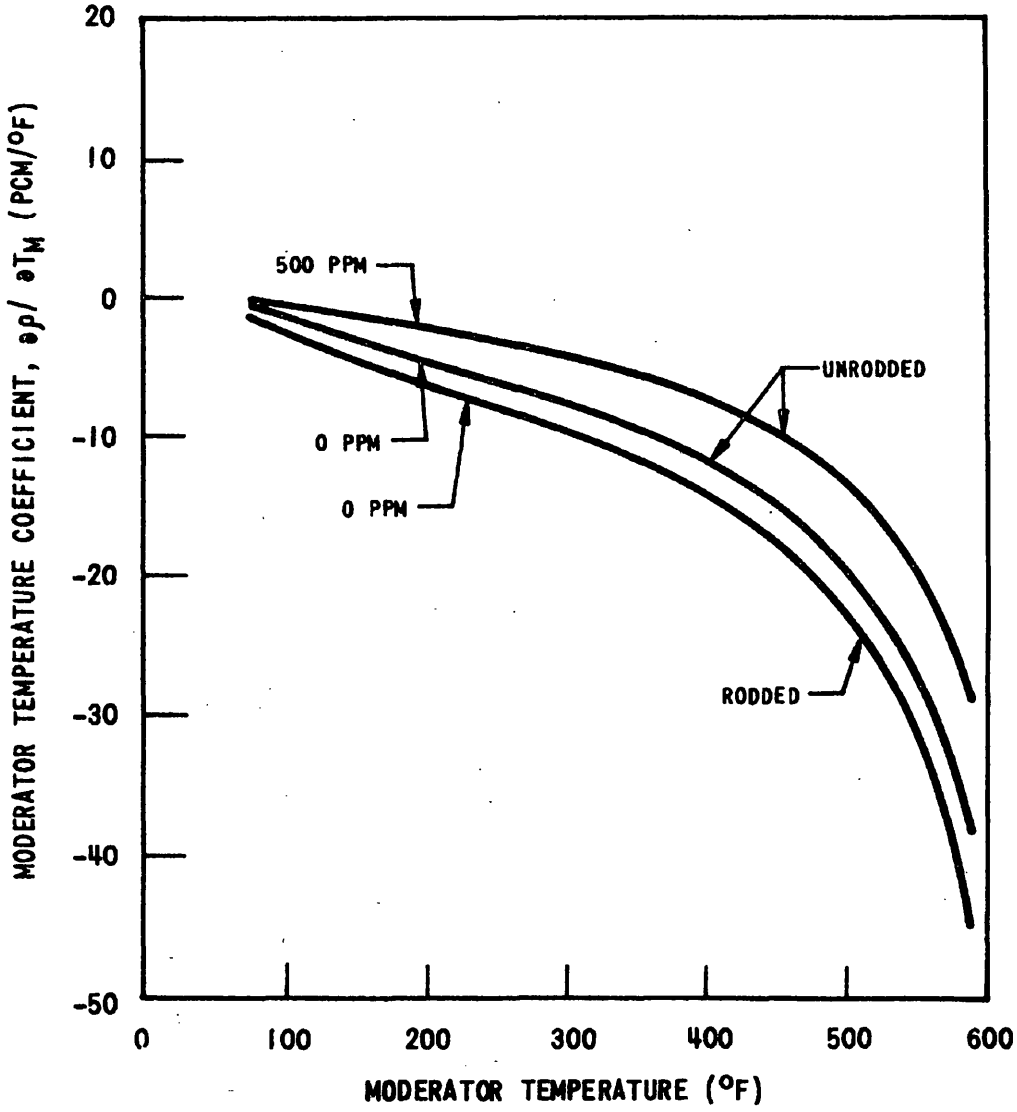

FIGURE 3.3-31
MODERATOR TEMPERATURE COEFFICIENT
EOL, CYCLE 1

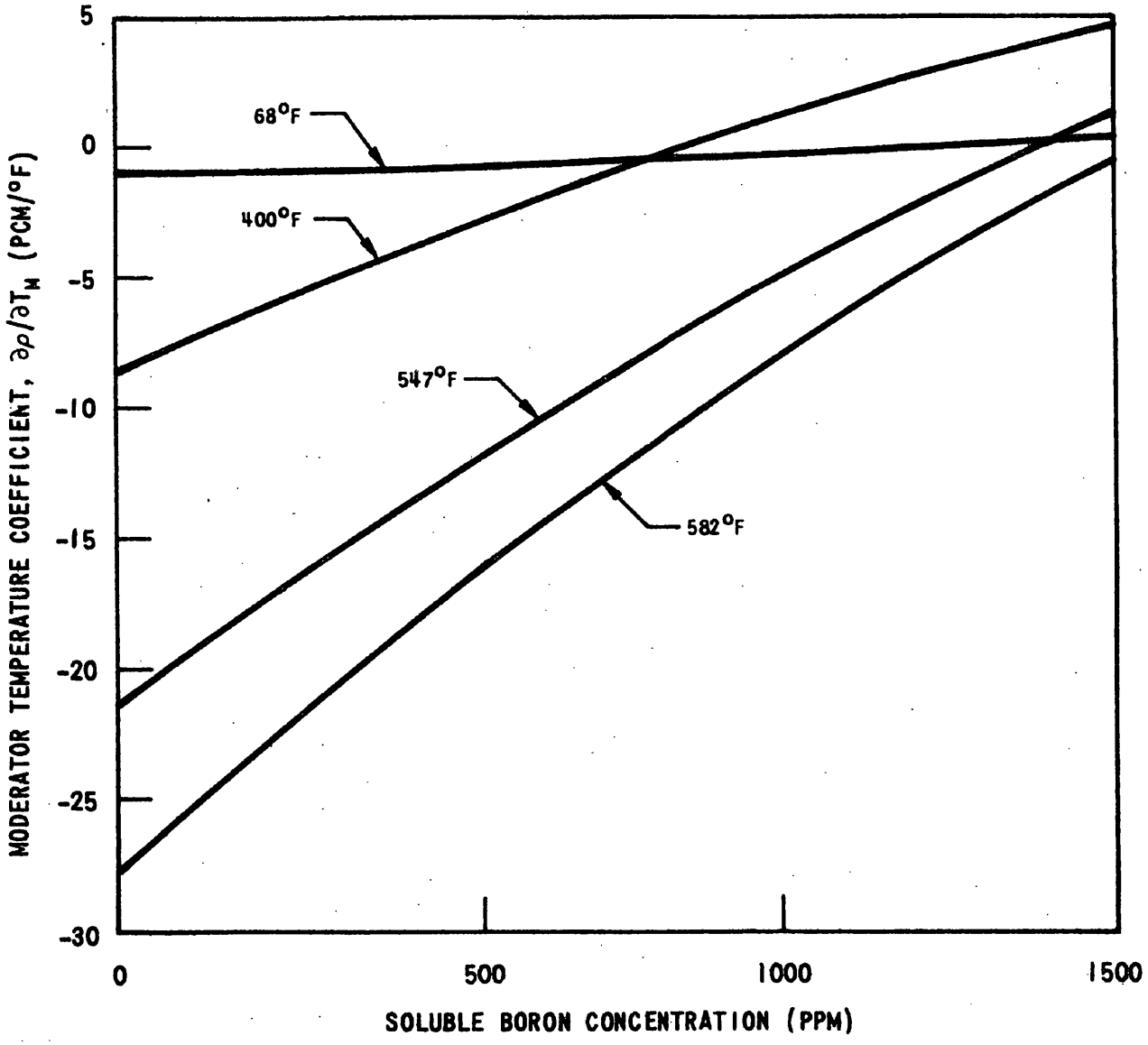

FIGURE 3.3-32
MODERATOR TEMPERATURE COEFFICIENT AS A FUNCTION OF BORON CONCENTRATION BOL CYCLE 1, NO RODS
BEAVER VALLEY POWER STATION UNIT NO. 1
UPDATED FINAL SAFETY ANALYSIS REPORT

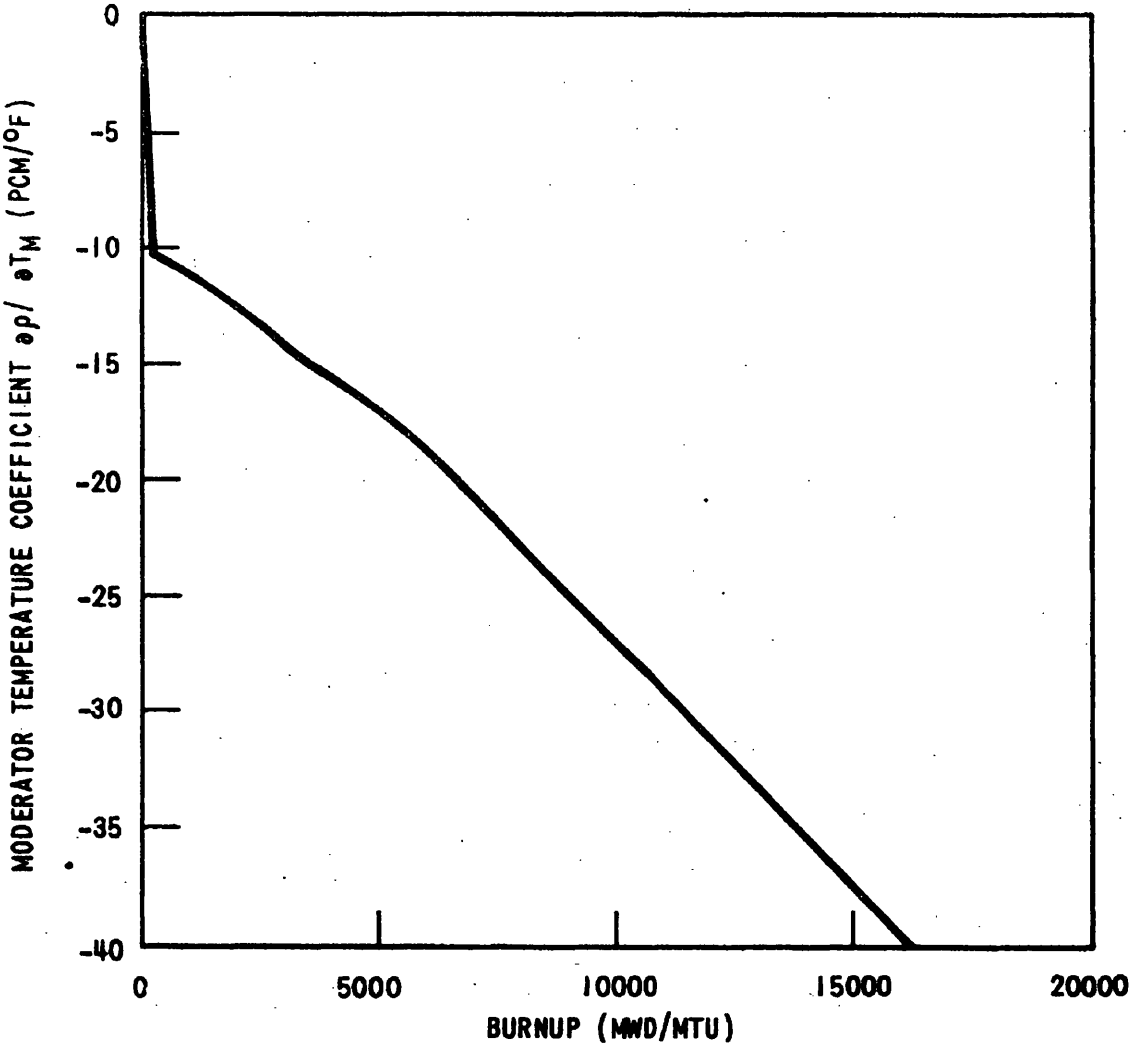

FIGURE 3.3-33
HOT FULL POWER TEMPERATURE COEFFICIENT DURING CYCLE 1 FOR THE CRITICAL BORON CONCENTRATION
BEAVER VALLEY POWER STATION UNIT NO. 1
UPDATED FINAL SAFETY ANALYSIS REPORT

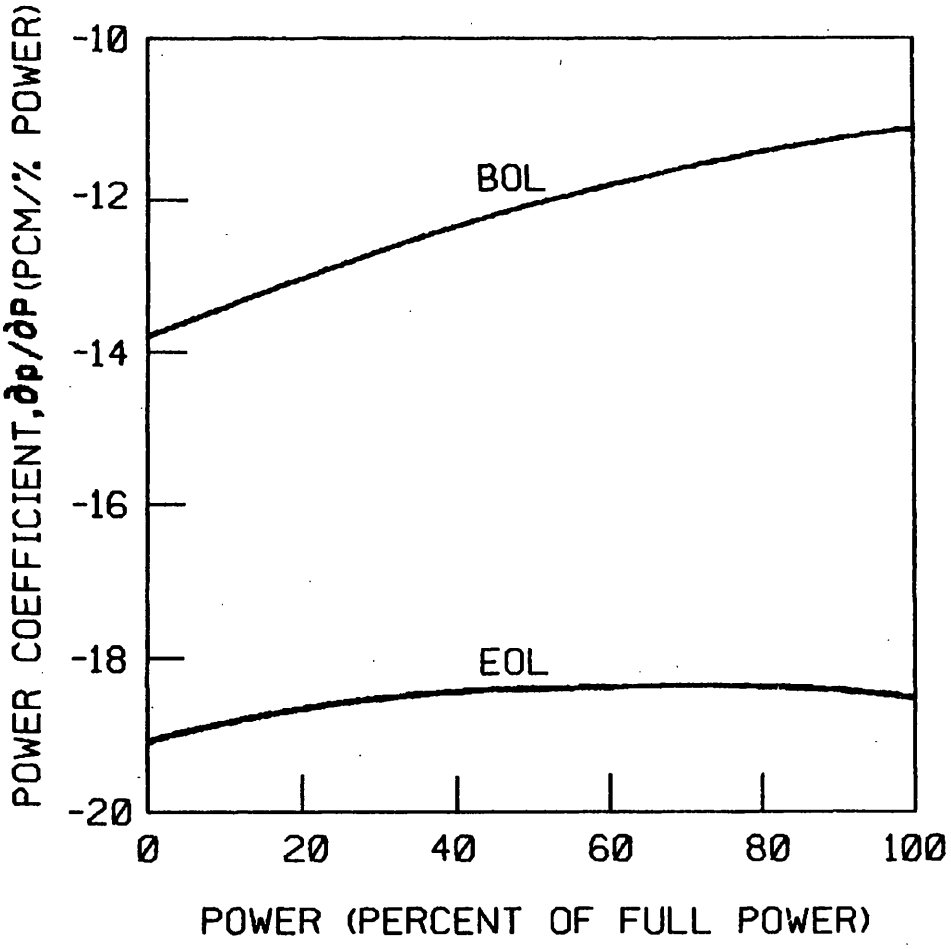

FIGURE 3.3-34

CYCLE 1
POWER COEFFICIENT VS. PERCENT FULL POWER FOR BOL AND EOL

BEAVER VALLEY POWER STATION-UNIT 1
UPDATED FINAL SAFETY ANALYSIS REPORT

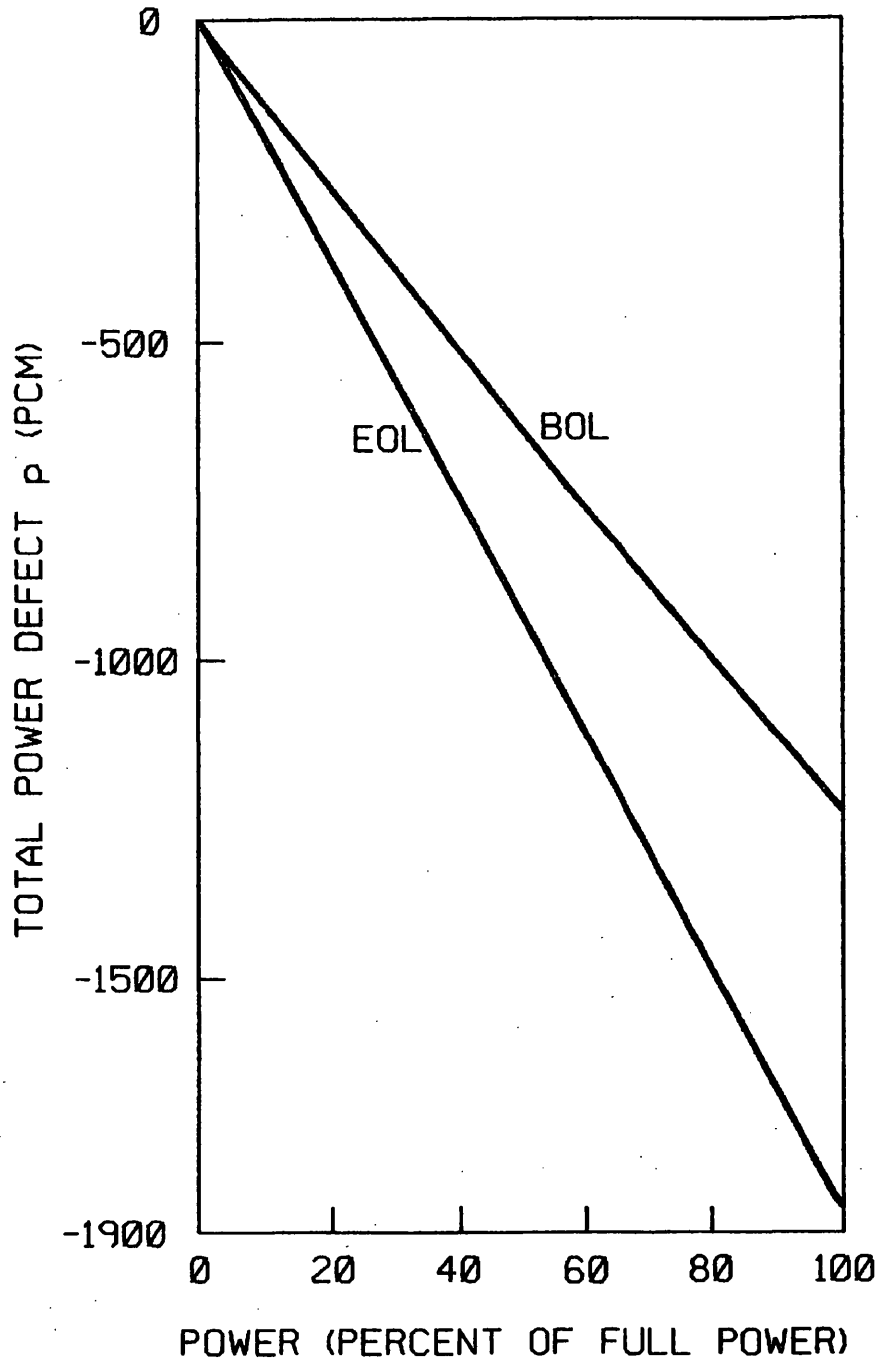

FIGURE 3.3-35

CYCLE 1
POWER DEFECT VS. PERCENT FULL POWER BOL AND EOL

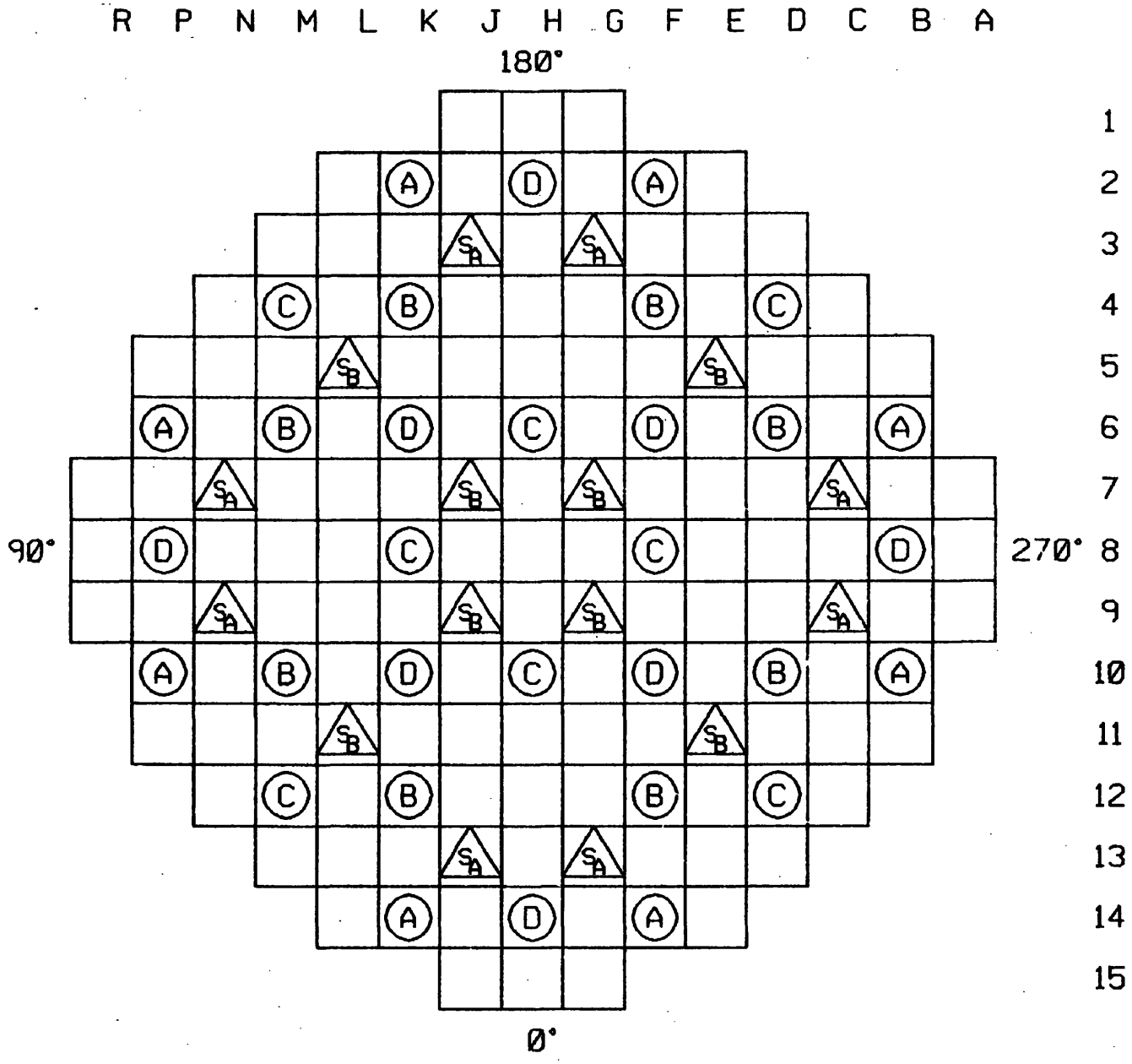

FUNCTION	NUMBER OF CLUSTERS
CONTROL BANK D	8
CONTROL BANK C	8
CONTROL BANK B	8
CONTROL BANK A	8
SHUTDOWN BANK S_B	8
SHUTDOWN BANK S_A	8

FIGURE 3.3-36

ROD CLUSTER CONTROL ASSEMBLY PATTERN

BEAVER VALLEY POWER STATION-UNIT 1
UPDATED FINAL SAFETY ANALYSIS REPORT

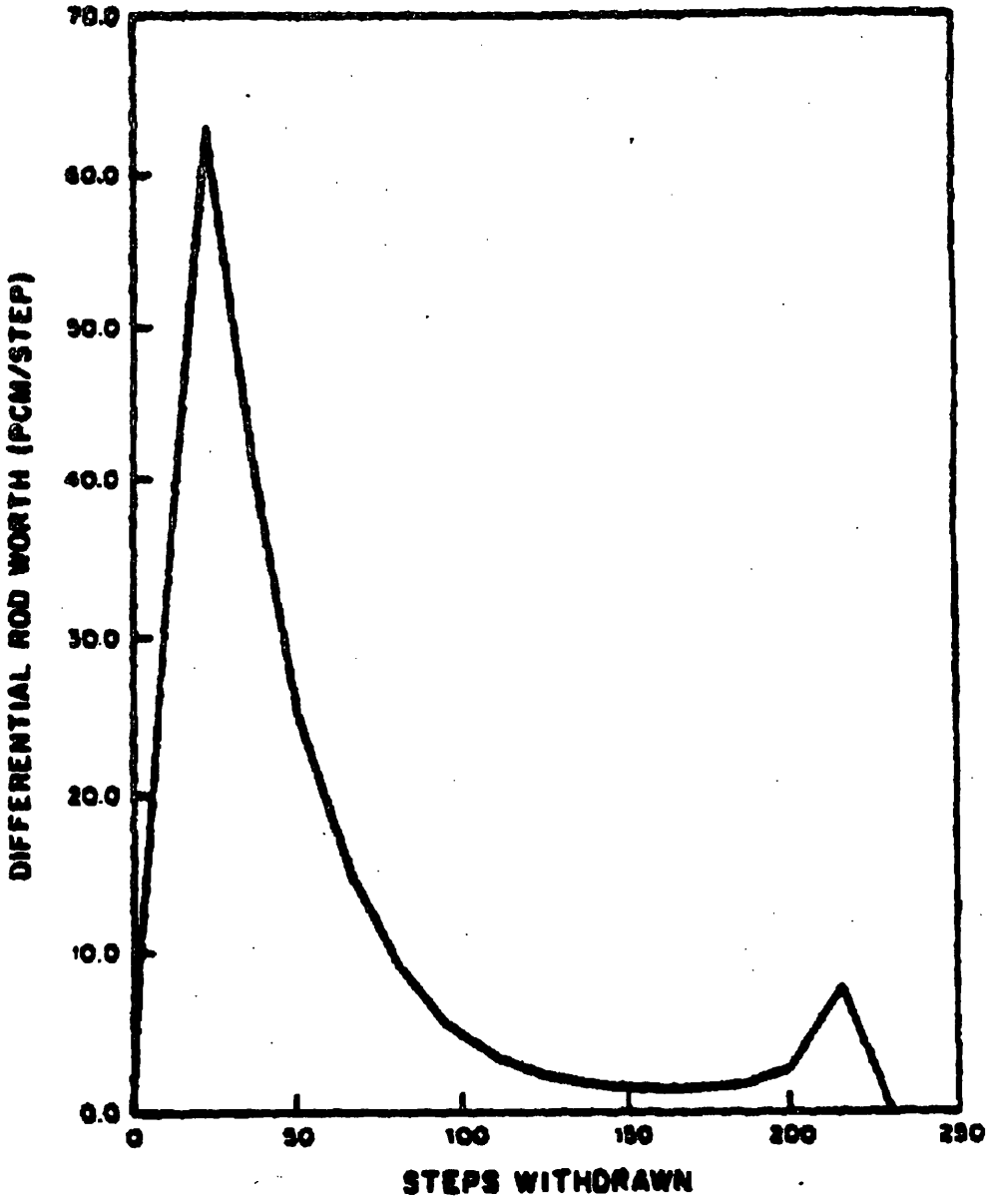

FIGURE 3.3-37
TYPICAL ACCIDENTAL SIMULTANEOUS
WITHDRAWAL OF TWO CONTROL BANKS
AT BOL, HZP, BANKS "A" AND "B"
MOVING IN THE SAME PLANE

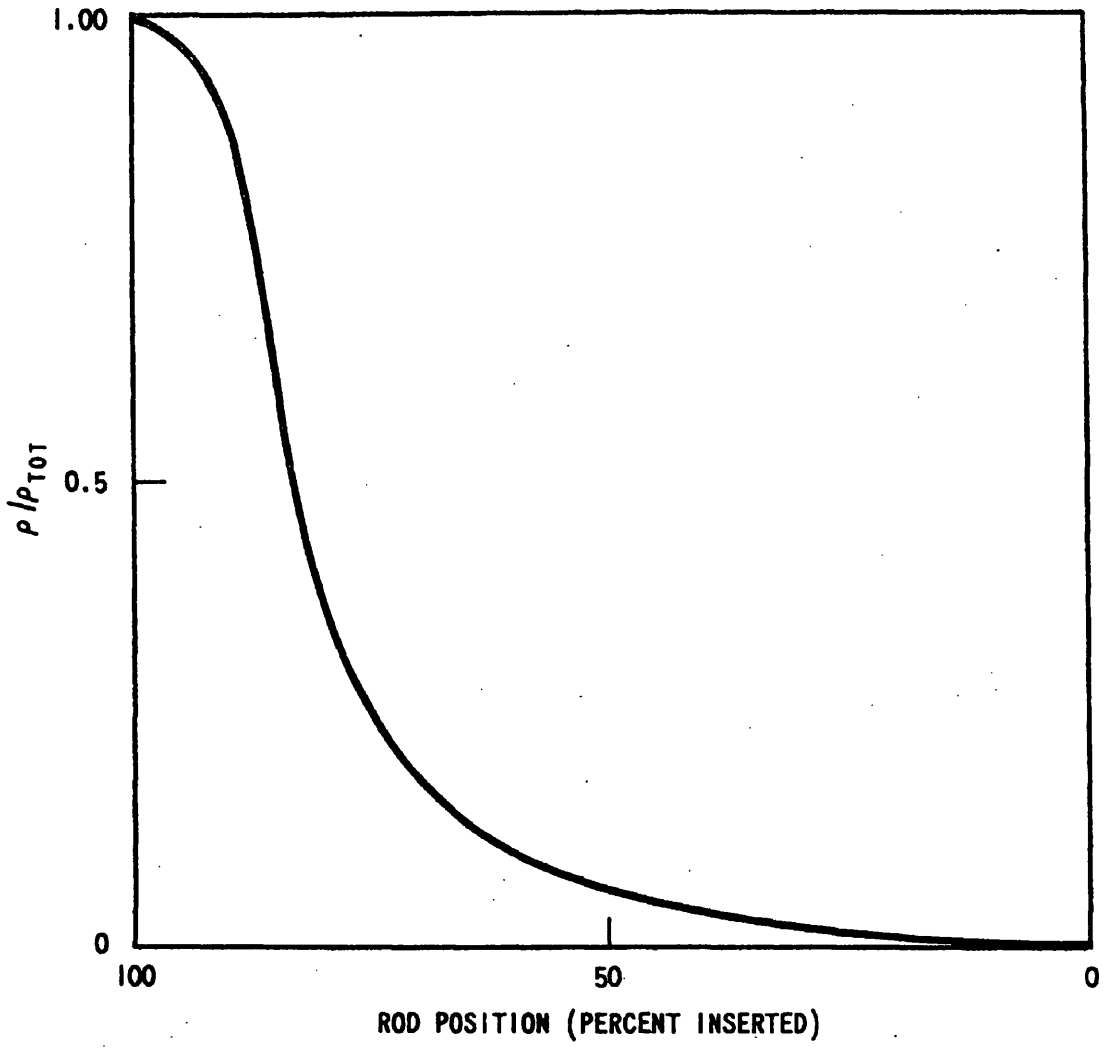

FIGURE 3-3-39
NORMALIZED ROD WORTH VS PERCENT INSERTION ALL RODS BUT ONE
BEAVER VALLEY POWER STATION UNIT NO. 1
UPDATED FINAL SAFETY ANALYSIS REPORT

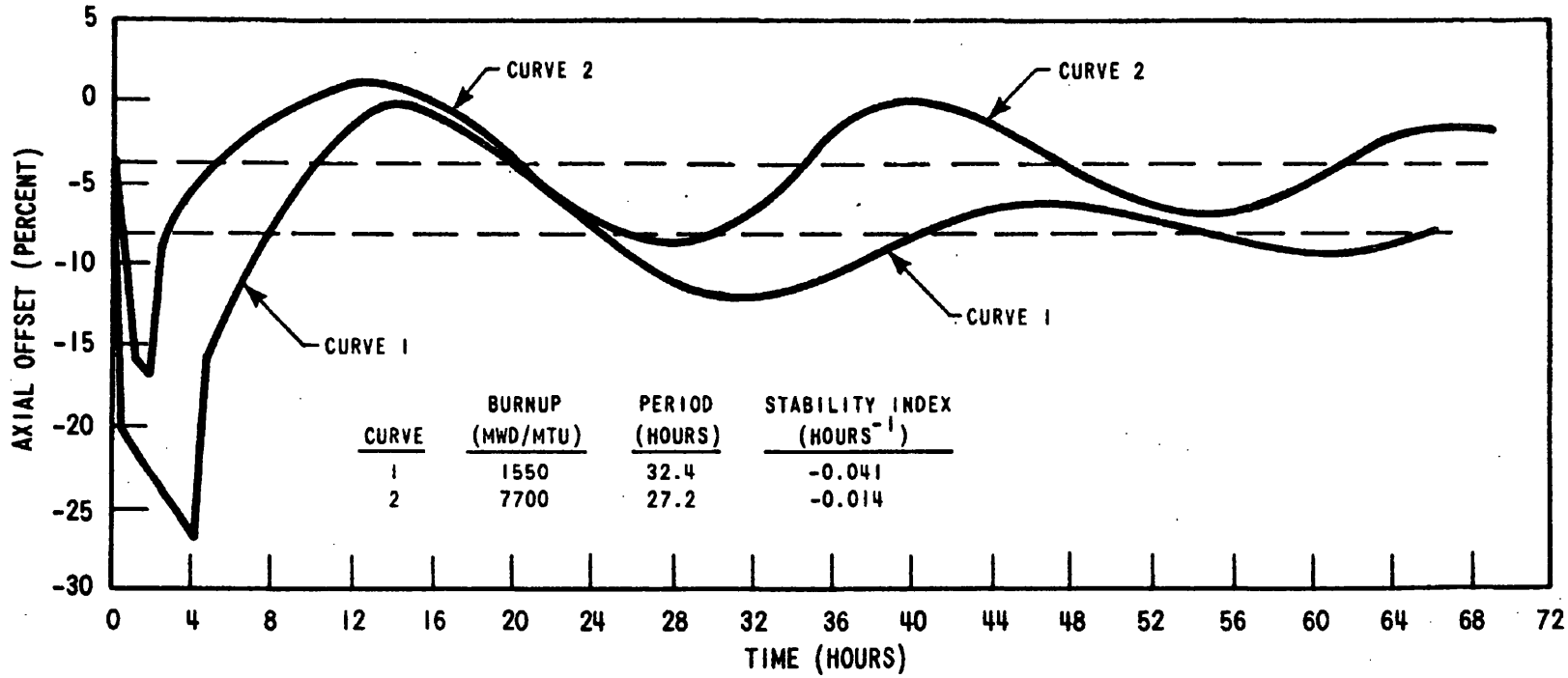

FIGURE 3.3-40
AXIAL OFFSET VS TIME PWR CORE WITH A 12-FT HEIGHT AND 121 ASSEMBLIES
BEAVER VALLEY POWER STATION UNIT NO. 1
UPDATED FINAL SAFETY ANALYSIS REPORT

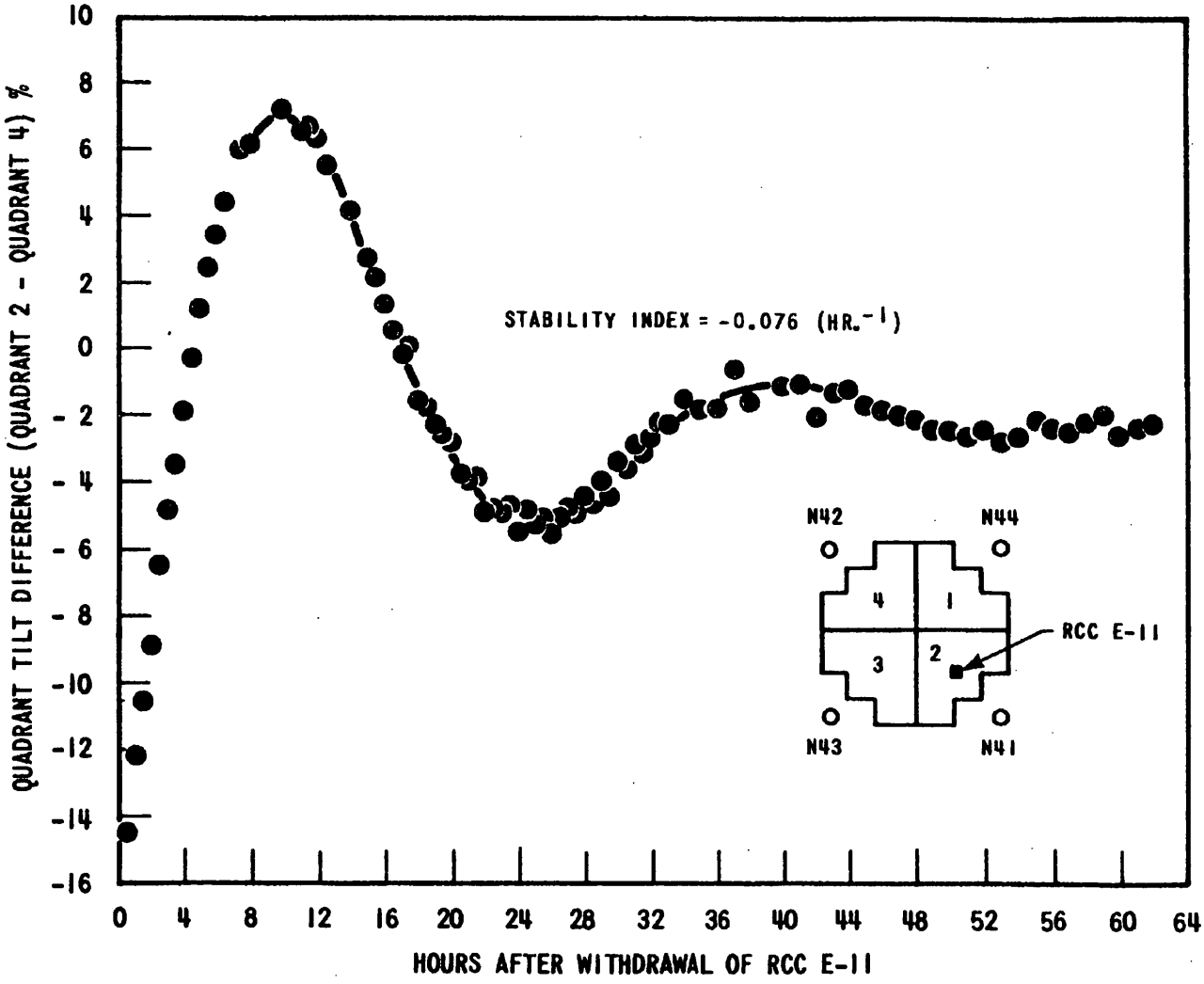

FIGURE 3-3-41
XY XENON TEST THERMOCOUPLE RESPONSE
QUADRANT TILT DIFFERENCE VS TIME
BEAVER VALLEY POWER STATION UNIT NO. 1
UPDATED FINAL SAFETY ANALYSIS REPORT

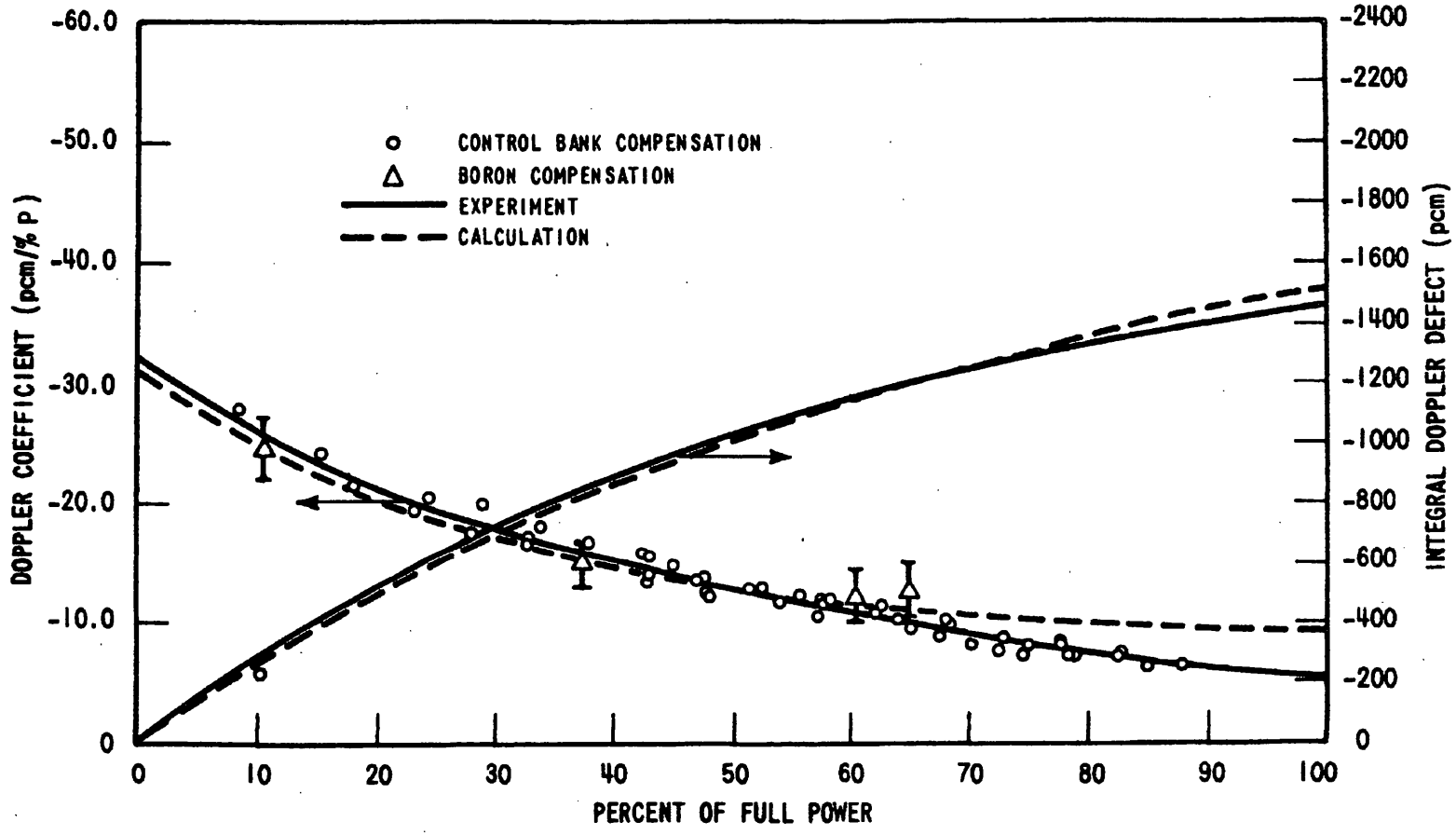

FIGURE 3.3-42
CALCULATED AND MEASURED DOPPLER DEFECT AND COEFFICIENTS AT BOL TWO-LOOP PLANT, 121 ASSEMBLIES, 12 FOOT CORE

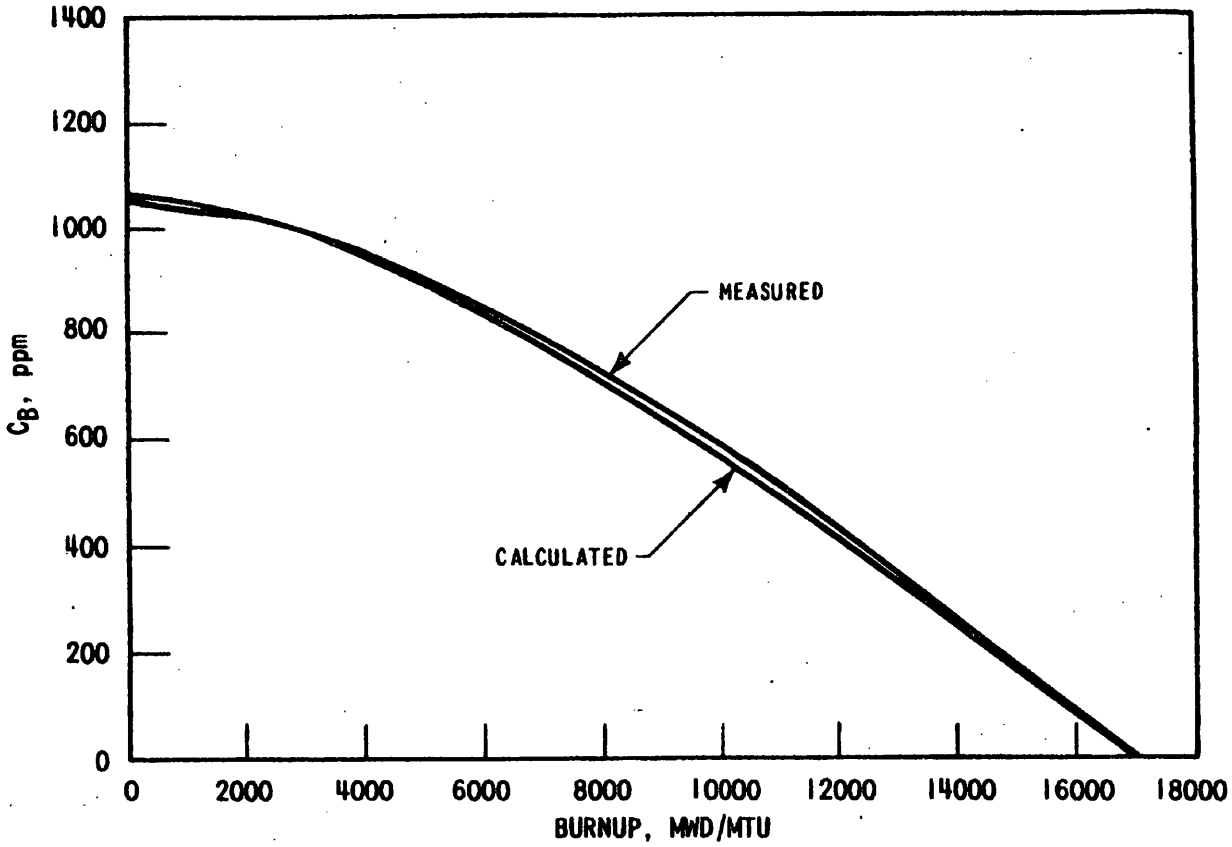

FIGURE 3.3-43
COMPARISON OF CALCULATED AND MEASURED BORON CONCENTRATION FOR 2 LOOP PLANT, 121 ASSEMBLIES, 12 FT CORE
BEAVER VALLEY POWER STATION UNIT NO. 1
UPDATED FINAL SAFETY ANALYSIS REPORT

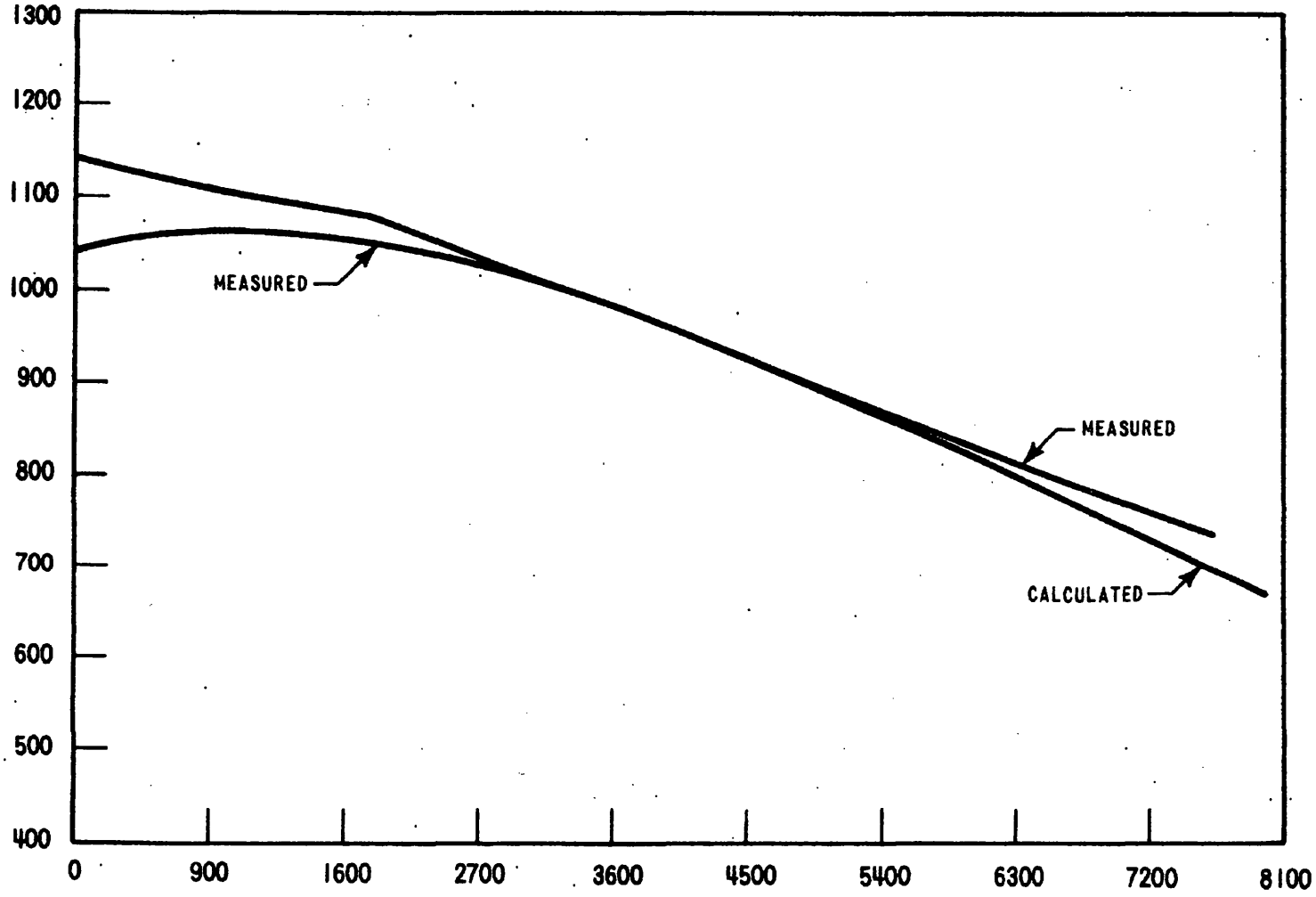

FIGURE 3.3-44
COMPARISON OF CALCULATED AND MEASURED C_B 2-LOOP PLANT WITH 121 ASSEMBLIES, 12 FOOT CORE

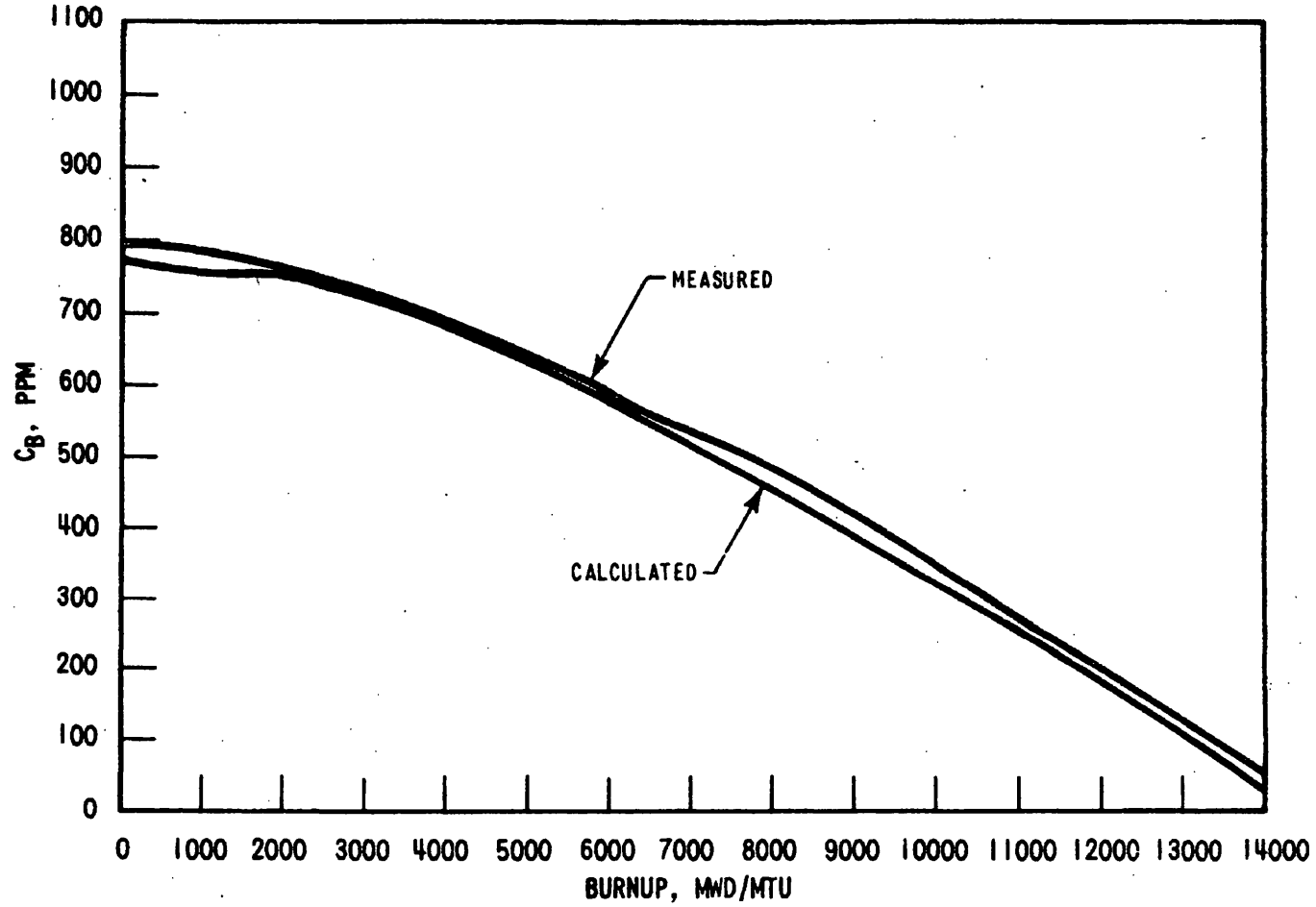

FIGURE 3.3-45
COMPARISON OF CALCULATED AND MEASURED C_B IN 3 LOOP PLANT, 157 ASSEMBLIES, 12 FOOT CORE

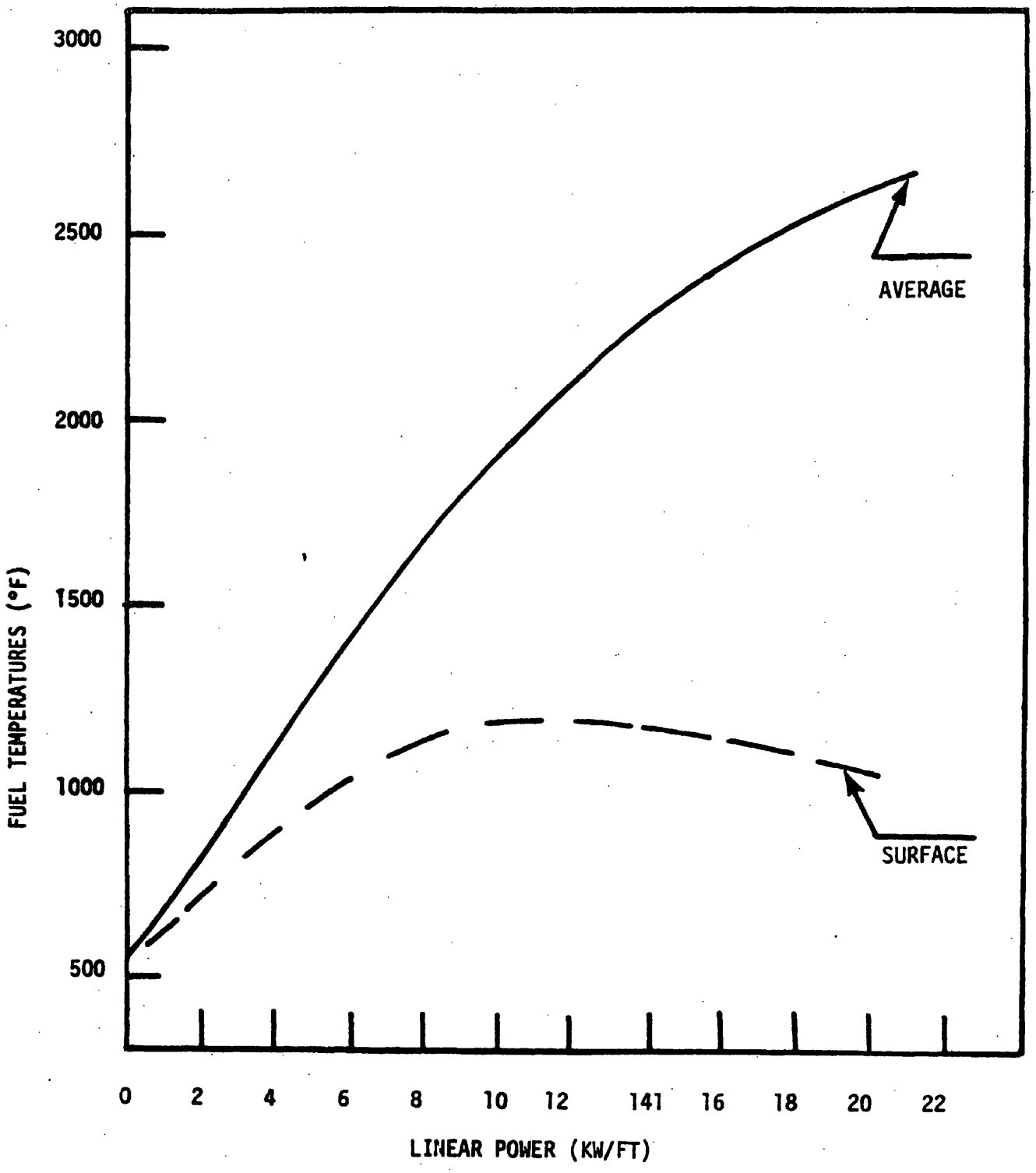

FIGURE 3.4-1
PEAK FUEL AVERAGE AND SURFACE TEMPERATURES DURING FUEL ROD LIFETIME VS LINEAR POWER
BEAVER VALLEY POWER STATION UNIT NO. 1
UPDATED FINAL SAFETY ANALYSIS REPORT

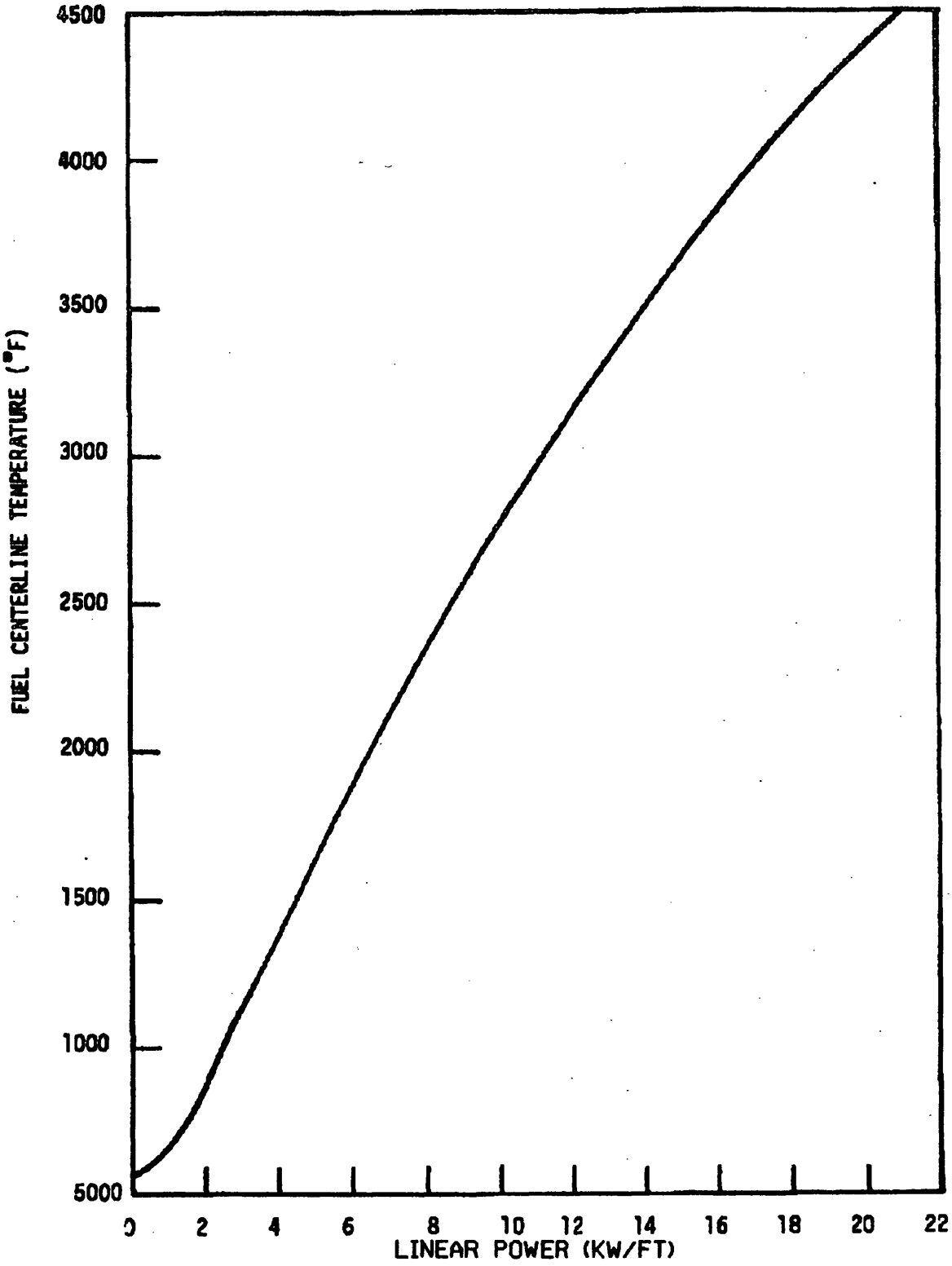

FIGURE 3.4-2
PEAK FUEL CENTERLINE TEMPERATURE DURING FUEL ROD LIFETIME VS LINEAR POWER
BEAVER VALLEY POWER STATION
UPDATED FINAL SAFETY ANALYSIS REPORT

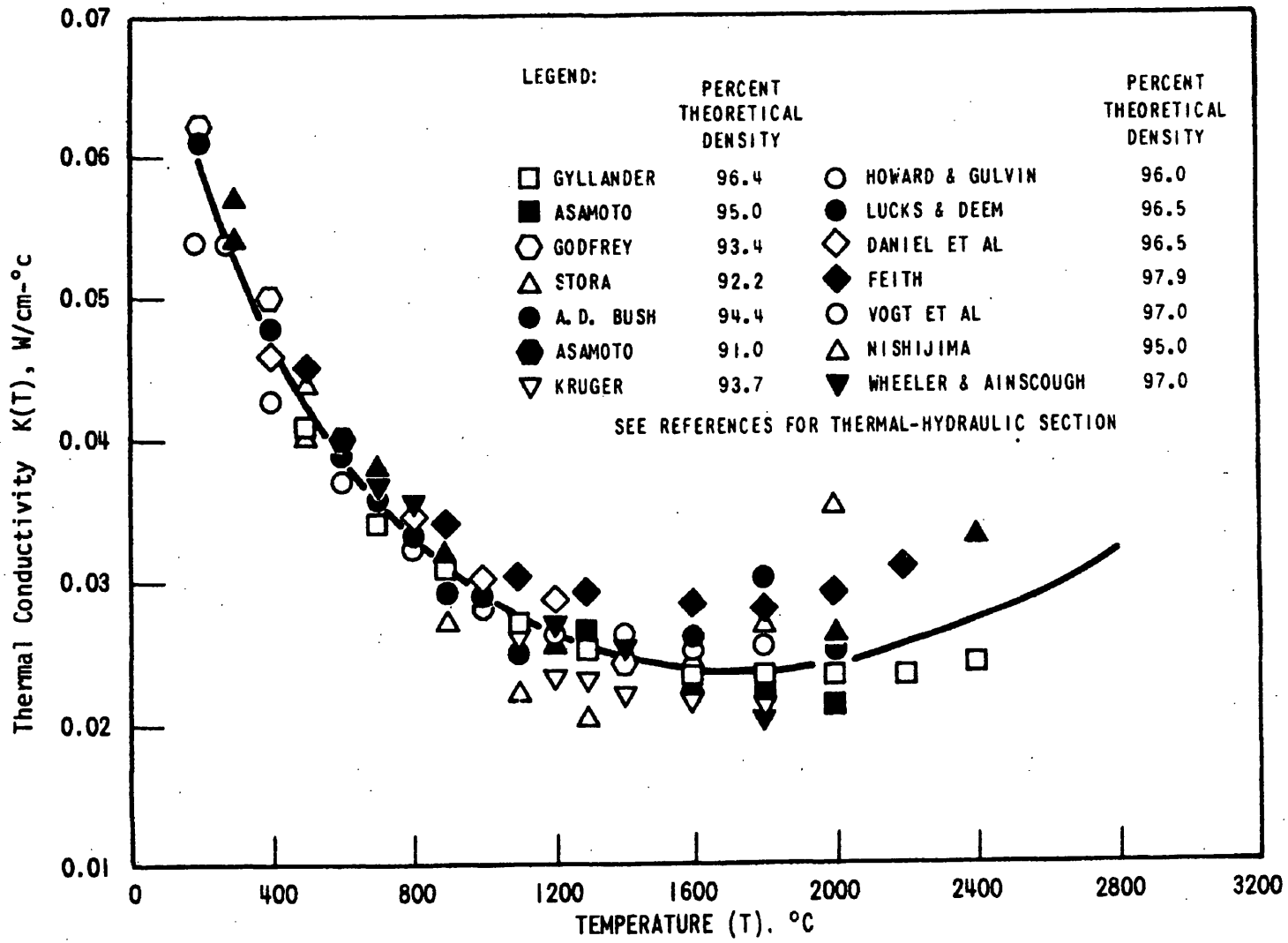

FIGURE 3.4-3
THERMAL CONDUCTIVITY OF UO_2 (DATA CORRECTED TO 95% THEORETICAL DENSITY)
BEAVER VALLEY POWER STATION UNIT NO. 1
UPDATED FINAL SAFETY ANALYSIS REPORT

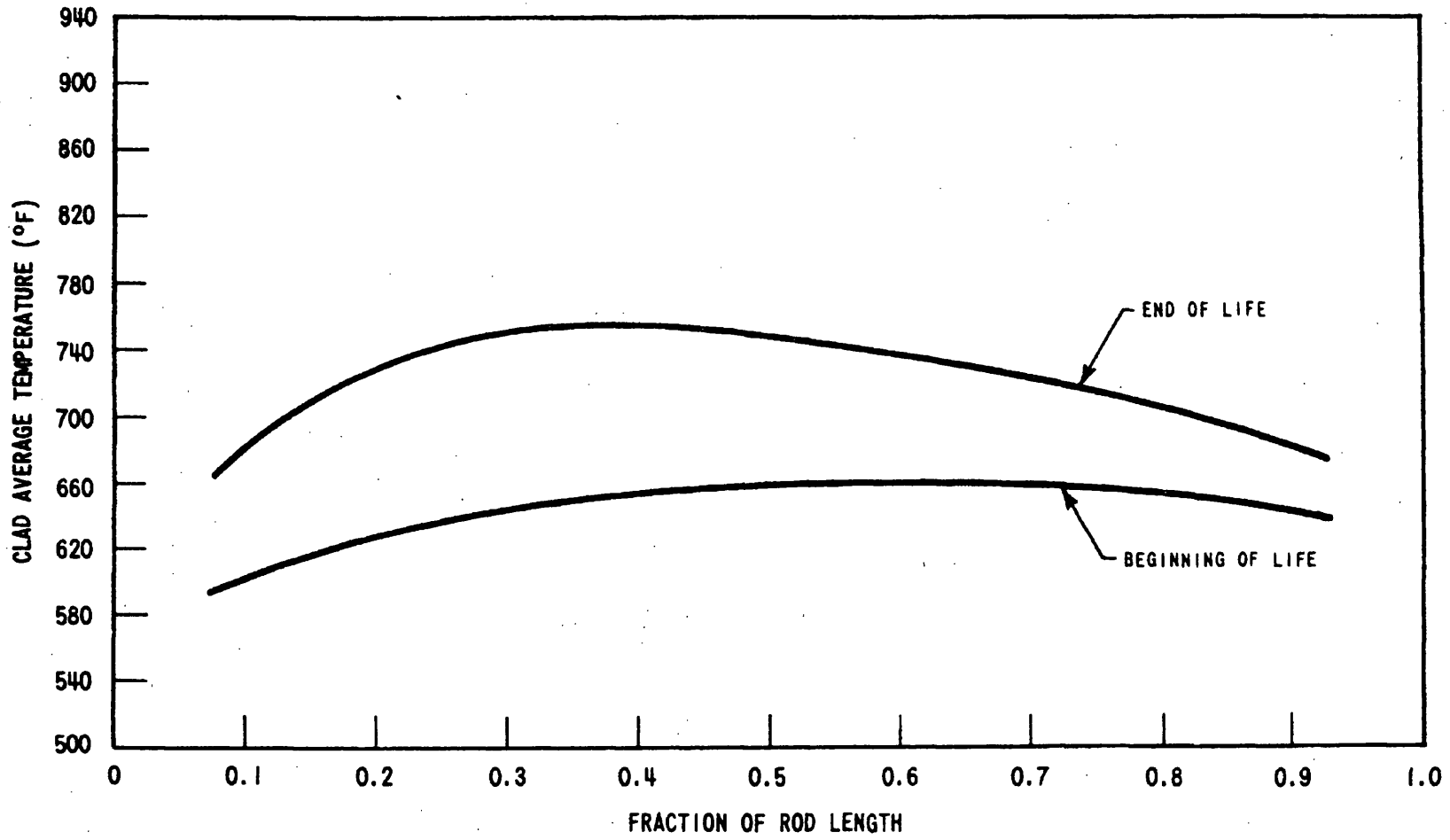

FIGURE 3.4-4
AXIAL VARIATION OF AVERAGE CLAD TEMPERATURE FOR ROD OPERATING AT 5.43 KW/FT

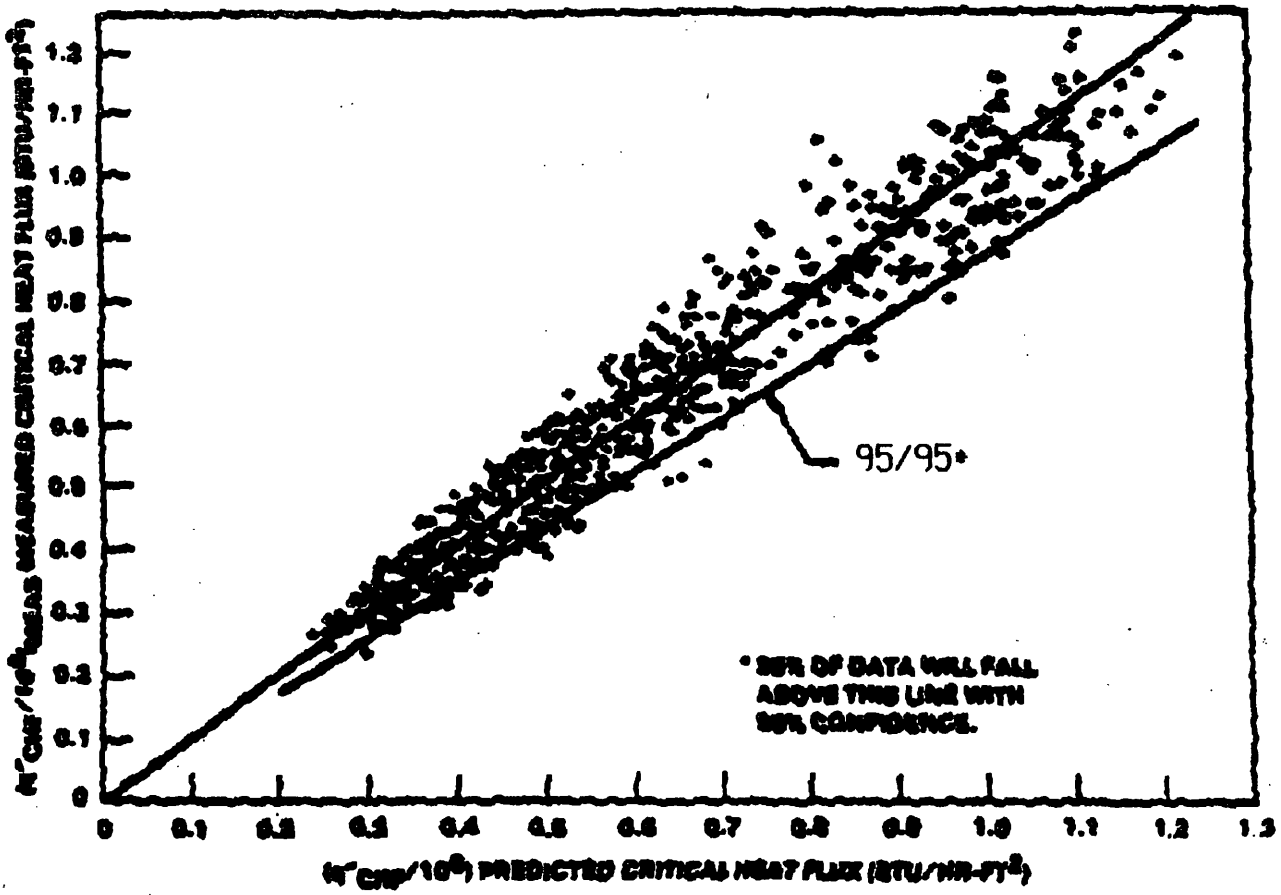

FIGURE 3.4-5
MEASURED VERSUS PREDICTED CRITICAL
HEAT FLUX - WRB-1 CORRELATION
BEAVER VALLEY POWER STATION UNIT NO. 1
UPDATED FINAL SAFETY ANALYSIS REPORT

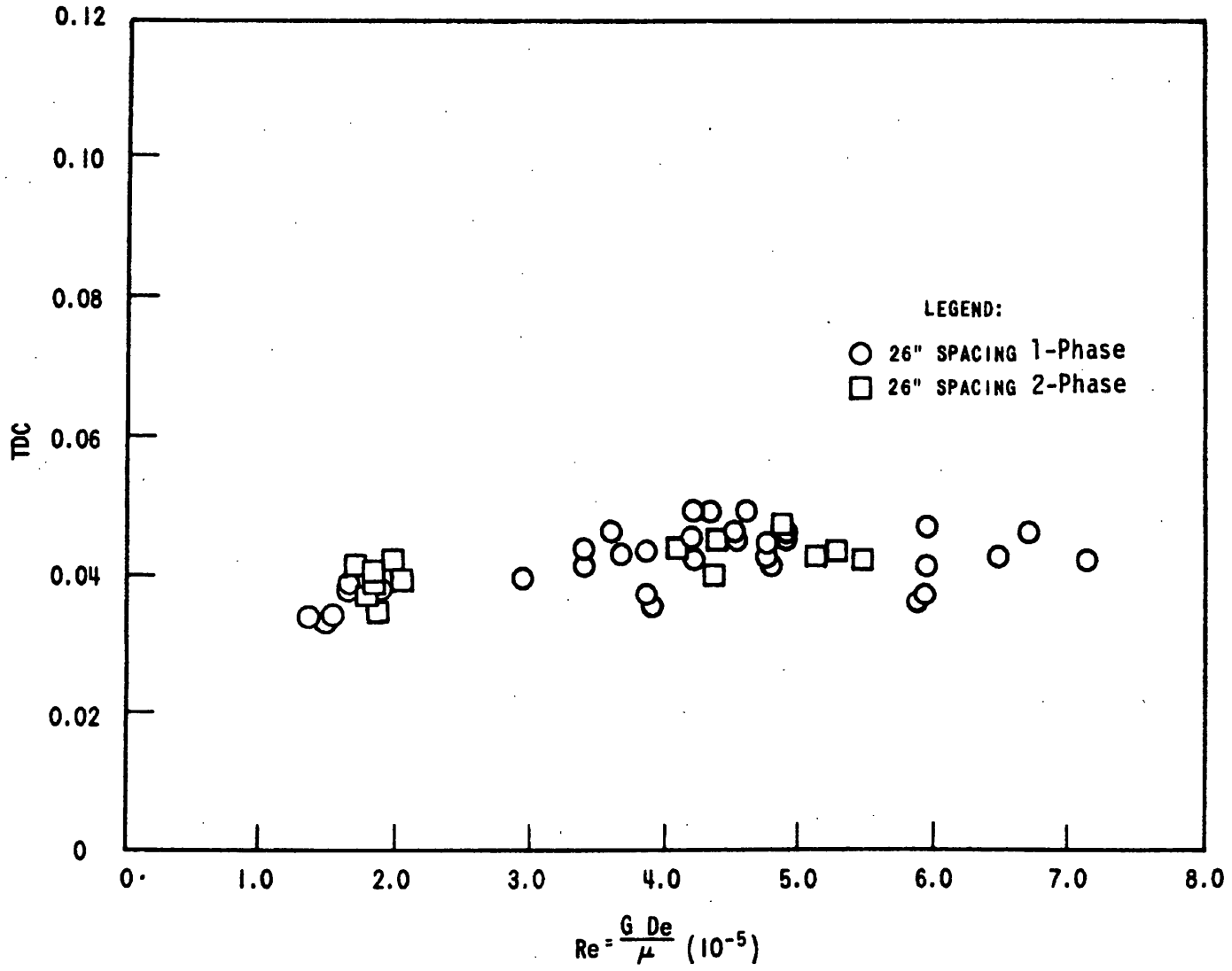

FIGURE 3.4-8
TDC VS REYNOLDS NUMBER FOR 26" GRID SPACING
BEAVER VALLEY POWER STATION UNIT NO. 1
UPDATED FINAL SAFETY ANALYSIS REPORT

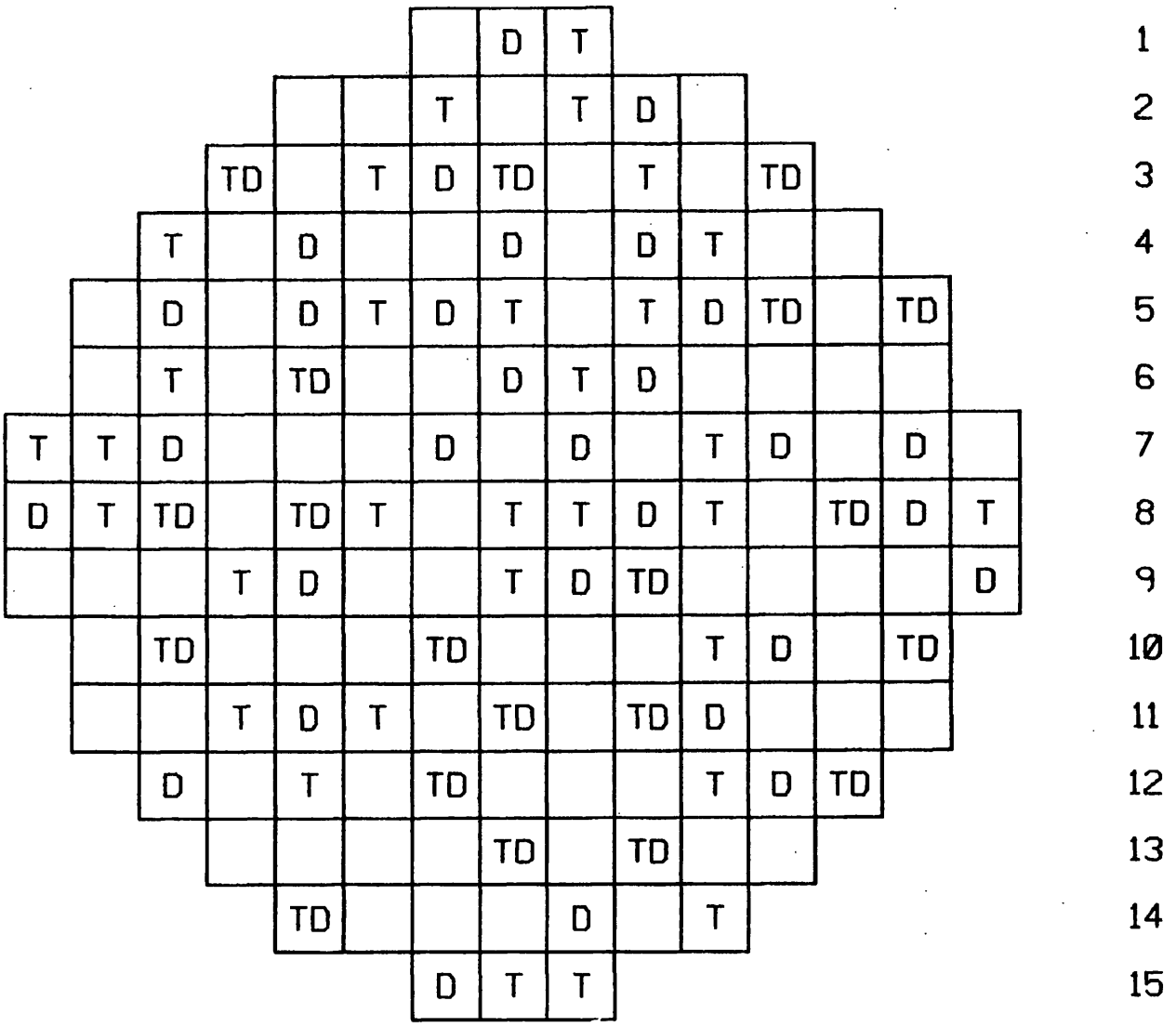

FIGURE 3.4-22

DISTRIBUTION OF IN-CØRE INSTRUMENTATION

BEAVER VALLEY POWER STATION-UNIT 1
UPDATED FINAL SAFETY ANALYSIS REPORT

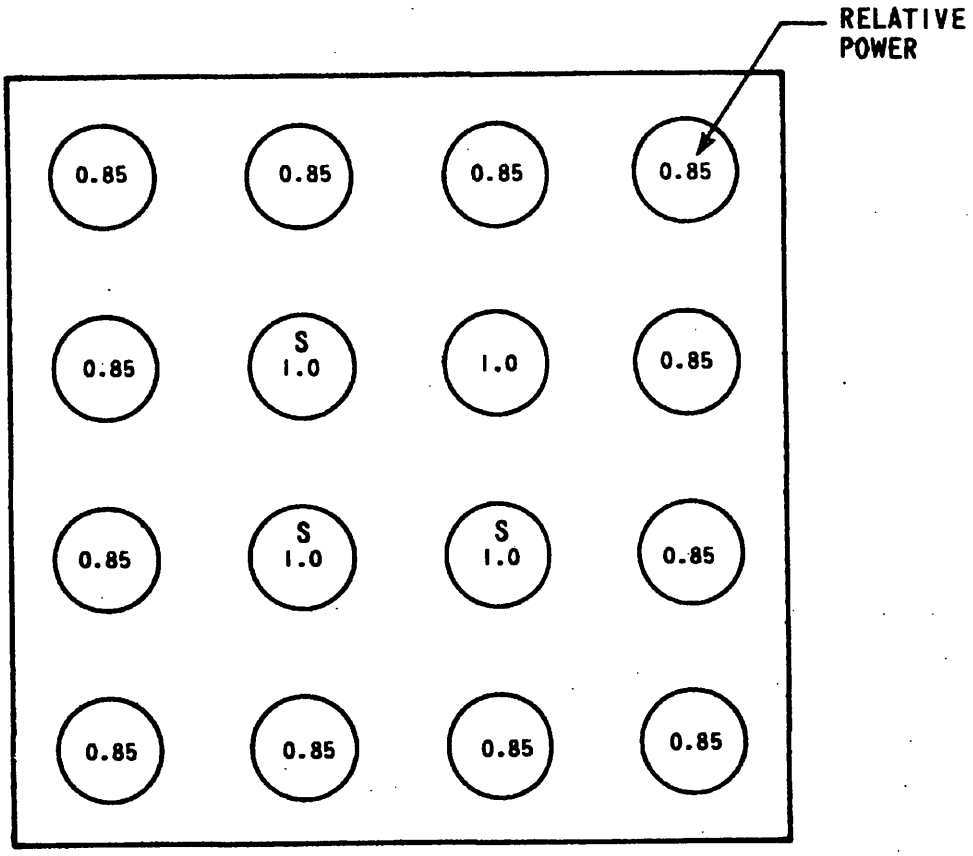

"S" - SPIKED ROD LOCATIONS

FIGURE 3.4-23
TEST SECTION CROSS-SECTION FOR DNB SPIKE TEST
BEAVER VALLEY POWER STATION UNIT NO. 1
UPDATED FINAL SAFETY ANALYSIS REPORT

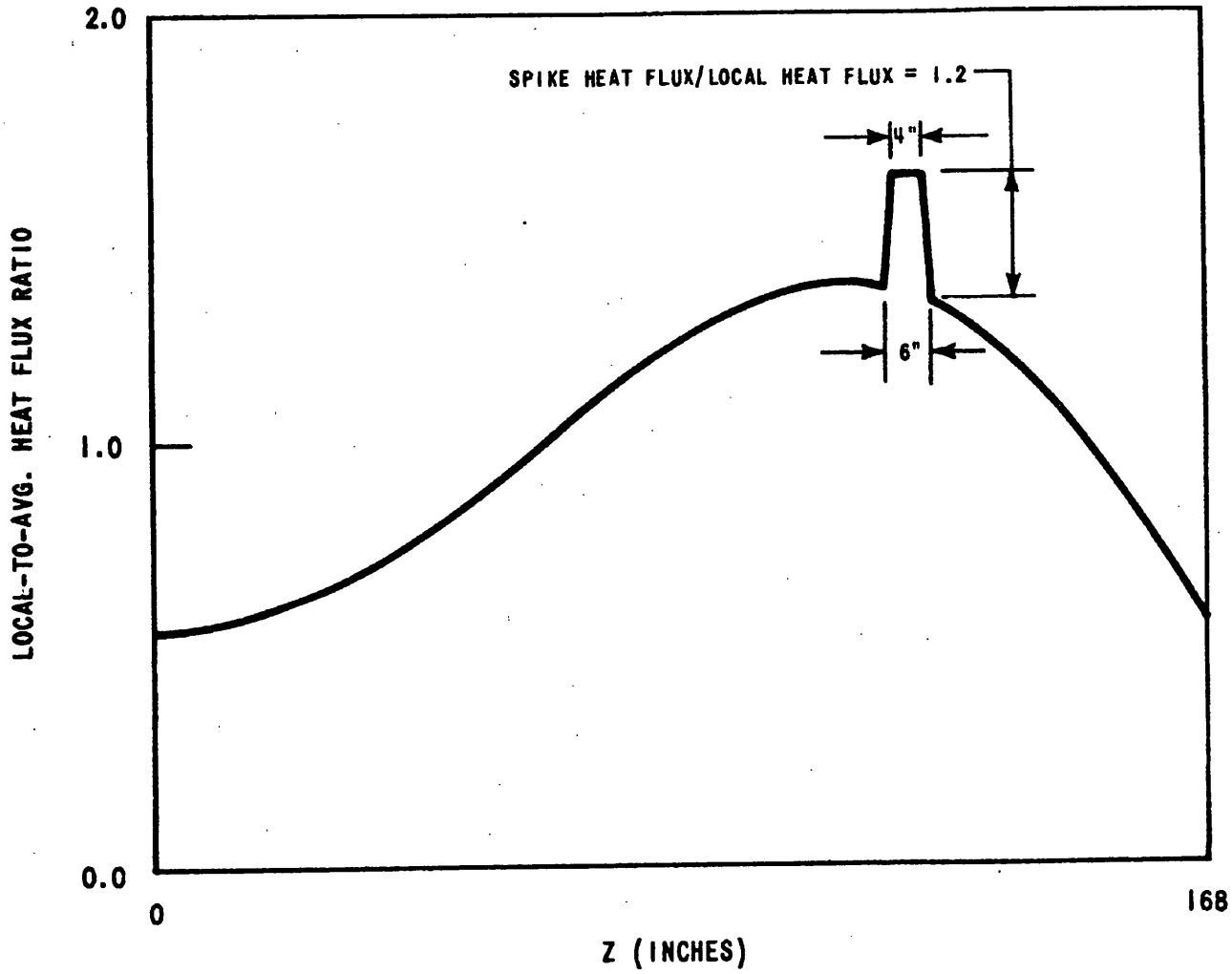

FIGURE 3.4-24
AXIAL HEAT FLUX PROFILE WITH 20% SPIKE FOR 168 INCH RODS
BEAVER VALLEY POWER STATION UNIT NO. 1
UPDATED FINAL SAFETY ANALYSIS REPORT